AFFDL-TR-67-82

APPROACHES TO STRUCTURAL VERIFICATION TESTING OF MACH 3-15 VEHICLES

H. D. DILL, J. M. FINN AND R. A. GARRETT

McDONNELL COMPANY

TECHNICAL REPORT AFFDL-TR-67-82

DECEMBER 1967

AIR FORCE FLIGHT DYNAMICS LABORATORY
RESEARCH AND TECHNOLOGY DIVISION
AIR FORCE SYSTEMS COMMAND
WRIGHT-PATTERSON AIR FORCE BASE, OHIO

NOTICE

When Government drawings, specifications, or other data are used for any purpose other than in connection with a definitely related Government procurement operation, the United States Government thereby incurs no responsibility nor any obligation whatsoever; and the fact that the Government may have formulated, furnished, or in any way supplied the said drawings, specifications, or other data, is not to be regarded by implication or otherwise as in any manner licensing the holder or any other person or corporation, or conveying any rights or permission to manufacture, use, or sell any patented invention that may in any way be related thereto.

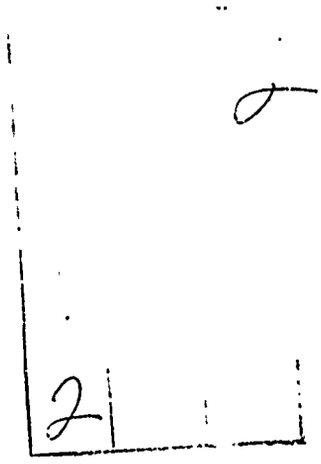

Copies of this report should not be returned unless return is required by security considerations, contractual obligations, or notice on a specific document.

200 - January 1968 - CO455 - 21-451

AFFDL-TR-67-82

APPROACHES TO STRUCTURAL VERIFICATION TESTING OF MACH 3-15 VEHICLES

H. D. DILL, J. M. FINN AND R. A. GARRETT

McDONNELL COMPANY

FOREWORD

This report was prepared by the McDonnell Company, St. Louis, Missouri under contract number AF33(615)-3418, dated 31 January 1966. This contract was initiated under Project 1347, "Structural Testing of Flight Vehicles," Task 134703. The contract was administered under the direction of the Air Force Flight Dynamics Laboratory of the Air Force Systems Command, Wright-Patterson Air Force Base, Ohio. Mr. William R. Johnston, AFFDL, was the Project Engineer.

The Structural Research Group of the McDonnell Strength Department had the responsibility for the performance of this program. The project leader for McDonnell was J. M. Finn, Chief Structural Research Engineer. Principal authors of this report are R. A. Garrett, Project Strength Engineer and H. D. Dill, Strength Group Engineer. Other contributors to the study include: J. H. Carlson, Thermodynamics Engineer; K. L. Denney, Senior Test Laboratory Engineer; F. W. Huster, Section Supervisor, Engineering Estimating; S. J. Kenjarski, Strength Engineer; and J. Noyes, Assistant Project Engineer, Producibility. Professor H. T. Corten, University of Illinois was retained as McDonnell consultant for this program.

In accordance with contractual requirements, the following consultants were retained to evaluate the results of this investigation: Dr. Bruno A. Boley, Columbia University; and Dr. H. L. Langhaar, University of Illinois.

This report covers work conducted from 1 February 1966 through 1 February 1967.

This technical report has been reviewed and is approved.

James C. Horsley Jr.
JAMES C. HORSLEY, JR., MAJOR, USAF
Chief, Experimental Mechanics Branch
Structures Division

ABSTRACT

Several alternate approaches have been investigated for the structural verification testing of future aerospace vehicles. The investigation had a two-fold objective: (1) to develop, evaluate, and select approaches for fatigue and ultimate strength verification testing of aerospace structures experiencing large thermal inputs over large areas, and (2) to establish a test program to confirm the validity of the selected approaches.

The advantages and disadvantages of reducing the size of the test article, and hence the thermal input required, have been investigated by evaluation of the scaled structural model approach and the component approach. The approach of simulating the thermal effects by mechanical means has also been evaluated. Two vehicle configurations have been studied to provide data for the relative evaluation: a large Mach 3-4 vehicle similar to the SST and a smaller Mach 12-15 hypersonic manned vehicle. Detailed thermodynamic, strength, test facility, and cost data relating to individual testing approaches, and combinations of these approaches, for these two configurations are presented. Costs for each of the combination testing approaches are developed and compared. The most attractive combination of approaches is selected and a testing program to confirm the val ity of the combination is defined.

(Distribution of this abstract is unlimited.)

TABLE OF CONTENTS

TABLE OF CONTENTS (Continued)

TABLE OF CONTENTS (Continued)

TABLE OF CONTENTS (Continued)

TABLE OF CONTENTS (Continued)

ILLUSTRATIONS

ILLUSTRATIONS (Continued)

ILLUSTRATIONS (Continued)

ILLUSTRATIONS (Continued)

ILLUSTRATIONS (Continued)

TABLES

SYMBOLS

A	Area, $ft.^2$
b	Width, in.
C	Joint conductance, $BTU/ft.^2\text{-}hr.\text{-}^\circ F$
c_p	Specific heat, $BTU/lb.\text{-}^\circ F$
d	Diameter, in.
E	Young's modulus, psi
F	Honeycomb shear strength, psi; blackbody radiation shape factor
F_c	Inter-rivet buckling strength, psi; column buckling strength, psi
F_{cc}	Crippling strength, psi
F_{cr}	Compressive buckling strength, psi
F_{cy}	Material compressive yield strength, psi
F_s	Rivet shear strength, psi
F_{tu}	Material ultimate strength, psi
F_{ty}	Material tension yield strength, psi
f	Stress, psi; natural frequency, cycles/sec.; cyclic rate, cycles/sec.
f*	Stress gradient, $lb./in.^3$
Δg	Load factor increment, g's.
H	Total heat, BTU
h	Convective heat transfer coefficient, $BTU/ft.^2\text{-}hr.\text{-}^\circ F$
K	Geometric proportionality factor
K_T	Stress concentration factor
k	Thermal conductivity, $BTU/hr.\text{-}ft.^2\text{-}^\circ F/ft.$
L	Geometry, ft.
L'	Effective column length, ft.

SYMBOLS (Continued)

M	External moment, ft.-lb.
N	Cycles to failure
n	Ratio model to prototype dimensions; cycles per load level
n_x) n_y) n_z)	Directional load factors, g's.
P	External load, lb.; spotweld strength, lb./in.
p	Pitch, in.
$\dot{q}$	Heat flux, BTU/ft.^{2}-hr.
R	Radius, in.; stress ratio = $\frac{\text{minimum stress}}{\text{maximum stress}}$
T	Temperature, °R
T'	Temperature difference, °R
T_{aw}	Stream adiabatic wall temperature, °R
T_s	Specimen surface temperature, °R
T_c	Coolant temperature, °R
t	Thickness, in.
V	Volume, ft.^{3}
δ	Deformation, ft.
Δ	Tolerances, in.
ε	Surface emissivity; creep, in./in.
ρ	Radius of gyration, in.; density, lb./in.^{3}
σ	Stephan-Boltzmann constant; surface finish, in.-R.M.S.
τ	Time, sec.
$\Delta\tau$	Time increment, sec.
τ_{cr}	Shear buckling strength, psi

Subscripts

C	Convection
c	Cooling system
f	Flight environment (design)
h	Heating system
I	Interface conduction
m	Model
p	Prototype
R	Radiation

SECTION I

INTRODUCTION

Traditionally, the structural integrity of military flight vehicles has been demonstrated by means of full-scale structural tests incorporating laboratory simulation of the most critical characteristics of the vehicle service environment, as required in appropriate Military Specifications. When the critical characteristics included only the application of a complex loading system, the task at hand was sometimes large but not insurmountable. But with large thermal inputs over large areas of the flight vehicle about to become one of the critical characteristics to be duplicated in the laboratory, the expected test complexity, duration, and costs dictated the need for alternate approaches to both ultimate and fatigue strength verification testing, by which the thermal requirements, both heating and cooling, could be reduced. The twofold purpose of the study reported herein is (1) to develop, evaluate, and select such alternate test approaches, and (2) to define a test program to confirm the validity of selected approaches.

The general purpose of structural verification tests is to demonstrate that the vehicle structure has the capability to withstand the most severe load and thermal environment within the requirements of the design specification. The need for such testing is not without statistical support; it has been shown that although significant improvements have been made in analytical techniques over the past 20 years, the number of major components of weapon systems failing below design ultimate load in tests has remained essentially constant. More complete data of this type are presented in Reference 1.

In the past, due to subsonic or low supersonic vehicle speed limitations, a room temperature environment for such tests has been adequately representative of the vehicle in-flight thermal environment, to within a small correction factor for temperature effects on material allowables. Little was changed in tests to demonstrate vehicle fatigue life except that the time duration of such tests became disturbingly long.

The advent of advanced weapon systems utilizing small vehicles of high supersonic or hypersonic speed capabilities posed the requirement that a portion of the structural verification tests must be conducted when the vehicle is subjected to a severe thermal environment in order to simulate the most critical structural design condition. This requirement brought about the development of lamps, capable of generating high heat at the expense of large electrical power, and associated control and monitoring systems. The use of these devices and controls in tests proved to be quite expensive, raising the cost of such tests by factors from 2-5, depending on the temperatures involved. The structural verification tests performed on the ASSET research vehicle, built and tested for USAF, may serve as an example. In steady state thermal tests in which no loads were applied simultaneously with temperatures, a maximum surface temperature of 2800°F was obtained; the vehicle surface area which was heated during the tests was approximately 10 square feet, and the heat flux was 60 BTU/ft.^{2}/sec. The total cost of this test program was approximately one million dollars; if similar techniques were applied to a vehicle up to 1000 times the surface area of ASSET, the resulting costs might immediately rule out such a test program regardless of whether the test could be performed or not. It can be concluded that present weapons systems and those foreseeable through 1975 may not permit the luxury of a full-scale structural verification test at

mission thermal environments for three reasons. First, the total costs of the program would be prohibitively large. Second, in the case of a long time fatigue test, there exists only a small probability of successfully completing such a test due to test apparatus failures. Finally, in all likelihood, the environment could not be properly simulated at all locations of the structure, and to simulate it only at selected points or areas would imply, inconsistent with the need for the test, prior knowledge of the critical area of the structure. It therefore becomes imperative that alternate testing approaches for future aerospace vehicles requiring large thermal inputs over large areas be developed.

It is realized that a complete structural test program for a weapon system includes many developmental tests, element tests, and major component tests (landing gear, control surfaces and systems, doors, etc.) prior to the ultimate or fatigue strength test of the airframe. Further, the airframe tests can be categorized into subassembly and system tests, fail-safe tests, and overall airframe ultimate and fatigue strength tests. Testing problems of the type described above are expected to be greater for the overall airframe ultimate and fatigue strength tests than the others; hence, the effort in this study has been restricted to evaluation of alternate approaches for such ultimate and fatigue strength tests.

SECTION II

SUMMARY

The purpose of the study reported herein was (1) to develop, evaluate, and select approaches for fatigue and ultimate strength verification testing of aerospace structures experiencing large thermal inputs over large areas, and (2) to establish a test program to confirm the validity of the selected approaches. The initial phase of the study was focused on the analytical determination of the portions of the mission thermal environment which must be simulated in the laboratory in order to obtain meaningful test results. The next phase was directed to the analysis of several alternate testing approaches and the selection of the particular approaches which best simulate these portions of the thermal environment at least cost. It has long been recognized that the simultaneous application of mechanical and thermal loadings is difficult. Further, as the severity of the thermal environment increases, the control requirements become more exacting and the test problems are disproportionately magnified and may become insurmountable; therefore, an evaluation of alternate approaches for testing of elevated temperature structures is required. Such evaluation, subsequent conclusions, and a test program to confirm the validity of the selected approaches are presented in this report.

To reduce the problems associated with the application of the thermal environment in tests, two possibilities have been considered in this study: (1) reduction of the physical size of the specimen to be tested by utilizing either components, representative of the prototype structure, or reduced scale structural models, and (2) simulation of some portion of the thermostructural effects of the thermal environment by mechanical means. In the first scheme, the surface areas of the test specimens to be heated are significantly decreased. The actual magnitude of this decrease depends on

the size of the selected components in the component approach or on the scaling factor in the structural model approach. The maximum temperature levels to be imposed on the specimens remain essentially the same as in the prototype mission thermal environment but the overall power requirements are reduced. In the second scheme, mechanical simulation of thermo-structural effects permits a lowering of the test temperature levels below those of the mission thermal environment, thus again decreasing the overall power requirements. Each of these schemes has been considered as a basic approach in the study. Including the approach of full-scale complete vehicle, a total of four basic approaches has been investigated:

(1) Full-Scale Complete Vehicle Testing

(2) Model Testing

(3) Component Testing

(4) Mechanical Simulation of Thermal Effects

As indicated in Section IV, it has been assumed that the testing to be considered would include only the final overall strength verification testing of the complete structure, either in fatigue or ultimate strength, and not the many elemental, developmental, and functional tests performed during the vehicle design, nor the many system tests, i.e., actuators, control surfaces, pressure bottle tests, etc., normally associated with vehicle approval or certification. Also, in this report, the complete vehicle test does not refer to a single test, nor is it assumed that such a single test at one time can substantiate the vehicle strength. It is recognized that in the case of ultimate strength testing, a sizable number of critical conditions must be applied to the vehicle structure to fully substantiate its strength, and although several conditions can sometimes be applied simultaneously, some of the remainder must be applied separately. It is this whole group of tests which are referred to as the complete vehicle test.

In order to form a base for a quantitative evaluation of approaches, the changes in the vehicle test thermal environment and the companion changes in material property degradation, creep effects, thermal stresses, etc., caused by the use of each of these basic approaches were first determined. Next, the effect of each of these changes on vehicle ultimate and fatigue strength was determined to ascertain any special provisions that must be made in the performance of tests to obtain satisfactory results. Finally, test facility requirements and test costs were determined. The results are presented in this report.

Two hypothetical vehicles, intended to represent the two extremes of elevated temperature testing problems were selected for analysis: one, a large, transport type, Mach 3-4 vehicle similar to a version of the SST (Supersonic Transport), for which peak temperatures are not excessive but where the size alone introduces facility problems; and the other, a smaller, Mach 12-15 vehicle for which local heating rates and temperatures rather than vehicle size constitute the critical test parameters. These two vehicles were selected in order to study two limits of facility problems: (1) the application of relatively moderate temperatures and heat fluxes over large areas, creating total power and power control problems, and (2) the application of high local heating rates with high temperatures over relatively small total areas. Verification testing approaches to both fatigue and ultimate strength were evaluated for the Mach 3-4 vehicle; however, only ultimate strength verification testing approaches have been evaluated for the Mach 12-15 vehicle because of the latter's relatively short assumed design life. For each vehicle, the configuration, mission speed-altitude profiles, local structural details, and surface temperature histories were defined to permit detailed analysis. The vehicle descriptions are presented in Section V.

The four basic approaches previously described for ultimate strength and

fatigue testing of the Mach 3-4 vehicle and the ultimate strength testing of the Mach 12-15 vehicle were individually considered. Ultimate strength is discussed in Section VI, and fatigue strength is discussed in Section VII. For each basic approach, an engineering analysis, test facility analysis, and cost analysis have been performed. In the engineering analysis, temperature and thermal stress data were determined to assess the quantitative effects of pertinent parameters such as emissivity, interface conductance, structural and thermal boundary conditions, etc. To date, only qualitative evaluations of these parameters have been reported in the literature.

The objective of the test facility analysis was to establish the test equipment required for the basic approaches and to evaluate the test problems likely to be encountered. A cost estimation was also performed for each basic approach with the primary objective of determining their relative costs. The major areas considered were (1) engineering design costs of the test specimen; (2) manufacturing costs of the test specimen, including tooling; and (3) testing costs, including jig design and fabrication, test equipment and material, and test performance, with the effects of down time. It should be noted that the costs estimates were derived from what are believed to be reasonably representative, typical data; however, they should be considered as gross, first level approximations to actual costs. The relative cost estimates have greater accuracy than any single absolute cost.

An evaluation of each basic approach led to the conclusion that not all of these approaches, applied individually, would satisfy the requirements of a meaningful vehicle strength verification test program. Accordingly, combination approaches were then developed. These are considered in Section VIII. A combination approach is an approach in which one or more of the several test types (full-scale complete vehicle test, structural model tests, full-scale

component tests, or mechanical simulation tests) is performed in one or more of the thermal environments (room temperature, constant elevated temperature, or mission temperature).

The full-scale complete vehicle test at mission temperatures was chosen as the basis for comparison of the technical merit of combination approaches; if it were not for test costs, time, and complications, this approach would be the prime candidate for testing. Combination testing approaches should have comparable test technical merit and should be obtainable at smaller costs, or in shorter time, or with less test complications.

The combination approaches for ultimate strength testing of both vehicles have been ranked by their respective costs; the combination approaches for fatigue testing of the Mach 3-4 vehicle have been ranked by their respective products of cost and elapsed time. These costs and cost-time products have been normalized to the values for the complete vehicle mission temperature test; reciprocals of these normalized values are termed the cost effectiveness and cost-time effectiveness factors for ultimate and fatigue strengths, respectively. The combination approaches found to have the highest effectiveness factors have been determined in Section VIII. They are presented, along with other conclusions of this study, in Section III.

The test facility at Wright-Patterson Air Force Base (WPAFB) has been used as a model for capacity and capability purposes to represent a typical existing large facility. Figure 1 indicates the limitations of that facility as a function of vehicle descriptors. It may be seen that the limitations of control equipment are more restricting than the limitations of building size or gross available power. These conclusions, obtained from the analyses presented in Sections VI and VII, are presented in Section III.

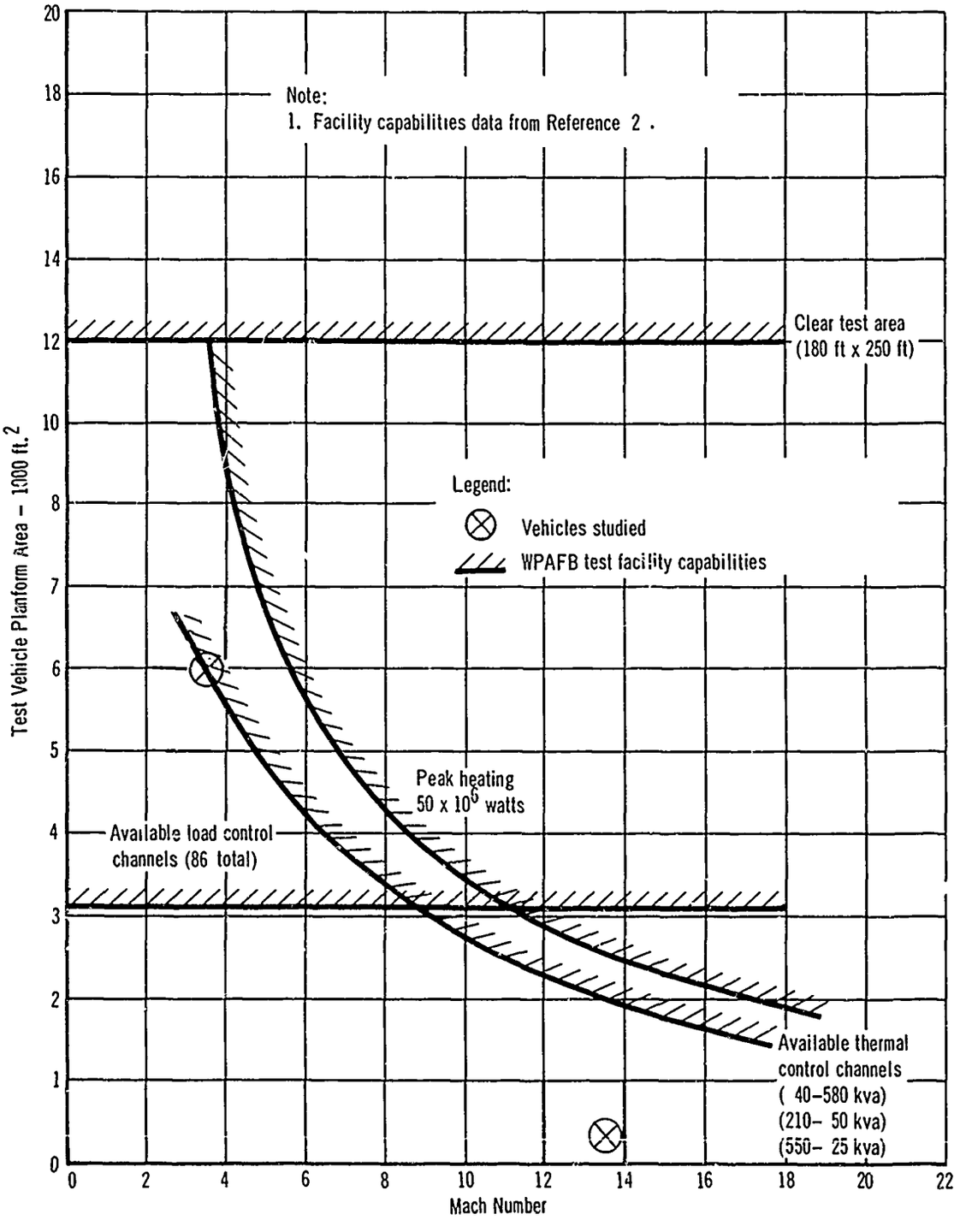

Figure 1 - Comparison of Study Vehicle Parameters and Test Facility Capabilities

The final goal of the study was the definition of a test program to confirm the validity of the selected approaches; this program is described in Section IX. Each of the selected approaches utilizes either a full-scale complete vehicle or an appropriate number of components, tested at room temperature or constant elevated temperatures to locate critical areas, followed by one or more components tested at mission temperature to determine the vehicle actual mission strength. As determined in Section VI, combination approaches using models had higher costs, basically because of the cost of tooling for test specimen fabrication.

The use of components does not require substantiation or confirmation; an awareness of the potential problems associated with components will usually lead to a satisfactory design and test. However, the correctness of the hypothesis that vehicles in constant temperature tests, whether at room or elevated temperature, will fail in the same areas, if not necessarily at the same load or life as in the mission profile temperature test, does require confirmation. A proposed test program, designed to evaluate the above hypothesis, has been formulated and is presented in Section IX.

Another possible approach is the utilization of a flight test program for the substantiation of the structural integrity of the vehicle. This approach would appear particularly applicable to fatigue strength evaluation of an aircraft, provided the timing of the program could be worked out satisfactorily. The flight test approach has the advantage of accumulating fatigue loadings in the true mission environment. It has been, however, considered outside the scope of the study and no detailed analyses pertaining to it have been performed.

SECTION III

CONCLUSIONS

The conclusions of this study are based upon engineering, test facility, and cost analyses of several alternate approaches to fatigue and ultimate strength verification testing of supersonic vehicles requiring large thermal inputs over large areas. The structures of two vehicles (Section V) were considered, with appropriate mission profiles and environments. Three types of conclusions have been reached: (1) conclusions pertaining to the technical validity, manufacturing problems, or testing difficulties of the various basic approaches (complete vehicles, models, components, mechanical simulation); (2) conclusions pertaining to the selection of suitable combinations of the above basic approaches for structural verification test programs; and (3) conclusions of a general overall nature, pertaining to the effects of mechanical and thermal loadings on the vehicle ultimate or fatigue strength. These three types of conclusions are presented in the following paragraphs.

1. Conclusions Pertaining to Basic Approaches

   1.1 Complete Vehicle Testing

   (a) For a test of a complete vehicle at mission profile temperatures of both vehicles studied, heating requirements, either $BTU/ft^2/hr$ or BTU/hr, are not a serious problem. Data and discussion are presented in Section VI.1.2.1, 1.2.2, 2.2.1, and 2.2.2. The real heating problems are associated with equipment reliability, the possibility of producing some serious,

unwanted, unforeseen thermal effect, and the difficulty of controlling temperatures in many locations over large areas.

(b) Cooling requirements are much more critical than heating requirements; this is especially true for vehicles requiring large cooling rates at moderate temperatures where radiation is not significant. See Section VI.1.2.2.

1.2 Structural Model Testing

(c) As described in Section VI.1.3.1, fabrication feasibility dictates that, for practical reasons, only scale factors of 1/4, 1/2, or 3/4 be considered, with 1/2 appearing most usable. Other scale factors would require a greater use of non-standard hardware or larger deviations from scaled geometry.

(d) As an extension of (b) above, cooling requirements for a particular vehicle may limit the extent of scaling possible, since heating and cooling rates vary inversely with scale factor, i.e., a scale factor of 1/2 requires that the cooling rate be increased by a factor of 2.

(e) Of all the thermal parameters known to be not scalable (radiation, interface conductance, etc.), the non-scalability of radiation has the greatest effect for the structures considered. The comparative effects of these parameters are discussed in Sections VI.1.2.1 and 1.3.1.

(f) Thermal stresses in models where test time has been scaled for conductive heat transfer tend to be greater than in full-scale structures due to the effects of internal radiation

which dictate a different test time scale factor. See Section IV.1.3.1.

(g) It has been demonstrated that thermal stresses in a model can be more closely duplicated through use of an intermediate time scale factor with a value between the values dictated by conductive and radiative heat transfer modes, as shown in Section VI.1.3.1.

(h) Structural models appear satisfactory for ultimate strength verification where the degree of thermal stress simulation has a relatively minor effect on test results, as described in Section VI.1.3.1.

(i) Serious drawbacks to the model approach include: (1) the high cost of tooling for, and the fabrication of a satisfactory structural model, as discussed in Section VI.1.3.3; (2) the engineering effort required to complete model drawings, discussed in Section VI.1.3.1; and (3) the difficulty of producing and monitoring the thermal environment inside a reduced size model due to limited available space, discussed in Section VI.1.3.2.

(j) Structural models are potentially less satisfactory for fatigue strength verification than for ultimate strength verification due to the greater sensitivity of fatigue life to small stress changes. See Sections VII.2.1 and 3.1. For this reason, it has been concluded that actual fatigue life of the prototype vehicle cannot be reliably determined by model tests alone.

1.3 Components

(k) Components for elevated temperature testing may become larger than for room temperature testing because of the additional structure required to provide suitable thermal boundary conditions, as described in Section VI.1.4.1. Therefore, little is saved in cost of test specimen fabrication using the component approach in elevated temperature testing, as compared to complete vehicle testing. The reduction of heating requirements, the reduction in required physical size of the test facility, and the capability to use more than one facility at a time are the significant advantages of the component approach.

(l) The effect of internal radiation within a component will generally result in thermal gradients larger than those of the prototype. See Section VI.1.4.1.

(m) Similar to (l) above, the maximum thermal stresses developed within a component may become larger than in the prototype because of the larger temperature gradients.

1.4 Simulation of Thermal Effects by Mechanical Means

(n) Meaningful simulation of thermal effects by mechanical means in a fatigue test requires knowledge not only of the most critical cross section, but also of the location of the potential failure in the cross section. Knowledge of the latter is required to calculate what changes in mechanical loading will simulate the thermal environment effects at that point. Such prior knowledge is usually not available; if it were, it is problematical whether a test would be necessary; hence, the usefulness of the

mechanical simulation approach appears limited. Additional discussion is presented in Section VI.2.5.1.

(o) An overall increase in applied loads to account for thermal effects on mechanical properties appears the most practicable use of the mechanical simulation approach. See Section VI.2.5.1.

2. Conclusions Pertaining to Selection of Combination Approaches

2.1 Ultimate Strength Verification - Mach 3-4 Vehicle

(a) Of the developed combination approaches, all of which have comparable technical merit, the least expensive combination approach (and therefore by the definitions of this study has the highest cost effectiveness) is the one in which a complete vehicle is tested at room temperature to locate the critical areas, followed by a test, at mission profile temperatures, of a small component containing the section which failed in the complete vehicle room temperature test, to establish the ultimate strength level under mission temperatures. This is the selected approach for the ultimate strength verification of the Mach 3-4 vehicle. See Section VIII.4.

(b) The basic approach using one complete vehicle at mission profile temperatures has approximately the same rating factor as the selected combination approach for ultimate strength testing of the Mach 3-4 vehicle described in (a) above. See Section VIII.4.

(c) The costs of technically satisfactory approaches utilizing structural models are the largest of all approaches considered due to additional engineering design, monitoring and tooling

costs, as shown in Section VIII.4.

(d) Tooling costs for the model fabrication are the largest single item in model testing costs. See Section VIII.4.

2.2 Ultimate Strength Verification - Mach 12-15 Vehicle - The conclusions obtained for the ultimate strength verification of the Mach 12-15 vehicle are identical to the four conclusions pertaining to the selection of approaches for the ultimate strength verification of the Mach 3-4 vehicle and are not repeated here. It is then appropriate to conclude that these same conclusions apply to ultimate strength testing of a great variety of vehicles in the range of the two studied.

2.3 Fatigue Strength Verification - Mach 3-4 Vehicle

(e) The selected combination approach is that which utilizes six large components (sufficient in size to survey the fatigue strength of the entire vehicle), tested at room temperature to locate fatigue critical areas, followed by two large components tested at mission profile temperatures to determine actual vehicle mission fatigue life. See Section VIII.4.

(f) The combination approach utilizing one complete vehicle tested at room temperature to locate critical areas, followed by two large components tested at mission profile temperatures to determine fatigue life has approximately the same rating as the selected combination approach described in conclusion (e) above. It is described in Section VIII.4.

(g) The combination approach using one complete vehicle at mission profile temperatures has the lowest rating and therefore the least

attractive synthesis of cost and test performance time for fatigue testing of the Mach 3-4 vehicle, as discussed in Section VIII.4.

(h) The costs of combination approaches using a half-scale complete vehicle are approximately the same as the costs for a full-scale complete vehicle test at mission profile temperatures, as shown in Section VIII 4.

3. Conclusions of a General Nature

The depth of the study does not allow for complete substantiation of the following general conclusions; they should be considered judgements based on limited information obtained in the study, which were insufficient to assure complete applicability to all situations, and therefore may be more properly termed conjectures.

(a) For vehicles designed for long fatigue life, such as the Mach 3-4 vehicle, analysis indicates that creep is not of major significance and hence its simulation is of secondary importance. See Section VII.2.1.2.

(b) Thermal stresses of the magnitudes considered in this study are not of significant importance for fatigue life simulation, if only flight loads are applied to the test article. However, if the ground-air-ground cycle is included in the testing program (as it should), the thermal stress simulation becomes much more important and may reduce the expected life by a factor of 2 to 5. Pertinent data are presented in Section VII.2.1.2.

(c) For the vehicles considered, thermal stresses are not important for ultimate strength verification of structural elements with compact, stable cross sections. See Section VI.2.2.1.

(d) Analysis presented in Section VII.2.1.2 has shown that ground-air-ground cycles are of significant importance in the fatigue life of the Mach 3-4 vehicle, and they may reduce the expected test fatigue life in certain areas of the vehicle by a factor of as much as 10. The method of analysis used to compute such a life reduction correlates well with spectrum fatigue test results reported in the literature.

(e) If ground-air-ground cycles were omitted from the fatigue test program for reasons of test complexity, attempts to include or simulate thermal stresses may also be omitted or greatly simplified, since the effects of thermal stresses on fatigue life without the application of ground-air-ground cycles are much smaller than their synergistic effect with the ground-air-ground cycles. Also, attempts to produce creep may be omitted because its effects on fatigue life are very small in comparison to the effects caused by the ground-air-ground cycle. The relative effect on fatigue life of each of these parameters is discussed in Section VII.2.1.2.

SECTION IV

ASSUMPTIONS, PARAMETERS, AND APPROACHES

This section defines the assumptions and parameters on which the study was based, and discusses the approaches considered. The results of the study are directly applicable only to the testing of the vehicles described in Section V. Their applicability to the testing of other vehicles can be best determined by an appraisal of the conformance of the geometry, construction, and mission profile of the vehicle in question to the descriptions of Section V, summarized in Subsection 1.1, and the general validity of the other assumptions, parameters, and approaches presented to the vehicle in question.

1. Assumptions

The primary objective of this study was to develop, evaluate, and select approaches for the fatigue and ultimate strength testing of aerospace structures. Accordingly, a set of assumptions was established to limit the scope of the analysis to permit greater concentration on the more pertinent areas, resulting in a quantitative evaluation of the approaches and a degree of specificity in the technical analysis. The other possibility would have been a broad brush qualitative attempt to cover the entire field of structural testing without any quantitative investigation. If this had been attempted, it is felt that the importance of some of the parameters considered could not have been adequately estimated.

1.1 Vehicle Definition and Testing Assumptions - The following assumptions were made with regard to the vehicle type and scope of testing to be considered. A more complete vehicle description and mission definition is presented in Section V.

(a) Two vehicles would be considered to evaluate the applicability of the various approaches to be studied; briefly, they are:

1. A relatively large, manned vehicle, planform area of approximately 6,000 square feet, whose speed-altitude regime and mission definition are somewhat similar to the Supersonic Transport - Mach 3-4 at 80,000 feet, a design service life of 20,000 missions and a maximum airframe temperature of 600°F. Criteria developed for this vehicle would be applicable to other structures where the total vehicle area to be thermally controlled during ultimate or fatigue testing would be of principal concern. The number of controllers required and the companion control difficulties create the fundamental test problem for this vehicle.

2. A small manned vehicle with planform area of approximately 350 square feet with a maximum airframe temperature of 1600°F (Mach 12-15 at 140,000 feet). For testing of this vehicle the complications of applying both high thermal loads and mechanical loads simultaneously are of principal concern.

(b) Testing criteria applicable through the year 1975 would be considered; hence it has been assumed that fatigue life verification testing of Mach 12-15 vehicles will not be a requirement in this time period. Such a vehicle has been assumed to be an advanced research vehicle, designed for a relatively short service life (less than 1000 flight hours), so only ultimate strength verification is believed to be appropriate for this vehicle. However, for the Mach 3-4 vehicle, both fatigue and ultimate strength verification would be considered.

(c) The testing to be considered has been assumed to include only the final overall strength verification of the complete structure in fatigue and/or ultimate strength as described previously, and not the many elemental, developmental, and functional tests performed during the vehicle design phase, nor the many system tests, i.e., actuators, control surfaces, pressure bottle tests, etc., normally associated with vehicle approval or certification.

(d) The testing to be considered would include only versions of laboratory testing and not any flight test program which, although potentially very useful for the vehicles considered, does not involve laboratory heating problems.

(e) It should be noted that, in the context of this report, the complete vehicle test program does not imply or assume a single test; nor is it assumed that such a single test can substantiate the strength of a complete vehicle in any meaningful manner. For instance, it is recognized that in the case of ultimate strength testing, a sizable number of critical conditions must be applied to the vehicle structure and although several conditions can sometimes be applied simultaneously, some of the remainder must be applied separately. It is this whole group of tests - all those which would normally be applied to the complete structure - which are taken to be, and are referred to as, the complete vehicle test. The exact definition of these tests and their sequence of application requires a much more detailed investigation of critical conditions for the vehicle in question, a more complete structural description, and a detailed evaluation of the specification requirements for the vehicle to be tested - all of which are considered outside the scope of the study.

1.2 Assumed Testing Facility Available

(a) The test facility at WPAFB has been used as a model to represent the capacity and capability of a typical existing large facility. As reported in Reference 2, the building has a clear floor area 180 feet by 250 feet and included among its many and varied support equipage are a radiant heating capability of almost 50 million watts for short time duration or 18 million watts of radiant heating on a continuing basis, a multiple channel programmed loading capability, and an extensive data collection and processing system. In addition, this facility has 80 power control channels rated at 580 KW with 40 channels being capable of division into 550 subchannels at 25 KW and 210 subchannels at 50 KW. These channels can be used for integrated heating and cooling control with only minor adaptation. In addition, 86 control channels are available for load control.

(b) For costing purposes in this study, it has been assumed that the fixed plant characteristics of this assumed facility such as enclosure size, floor and wall strength, control monitors, etc. are either available or acquirable and are adequate to perform the required testing; hence, they were not included in test cost estimates presented in Sections VI and VII.

(c) Expendable items, such as lamps, strain gages, thermocouples, and hardware designed specifically for the vehicle to be tested, such as whiffletrees, loading beams, etc. are all included in the final cost estimate.

1.3 Assumed Engineering Effort - The following assumptions have been made with regard to the engineering effort required to support the test programs considered:

(a) A complete set of engineering drawings of the prototype vehicle would be available, so no further engineering effort would be required in that area.

(b) All components must be designed, component quantities defined, component boundaries determined, edgings designed, thermodynamic and stress analysis performed, etc.

(c) All testing structures and jig hardware must be designed.

(d) For the modeling approach, the required engineering effort would include engineering design of the half-scale specimen.

(e) An appropriate amount of data reduction would be required for all approaches.

(f) All lamp arrangements, requirements, and controls must be completely engineered.

1.4 Assumed Manufacturing Effort

(a) All test specimens, regardless of the approach considered, must be manufactured as part of the test program and the associated costs included.

(b) Tooling for the half-scale model must be fabricated.

(c) Tooling developed for the full-scale complete vehicle is available for component fabrication.

2. Parameters

The parameters which affect the vehicle ultimate and fatigue strength in laboratory tests may be grouped under the headings of mission parameters and

laboratory parameters. The mission parameters are those associated with the anticipated usage of the structure, such as load and thermal environment, corrosive environment, etc., while laboratory parameters are those resulting from the manner and means of simulating the vehicle mission environment in the laboratory, such as factors affecting accuracy of load and thermal control, etc. The total number of these two groups of parameters is large for a structure operating near room temperature, but increases sharply for structures experiencing a broader thermal environment.

A further increase in the number of parameters occurs when verification testing is performed using components or models. In both cases, the desire is to test a specimen identical in performance with the prototype; this may require a change in a physical characteristic of the test specimen from that ordinarily obtained without special attention. For example, if structural models are to be used, it can be shown that the desired surface emissivities to create the correct thermal gradients in a half-scale model are twice those of the full-scale prototype, as discussed in Section VI. Controlling the value of such a parameter in the test article is difficult, but doubling the value could be impossible.

The following parameters of both types have been considered in the evaluation of various testing approaches in this study:

(a) Creep effects

(b) Strain rate (load frequency)

(c) Load spectrum

(d) Load randomization

(e) Ground-air-ground cycle

(f) Material degradation caused by temperature

(g) Metallurgical changes

(h) Corrosion

(i) Manufacturing residual stresses

(j) Size effects (modeling effects):

Surface finish

Size

Tolerances

Stress gradient

(k) Parameters affecting thermal stress:

Environmental air pressure

Surface emissivities

Surface (interface) conductances

Boundary conditions

(l) Boundary conditions (component size)

(m) Specimen-to-specimen variability

3. Approaches

Several alternate approaches have been evaluated in this study. All are predicated on the fundamental premise that full-scale thermal testing of complete vehicle structures is not a satisfactory solution due to excessive demands it places on facilities, particularly thermal control, and that these demands must be reduced to render the structural verification test program feasible. Such reduction can be achieved: (a) by decreasing the physical size of the specimens to be tested through use of components or models, (b) by decreasing the thermal inputs into the test specimens through (partial) simulation of thermal effects by mechanical means, and (c) by some other method such as a suitable flight test program. Approaches (a) and (b) are considered in this study; a flight test program has been deemed to be outside the scope of the study.

There are two basic alternate approaches which reduce the size of thermal test specimens, namely, model testing and component testing.

3.1 Model Testing - In the evaluation of this approach, it has been assumed that the prototype vehicle must be analyzed to determine the scale factor to be used, and the configuration of the test article required for a valid test program. Upon fabrication of the necessary hardware, the verification test program must be performed with the environment parameters such as loads, temperature, and time, adjusted in accordance with the scale factor used.

In some cases for the modeling approach, scaling laws indicate that a simple reduction of geometric size satisfies scaling requirements; that is to say, thicknesses and widths of a half-scale model should be half that of the full-scale prototype. In other cases, a non-proportional change is required in order to retain scale structural characteristics. An additional important consideration in the modeling approach is that there exist practical limitations to the scaling down of material gages, fastener diameters, and other items normally considered scalable. For this reason, only one-half scale models have been considered in this study.

3.2 Component Testing - In the component testing approach, full-scale portions of the prototype structure have been considered as separate test articles. For the vehicle in question, the prototype areas to be represented must be selected, the component configurations such as size, type, and degree of simulation of the prototype structure defined, and the number of specimens needed for a valid test program established. An important consideration consists of allowing for the local structural effects at the component-test jig juncture. The number of test specimens and the scope of the test program requires definition for the vehicles considered, based on

their structural characteristics, mission profile, and other pertinent parameters.

3.3 Mechanical Simulation of Thermal Effects - The two primary effects of a severe thermal environment upon a load-carrying structure are: (a) the degradation of mechanical properties of the materials used to fabricate the load-carrying structure, and (b) the creation of thermal stresses due to incompatible and/or restricted thermal expansions. Some adjustment of the magnitude of the applied mechanical loads may be used to compensate for a fraction of the material degradation due to temperature. Also, it is theoretically possible to reproduce the induced thermal stresses in small portions of the structure without the application of the thermal gradient by means of mechanical loads. The use of this technique would require that a suitable analysis be performed to define either the changes in loads or the added loading arrangements that should be applied to the specimens so as to produce the same effect as the (then omitted) thermal environment. Some moderate heating may be included as a part of this approach to induce overall material property temperature degradation effects. As described later in this report, the mechanical simulation approach has some merit for ultimate strength testing where thermal strain simulation is of little importance, but little merit for fatigue life verification where a more exact simulation of local strains over a large test area is required.

3.4 Combination Approaches - The approaches previously described are termed basic approaches in the context of this report. More useful approaches for verification testing have been formed of combinations of more than one basic approach; these combination approaches are discussed in Section VIII. They were developed to provide a means of structural verification testing

comparable in merit to complete vehicle mission temperature testing. Since the combination approaches were derived from the basic approaches, the descriptions of the basic approaches will, in general, apply to the combination approaches.

SECTION V

VEHICLE DEFINITIONS

The definition of vehicles used in this study to evaluate various test approaches was predicated on configurations and missions which may require testing through 1975. In order to allow quantitative evaluations, i.e., to allow the thermodynamic, strength, test facility, and cost analyses to be performed in a quantitative manner, definite vehicle types and configurations were selected. The conclusions drawn from these analyses are expected to be valid for a range of vehicle types and configurations; however, each specific application should be evaluated individually.

Expected mission design environments for present and future aerospace vehicles are shown in Figure 2. In view of the temperature and load application problems described in the previous sections, and in order to develop approaches to testing of appropriate future configurations, two types of vehicles were selected for evaluation and are shown in Figures 3 and 4.

(a) Mach 3-4 Vehicle - A relatively large manned vehicle, with planform area of approximately 6,000 square feet, whose speed-altitude and mission definition is somewhat similar to the SST - Mach 3-4 at 80,000 feet, a design service life of 20,000 missions and a maximum airframe temperature of 600°F. Approaches developed for this vehicle would be applicable to other structures where total heating and cooling rates (BTU/sec) or thermal control requirements during fatigue testing would be of principal concern.

(b) Mach 12-15 Vehicle - A relatively small manned vehicle, with planform area of approximately 350 square feet and a maximum surface temperature of 1600°F (Mach 12-15 at 140,000 ft.).

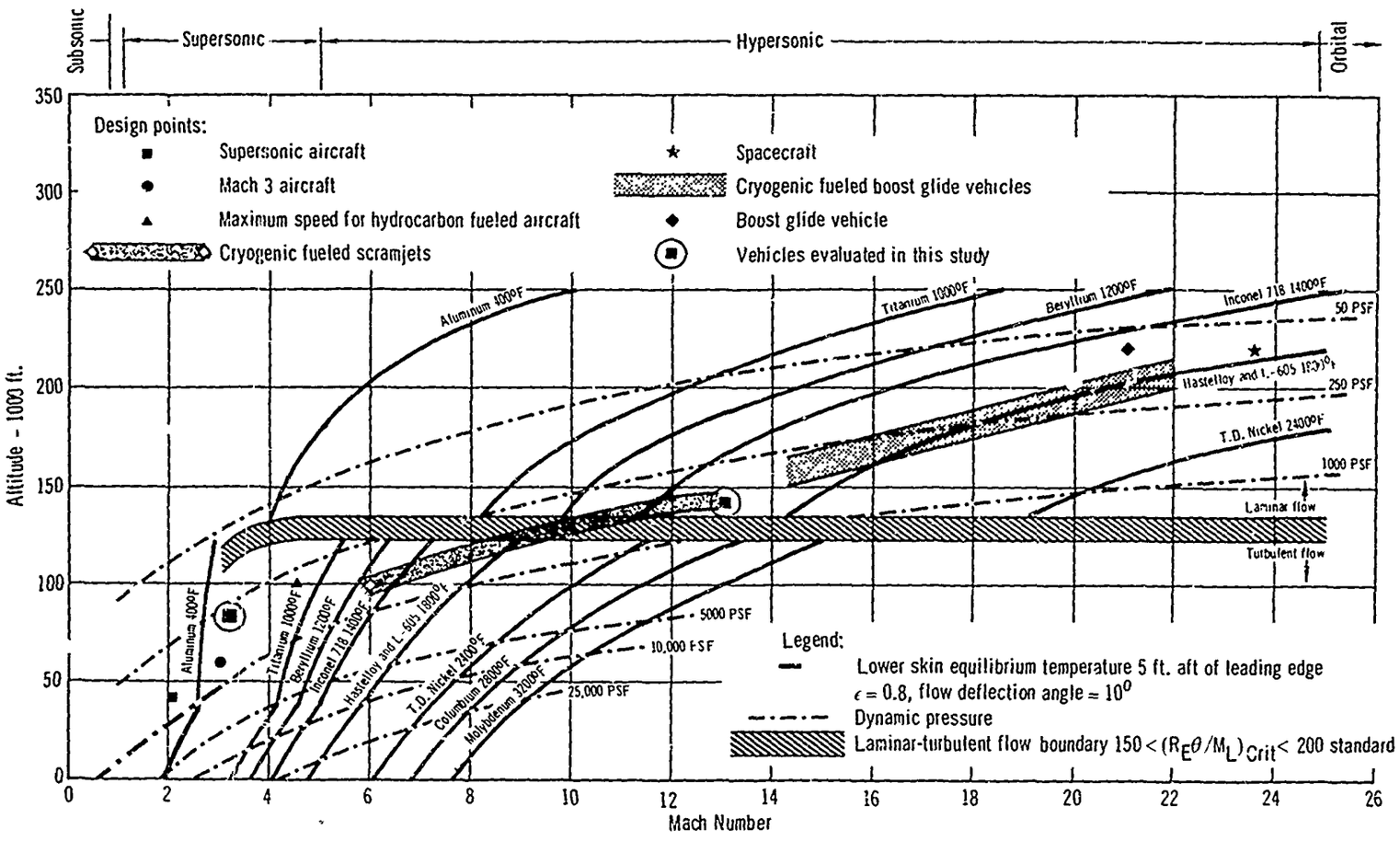

Figure 2 .. Design Environment of High Temperature Vehicles

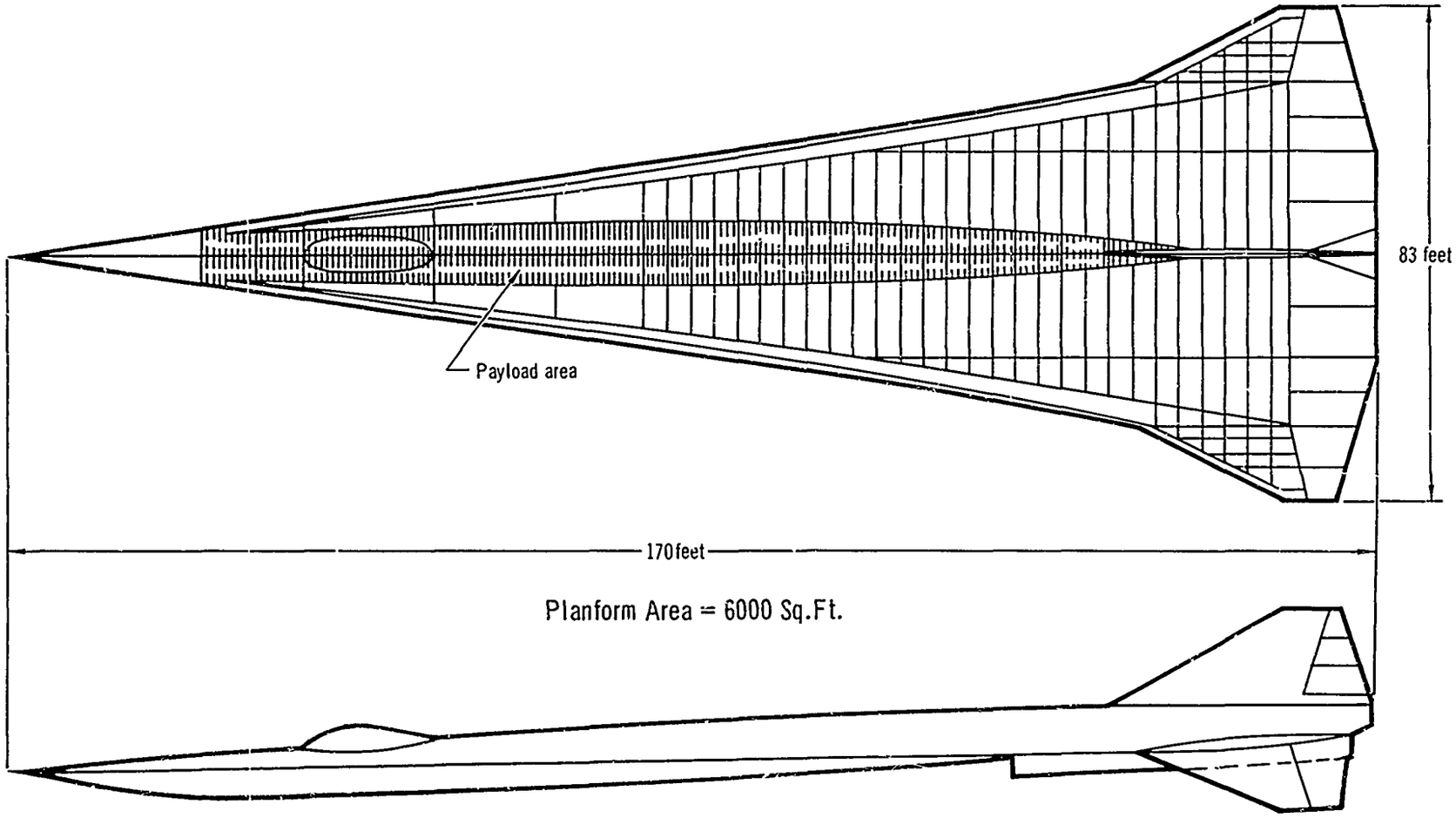

Figure 3 - Mach 3-4 Vehicle Configuration

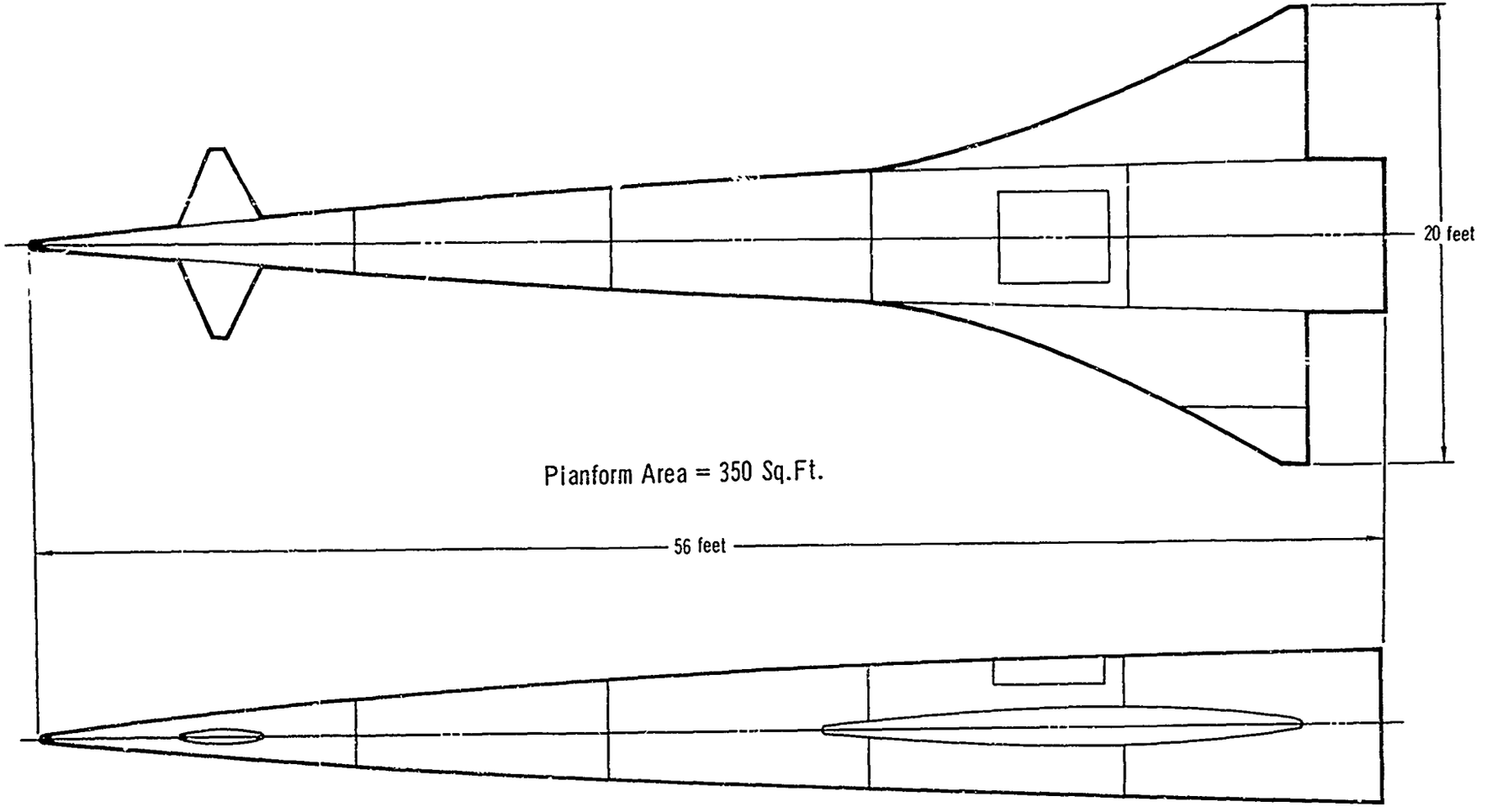

Figure 4 - Mach 12-15 Vehicle Configuration

Because of the vehicle size, the complication of simultaneously applying both high heat fluxes (BTU/ft^2-sec) and mechanical loads is of more importance than the total heating rate. For purposes of this study, only ultimate strength verification will be considered for this vehicle. Each of these vehicles is described more completely in the following paragraphs.

1. Mach 3-4 Vehicle

1.1 Structural Configuration - The planform of the Mach 3-4 vehicle used in this study is shown in Figure 3. The major features of the vehicle are:

(a) A configuration in which lifting airloads on each local area of the vehicle tend to be balanced by inertia loads (fuel and/or weight empty) developed in that same area.

(b) The fuel is stored in bladder cells in the fuselage and inboard wing.

(c) Multiple spars, with a large (deep) root rib and several intermediate ribs.

(d) Wing panels formed of double-face corrugated skins.

(e) Construction details consistent with the philosophy of minimizing thermal stresses.

In conventional aircraft which have the wing and tail connected by a length of fuselage, the tail loads are balanced by the wing loads which induce bending in the connecting structure. The delta configuration of the vehicle used in this study allows wing airloads, major inertia loads, and balancing elevon loads to be applied near each other, eliminating long expanses of cantilevered connecting structure. This approaches the ideal structural configuration in which all distributed airloads are exactly balanced locally by inertia loads.

This configuration provides multiple load paths, and is, therefore, typical of a "fail-safe" design. This inherent structural redundancy does, however, complicate the structural analysis and the verification testing.

The basic wing structure consists of: (1) cover panels which carry the axial loads due to overall wing bending and beam the airloads and fuel loads to the spars; (2) spars which function as shear members and stabilize the compression covers; and (3) ribs which redistribute concentrated loads and support mass items.

Possible structural arrangements for wing cover panels include skin-stringer, honeycomb sandwich, and corrugation stabilized sandwich (double-face corrugated skins). The latter configuration was selected for this study, being representative of expected designs and having a reasonable compromise of weight, cost, and producibility. The panels are required to support normal airloads and fuel loads, bi-axial in-plane loads, with large rib and spar spacings. The wing structure has been assumed continuous through the fuselage. The upper skin cover is designed by bi-axial compression loads generated by spanwise and chordwise bending combined with local effects of beaming the airloads to the spars. The lower cover is designed by a combination of bending, resulting from local effects of beaming airloads and fuel loads to the spars, and the tension effects of spanwise bending.

The multiple spars are tubular member trusses, except where reduced wing thickness makes a corrugated web more efficient or where fuel cells require fuel pressure supporting structure. Main ribs are located at the aircraft centerline, the fuselage sidewall, and the leading edge of the wing, with one intermediate rib between the sidewall rib and leading edge rib. The general structural arrangement is indicated in Figure 3. Additional auxiliary ribs are required at control surface actuator support points and at engine nacelle

support locations. The leading edge of the wing is constructed in sections and attached to the inboard leading structure with slip joints to reduce thermal stresses in this area of highest temperatures.

The assumed fuselage structure for the Mach 3-4 vehicle is of semi-monocoque skin-stringer construction. The fuselage is continuously attached under the wing, with the side wall in line with the root rib. The centerline rib and the ribs at the fuselage side wall provide the primary vertical bending stiffness for the vehicle. The fuselage and wing inboard of the rib at the fuselage side wall have been assumed to be pressurized.

The assumed structural airframe material in this study was duplex annealed 8Al-1Mo-1V titanium alloy. It is recognized that this alloy exhibits some susceptibility to stress corrosion; however, the conclusions drawn for this alloy are generally applicable to any other current high strength titanium alloy.

1.2 Mission Profile - The basic mission characteristics of a supersonic transport type vehicle are presented in Table I. The mission profile for the Mach 3-4 vehicle is shown in Figure 5 and is patterned after results of a study of the SST mission and expected usage (Reference 3). The anticipated gust and maneuver load factor spectra are shown in Tables II, III, and IV and are based on data of Reference 3. To allow for a more quantitative evaluation of problems associated with the ultimate strength testing, panel point loads were determined for the vehicle; these loads are presented in Figure 6. Similar loads have been determined for the fatigue testing of this vehicle. Panel point load values include both airloads and inertia loads and are based on a vehicle gross weight of 340,000 pounds.

1.3 Structural Cross Section - To focus the analysis effort, it was decided that some particular "typical" area would be selected for numerical analysis; the area selected is a representative wing cross section of the

TABLE I

SUPERSONIC AIRCRAFT MISSION CHARACTERISTICS

Phase of Mission	Expected Loads	Expected Temperature and Thermal Stresses
Taxi, take-off and climb at subsonic speeds.	Taxi loads, first half of ground-air-ground cycle, gust and maneuver loads. First half of fuselage pressurization cycle.	Skin temperature from 100°F to zero. Negligible thermal stresses.
Climb at supersonic speeds.	Gust and maneuver loads.	Skin temperature increases with Mach number and altitude. Thermal stresses increase.
Cruise at supersonic speeds.	Gust and maneuver loads.	Skin temperatures determined by Mach number and altitude. Temperature of internal structure increases. Thermal stresses diminish.
Descent at supersonic speeds.	Gust and maneuver loads.	Skin temperature decreases with Mach number and altitude. Temperature decrease of internal structure lags. Thermal stresses increase, are opposite in sign from climb.
Descent at subsonic speeds, landing and taxi.	Gust and maneuver loads, second half of fuselage pressurization and ground-air-ground cycles, landing and taxi loads.	Temperature of outer skin decreases and internal structure cools. Thermal stresses diminish.

TABLE II

GUST LOAD SPECTRUM
MACH 3-4 VEHICLE

Flight Phase	Climb	Climb	Climb	Climb	Cruise	Descent	Descent	Descent	Descent
Altitude (1000 ft.)	≤ 40	40–50	50–60	60–70	70–80	80–70	70–60	60–50	≤ 50
Mission time (hr)	≤ 0.22	0.22–0.27	0.27–0.33	0.33–0.46	0.46–1.66	1.66–1.79	1.79–1.86	1.86–1.89	≥ 1.89
$\Delta g = 0.2$	87,381	926	289	146	434	18	26	44	12,045
$\Delta g = 0.4$	2,315	16	6						96
$\Delta g = 0.6$	293								4
$\Delta g = 0.8$	46								
$\Delta g = 1.0$	11								
$\Delta g = 1.1$	2								

Notes: 1. Load during cycle is $1g \pm \Delta g$.
2. Spectrum is for 20,000 flights in 40,000 hours.
3. Data from Reference 3.

TABLE III
MANEUVER LOAD SPECTRUM
MACH 3-4 VEHICLE

Flight Phase	Climb	Climb	Climb	Climb	Cruise	Descent	Descent	Descent	Descent
Altitude (1000 ft.)	≤42	42–48	48–61	61–70	70–80	80–76	76–65	65–42	≤42
Mission time (hr.)	≤0.23	0.23–0.26	0.26–0.34	0.34–0.46	0.46–1.66	1.66–1.73	1.73–1.84	1.84–1.91	≥1.91
Δg = 0.2	95,000	307,700	575,800	893,600	2,087,000	1,082,000	590,000	265,700	669,000
Δg = 0.4	4,220	2,215	4,040	6,170	12,440	17,320	9,620	4,140	10,590
Δg = 0.6	173	82	156	111	534	642	359	151	388
Δg = 0.8	7	3	6	9	25	36	20	9	21
Δg = 1.0					1	2	1		1

Notes: 1. Load during cycle is $1g \pm \Delta g$.
2. Spectrum is for 20,000 flights in 40,000 hours.
3. Data from Reference 3.

TABLE IV
GUST PLUS MANEUVER LOAD SPECTRUM
MACH 3-4 VEHICLE

Flight Phase	Climb	Climb	Climb	Climb	Cruise	Descent	Descent	Descent	Descent
Altitude (1000 ft.)	≤42	42–48	48–61	61–70	70–80	80–76	76–65	65–42	≤42
Mission time (hr.)	≤0.23	0.23–0.26	0.26–0.34	0.34–0.46	0.46–1.66	1.66–1.73	1.73–1.84	1.84–1.91	≥1.91
Δg = 0.2	782,381	308,626	576,089	893,746	2,087,434	1,082,018	590,026	265,744	681,045
Δg = 0.4	6,535	2,231	4,046	6,170	12,440	17,320	9,620	4,140	11,686
Δg = 0.6	466	82	156	111	534	642	359	151	392
Δg = 0.8	53	3	6	9	25	36	20	9	21
Δg = 1.0	11				1	2	1		1
Δg = 1.1	2								

Notes: 1. Load during cycle is $1g \pm \Delta g$.
2. The maneuver load spectrum is far more severe than the gust load spectrum, consequently, in combining the two spectra, the maneuver load altitude profile was used.

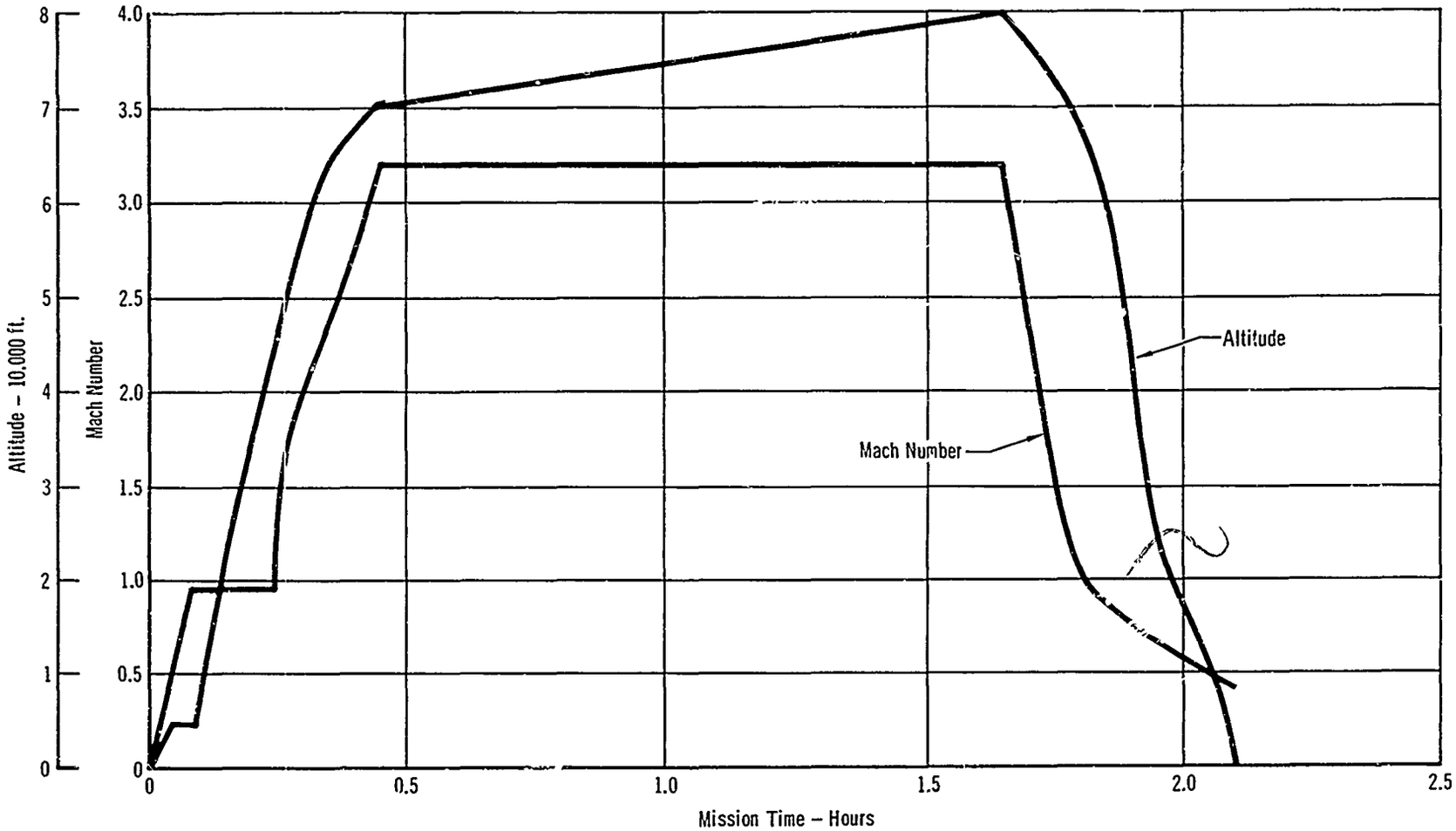

Figure 5 - Mission Profile
Mach 3-4 Vehicle

Panel Point	Ultimate Design Load	Panel Point	Ultimate Design Load
1	−13590	21	−10650
2	−25220	22	+15010
3	−46540	23	+28220
4	−45810	24	+20560
5	−26970	25	+ 9780
6	− 8460	26	+ 560
7	− 6030	27	− 9930
8	+17680	28	+11670
9	− 7450	29	+29760
10	−27980	30	+24210
11	−23140	31	+ 9600
12	− 5560	32	− 5300
13	− 2120	33	−11810
14	−12110	34	+30950
15	+14750	35	+15890
16	+24070	36	− 3040
17	− 3450	37	+11590
18	−10920	38	+10650
19	− 6250	39	+17410
20	− 890		

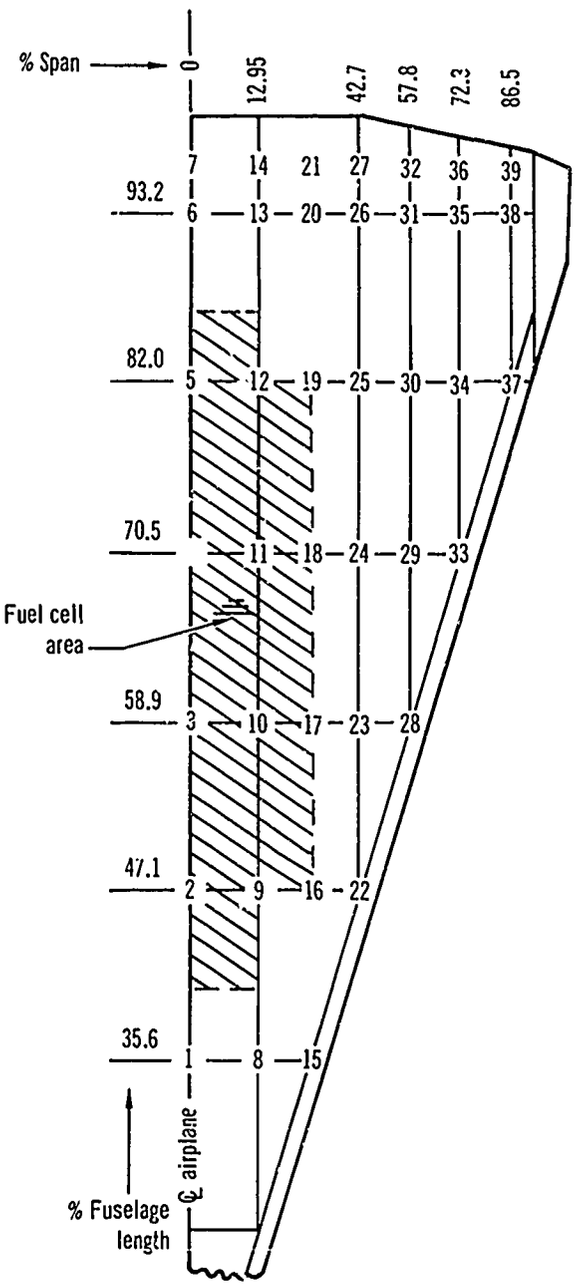

Notes: 1. Design condition is symmetrical pull-up, $n_x = 0$, $n_y = 0$, $n_z = 2.00 \times 1.5 = 3.00$ ultimate
2. All panel loads are net ultimate (airload + inertial), values in pounds.
3. Airplane gross weight is 340,000 pounds.

Figure 6 - Wing Planform Panel Loads Mach 3-4 Vehicle

structure previously described. Two types of wing structures were investigated: a corrugated sandwich configuration (shown in Figure 7) and a skin-stringer configuration. They are shown with their mathematical models in Figures 8 and 9. Primary emphasis was placed on the corrugated sandwich configuration since it was felt that it is more critical with regard to the temperature gradients and thermal stresses than the other possible configurations. As described in the sections which follow, limited investigations using the skin-stringer configuration yielded similar results as the corrugated sandwich; hence, conclusions drawn for the latter configuration are assumed applicable to both structures. A reference temperature spectrum, in the form of surface temperatures as a function of time, is shown in Figure 10. The straight line variation of temperature with time was chosen for simplicity; the difference between these data and true temperature histories is considered unimportant. These surface temperatures were used as "input" data for all computer runs described subsequently; that is, all internal temperatures, external heating rates, and thermal stresses regardless of scaling factor, size, etc., are completely consistent and are based on these surface temperatures. Maximum temperatures and heating rates on other portions of the structure are shown in Figure 11.

2. Mach 12-15 Vehicle

2.1 Structural Configuration - This vehicle is intended to represent an advanced, hypersonic, manned vehicle. The configuration and details of this vehicle are defined in less depth than those of the Mach 3-4 vehicle. The selected planform is presented in Figure 4. The vehicle gains much of its lift from its body, therefore the distributed airloads tend to be balanced by the inertia loads. The centerbody is of monocoque construction, and the skin is double-face corrugation formed of Rene' 41 material. Circumferential rings are

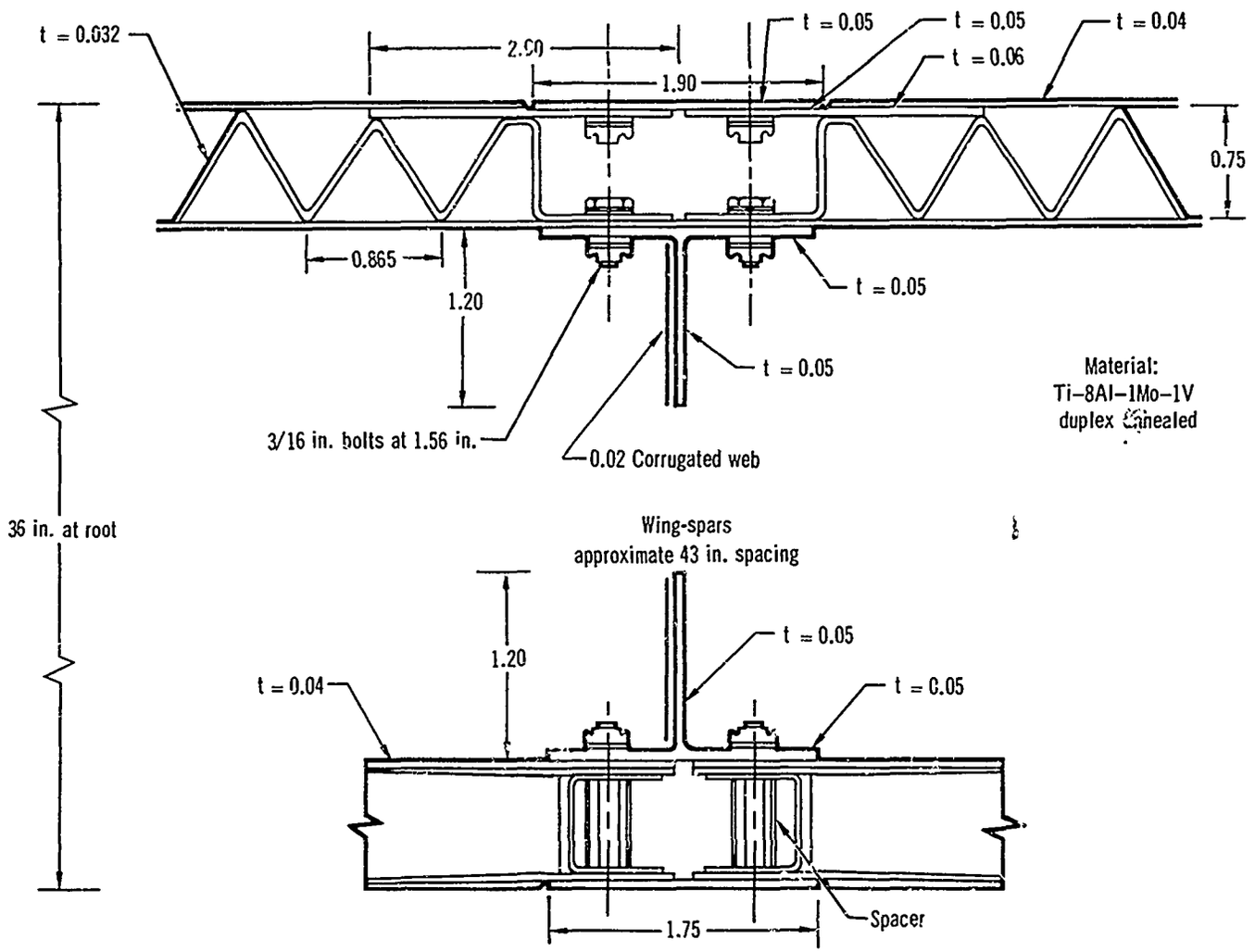

Figure 7 - Wing Structure Cross Section
Mach 3-4 Vehicle

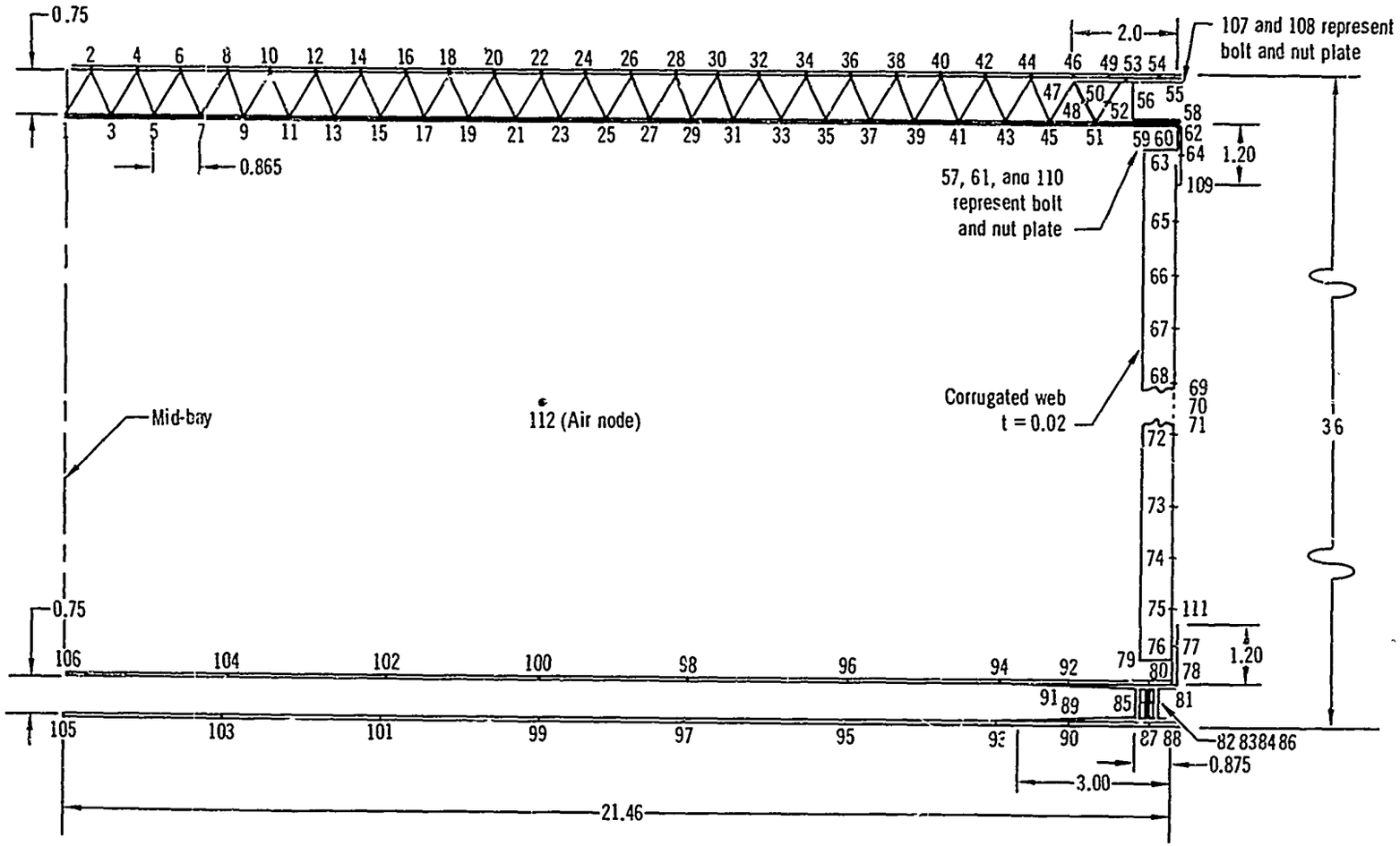

Figure 8 - Wing Cross Section Nodal Numbering System
Corrugated Sandwich Lower Surface Configuration
Mach 3-4 Vehicle

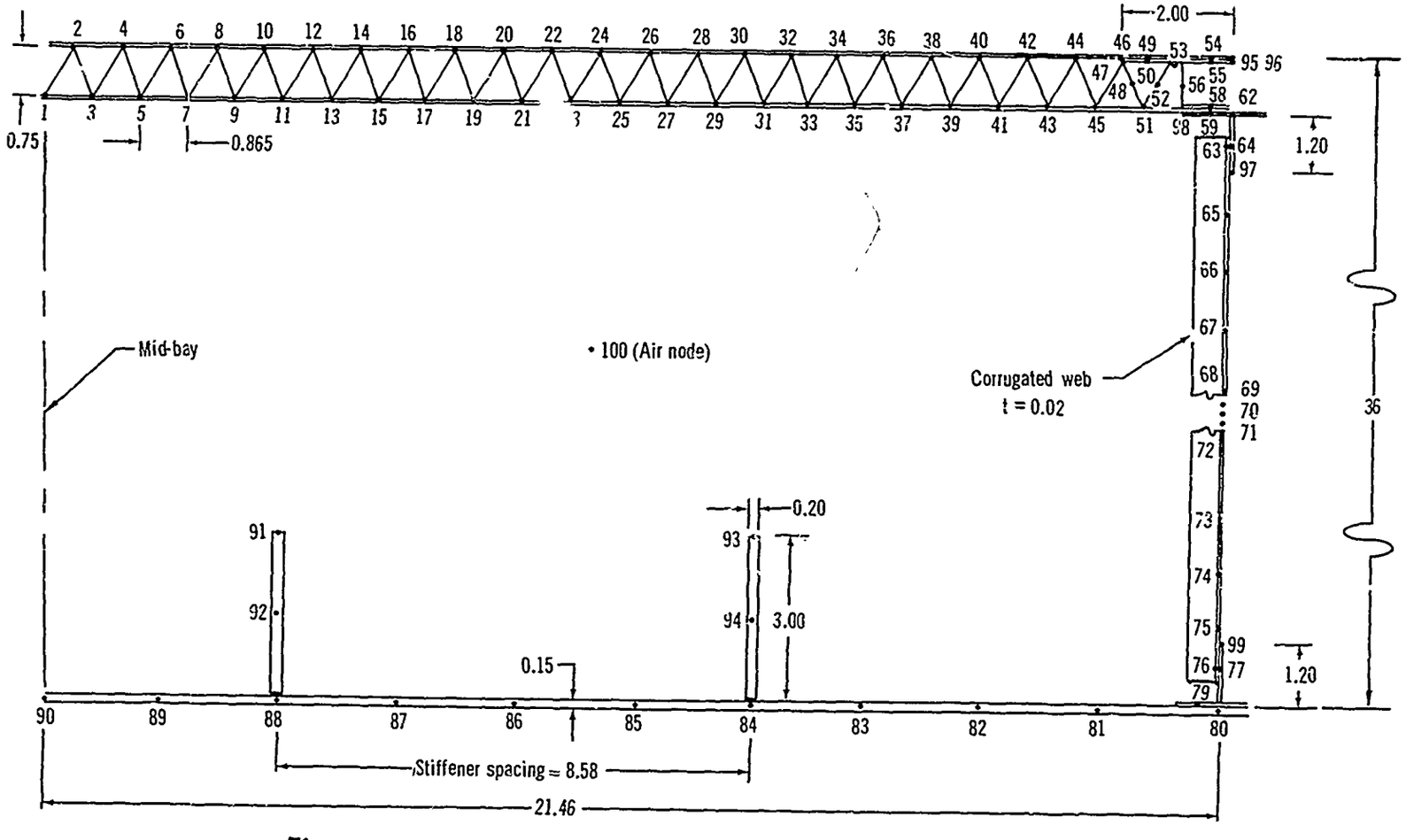

Figure 9 - Wing Cross Section Nodal Numbering System
Skin-Stringer Lower Surface Configuration
Mach 3-4 Vehicle

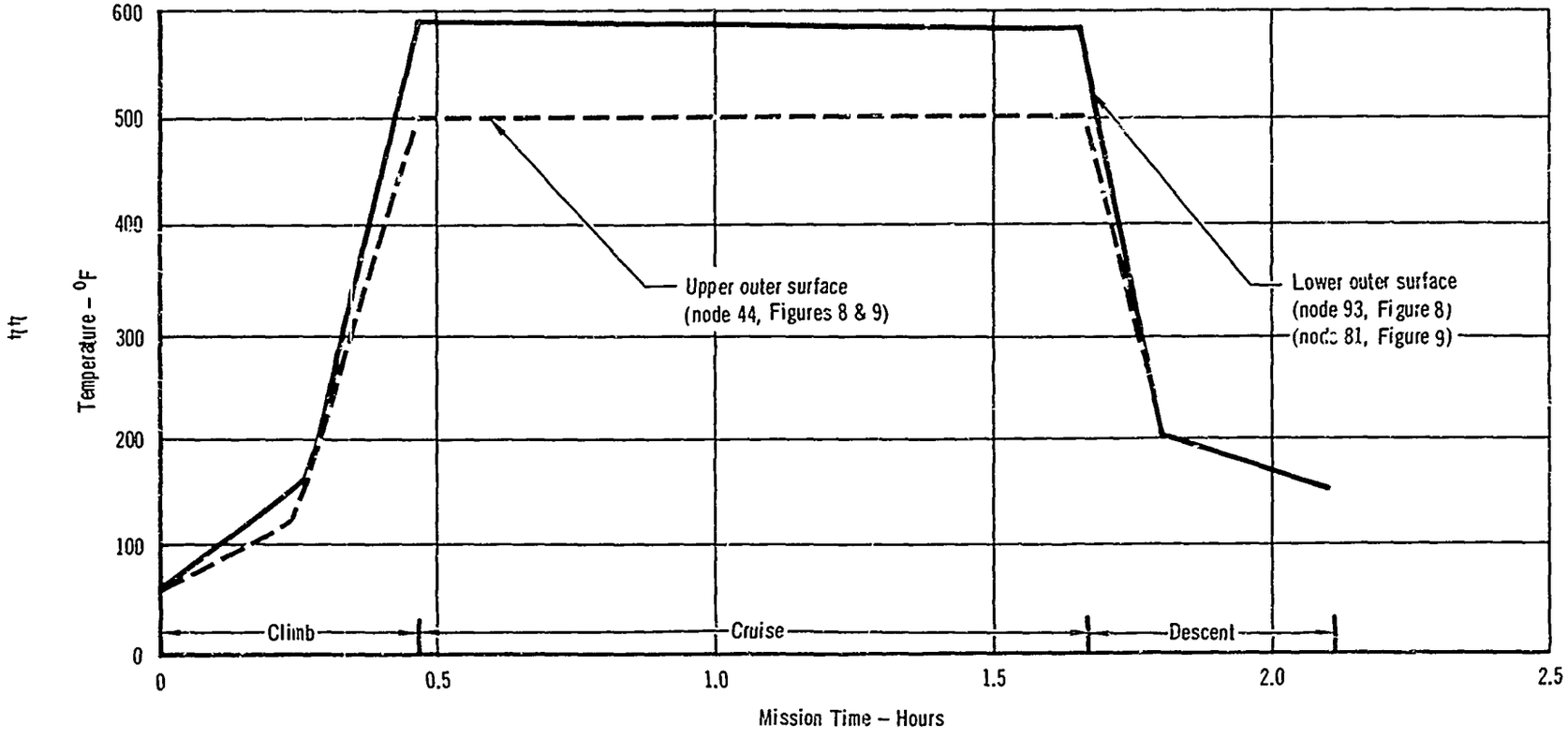

Figure 10 - Mission Temperature Profile
Mach 3-4 Vehicle

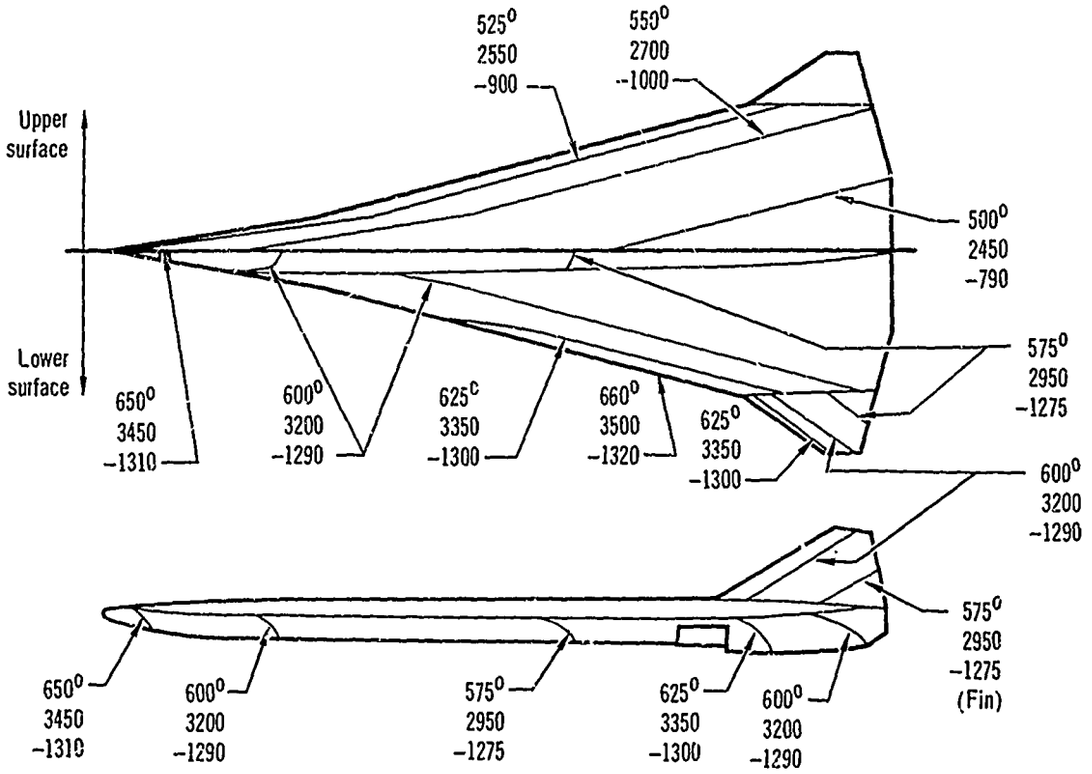

Figure 11 - Equilibrium Temperatures and Peak Aerodynamic Heating and Cooling Rates Mach 3-4 Vehicle

provided to stabilize the shell and distribute lateral airloads and concentrated equipment loads to the shell. The small control surfaces could be similar in construction to those of the Mach 3-4 vehicle, although greater use of the "shingle" concept is expected; i.e., the surface skin panels could be made free-floating for thermal expansion reasons by means of oversize holes upon spar and ribs which are the load-carrying structure. If the wings were formed in this manner, the expected thermal stresses would be lowered, but at a certain weight cost, since the free floating skin panels cannot carry any of the spanwise wing bending loads resulting in increased weight in the spar caps.

2.2 Mission Profile - The mission characteristics of the Mach 12-15 vehicle are quite similar to those presented in Table I for the Mach 3-4 vehicle; the values of stresses and temperatures are, of course, significantly different from those of the Mach 3-4 vehicle. The mission profile in terms of speed-altitude variations is shown in Figure 12.

2.3 Structural Cross Section - A lesser effort was directed to the investigation of this vehicle and only a single type of construction was considered in detail. Conclusions drawn for this construction are considered applicable to most other proposed methods of construction of this type vehicle. The portion of the vehicle selected for study is the centerbody; a cross section of this centerbody is shown in Figure 13 along with the side wall description. Figure 14 presents the mathematical model of this cross section. The alloy selected for evaluation was René 41 nickel base alloy. The mission temperature profile used in the analysis is shown in Figure 15.

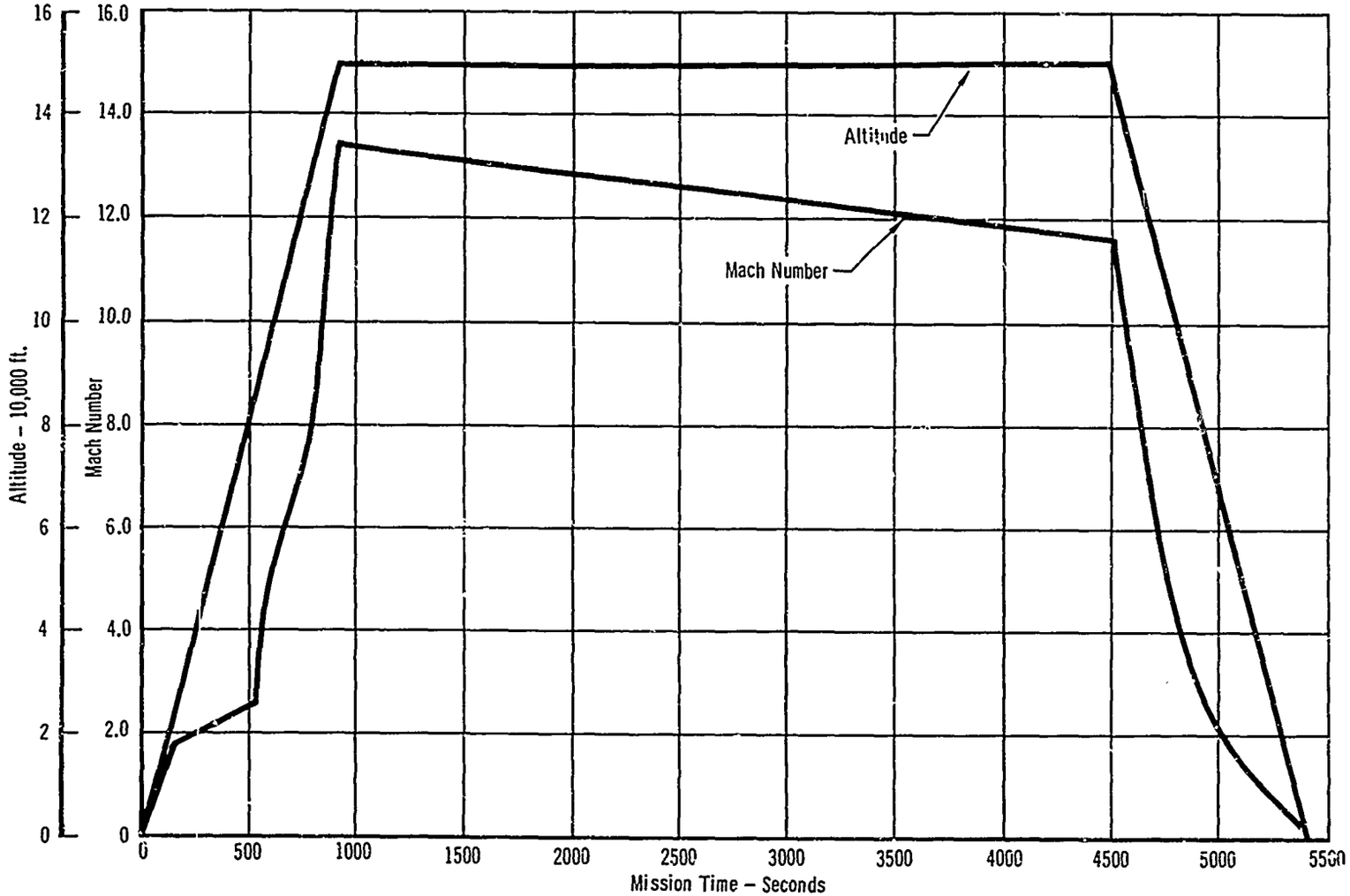

Figure 12 - Mission Profile
Mach 12-15 Vehicle

Payload:

Density = 0.015 lb./in.^{3}
Specific heat, c_p = 0.24 BTU/lb-^{0}F
Thermal conductivity,
k = 2 BTU/hr.-ft.$^{2-0}$F/ft.

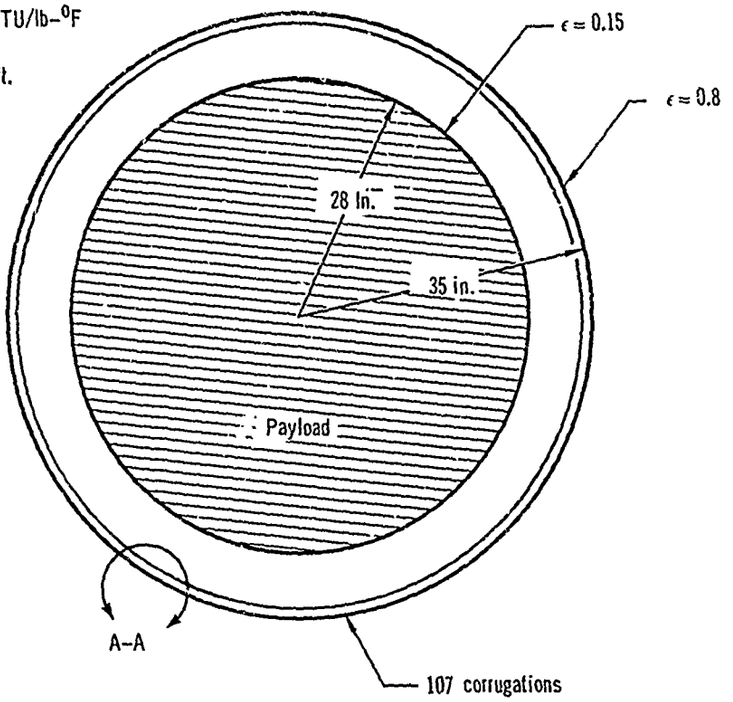

Structure:

Rene'41
Density = 0.300 lb./in.^{3}
Specific heat, c_p = 0.108 BTU/lb.-^{0}F
Thermal conductivity (k),
BTU/hr.-ft.$^{2-0}$F/ft.

Temperature (^{0}F)	k
400	6.2
1200	9.8
1600	14.6

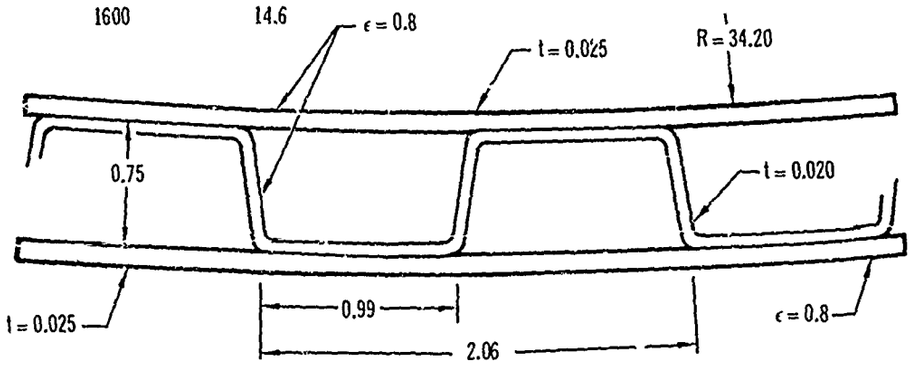

View A–A

Figure 13 - Centerbody Structure Cross Section Mach 12-15 Vehicle

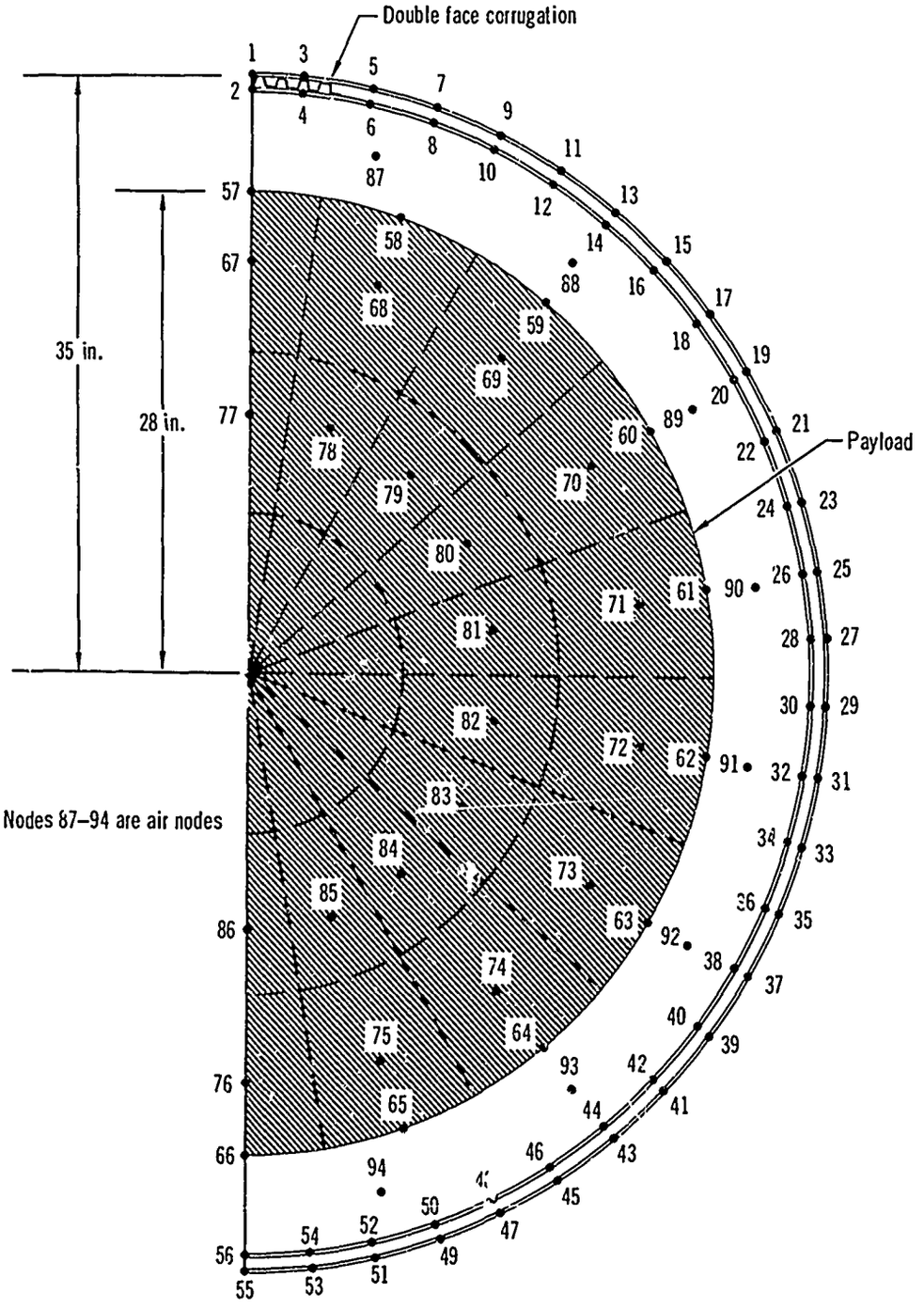

Figure 14 - Centerbody Cross Section Nodal Numbering System Mach 12-15 Vehicle

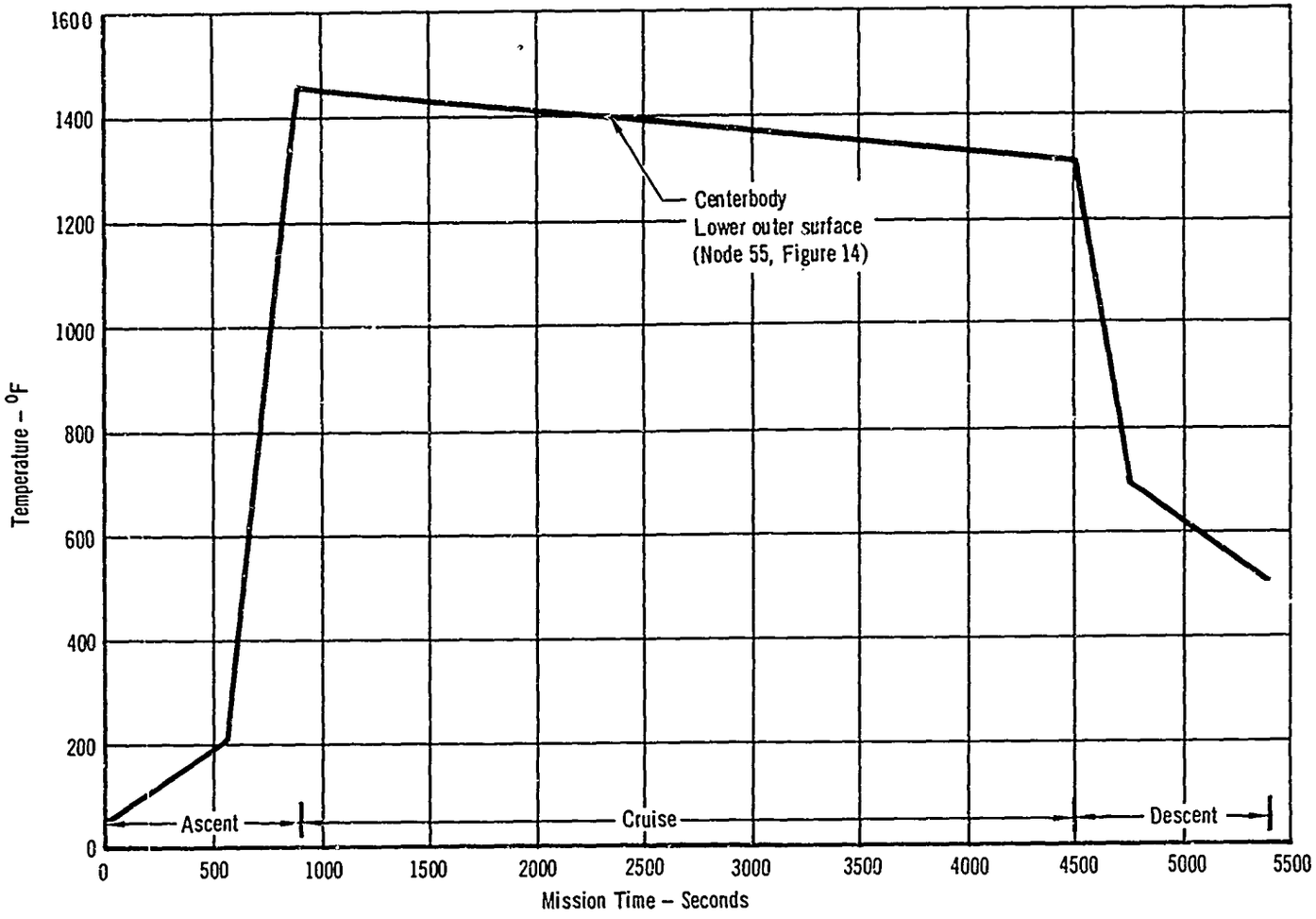

Figure 15 - Mission Temperature Profile
Mach 12-15 Vehicle

SECTION VI

ULTIMATE STRENGTH VERIFICATION TESTING

BASIC APPROACHES

In this section, four basic approaches to ultimate strength testing of the Mach 3-4 and 12-15 vehicles are considered. These basic approaches are: complete vehicle testing, model testing, component testing, and mechanical simulation of thermal effects. The two vehicles are treated separately. For each basic approach, engineering, test facility, and cost analyses have been performed under the assumptions discussed in Section IV.

The engineering analysis consists of thermodynamic and strength analyses. The purpose of the former was to determine the importance of various phenomena such as internal radiation, interface conductance, and control temperature error. The extent to which these phenomena were affected by the basic approaches, and the effects of changes in the phenomena on significant parameters such as thermal stress or material degradation were evaluated in a quantitative manner. The basic purpose of the strength analysis was to evaluate for each approach:

(a) The capability to produce prototype transient thermal stresses.

(b) The capability to produce and demonstrate an ultimate strength equivalent to that of the prototype vehicle.

The objective of the test facility analysis was to define the test equipment required in the use of each of the basic approaches and to identify the test problems likely to be encountered. The results of the test facility analysis were used in the determination of the man-hour and dollar costs of the basic approaches.

A cost analysis has been performed for each approach with the primary objective being the determination of relative costs. The major areas

considered were: (1) engineering design costs of the test specimen, (2) manufacturing costs of the test specimen, including tooling, and (3) testing costs, including jig design and fabrication, test equipment and material costs, and test performance.

The conclusions drawn from the three analyses for each basic approach allow the development of combination approaches of comparable technical merit and the determination of the associated costs. The need for such combination approaches resulted from the fact that most basic approaches were judged to be unsatisfactory for the purposes of structural verification. These combination approaches are discussed in Section VIII.

For ultimate strength verification of the Mach 3-4 vehicle, the complete vehicle basic approach is discussed in Subsection 1.2; the model basic approach in Subsection 1.3; the component basic approach in Subsection 1.4; and the mechanical simulation basic approach in Subsection 1.5. The corresponding subsections for the Mach 12-15 vehicle are 2.2, 2.3, 2.4, and 2.5, respectively.

1. Mach 3-4 Vehicle

1.1 Parameters - Many of the parameters discussed in Section IV are relatively unimportant in ultimate strength testing. Consideration of the load spectrum, load randomization, and ground-air-ground cycle is not applicable to the analysis of ultimate strength except for the case of residual strength of fatigue damaged structure, which was not considered in this study. Creep and strain rate (load rate) may have an effect, but such effects have been found to be relatively unimportant for the vehicles considered in this study. Corrosion may significantly affect the strength of actual vehicle in service usage; traditionally, however, its effect is investigated using element tests, and is not introduced in the basic verification program. The remaining parameters that were deemed to be important in ultimate strength verification testing

include:

Material degradation caused by temperature

Metallurgical changes caused by time at temperature

Size effects (modeling effects)

Thermal stresses

Boundary conditions (component size)

Specimen-to-specimen variability

The effects of these parameters on the ultimate strength verification testing of the Mach 3-4 vehicle are discussed in the following subsections.

1.2 Complete Vehicle Testing - Complete vehicle mission temperature testing is defined as the test of a full-scale complete airframe with the temperatures expected in flight duplicated during the laboratory testing. The primary purpose of the analysis of this basic approach was to develop a basis of data to which the results of the analyses of other approaches could be compared. The analysis is divided into three subsections; this same grouping is used for all subsequent analyses: engineering analysis, test facility analysis, cost analysis, followed by conclusions.

1.2.1 Engineering Analysis - In order to compute structural temperatures of the wing cross section chosen for analysis, described in Section V, a thermal idealization was developed and analyzed utilizing the McDonnell General Heat Transfer Program. The wing cross section was divided into 112 nodes (shown in Figure 8) which were thermally connected through the following modes of heating:

Internal convection

Internal radiation

Conduction through continuous material and interfaces including fastening

Radiation to external surroundings

A single node was selected to represent the air within the wing cross

section to permit calculation of its heat storage and convective heat transfer. Temperature-time profiles for locations on upper and lower wing outer surfaces were established and are compatible with flight Mach numbers and altitudes described in Section V; these profiles are shown in Figure 10. Several simplifications were made to reduce the computation effort. These are as follows:

(a) Straight-line temperature-time variations were assumed for the two control nodes; actual flight temperatures at these locations would not follow the abrupt changes in temperature slope shown in Figure 10.

(b) Infinite spanwise depth perpendicular to the plane of the cross section and similar adjacent sections in the chordwise direction were assumed. Wing temperature gradients and the rate of change of geometry in the spanwise and chordwise directions are usually small in comparison to the wing depth; therefore, this assumption was judged reasonable.

(c) Similar to (b), the heating rates were assumed to be functions of time, but constant, albeit different, for the upper and lower surfaces, with the actual values determined by the control node temperature-time profile for each surface. Node 44 was the temperature control node for the upper surface, and node 93 for the lower surface; both are shown in Figure 8. The slope discontinuities in the time-temperature histories at the intersections of the linear portions, described in (a), resulted in a spiked heating rate whose peak value is larger than the expected mission value. However, the heating and cooling rates at other times in the idealized mission closely approximate what would be expected in the true mission temperature-time profile.

(d) For the initial analyses, internal air pressure was assumed to be

equal to the flight altitude free stream value. Subsequent analyses using laboratory pressure (at 1 atmosphere) showed negligible change in structural temperature histories and thermal stresses.

(e) The emissivities of the internal surfaces of the double-face corrugated sandwich panels were assumed equal to .66 for most of the analyses. The emissivities of the surfaces outlining the wing cross section enclosure - the inner surface of the inner skin of the sandwich panel, the spar-web, and the spar-web attachment tee - were assumed equal; for most analyses a value of .66 was assumed.

The computed structural temperatures were used to determine elastic thermal stresses for the wing cross section, using the following assumptions:

(a) The free expansion thermal elongation for each of the structural elements was determined relative to their length at 70°F.

(b) The materials were assumed to remain linearly elastic.

(c) The variation of the coefficient of expansion and of the modulus of elasticity with temperature was included in the analysis.

(d) Computations were based on the assumptions of elementary beam bending theory (plane cross sections remain plane).

(e) The wing cross section was assumed to be free of axial or bending restraint.

The analytical model of the cross section is similar to that used for the thermodynamic analysis presented in Figure 8. Temperatures and thermal stresses have been computed for the two configurations of the wing cross section: one utilizing a corrugated sandwich lower surface; and the other, a skin-stringer lower surface.

Based on the assumed temperature profiles shown in Figure 10, the temperatures and thermal stresses produced during a typical Mach 3-4 flight have been

computed for all 112 nodes of the sandwich configuration. The heating rates for the wing surfaces have also been computed for the full-scale complete vehicle and are presented in Figures 16 and 17; the other data presented on these figures will be discussed in other subsections.

The effects of external surface radiation cause a significant difference between the heat inputs required for the testing of a structure in the laboratory and the actual flight heat input to the same structure. In a flight vehicle, the aerodynamic heating to the surface must exceed the surface radiant emission to the outside before the structure becomes heated. Mission heating rates determined by computer analysis in this study have included this radiation term. However, in the laboratory, heating is accomplished by using radiant lamps with a highly reflective backing; in an ideal test system, with a perfect reflector, none of the radiant energy from the surface is lost, thus the laboratory heating requirement is reduced by the radiation term ($\sigma\epsilon T^4$). The results of an analysis of this phenomenon using expected laboratory system efficiencies are presented in Figure 18. This figure indicates that although the peak mission and laboratory heating rates are not appreciably different, the laboratory total heat requirements are much lower.

Temperatures and thermal stresses for several nodal locations are presented in Figures 19 through 23. Temperatures at node 70 are presented in Figure 19. This location heats up and cools off more slowly than other nodes in the structure during a typical mission due to its greater distance from the outer surface nodes. Temperatures and stresses for two nodes of the sandwich lower surface are presented in Figures 20, 21, 22, and 23; for node 90, because it is near the spanwise joint in the area of maximum stress concentrations, and for node 111, because it is at the location of maximum tensile thermal stress. For strength analysis, thermal stresses are additive to the sum of

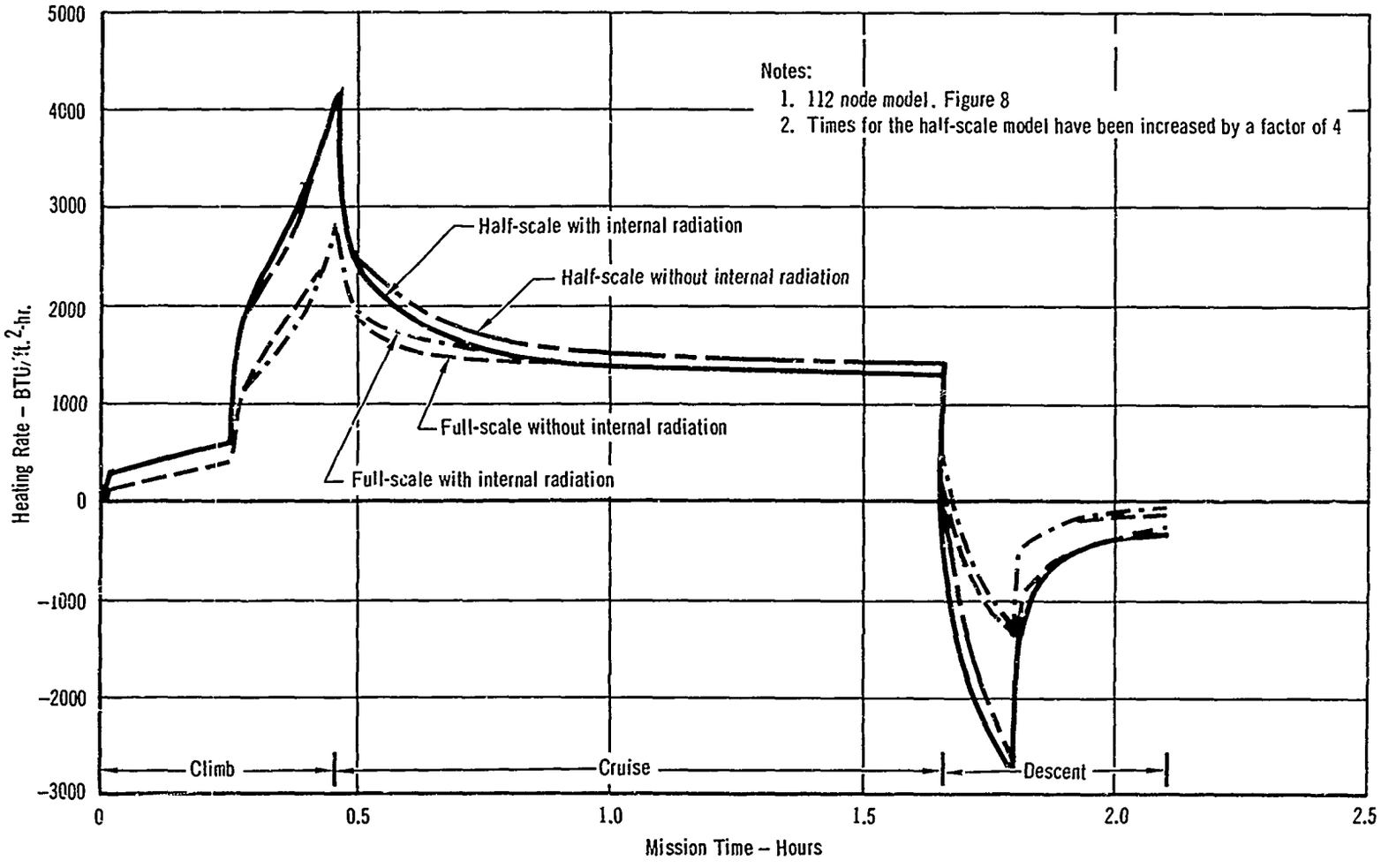

Figure 16 - Scaling and Radiation Effects on Wing Lower Surface Heating Rate Mach 3-4 Vehicle

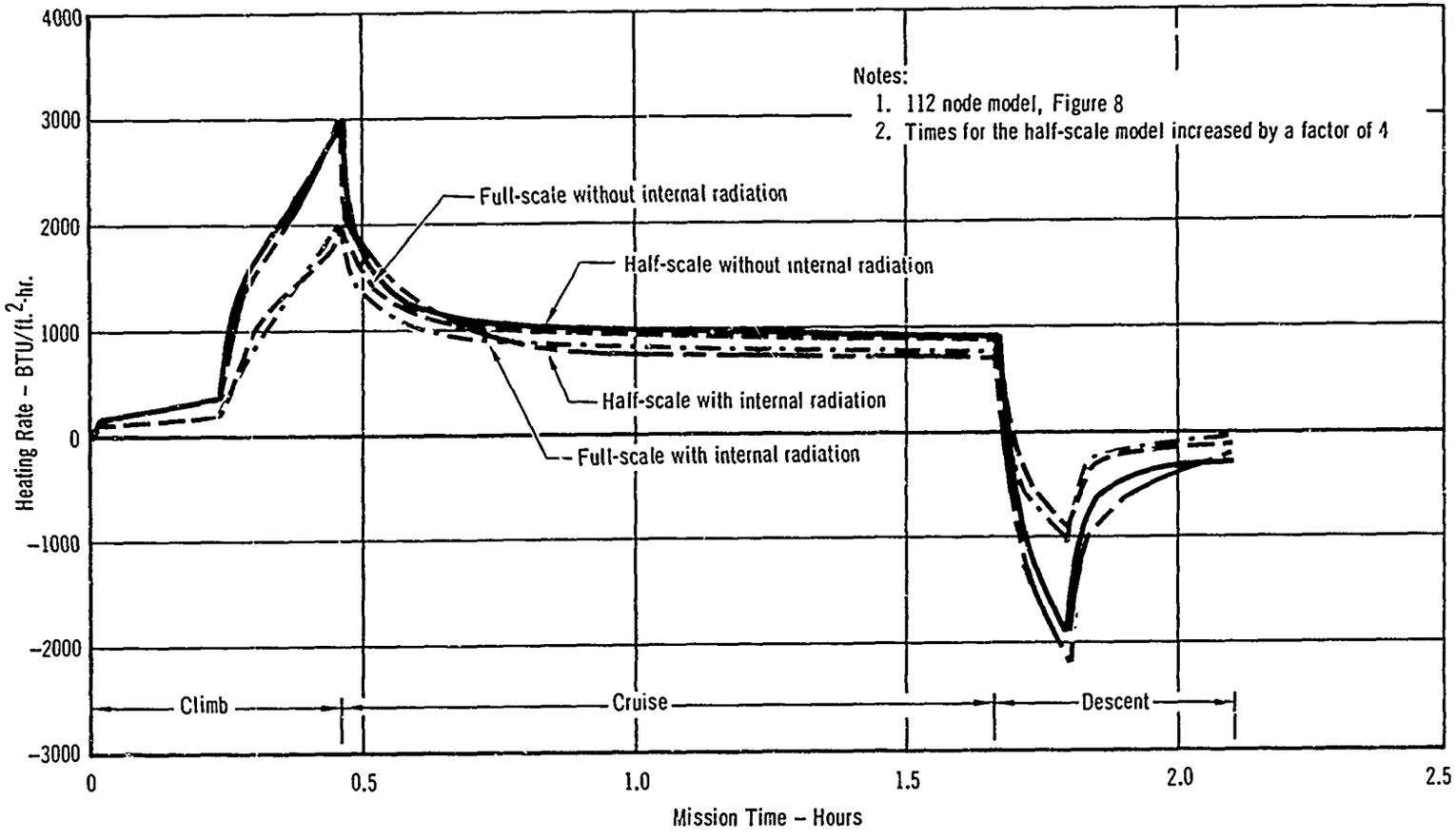

Figure 17 - Scaling and Radiation Effects on Wing Upper Surface Heating Rate Mach 3-4 Vehicle

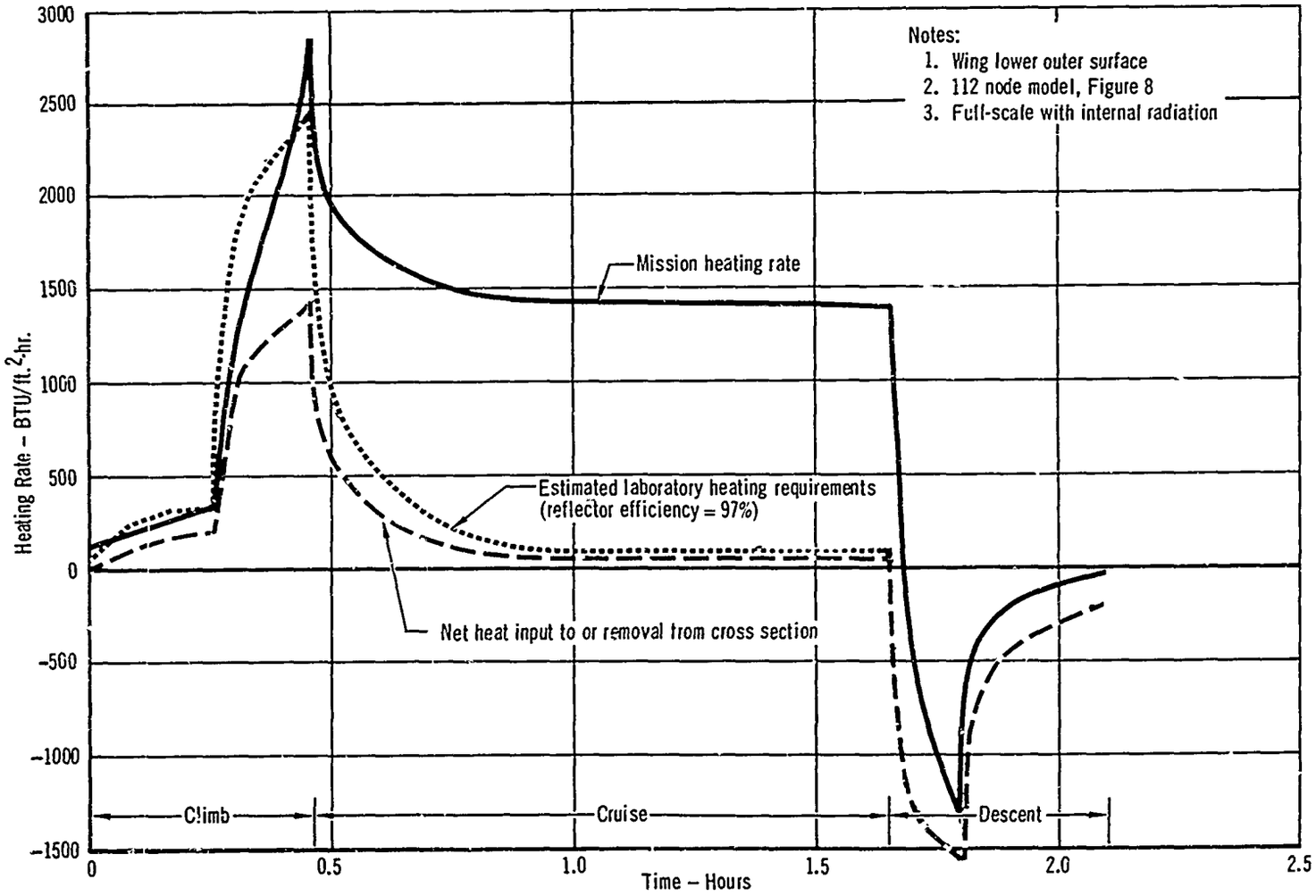

Figure 18 - Comparison of Mission and Laboratory Heating Rates Mach 3-4 Vehicle

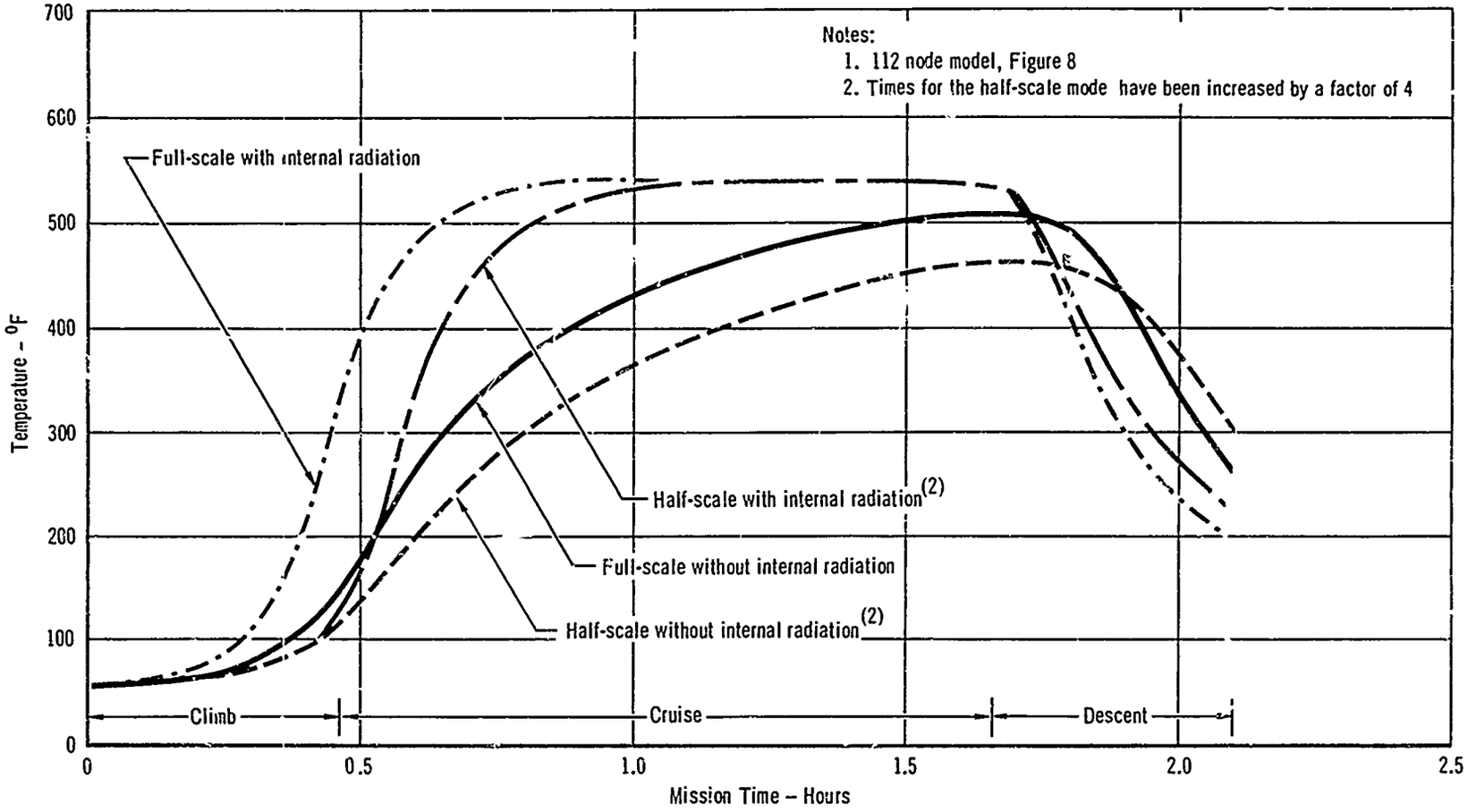

Figure 19 - Scaling and Radiation Effects on Temperature at Node 70
Mach 3-4 Vehicle

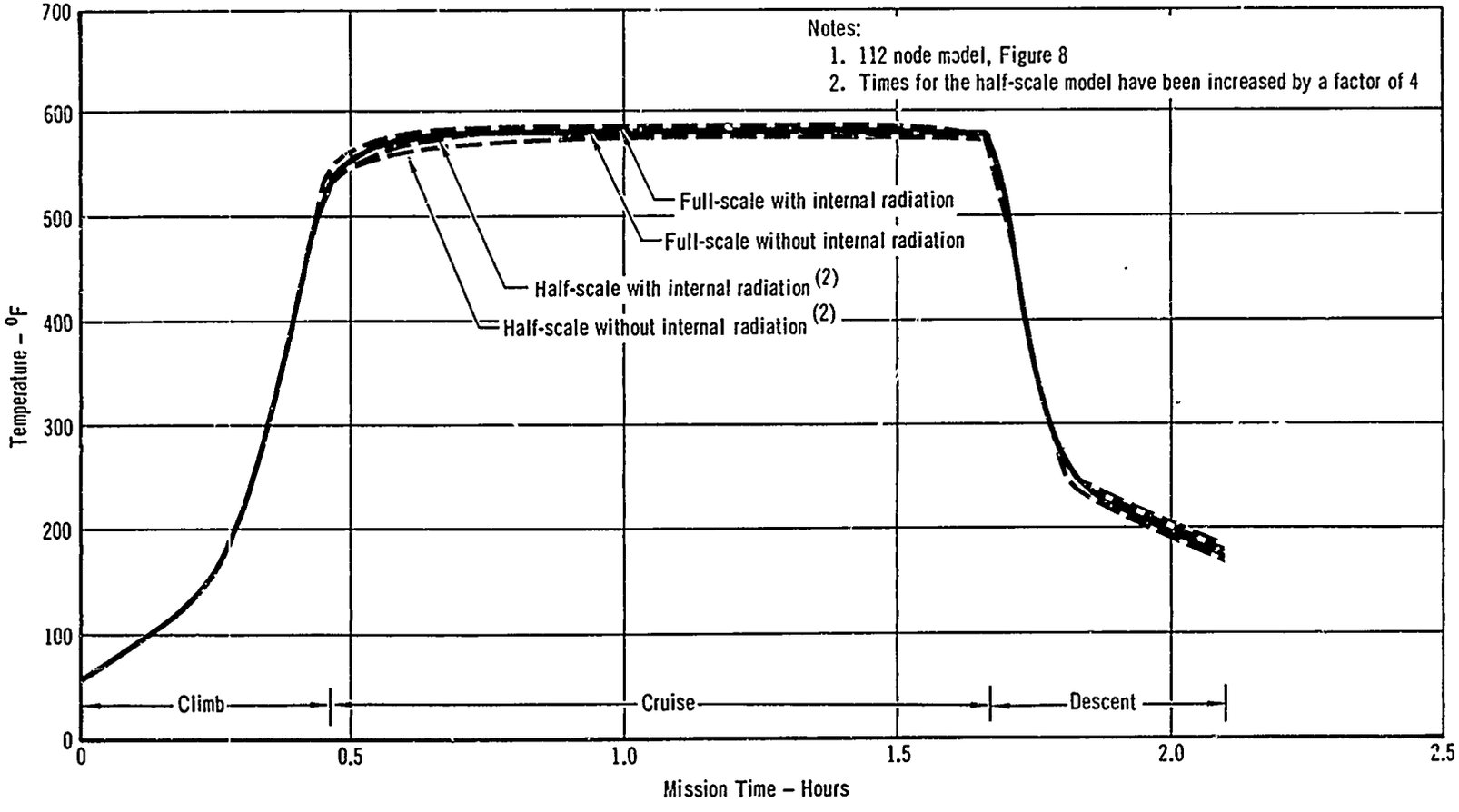

Figure 20 - Scaling and Radiation Effects on Temperature at Node 90 Mach 3-4 Vehicle

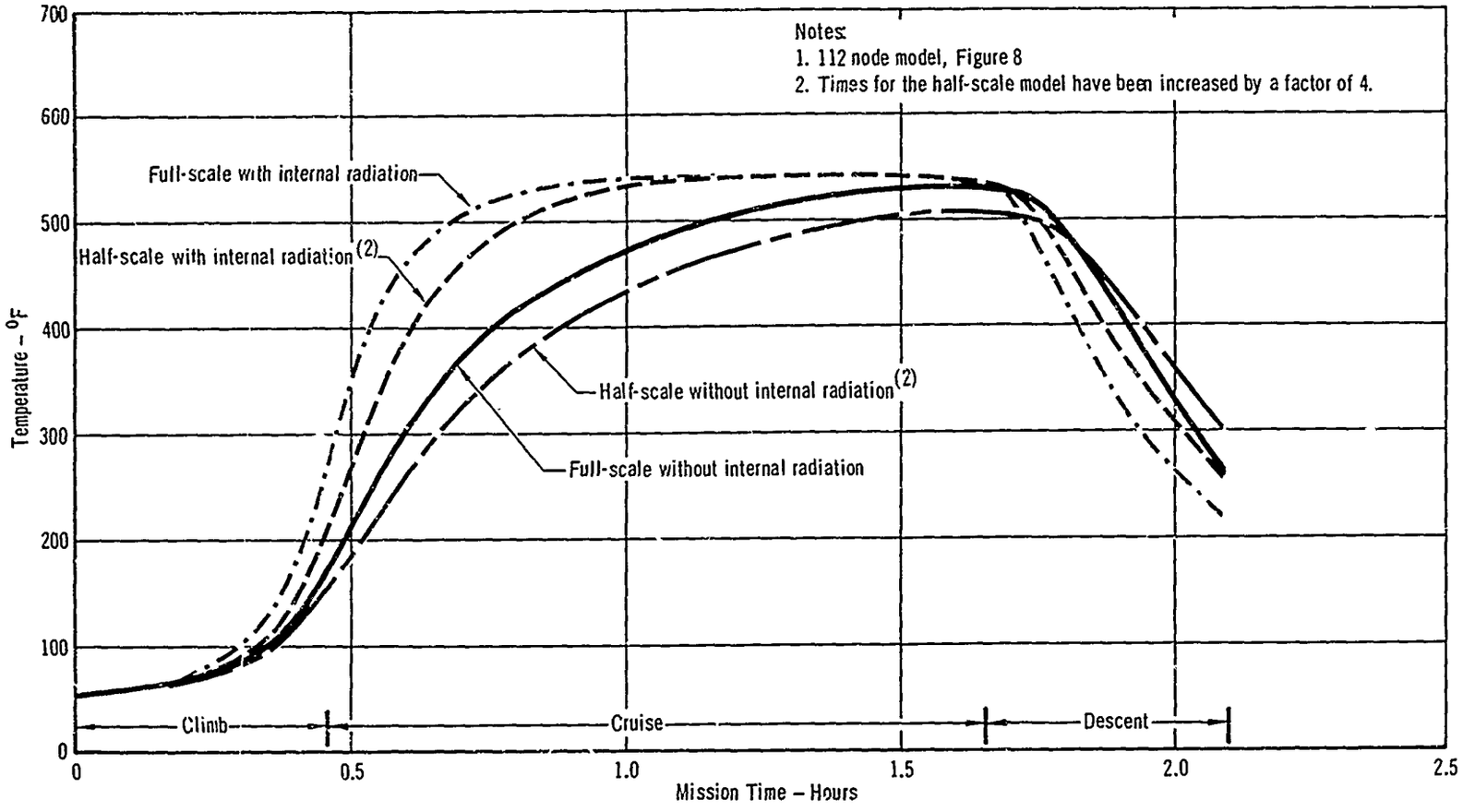

Figure 21 - Scaling and Radiation Effects on Temperature at Node 111 Mach 3-4 Vehicle

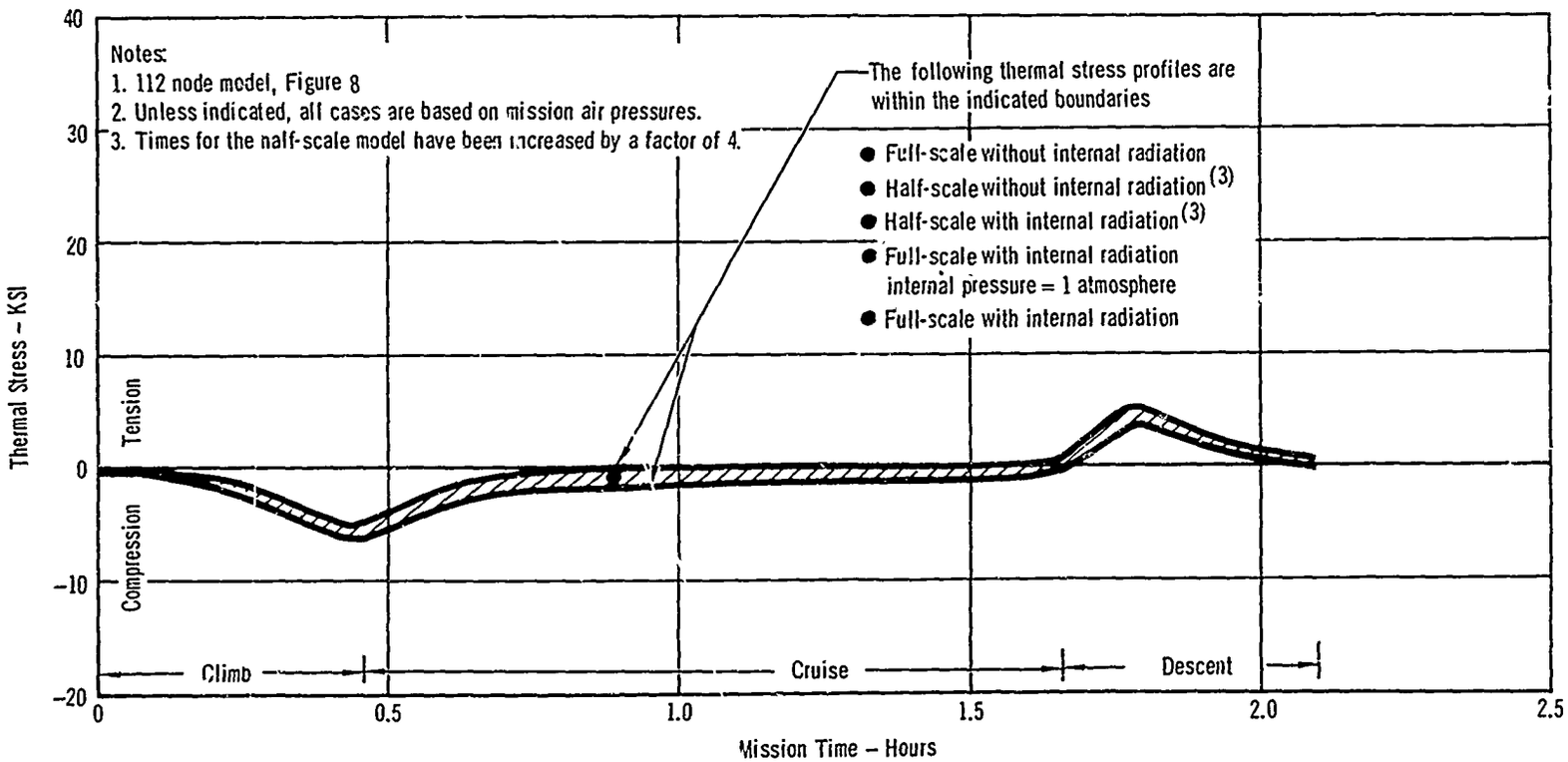

Figure 22 - Scaling and Radiation Effects on Spanwise Thermal Stress at Node 90 Mach 3-4 Vehicle

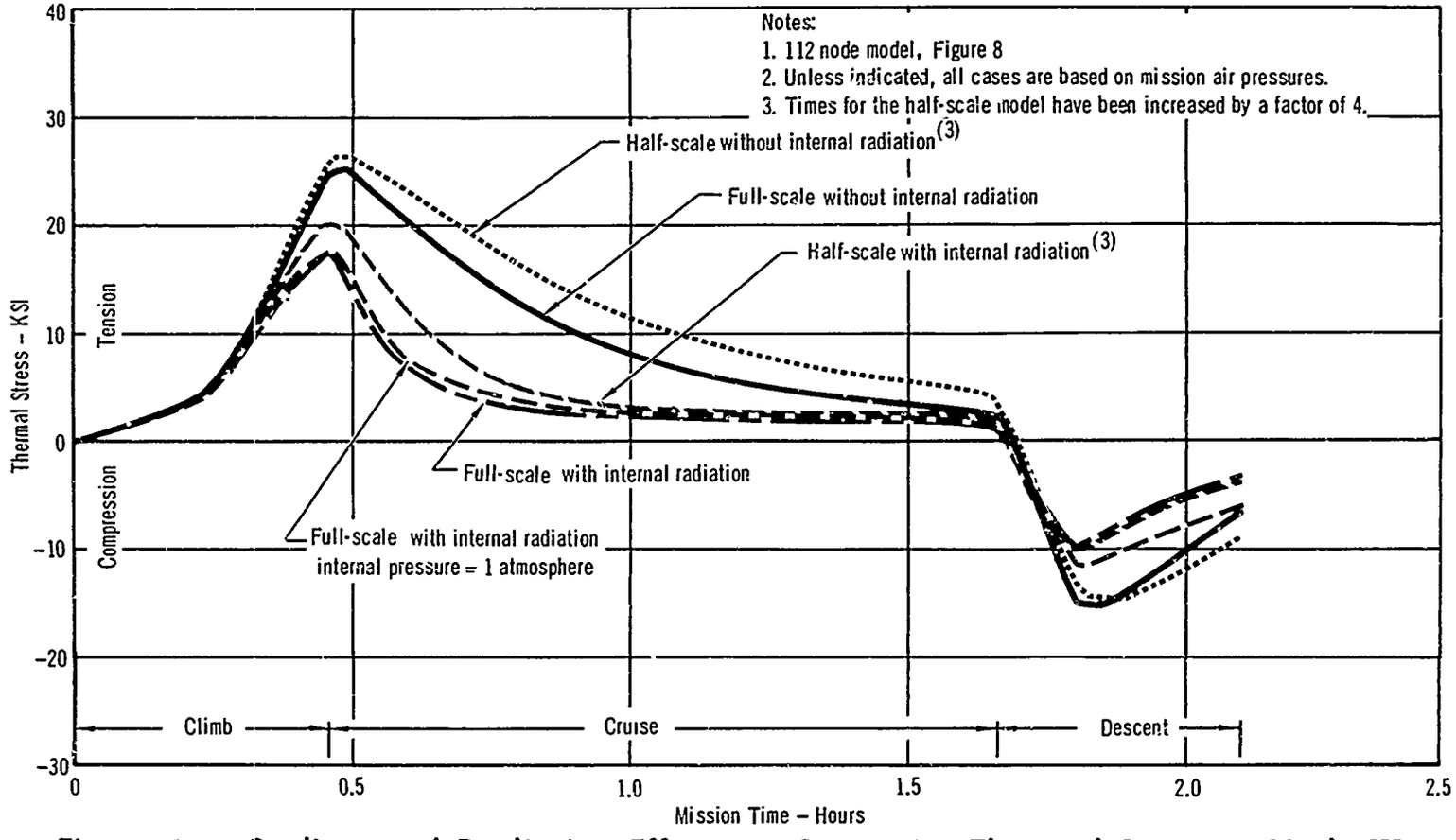

Figure 23 - Scaling and Radiation Effects on Spanwise Thermal Stress at Node 111

Mach 3-4 Vehicle

maneuver or gust alternating stresses and the mean (1g) flexural stresses. Figures 24 and 25 present the variations of spanwise thermal stresses in the chordwise direction of the full-scale wing cross section at the time of peak thermal stresses for nodes 90 and 111 (mission time = .46). The comparison of the chordwise variations shown in these two figures is typical for this type of structure; the outer face of the sandwich lower wing surface is in compression, as shown in Figure 24, and the inner surface is in tension, as shown in Figure 25. The change in stresses in the faces near the spar-web are a result of the heat sink effect of the spar, i.e., the inner face tensile stresses are increased and the outer face compressive stresses are decreased.

Using the 112 node sandwich lower surface model, numerous studies of the effect of various parameters on temperature and thermal stress were conducted; the more significant of these studies are:

Effects of internal radiation

Effects of interface conductance

Effects of internal air pressure

Effects of control temperature error

In addition, the effect of thermal environment on wing cross section ultimate strength was investigated. Each is discussed in the following paragraphs.

1.2.1.1 Effects of Internal Radiation - Structural temperatures and thermal stresses were calculated for both full-scale and half-scale wing cross section with the range of internal emissivity values $0.0 \leq \varepsilon \leq 1.0$. The use of $\varepsilon = 0.0$ approximated the situation where the inside of the enclosure is coated with a low emissivity covering, resulting in maximum thermal gradients and stresses. These maxima occurred at the transition between climb and cruise, mission time = .46 hr., as shown in Figures 22 and 23. The actual emissivity cannot be zero; therefore, the true maximum thermal gradients and stresses will

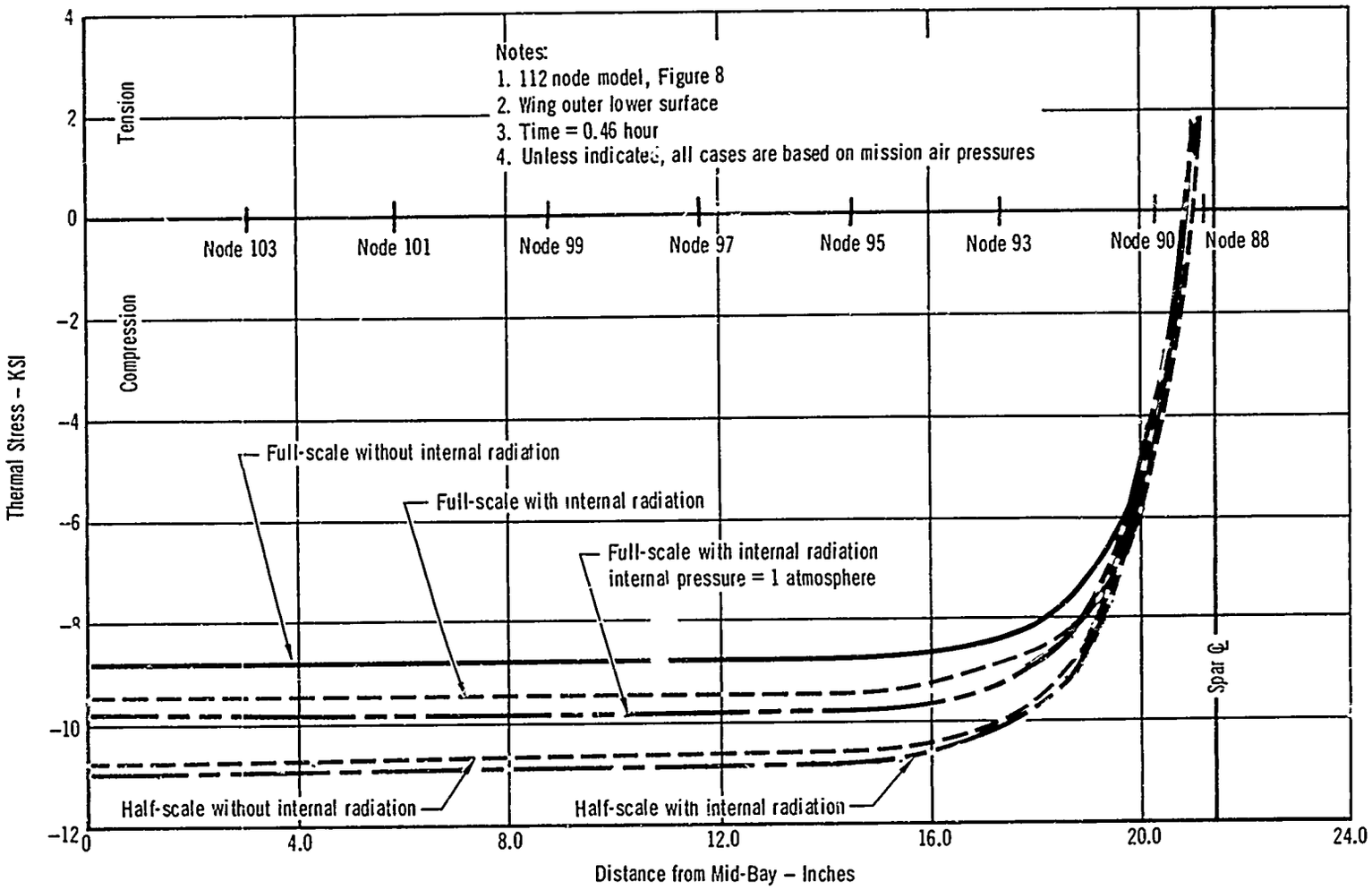

Figure 24 - Scaling and Radiation Effects on Chordwise Variation of Spanwise Thermal Stresses in Wing Outer Surface Mach 3-4 Vehicle

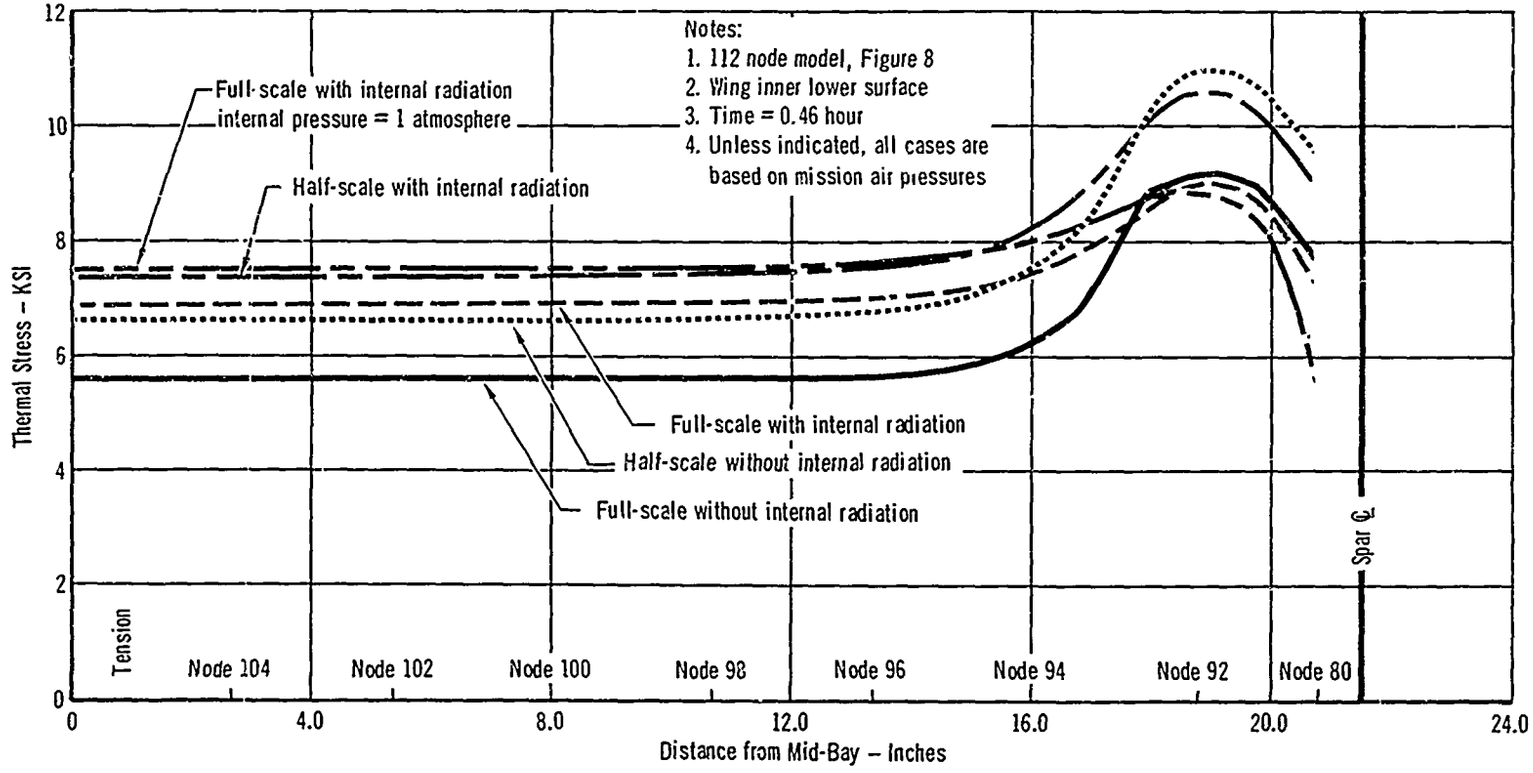

Figure 25 - Scaling and Radiation Effects on Chordwise Variation of Spanwise Thermal Stresses in Wing Inner Surface Mach 3-4 Vehicle

always be less than for this limiting case. In the analysis, the emissivities of the internal surfaces of the double-face corrugated sandwich were assumed equal to a single value. The single value of emissivity for these surfaces has been termed external emissivity. The emissivities of the surfaces outlining the wing cross section enclosure were also assumed equal to a single value; these surfaces include the inner surface of the inner skin of the sandwich panel, the spar-web, and the spar-web attachment tee. The single value of emissivity for these surfaces has been termed internal emissivity. Figure 26 indicates the effect of emissivity on the maximum thermal stress achieved at node 111. It may be noted that these digital computer analyses indicate a linear variation in thermal stress with emissivity, obtained when the external emissivity is equal to the internal emissivity, for the configuration and assumptions of this investigation.

The effects of internal radiation can also be determined in Figures 22, 23, 24, and 25; these figures present the results obtained when internal emissivity is equal to .66 and to 0.0, and when external emissivity is equal to .66.

1.2.1.2 Effects of Interface Conductance - A variable which would be largely uncontrollable in a structure is that of interface thermal conductance offered by less than perfect contact between adjacent faces. Interface conductance would be a consideration, for example, between nodes 46 and 47 or 54 and 55 of Figure 8. Interface conductance values in the range of 500 to 5000 BTU/ft^2-hr-$^\circ$F seem probable for these particular joints. In this study, the lowest of these values was selected for most of the analyses in order not to understate the importance of interface resistance in later comparisons. An analysis was made to determine the effect of this variable; increasing the value simultaneously at all joints from 100 BTU/ft^2-hr-$^\circ$F to infinity increased the temperature at node 111 less than 10°F at time of peak thermal stress.

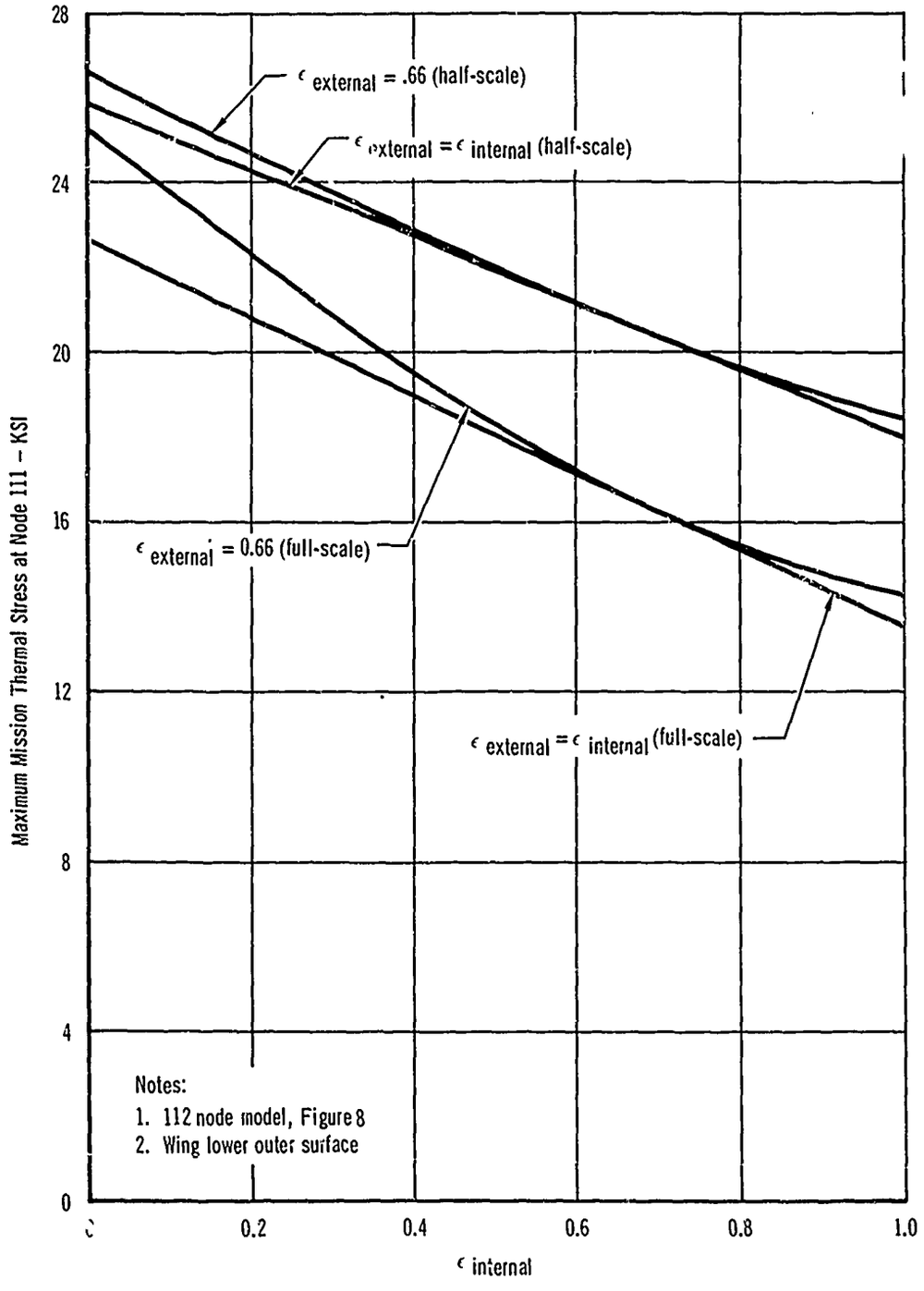

Figure 26 - Emissivity and Scaling Effects on the Maximum Thermal Stress at Node 111 Mach 3-4 Vehicle

Therefore, little variation in thermal stress would be expected as a result of variations in interface conductance; and no further evaluation of interface conductance was performed.

1.2.1.3 Effects of Internal Pressure - While simulation of internal pressure within the test specimen may be desirable in the laboratory from the standpoint of accurately duplicating mission conditions, the complexity and cost of such a test would be appreciably reduced if enclosure air at one atmosphere pressure could be utilized. Temperatures computed for the wing cross section using mission pressure agreed well with those using atmospheric air pressure; the greatest discrepancy in structural temperatures generally occurred at node 70 and was less than 15°F. Figure 27 presents the calculated wing enclosure air temperature history for both mission air pressures and atmospheric pressure in the wing. When compared with the expected flight temperatures, 500°F to 600°F, the magnitude of the temperature variations is small, indicating close simulation may be obtained by using air at one atmosphere in the internal cavity of the test specimen.

Figure 23 presents a comparison of thermal stresses determined when internal convective heat transfer is based on mission and atmospheric pressures. The thermal stresses for these two cases were found to be almost identical; therefore, the use of laboratory pressure during testing is not expected to affect the accuracy of the thermal stress simulation.

1.2.1.4 Effects of Control Temperature Error - An investigation of the effect of control temperature error on structural temperatures and stresses was performed utilizing modified control temperature histories for the climb and cruise portion of the mission; these profiles are shown in Figure 28. While the control temperature profiles are not appreciably different, the associated required heating rate histories shown in Figure 29 differ more significantly,

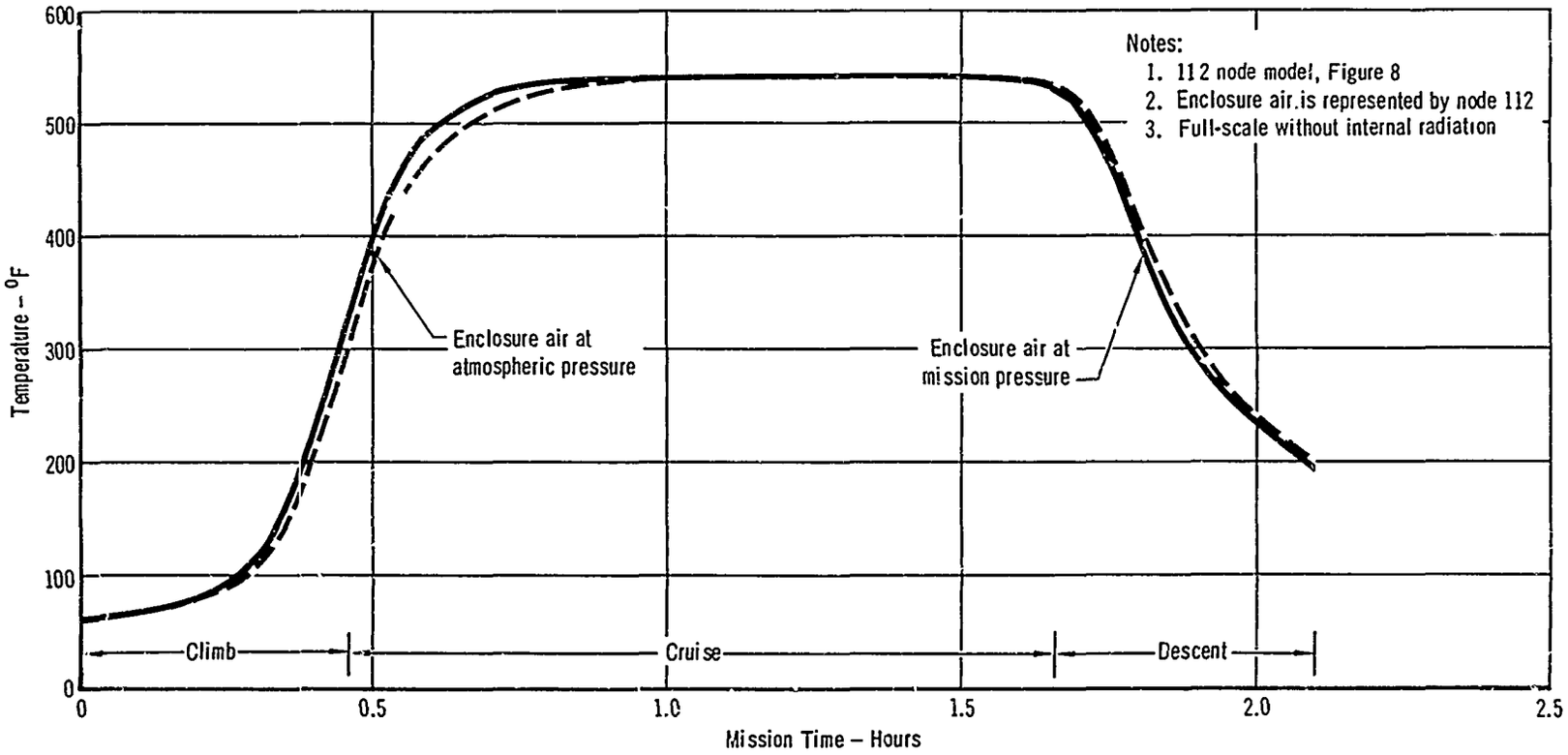

Figure 27 - Effect of Air Pressure Variation on the Temperature of the Enclosure Air Mach 3-4 Vehicle

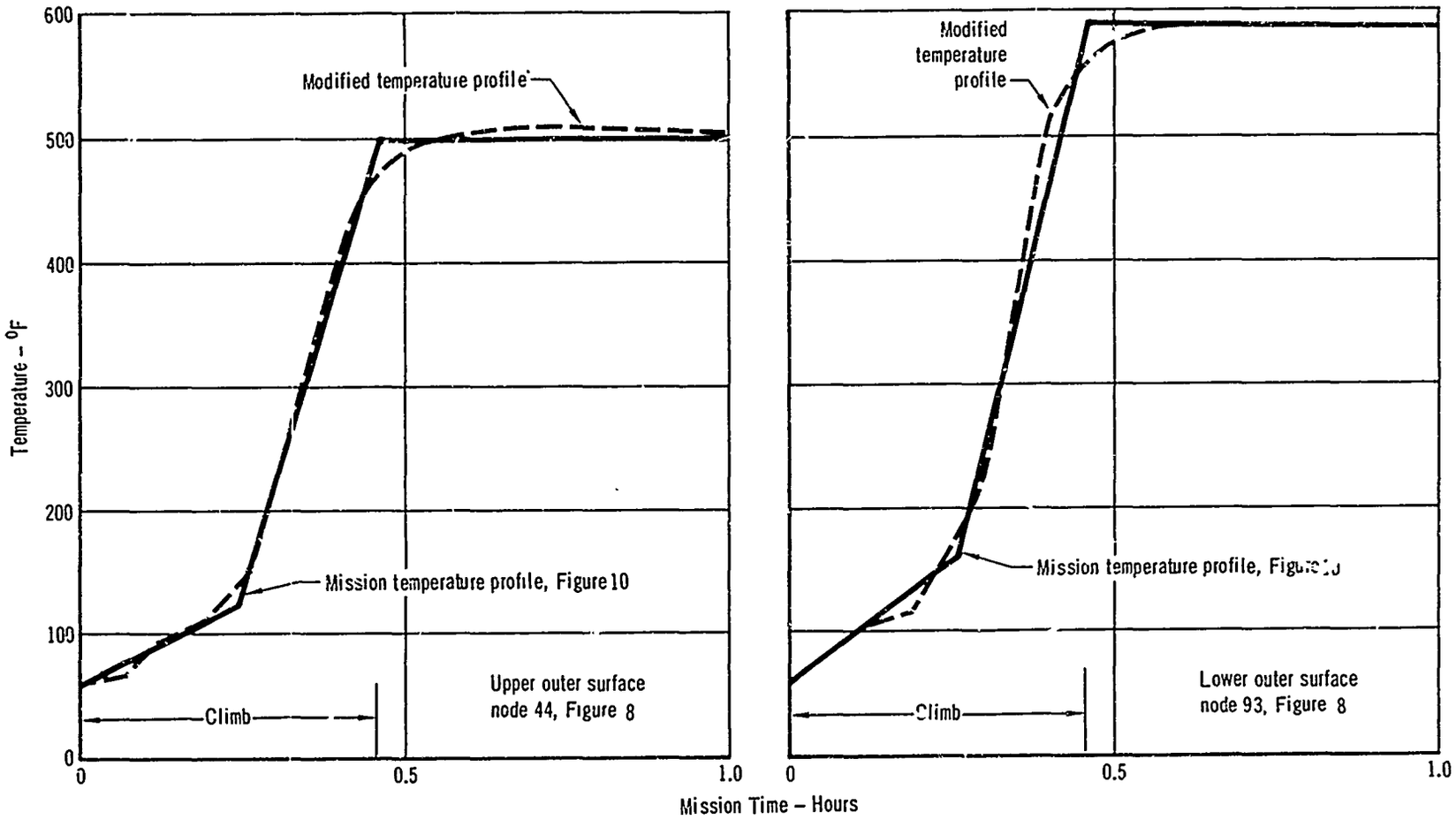

Figure 28 - Modified Control Node Temperature Profiles
Mach 3-4 Vehicle

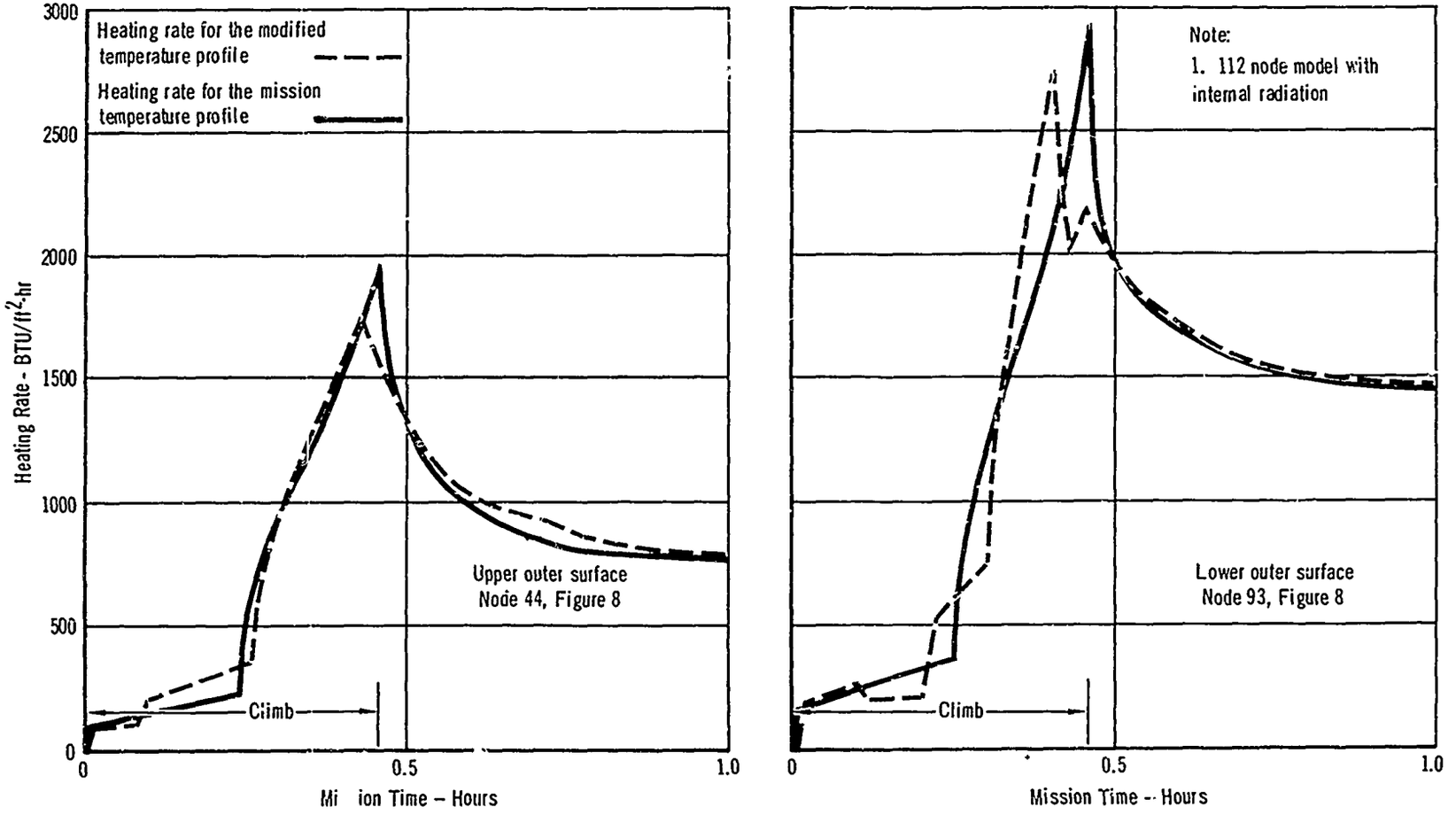

Figure 29 - Effect of a Modified Temperature Profile on Outer Surface Heating Rates Mach 3-4 Vehicle

both in magnitude and time of occurrence. As previously discussed, the peaks and troughs of the heating rate histories result from discontinuities in the slopes of the temperature history curves, which are linear idealizations of in-flight temperature-time curves, but it is seen that a slight change in the shape of the temperature-time curve for the control node has a significant effect on the heating rate curve. A comparison of the thermal stresses calculated for the base temperature profile and for the modification of this temperature profile is presented in Figure 30. As shown in this figure, the maximum thermal stress for the modified temperature profile is approximately 13% greater than the peak stress for the original temperature profile. Since the extent of a alteration of the control node temperature profile was slight, this variation of temperature and resulting variation of thermal stress can be expected to occur in all laboratory tests because of control inaccuracies. It is apparent that errors resulting from control temperature variations may easily be as significant as errors resulting from variation in other parameters.

1.2.1.5 Effect of Thermal Environment on Wing Cross Section Ultimate Strength - Figure 31 presents the results of an analysis of the compressive strength of the upper surface of the Mach 3-4 vehicle, with and without thermal stresses. This surface is assumed critical for the wing of the Mach 3-4 vehicle during ultimate strength verification. The temperature distributions used in the analysis are those resulting from surfaces emissivities equal to 0.66. The thermal stresses cause a maximum of 1.7% reduction in compressive strength (time ≈ .46 hours, panel buckling). The wing panel buckling is allowable for the assumed geometry was found to be considerably smaller than the crippling allowable; if the geometry were changed to allow the panel buckling stress to approach the panel crippling stress, the effects of thermal stresses would be further reduced. In either case, the effects of thermal stresses on panel ultimate strength are not as significant as temperature degradation effects.

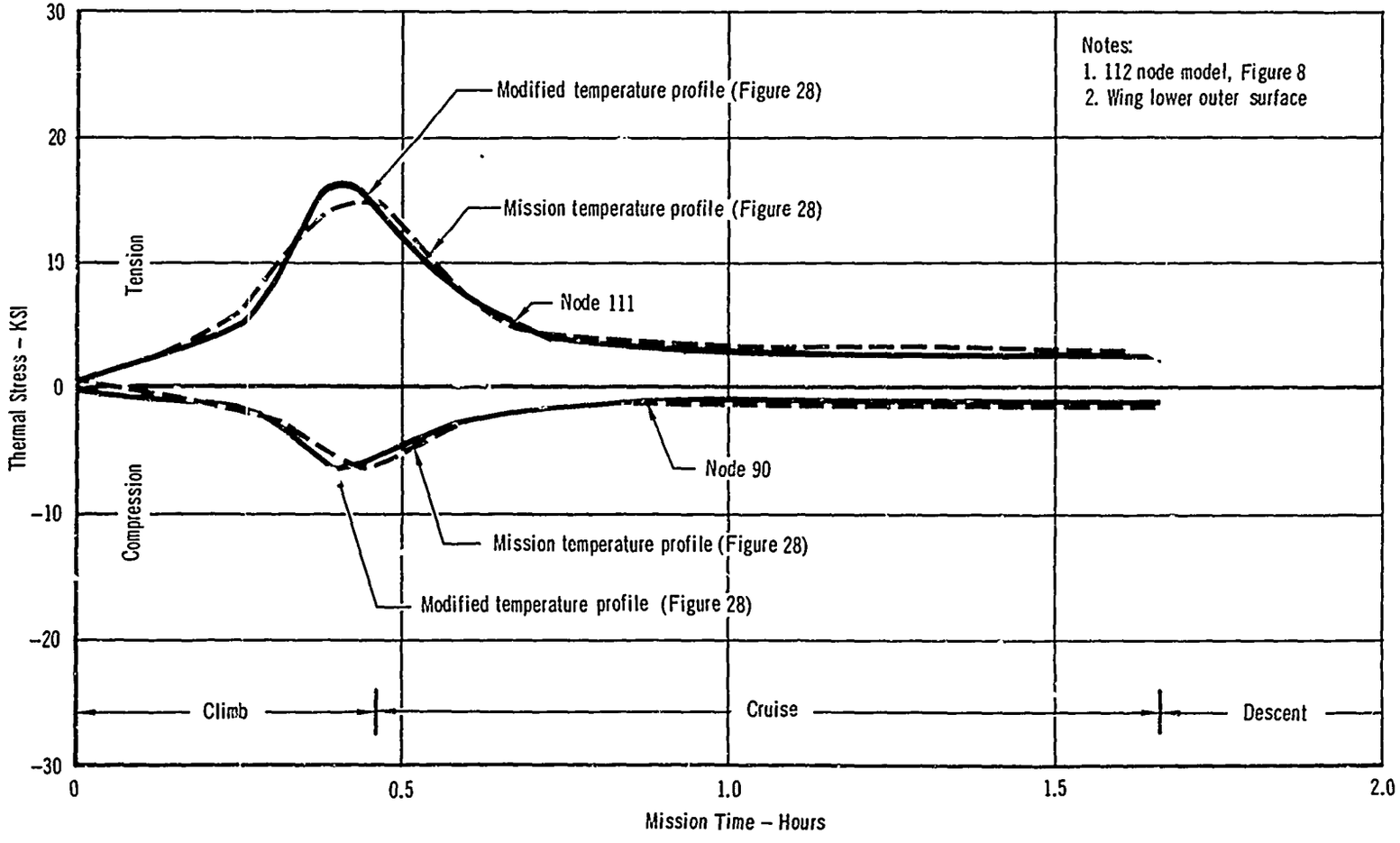

Figure 30 - Effect of Temperature Profile on Spanwise Thermal Stress Mach 3-4 Vehicle

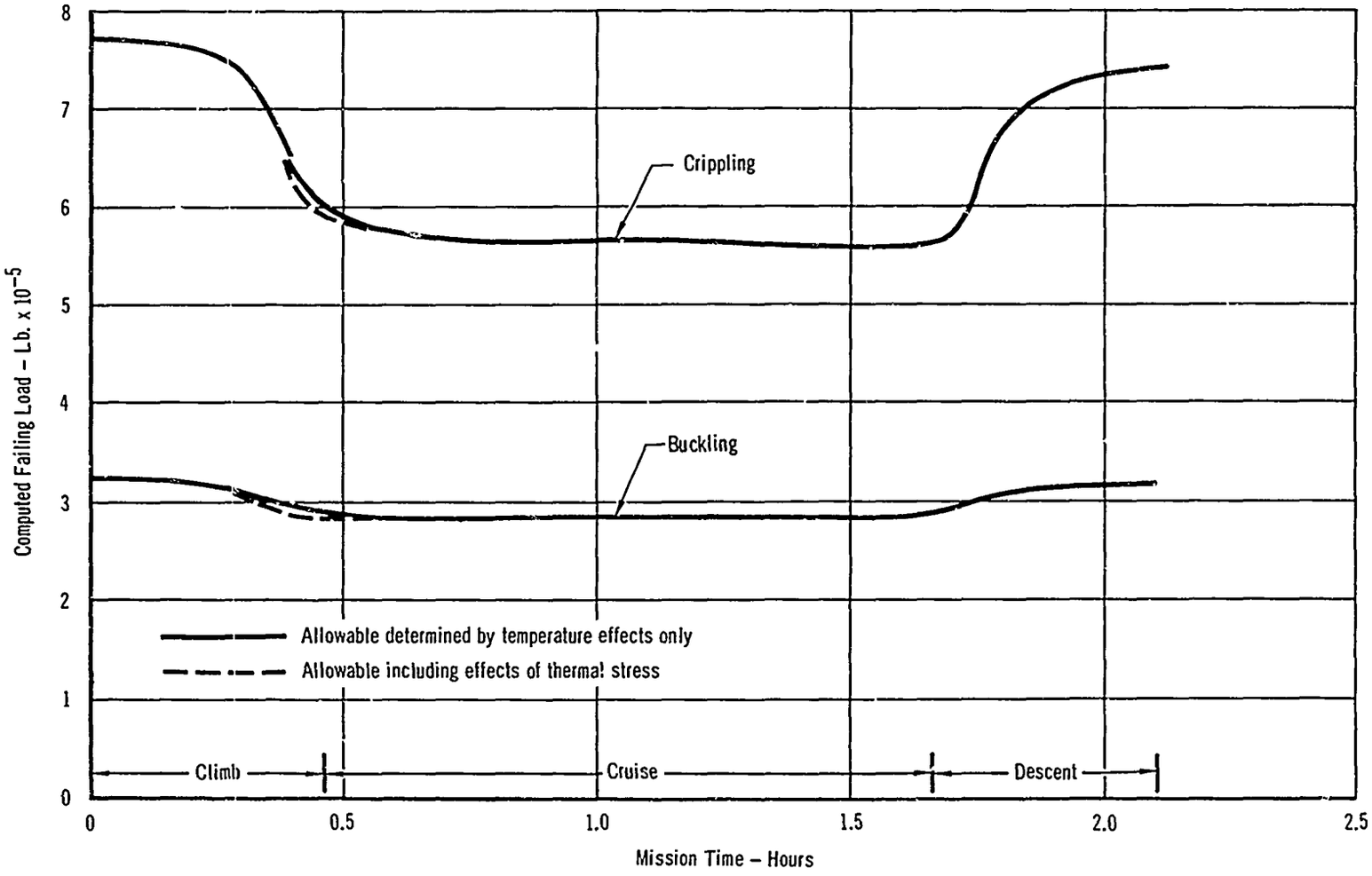

Figure 31 - Effect of Mission Environment on Computed Wing Upper Surface Panel Failing Load Mach 3-4 Vehicle

1.2.1.6 Analysis of the Skin-Stringer Lower Surface Wing Cross Section - The previous analyses were performed for the double-face sandwich configuration of the lower wing surface. In order to determine the applicability of these analyses and of subsequent conclusions to other configurations, a brief investigation of an alternate skin-stringer lower wing surface configuration was performed. Figure 9 describes the configuration of the cross section and the nodal numbering system. Temperatures and thermal stresses were computed for all 90 nodes of the cross section. Figures 32 and 33 present the temperatures and thermal stresses, respectively, for nodes 91, 93, and 99 of the wing lower surface; that is, the inboard ends of the web attachment tee and the stiffeners (see Figure 9), which are the locations of maximum thermal stress. Node 99 corresponds to node 111 for the corrugated configuration. Since the peak temperatures and thermal stresses for the two configurations are not significantly different, it is judged that conclusions for the corrugated configuration are also applicable to the skin-stringer configuration.

1.2.2 Test Facility Analysis - Similar procedures were employed in designing test systems for all test articles considered in this study (i.e., complete vehicle, model, or component, for the Mach 3-4 vehicle and the Mach 12-15 vehicle). The procedure for designing heating and cooling systems and their integration with the structural loading system is discussed first, followed by a summary of the testing requirements for the Mach 3-4 vehicle.

The state-of-the-art made it necessary to estimate facility requirements through detailed computations because general parametric studies of test facilities are not available. The following data are generally required for the computation of facility requirements:

(a) Detail specimen configuration and geometry

(b) Test loads

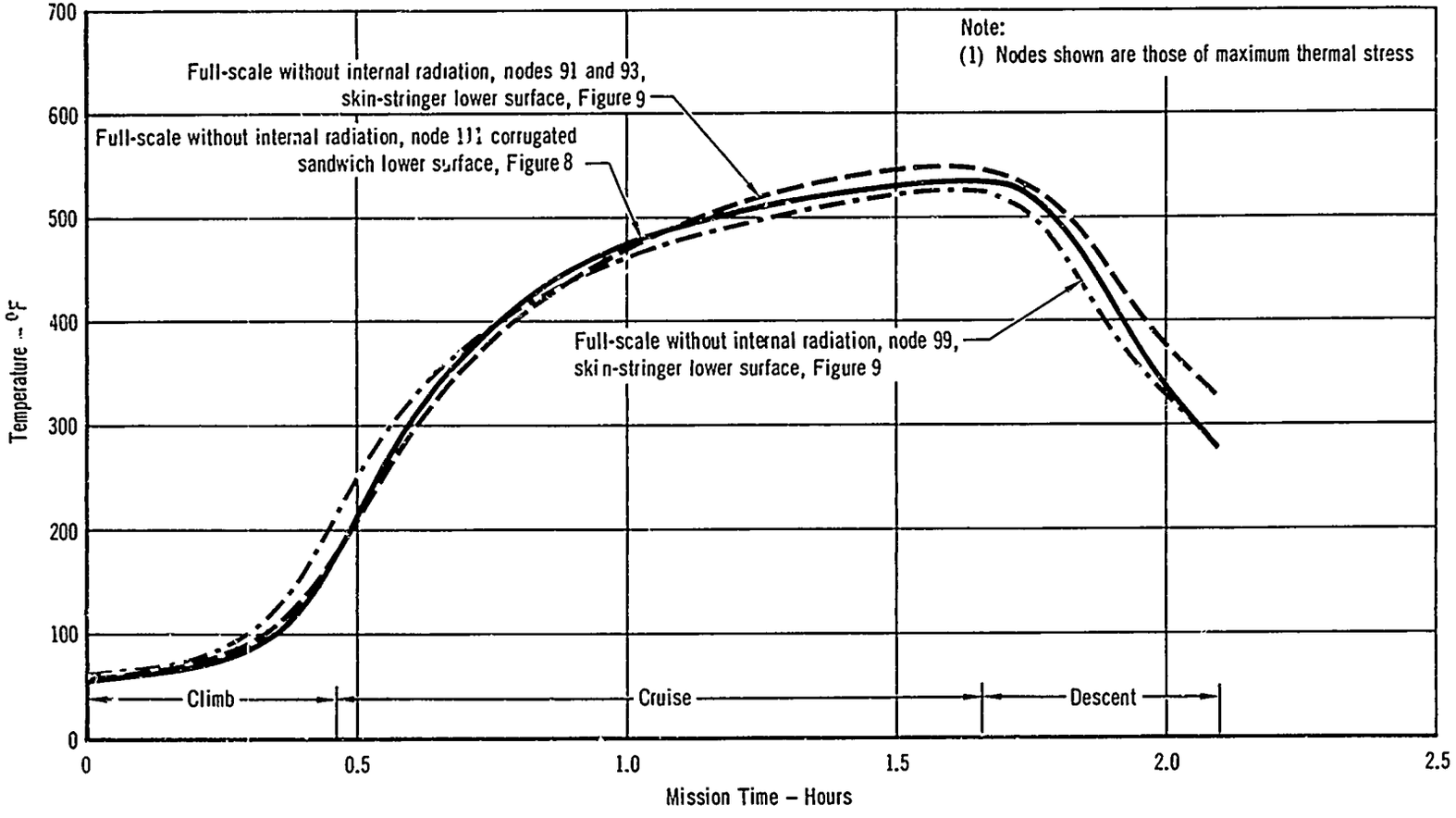

Figure 32 - Comparison of Temperatures for Two Structural Configurations Mach 3-4 Vehicle

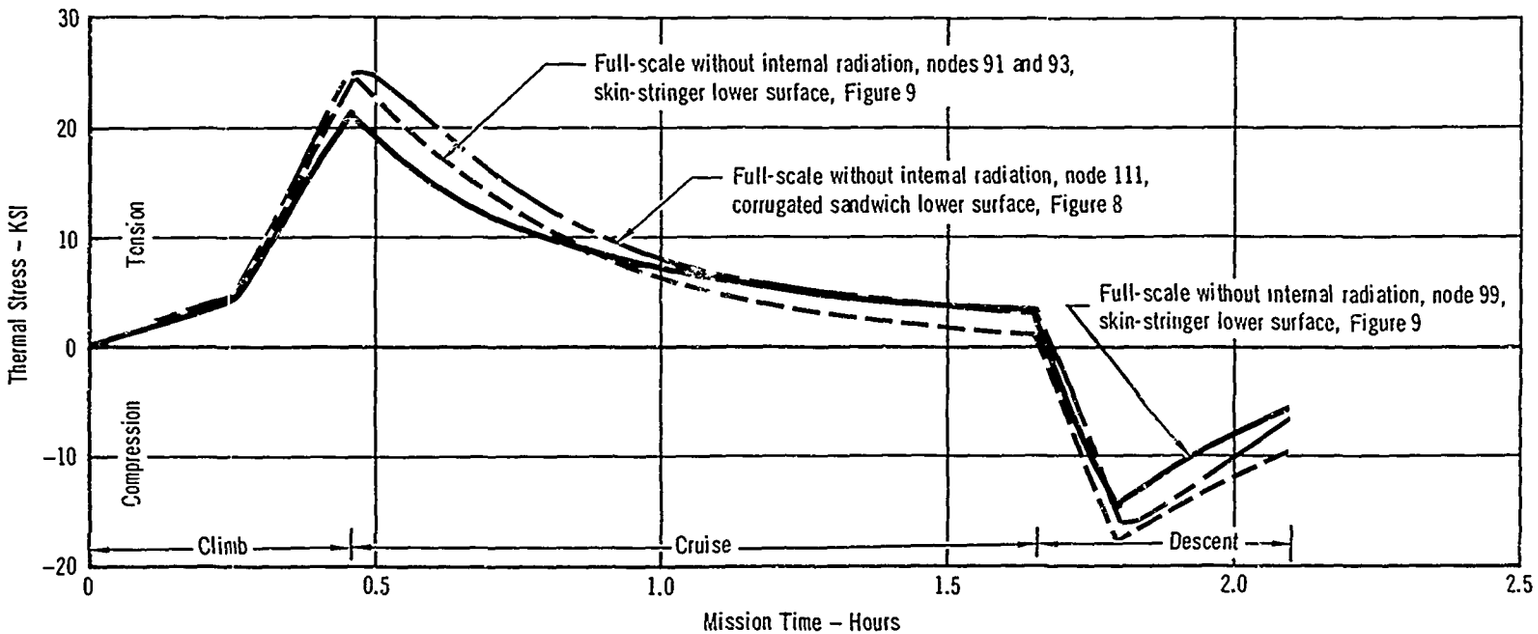

Figure 33 - Comparison of Spanwise Thermal Stress for Two Structural Configurations Mach 3-4 Vehicle

(c) Critical test thermal conditions, temperature-time profiles

(d) Instrumentation and inspection requirements

(e) Length of test time and test cycles for application to equipment design

(f) Fatigue criteria, including spectrum and allowable cycle rate

(g) Test data required

Two separate systems must be considered: the mechanical loading system and the thermal loading system. The procedure used for developing the mechanical loading system is discussed first, followed by a discussion of a method used for designing heating and cooling systems and their integration with the loading system.

1.2.2.1 Mechanical Loading System Design Methods - Alternates to the typical whiffletree-loading pad arrangement of applying loads include penumatic or hydrostatic pressure systems. The use of either loading system requires sealing of the test structure. Sealants are undesirable on structural test vehicles because they tend to conceal incipient failures. Also, the complexity of a distributed pneumatic or hydrostatic pressure loading system for the testing of a large structure is prohibitive; especially when inertia loads and thermal conditions are to be applied simultaneously. Therefore, the whiffletree system remains the most attractive loading technique for the structures considered.

The use of bonded loading pads over a large portion of the loaded surface is satisfactory for room temperature or steady state elevated temperatures up to about 500°F (limited by the adhesive). However, the presence of the overall pad system changes the thermal mass of the test article and the pad system interferes with the heating and cooling system because it covers the surface.

The best approach to the simultaneous simulation of transient thermal environment and loads has been judged to be the application of a limited

number of concentrated external loads which may cause undesirable localized thermal and structural discontinuities but will develop the proper overall structural and thermal loadings. This approach may require some supplementary element tests to determine and verify local effects. The loading of the structure can be accomplished by straight-forward application of successive single tree-whiffletree systems to combine many individual loads into a minimum number of applied consolidated loads.

Using the loading requirements and methods previously described, the number of structural loading control channels required for fatigue and ultimate strength testing of the Mach 3-4 vehicle has been determined and is shown in Table V. It can be seen, as also shown in Figure 1, that the 86 channels for structural loading reportedly available at the WPAFB facility are not sufficient for all approaches; 315 channels would be required for structural loading of the full-scale complete vehicle.

1.2.2.2 Thermal System Design Methods - Three alternate methods were considered to develop flight temperature distributions within a laboratory specimen:

(a) Program heat fluxes on the surface skins using analytically determined or flight-measured values

(b) Program external and internal temperatures to match desired thermal stresses (or program thermal stresses and control the temperatures to match the desired thermal stresses)

(c) Program external surface temperatures to match analytically determined or flight measured values

The latter approach was selected to compute test facility requirements. This choice of thermal environment control may affect absolute costs but not relative costs between the various techniques.

Usual systems of simulating flight thermal environments on large test

TABLE V
SUMMARY OF ESTIMATED TEST FACILITIES REQUIREMENTS
MACH 3-4 VEHICLE
FATIGUE AND ULTIMATE STRENGTH TESTING

	Test Article (1)	Maximum Mission Heat Flux BTU Ft²-Hr	Maximum Test Flux Required (2) BTU Ft²-Hr		Effective Maximum Temperature °F	Area Heated by Lamps Ft²	Lamps Required	Maximum Power Required KW	Maximum Coolant Air Required TA = 80°F SCFM (4)	Heating KW-Hr Flight	Coolant Air SCF Flight	Control Channels		Instrumentation		
			Heating	Cooling								Heating (3)	Structural	Strain Gages Rosettes	Deflection Gages	Thermo Couples
Room Temperature	Full scale vehicle	2700	0	0	70	0	0	0	0	0	0	0	315	5175	325	0
	Half scale vehicle	5400			70								450	5310	325	
	1 Wing component	2950			70								35	250	15	
	2 Engine component	2700			70								60	175	10	
	3 Landing gear component	2325			70								65	265	15	
	4 Fuselage component	2700			70								50	490	10	
	5 Cabin component	2950			70								45	160	10	
	6 Nose component	3450	0	0	70	0	0	0	0	0	0	0	10	30		
Constant Elevated Temperature	Full scale vehicle	2700	360	0	575	14 000	20 200	2 270	0	3130	0	A 510 B 195 C 40	315	5175	325	950
	Half scale vehicle	5400	720		575	3 500	10 100	1 135		390		A 510 B 195 C 40	450	5310	325	475
	1 Wing component	2950	380		600	290	420	50		70		45	35	250	15	235
	2 Engine component	2700	380		550	1 820	2 620	310		425		295	60	175	10	1475
	3 Landing gear component	2325	330		540	940	1 350	140		190		120	65	265	15	730
	4 Fuselage component	2700	360		575	500	720	80		110		65	50	190	10	340
	5 Cabin component	2950	380		600	295	425	50		70		35	15	160	10	235
	6 Nose component	3450	420	0	650	135	195	25	0	35	0	25	10	30	2	145
Mission Profile Temperature	Full scale vehicle	2700	2100	1295	575	14 000	20 200	13 180	796 000	3780	890 000	A 510 B 195 C 40	315	5175	325	9500
	Half scale vehicle	5400	4200	2590	575	3 500	10,100	6 590	398 000	475	111 350	A 510 B 195 C 40	450	5310	325	4750
	1 Wing component	2950	2270	1395	600	290	420	295	17 800	80	17 150	45	35	250	15	2350
	2 Engine component	2700	2300	1285	550	1 820	2 620	1 900	103 000	515	106 000	295	60	175	10	14750
	3 Landing gear component	2325	1820	1319	540	940	1 350	775	54 200	240	57 100	120	65	265	15	7300
	4 Fuselage component	2700	2100	1295	575	500	720	470	28 500	135	31 800	65	50	490	10	3400
	5 Cabin component	2950	2270	1395	600	295	425	305	18 100	85	17 450	35	15	160	10	2350
	6 Nose component	3450	2660	1530	650	135	195	160	9 070	45	8 750	25	10	30	2	1450

Notes

(1) See Figure 51 for component locations.

(2) Maximum test flux required is that flux which must be applied to the test article to achieve the desired mission condition

(3) Control Channels A – Capacity = 25 KVA B – Capacity = 50 KVA C – Capacity = 580 KVA

(4) Cooling not expected to be required for ultimate strength testing

articles apply heat by electrically powered and controlled lamps, and remove heat by radiation heat sinks and/or forced external convection. In-flight cooling of a vehicle generally includes both free surface radiation and convective losses; however, cooling in the laboratory must be obtained by external convection with rates large enough to compensate for the lack of free surface radiation. The laboratory thermal environment control system must therefore effectively couple a radiant heat source with a convective heat sink to accomplish the necessary programming of both heating and cooling rates or temperature vs. time profiles. Heating requirements generally are evaluated under the assumption that the vehicle external surfaces are radiating to a free atmosphere at a temperature of -60° to +80°F. In a thermal test set-up using infrared lamp-reflector systems, the vehicle external surfaces re-radiate to the heating system reflector which may be allowed to approach the vehicle surface test temperature or may be kept cool; but in either case, it will generally be, by its design, a good infrared reflector. Therefore, the test heating requirement will be less than mission requirements, and the cooling requirements will be greater than those shown in the heating and cooling requirements curves determined for mission conditions.

A comparison of the equations governing in-flight heat transfer and test facility heat transfer is useful in evaluating this difference in heating requirements. In-flight heating is basically convective (neglecting hypervelocity shock front radiance) and can be represented in the form

$$\dot{q}_{f(local)} = h_{f(local)}(T_{aw} - T_s)_{(local)} \qquad (1)$$

In the test, an actual control point temperature is measured by a thermocouple suitably attached to the test vehicle at the control point location. The thermocouple output is continuously compared with the required temperature. An imbalance between the thermocouple output and the function generator output

results in an error signal. Heat is controlled by regulating the effective voltage applied to the heat lamps; coolant regulation systems employ valve control of the coolant. The surface heating rate at any point in the test control zone is directly proportional to the surface heating rate demand at the program control point (control thermocouple) location and is independent of the local surface temperature at any other point in the test control zone. This may be stated:

$$\dot{q}_{h(local)} = k_h \dot{q}_{h(control\ point)} \tag{2}$$

The local cooling rate (negative heating rate) control is accomplished by variations in the local coolant mass flow rate which, in turn, is controlled by coolant source pressure regulation. Regulation of coolant source pressure is, in effect, a programmed regulation of the convective heat transfer coefficient (h_c). Assuming a constant coolant source temperature, the local surface cooling rate at any point can be expressed by:

$$\dot{q}_{c(local)} = -h_{c(local)}(T_c - T_s)_{(local)} = -k_c h_{c(control\ point)}(T_c - T_s)_{(local)} \tag{3}$$

It can be seen from Equation 3 that the local cooling rate at any point is dependent upon the local surface temperature as well as upon the control point cooling rate.

Inspection of Equations 1, 2, and 3 will show that the test local cooling rates can closely approximate mission local cooling rates in control zones, with a wide variation of local surface temperatures, if test heat transfer coefficients do not have large local variations. This is not the case for the test heating simulation. The test local heating rates can approximate the flight local heating rates only when the flight surface temperatures do not have large variations within the control zone. This is because in-flight heating is a function of the difference of the surface and boundary layer temperature, while laboratory heating is a function only of the heating rate required at the control node.

In the past, the non-homogeneous heat capacity of structures and the resulting temperature non-uniformities causing the simulation difficulties previously described have been partially compensated by the use of a relatively high density of control zones on the specimen surface to minimize the range of temperature in any zone. This has been possible because of the relatively small size of specimens and an adequate number of control channels have been available. However, in attempting to test a structure with a very large heated area with relatively low local heating rates, the test system may be unable to provide a sufficient number of control zones to obtain the proper (design) temperature distributions.

1.2.2.2.1 Heating Rate Control - A study of available information on lamp system energy outputs and applied power requirements was made to determine radiant heat lamps and lampbank configurations that could be best utilized in obtaining required specimen heating rates.

The heat flux levels one inch away from the center of operating lampbanks with gold reflectors within 1.5 inches from the lamps was experimentally determined and permitted the computation of lamp efficiency. These calculations indicated that a 65 percent lamp efficiency can be expected at that distance from the lampbank; that is, a black body surface would receive 65 percent of the power that the heating system consumed. Variation in reflector type or in reflector lamp separation will result in somewhat different efficiencies. The variation of system efficiency with the distance from the lamp filaments to the irradiated specimen was also determined experimentally. The heat flux was measured at various distances from the center of a lampbank operating at several power input levels. Similar measurements for lamps of different power rating indicated the same efficiency variation with spatial position. The results of these efficiency studies are shown in Figure 34.

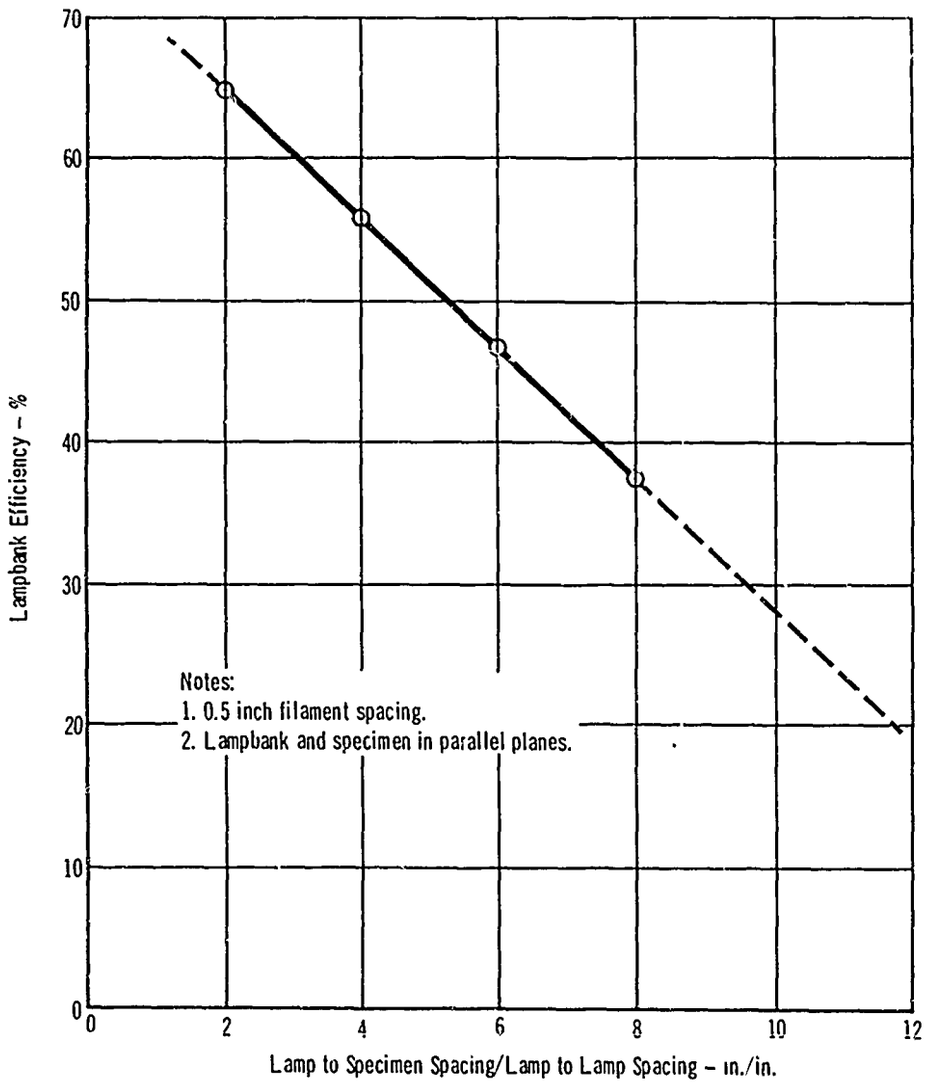

Figure 34 - Lampbank Efficiency

Curves of heat flux have been plotted in terms of lamp applied voltage and current; an example is presented in Figure 35. The combined use of data similar to that presented in Figures 34 and 35 with required heating rate data presented in Subsection 1.2.1 allowed the selection of specimen to lamp distance, lamp filament spacing, and lamp type for the testing considered.

1.2.2.2.2 Cooling Rate Control - The specimen cooling rates are equally as important as the heating rates in their effect upon the structure, and in some cases are more difficult to obtain and control. A vehicle in the descent and landing portion of a flight is cooled by forced convection and by external radiation, while in the laboratory, there is only a small amount of heat removal by natural convection. Since laboratory radiation heat transfer rates are less than those experienced in flight, there remains a net cooling required which can be met only by the use of a controlled convective cooling system. At typical temperatures of the Mach 3-4 vehicle, the effectiveness of heat removal by radiation rapidly diminishes as the temperature of the structure approaches the laboratory ambient temperature, as shown in Figure 18. It is, therefore, necessary to provide a convective cooling method if this portion of the flight is to be simulated. However, as indicated in Figure 31, the critical design condition or conditions for ultimate strength are expected to occur during the climb or cruise portions of the flight; hence, cooling is not usually required for ultimate strength verification testing. However, for continuity and completeness, the cooling system design will also be discussed in this section rather than in Section VII where it will be required for mission temperature testing.

By using cooling discharge orifices in the surfaces of the reflectors of the heating system, it is possible to incorporate a cooling system within the heating system, thus producing a modular temperature control unit. Streams of air (or cooled gas) issuing from these orifices, passing between the heat lamps

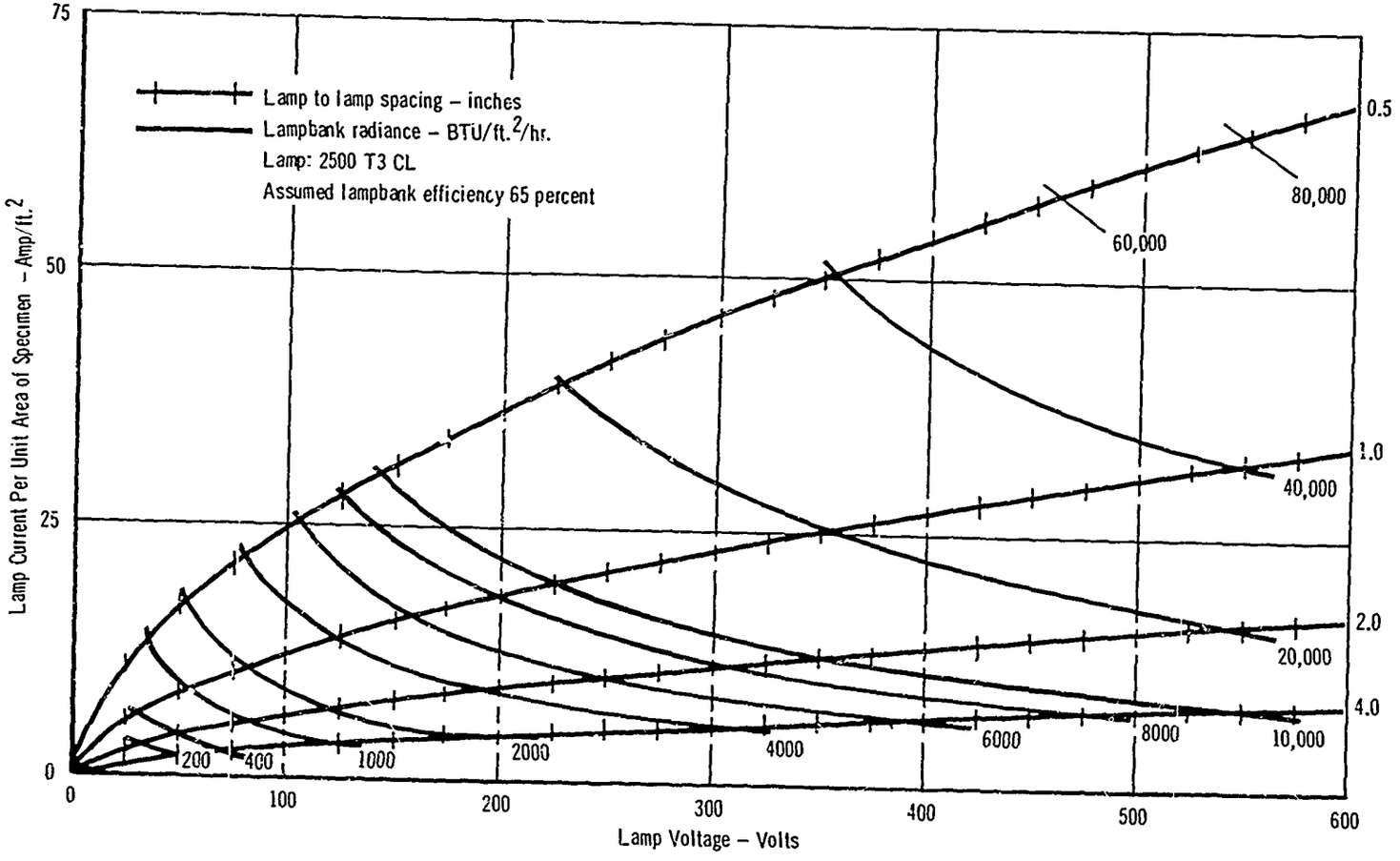

Figure 35 - Current Density and Voltage as a Function of Lampbank Radiance and Lamp Spacing

and impinging normally on the surface to be cooled, result in a relatively efficient and controllable cooling system. The cooling rate can be controlled by varying the coolant air mass flow rate and/or the coolant air temperature and by applying power to the lamps (to lower the cooling rate). The coolant mass flow rate can be readily varied by controlling the pressure upstream from the orifice; however, the coolant air temperature cannot be varied without the inclusion of more elaborate hardware in the system. Therefore, maintaining the coolant air temperature constant at laboratory supply temperatures and varying the coolant mass flow rate appears to be the best method of cooling rate control. Integration of the heating and cooling systems also provides for interlocking temperature control during all phases of the thermal cycle.

To facilitate the general design of a system capable of producing the cooling rates required in any given test, a collection of parametric curves was developed based on the data appearing in Reference 4. The geometric, pressure, and orifice parameters were combined to allow graphical determination of specimen-to-orifice spacings, orifice-to-orifice spacings and orifice diameter for specified design conditions. These design conditions included specimen temperature, required cooling rates, coolant pressure and temperature, and compatibility of the heating and cooling system spacings. Having determined the size and spacing of orifices necessary to obtain the required specimen cooling rate and knowing the maximum pressure to be used, it is then possible to calculate the total required instantaneous volumetric airflow. By multiplying the orifice discharge rate by the number of orifices in the system, the maximum instantaneous volumetric demand on the source is determined.

Greater uncertainty exists in the analytic design of the cooling system than of the heating system, resulting in greater uncertainty in the computed values of required mass flow, number of controllers and orifices, etc., than in the computed values for heating system.

1.2.2.3 Application of Thermal System Design Methods - The data presented in the previous paragraphs have been used to determine the system requirements for heating and cooling the complete Mach 3-4 vehicle.

Using the maximum heating rates computed for various areas of the vehicle, efficient heat lamp size and spacing were determined, and the required voltage and current density computed. It was found that to obtain the minimum current density (power controller applications are generally limited by current requirements), a 2500 T3CL lamp at 4 inch spacing must be used throughout, and peak operating levels would be from 230 to 270 volts across each lamp with current densities of 5 to 5.5 amps/ft^2.

The peak power required to heat the complete Mach 3-4 vehicle is about 13,200 KW, which is well within the capabilities of the WPAFB facilities. This power was computed using a current density of 5.5 amp/ft^2 and a voltage of 275 volts. Approximately 20,200 lamps would be required to heat the full-scale complete vehicle. Because of the increase in system application efficiency by operating at high voltage-low current, the lamps could be connected in series pairs and operate at near the 600 volt capacity of the system. This would reduce the number of control channels required, while keeping the current low. A disadvantage in connecting the lamps in series is that if one lamp fails both lamps will become inoperable. This effect could be minimized by alternating spacings of serviced lamp pairs so that adjacent lamps were not in series.

With the power input and the number of lamps established for peak heating requirements, the number of channels required to control heating can be approximated. The test facilities at WPAFB, as reported in Reference 2, have a capacity of 80 power control channels at 580 KW with 40 channels being capable of division into 550 sub-channels at 25 KW and 210 sub-channels at 50 KW, all operating at 600 volts. It is estimated that these facilities would be adequate for the

operation of the approximately 20,200 lamps in series pairs required for heating and cooling the full-scale complete Mach 3-4 vehicle studied in this report.

The required cooling rates, orifice spacings, and coolant flow requirements were determined using the previously discussed cooling system design methods. A source pressure of 80 psia was assumed. An orifice diameter of 1/8 inch with orifices spaced approximately 5.75 inches apart and with a test specimen to orifice spacing of 5 inches was found to provide the required cooling rate (BTU/ft^2-hr) shown in Table V. The test specimen to orifice spacing of 5 inches was selected to provide the required cooling rate; this is consistent with the expected specimen to lamp spacing. The orifice-to-orifice spacing provides reasonably small cooling gradients in the plane of the surface; a larger orifice spacing would generate larger cooling gradients in the plane of the surface which would alter the thermal stresses.

With the assumed orifice diameter and air source pressure, an air flow per orifice of 14.75 SCFM is required. With the orifice coverage areas established and using a full-scale planform area of 6000 square feet, it was possible to evaluate the rates of air flow at 80°F required to cool the specimen; the full-scale Mach 3-4 aircraft would require approximately 796,000 SCFM.

If the coolant air temperature were lower than room temperature, the amount of coolant required would be decreased; however, the cost to cool the air may be greater than the cost to provide a greater volume of air at room temperature.

1.2.3 Cost Analysis - To establish cost effectiveness of the various alternate approaches, a cost estimate for each approach was determined; however, the primary objective in performing such cost analyses in this study was the determination of relative costs. The major areas considered were:

(a) Engineering design costs

(b) Manufacturing costs

(c) Testing costs

The cost for engineering design includes drawing preparation, test monitoring, and analysis. However, for full-scale complete vehicle testing these costs were found not to be significant because it was assumed that none of the prototype design costs need be included, i.e., prototype drawings are available, and test monitoring and analysis, although important in the attainment of valid test results, did not significantly add to the test costs. Therefore, engineering costs have been concluded to be relatively unimportant in complete vehicle testing.

The cost for manufacturing includes tooling and fabrication of the test specimen. As in the engineering cost analysis, it was assumed that tooling for the prototype vehicle was available, so its cost was not included in complete vehicle testing costs. Fabrication of the test specimen and the test specimen material have been included. Material costs were computed in a direct manner, based upon the estimated structural weight of the vehicle. Fabrication costs have been determined using the usual estimation techniques; that is, a combination of the statistical approach based upon planform area and weight and judgment of the complexity of the construction.

Laboratory testing costs include design of the test jig, design of instrumentation and monitoring system, fabrication of the test jig, installation of test specimen and instrumentation, and test performance. The design and fabrication costs were determined using a combination of the statistical approach based upon planform area and weight and judgment of complexity; test jig costs were determined from the estimate of jig weight and the number of strain gages, thermocouples, actuators, and lamps required; and the equipment reliability and useful life were also included in the cost estimation. Since it was assumed

that all control equipment needed would be available, the cost for such equipment was not included in the analysis. Test performance costs, i.e., the man-hours required for actual test conductance, were found not to be significant for ultimate strength testing in comparison to the other costs.

Although the test cost of any technique would be influenced by the choice of test facility, the priority of the test program, and by the degree of accuracy desired, the relative costs would not be significantly affected by these choices; therefore, all costs are presented on a relative basis. The base cost value for comparison purposes is the ultimate strength verification of the full-scale complete vehicle, performed at room temperature. The relative man-hour costs are shown in Figure 36, and the dollar costs in Figure 37. The total man-hour cost of this test is in the range of 1.5 to 2.5 million man-hours and the corresponding dollar cost is 20 to 40 million dollars. It should be carefully noted that the costs, both unit and total, are based on estimates derived from what are believed to be reasonably representative, typical data; however, they should be considered as gross, first level approximations to actual costs. The relative cost estimates have greater accuracy than any single absolute cost.

1.2.4 Conclusions - The following conclusions may be drawn relating to the full-scale complete vehicle ultimate strength verification testing of the Mach 3-4 vehicle:

(a) The effects of internal radiation within the wing enclosure on thermal stresses are significant.

(b) The effects of variations in the interface conductance between the surfaces of the wing cross section on thermal stresses are not significant.

(c) The effects of variations in air pressure within the wing cross section enclosure on thermal stresses are not significant.

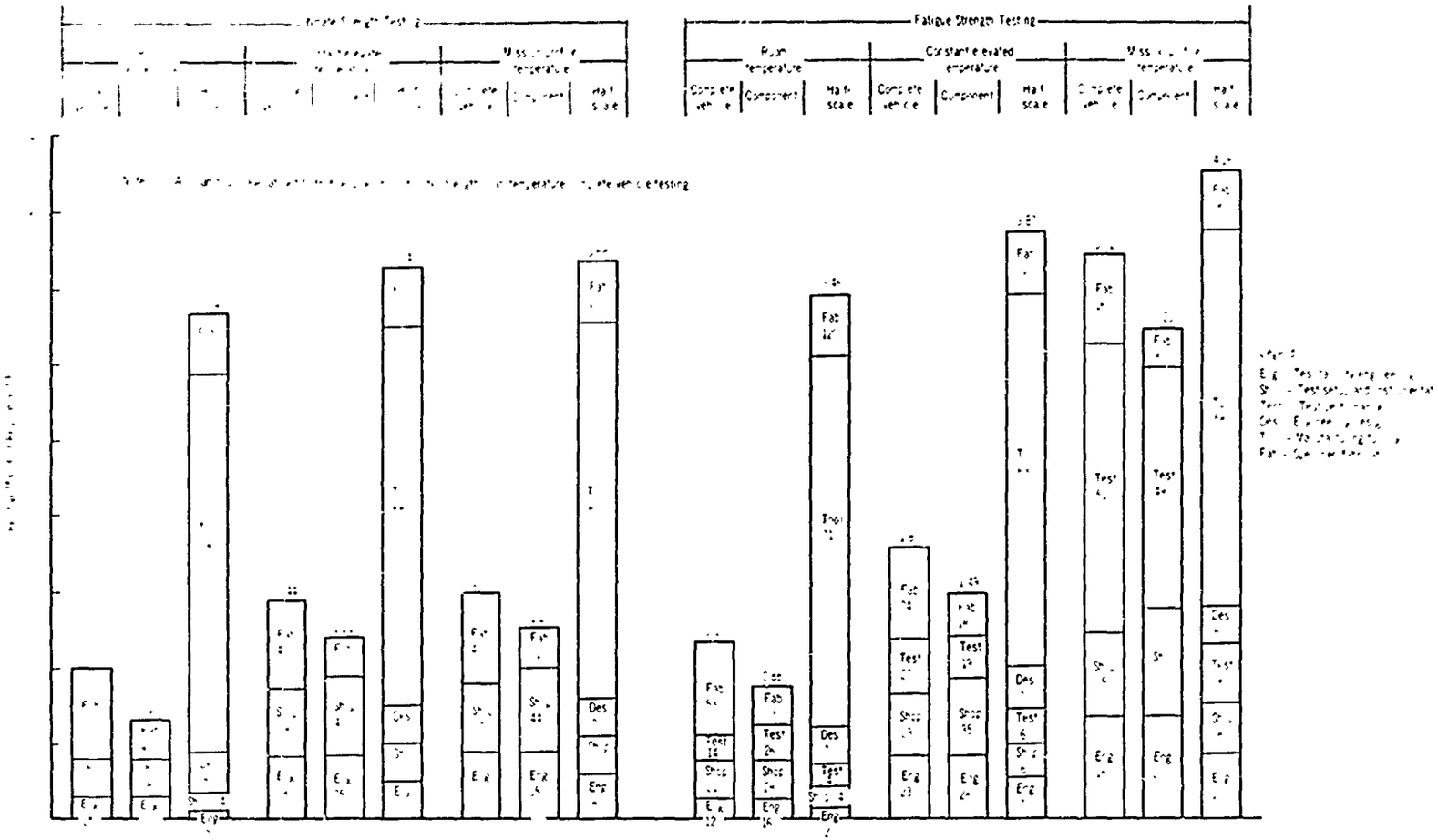

Figure 36 - Comparison of Relative Man-hour Requirements for Basic Approaches Mach 3-4 Vehicle

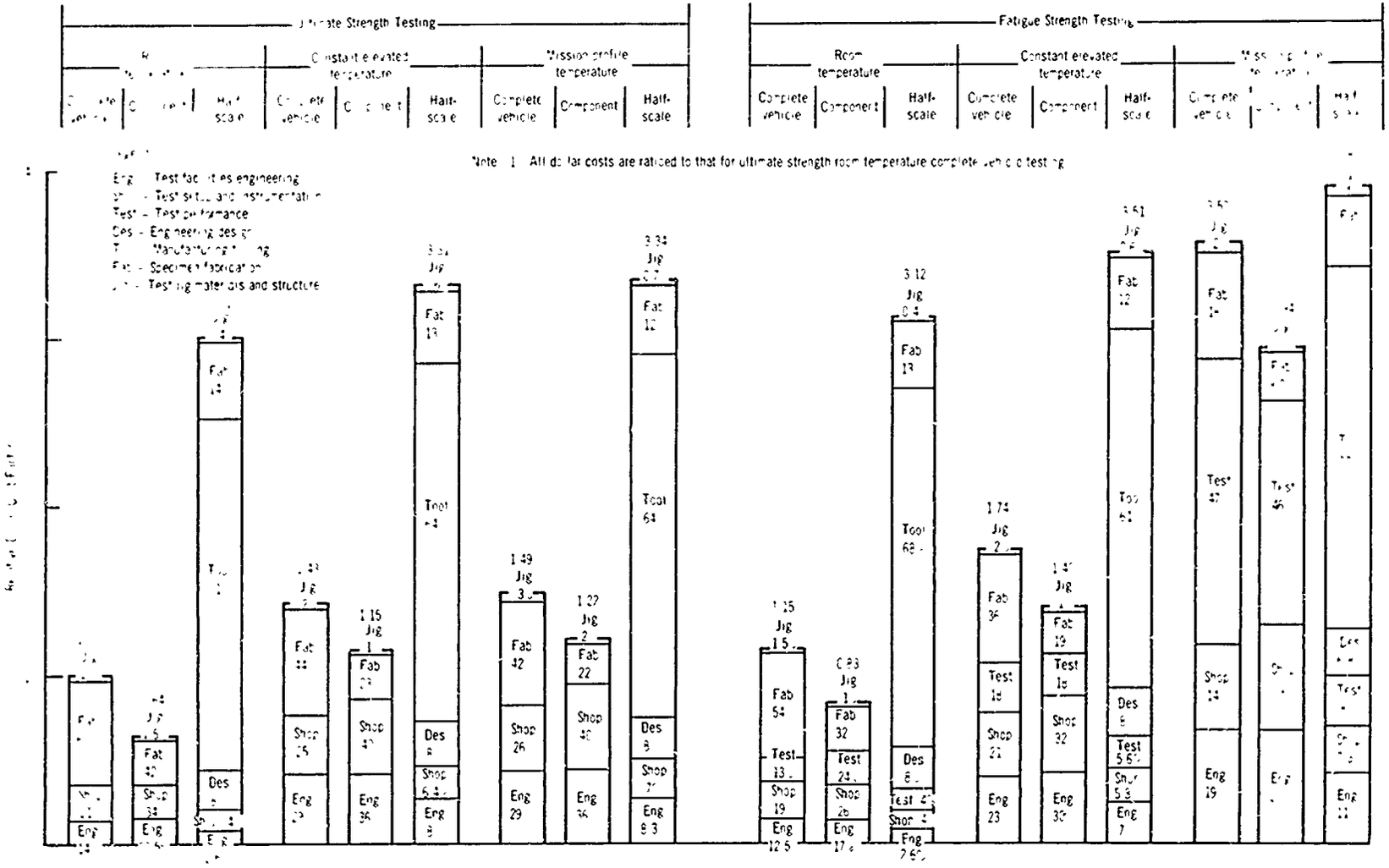

Figure 37 - Comparison of Relative Dollar Costs for Basic Approaches Mach 3-4 Vehicle

(d) Relatively small test control temperature error may be expected to cause significant deviations in thermal stresses.

(e) Thermal stresses do not significantly affect the ultimate strength of the wing cross section, mitigating any errors in thermal stress simulation caused by (a) or (d).

(f) For the mission temperature test of a complete Mach 3-4 vehicle, heating requirements, either BTU/hr or BTU/ft^2-hr, are not a serious problem. The significant heating problems are associated with equipment reliability, the possibility of producing some serious unwanted and unforeseen thermal effect, and the difficulty of controlling temperatures over large areas.

(g) Test cooling requirements for the Mach 3-4 vehicle are much more restrictive; this is true since this vehicle requires large cooling rates at moderate temperatures where re-radiation is not significant.

(h) The cost of test jig design and fabrication and of specimen fabrication are the most significant costs for complete vehicle ultimate strength tests.

1.3 Model Testing - In the following subsection the ultimate strength verification of the Mach 3-4 vehicle is discussed as affected by the basic approach of model testing. The engineering analysis, test facility analysis, cost analysis, and conclusions are presented in separate subsections. The effects of the modeling approach on vehicle strength in test are determined by comparisons to results obtained in Subsection 1.2.

1.3.1 Engineering analysis - Theoretical evaluation of structural models using dimensional analysis methods reveals three types of variables:

(a) Variables that are easily scalable

(b) Variables that are clearly not scalable

(c) Variables that may be scalable in themselves but are not compatible with the scaling requirements of other variables

A summary of the scaling laws for the first type of variables is presented in Table VI. Many of these scaling laws are given in the literature; most can be derived by simple analysis. For example, when transient heat transfer is restricted to the conduction mode, it can be shown that in order to maintain the same (homologous) temperature distribution in the model as in the prototype, both made of the same material:

$$\frac{\Delta\tau_m}{\Delta\tau_p} = n^2$$

This equation states that the time required to produce the prototype thermal stress in the model is scaled as the square of the geometric scale factor when conduction is the heat transfer mode. An event occurring in four minutes in the prototype would occur in one minute for a half-scale model, with the temperatures and thermal stresses being the same in both cases. The development of this relationship is presented in Subsection 1.3.1.1. If radiation is the heat transfer mode, a different result, $\Delta\tau_m/\Delta\tau_p = n$, would be obtained; also, consideration of convective heat transfer would yield approximately the same result. The following criteria must be met for exact true scaling to occur for all modes of heat transfer, if time is scaled as required for conduction ($1/n^2$):

$$\varepsilon_m = \frac{1}{n}\,\varepsilon_p$$

$$h_m = \frac{1}{n}\,h_p$$

$$c_m = \frac{1}{n}\,c_p$$

TABLE VI
SUMMARY OF SCALING RELATI ONSHIPS

General Scalable Relationships

Parameter	Units	Symbol	Scale Factor
Geometry	Ft.	L	$L_m/L_p = n$
Temperature (1)	^oR	T	$T_m/T_p = 1$
Stress (1)	Lb/ft^2	f	$f_m/f_p = 1$
Time	Sec	τ	$\tau_m/\tau_p = n^2$
Total heat	BTU	H	$H_m/H_p = n^3$
Heat flux	BTU/ft^2-sec	$\dot{q}$	$\dot{q}_m/\dot{q}_p = 1/n$
Deformation	Ft	δ	$\delta_m/\delta_p = n$
External load	Lb	P	$P_m/P_p = n^2$
External moment	Ft-lb	M	$M_m/M_p = n^3$

Strength Relationship

Loading	Strength is a Function of:	Scale Factor
Local element crippling	$F_{cy}, \frac{b}{t}\sqrt{F_{cy}/E}$	$F_{cc\text{-}m}/F_{cc\text{-}p} = 1$
Local element buckling	$F_{cy}, \frac{b}{t}\sqrt{F_{cy}/E}$	$F_{cr\text{-}m}/F_{cc\text{-}p} = 1$
Inter-rivet buckling	p/t	$F_{c\text{-}m}/F_{c\text{-}p} = 1$
Rivet shear strength	d/t	$F_{s\text{-}m}/F_{s\text{-}p} = 1$
Flat web shear buckling	t/b	$\tau_{cr\text{-}m}/\tau_{cr\text{-}p} = 1$
Column buckling (long)	L'/ρ	$F_{c\text{-}m}/F_{c\text{-}p} = 1$
Column buckling (short)	$L'/\rho, F_{cc}$	$F_{c\text{-}m}/F_{c\text{-}p} = 1$

Assumptions: 1. Identical model and prototype materials, temperatures and stress levels.
2. Conduction is the primary mode of heat transfer within the structure.

Subscripts: m = Model
p = Prototype

The many other variables which fall into categories (b) and (c) are summarized in Table VII. It is these variables that have received the greatest attention during this study.

1.3.1.1 Aspects of Modeling - In some situations, an experimental investigation has, as a primary purpose, the determination of temperatures and temperature gradients. Several methods of thermodynamic modeling with the above objective appear in the literature; they can be categorized as either "temperature preservation" or "material preservation." In the "temperature preservation" method, temperatures at homologous locations in model and prototype are identical, and thermal conductivity of materials in the scale model may differ from those of prototype through use of a different material. The second alternative is "material preservation," where identical materials are employed in the model and in the prototype. Temperatures at homologous locations in model and prototype are not identical, but are in a fixed ratio, depending on the geometric scale factor. Prototype geometry is usually scaled identically in all directions.

While the above techniques prove useful for applications where only information concerning temperature distributions is required, they are not applicable to a thermal-structural verification program. The use of different materials in the model and the prototype would not be acceptable in such a program; the engineering confidence in the test results would be low. Similarly, the use of a model with geometries scaled differently along the three orthogonal axes (which may be done to obtain more exact temperature distributions) is also not acceptable. Table VI indicates that theoretically, all dimensions should be scaled proportionally, if all strengths are to be scaled proportionally, and the prototype and model must be fabricated of the same materials, if adequate confidence in the approach is to be attained.

A discussion of scaling relationships for thermal-structural modeling may

TABLE VII
SUMMARY OF NON-SCALABLE PARAMETERS

Parameter		Units	Symbol	Expected Scale Factor (3)	Desired Scale Factor (4)	Category(1,5)
Natural frequency		Cycles/sec	f	$f_m/f_p = n$	$f_m/f_p = n^2$	b.
Joint conductance		BTU/ft^2-sec^{0}R	C	$C_m/C_p \approx 1$	$C_m/C_p = 1/n$	b.
Surface emissivity		None	ϵ	$\epsilon_m/\epsilon_p \approx 1$	$\epsilon_m/\epsilon_p = 1/n$	b.
Creep		In./in.	ϵ	$\epsilon_m/\epsilon_p < 1$	$\epsilon_m/\epsilon_p = 1$	b.
Convective heat transfer		BTU/ft^2-sec^{0}F	h	$h_m/h_p \approx 1$	$h_m/h_p = 1/n$	b.
Spot weld strength		Lb/in.	P	$P_m/P_p > 1$	$P_m/P_p = 1$	c.
Honeycomb shear strength		Lb/in.^{2}	F	$F_m/F_p < 1$	$F_m/F_p = 1$	c.
Material ultimate strength		Lb/in.^{2}	F_{tu}	$F_{tu\text{-}m}/F_{tu\text{-}p} > 1$	$F_{tu\text{-}m}/F_{tu\text{-}p} = 1$	c.
Material yield strength		Lb/in.^{2}	F_{ty}	$F_{ty\text{-}m}/F_{ty\text{-}p} > 1$	$F_{ty\text{-}m}/F_{ty\text{-}p} = 1$	c.
Fatigue life (general)		Cycles	N	$N_m/N_p > 1$	$N_m/N_p = 1$	c.
Ratio N_m/N_p as affected by:						
Factor	N_m/N_p					
Surface finish	< 1	In.-R.M.S.	σ	$\sigma_m/\sigma_p \approx 1$	$\sigma_m/\sigma_p = n$	c.
Specimen size	> 1	In.	L	$L_m/L_p = n$	$L_m/L_p = 1$	c.
Tolerances	< 1	In.	Δ	$\Delta_m/\Delta_p \approx 1$	$\Delta_m/\Delta_p = n$	b.
Cyclic rate	> 1	Cycles/sec	f	$f_m/f_p = 1/n^2$	$f_m/f_p = 1$	c.
Stress gradient	> 1	Lb/in.^{3}	f*	$f^*_m/f^*_p = 1/n$	$f^*_m/f^*_p = 1$	b

Notes:

(1) Assumptions: Identical model and prototype materials, temperatures and stress levels.
Conduction is the primary mode of heat transfer within the structure.

(2) Subscripts: m – Model
p – Prototype

(3) Values which will result from available fabrication techniques and material gauges.

(4) Scale factor desired, compatible with assumption of conduction as primary mode of heat transfer.

(5) Categories as described in Subsection 1.3.1.
b. Parameters clearly not scalable or scalable with great difficulty.
c. Parameters sometimes not scalable.

be used for illustration. Initially, conduction is assumed to be the only mode of heat transfer within the structure. In either the model or the prototype, the net heat transferred to or from an element by conduction is balanced by a subsequent increase or decrease in stored energy resulting in a temperature change:

$$\rho \, Vc_p \frac{dT}{d\tau} = kA \frac{dT}{dL} \tag{4}$$

Within the prototype and the model, respectively:

$$\rho_p \, V_p \, c_{p\text{-}p} \frac{dT_p}{d\tau_p} = k_p \, A_p \frac{dT_p}{dL_p} \tag{5a}$$

$$\rho_m \, V_m \, c_{p\text{-}m} \frac{dT_m}{d\tau_m} = k_m \, A_m \frac{dT_m}{dL_m} \tag{5b}$$

The length, area, and volume scale from prototype to model in the following manner:

$$L_m = nL_p \tag{6a}$$

$$A_m = n^2 A_p \tag{6b}$$

$$V_m = n^3 V_p \qquad (n < 1) \tag{6c}$$

Requiring the temperature distributions to remain the same in prototype and model:

$$T_p \, (\tau_p, \, L_p) = T_m \, (\tau_m, \, L_m) \tag{7}$$

Substituting equations 6 and 7 into equation 5b:

$$n^3 \, \rho_m \, V_p \, c_{p\text{-}m} \frac{dT_p}{d\tau_m} = n \, k_m \, A_p \frac{dT_p}{dL_p} \tag{8}$$

Requiring the material to be the same in prototype and model:

$$k_p = k_m \tag{9a}$$

$$\rho_p = \rho_m \tag{9b}$$

$$c_{p\text{-}p} = c_{p\text{-}m} \tag{9c}$$

Substitution of equations 9 into equation 8 results in:

$$n^3 \rho_p V_p c_{p-p} \frac{dT_p}{d\tau_m} = n k_p A_p \frac{dT_p}{dL_p} \tag{10a}$$

Simplifying:

$$n^2 \rho_p V_p c_{p-p} \frac{dT_p}{d\tau_m} = k_p A_p \frac{dT_p}{dL_p} \tag{10b}$$

Comparison of equations 5a and 10b clearly requires

$$\frac{d\tau_m}{d\tau_p} = n^2 \tag{11}$$

Thus, scaling for a conduction heat transfer process requires that times between prototype to model systems be scaled as n^2. An event occurring in four minutes for the prototype must, therefore, occur in one minute for a half-scale model in order to have the same T_p and T_m.

Heat transfer rates obtained from other modes of energy transfer must be the same as indicated in equations 5a and 5b in order to preserve this time scaling. The rates of heat transfer for a scaled element to the rate for the prototype element must be:

$$\frac{A_m \dot{q}_m}{A_p \dot{q}_p} = \frac{\dot{q}_{storage,m}}{\dot{q}_{storage,p}} = \frac{\rho_m V_m c_m dT_m d\tau_p}{\rho_p V_p c_p dT_p d\tau_m} = n^3 \frac{d\tau_p}{d\tau_m} \tag{12}$$

Substituting equation 11 into equation 12 leaves

$$\frac{A_m \dot{q}_m}{A_p \dot{q}_p} = n^3(1/n^2) = n \tag{13}$$

This means that all model heat transfer rates (in BTU/hr) from element to element must be n times that of the prototype for all modes. The heat transfer rates of radiation, convection, and interface conduction are described by:

$$\dot{q}_R = F\sigma\varepsilon(T_1^4 - T_2^4) \tag{14a}$$

$$\dot{q}_c = h\,(T_1 - T_2) \tag{14b}$$

$$\dot{q}_I = C\,(T_1 - T_2) \tag{14c}$$

In order that the relationship indicated by equation 13 be satisfied, the material constants ε, h, C of the model must have particular values, proportional to those of the prototype:

$$\frac{A_m \dot{q}_m}{A_p \dot{q}_p} = \frac{\varepsilon_m A_m}{\varepsilon_p A_p} = \frac{\varepsilon_m n^2}{\varepsilon_p} = n \qquad \text{Therefore } \varepsilon_m = \frac{\varepsilon_p}{n} \tag{15a}$$

$$\frac{A_m \dot{q}_m}{A_p \dot{q}_p} = \frac{h_m A_m}{h_p A_p} = \frac{h_m n^2}{h_p} = n \qquad \text{Therefore } h_m = \frac{h_p}{n} \tag{15b}$$

$$\frac{A_m \dot{q}_m}{A_p \dot{q}_p} = \frac{C_m A_m}{C_p A_p} = \frac{C_m n^2}{C_p} = n \qquad \text{Therefore } C_m = \frac{C_p}{n} \tag{15c}$$

Thus, with time scaling as n^2, which is obtained by considering the conductive heat transfer to be governing, it is required that the emissivity, the convective heating coefficient, and the joint conductance scale inversely with the geometric scale factor.

Re-examination of the heat balance equations by considering only radiation yields a different time scaling factor:

$$\rho V c_p \frac{dT}{d\tau} = F\varepsilon\sigma(T_1^4 - T_2^4) A_R$$

Utilizing the properties of homologous temperature distribution and material preservation, including $\varepsilon_m = \varepsilon_p$, a time scaling for a pure radiative process yields:

$$\frac{d\tau_m}{d\tau_p} = n$$

The natural convection within an enclosure of the vehicle is also a mode of heat transfer between elements. The convective heating coefficient is a function of wall geometry and temperature gradient between the air and wall and varies proportionally with the square root of pressure. The analyses performed for the two vehicles studied indicate that this natural convection is negligible in the overall heat transfer process. The use of either mission or laboratory

(1 atmosphere) pressure for half-scale models has been found to have an insignificant effect of the overall heat transfer process, similar to the full-scale complete vehicle conclusion discussed in Subsection 1.2.1.

The final heat transfer process to be considered is that of the interface conductance, which is dependent upon material hardness, surface roughness, surface flatness, joint contact pressures, and the presence of interstitial material. While the emissivity and convective heating coefficients may be predictably changed, the interface conductance in general cannot be knowingly adjusted. However, no great difficulties are expected; computer analysis of the Mach 3-4 vehicle wing cross section indicate that for the range of expected values of interface conductance, 500 to 5000 BTU/ft^2-sec., the effect on structural temperatures is negligible for both full and half-scale structures.

To summarize, Figure 38 illustrates the basic conflicts existing between the four heat transfer processes being considered. The fundamental differentiation between conduction and the other processes is that the reduction in the distance between the elements also enhances the conduction; that is, conduction is affected by all three dimensions, while the other processes are affected by area alone. Reducing the distance between elements does not enhance radiation, since it is a geometric function of the area only. Reducing the distance between the elements enhances the convective process somewhat but, as a rough approximation, it is also a function of the area only. Similarly, for a single value of interface conductance, C, the heat transfer rate is a function of area only. Therefore, under nominal conditions, model emissivity, convective heat transfer, and interface conductance are, for a half-scale model, only half what they should be when the time scale is predicted with conductive heat transfer; their respective coefficients require doubling over the value present in the prototype structure to be consistent with the conductive time scale factor.

Full-Scale

Conduction	Radiation	Convection	Interface conduction
Volume = V Area = A Dimension = L			
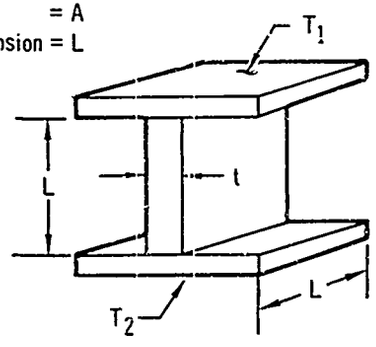	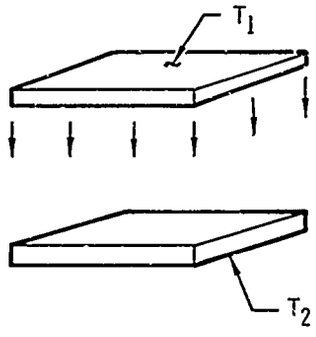	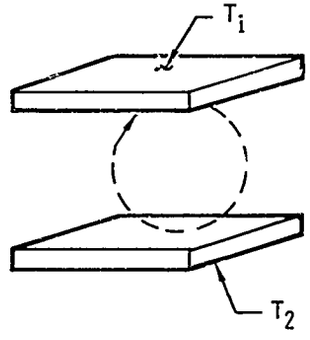	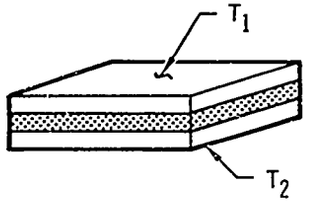
$\dot{q} = ktL\,(T_1 - T_2)/L = Kt\,(T_1 - T_2)$	$\dot{q} = \sigma\epsilon A(T_1^4 - T_2^4)$	$\dot{q} = h\,A\,(T_1 - T_2)$	$\dot{q} = CA\,(T_1 - T_2)$

Half-Scale

Volume = V/8 Area = A/4 Dimension = L/2			
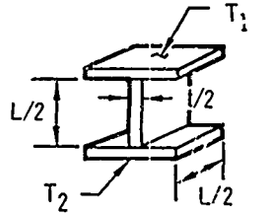	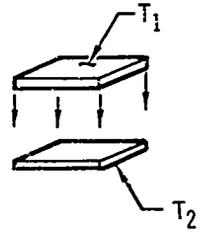	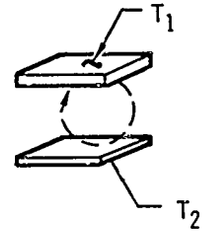	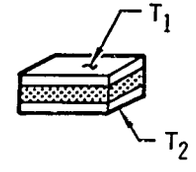
$\dot{q} = ktL/4\,(T_1 - T_2)/L/2 = Kt/2(T_1 - T_2)$ $= \frac{1}{2}\,\dot{q}$ (full-scale)	$\dot{q} = \sigma\epsilon\,A/4\,(T_1^4 - T_2^4)$ $= \frac{1}{4}\,\dot{q}$ (full-scale)	$\dot{q} \approx h\,A/4\,(T_1 - T_2)$ $\approx \frac{1}{2}\,\dot{q}$ (full-scale)	$\dot{q} = CA/4\,(T_1 - T_2)$ $= \frac{1}{4}\,\dot{q}$ (full-scale)

Note: $\dot{q}$ shown has units of heat transfer, BTU/sec.

Figure 38 — Effects of Scaling on Heat Transfer Processes

These modeling effects were studied in detail by analysis of a half-scale model of the wing cross section described in Subsection 1.2.1. Discrepancies between the full-scale and half-scale wing cross section temperatures occur primarily during the climb portion of the mission. After peak heating occurs, at the transition between climb and cruise, surface and near-surface structural temperatures during cruise quickly reach equilibrium, which reduces the differences between the prototype and the model results. Internal nodes of the half-scale model heat up and cool more slowly during transition periods, but steady-state temperatures in both the full-scale and half-scale structure were found to be nearly the same. The temperatures for node 70, shown in Figure 19, are of interest since they occur at the location which heats up more slowly than any other location. Nodes 90 and 111, whose temperature histories are shown in Figures 20 and 21, respectively, are of interest because they are located in regi is of maximum stresses. The time axis of these figures represent actual time for the full-scale structure and a scaled time, $\tau_m = 1/n^2\tau_p$, $\tau_m = 1/4\tau_p$, for the half-scale structure. Were all modes of heat transfer properly scaled, the temperature time histories for the full-scale prototype in actual time and the half-scale model in scaled time would coincide exactly. However, no attempt has been made to improve the scaling; rather, values for emissivity, interface conductance, and convective heating coefficients used for the half-scale model were those that would be obtained without intentional modifications.

1.3.1.2 Effects of Modeling on Strength Prediction - The purpose of this portion of the study is to evaluate the effect of modeling on:

(a) The capability to produce prototype thermal stresses in a structural model.

(b) The capability to demonstrate the ultimate strength of the prototype vehicle using a structural model.

Each is discussed in the following subsections.

1.3.1.2.1 Effect of Modeling on Thermal Stresses - Using the temperature distributions previously described, the thermal stresses for the wing cross section with the corrugated lower wing surface have been computed for a half-scale model. Figures 22 and 23 present the calculated thermal stresses in the wing structure at nodes 90 and 111, respectively. These nodal locations are shown in Figure 8. As described previously, node 90 is near the spanwise joint and is, therefore, in the area of maximum stress concentration; node 90 is at the location of maximum tensile thermal stress. Figures 22 and 23 indicate that the effects of scaling are not as large as those associated with changes in internal radiation. Figure 26 indicates the effect of emissivity on the maximum thermal stress achieved at node 111 for full-scale and half-scale cross sections. Variations of emissivity can therefore be expected to cause significant variations in thermal stress.

The effect of thermal stress upon ultimate strength is small, as shown in Figure 31; therefore, the variations in thermal stresses caused by modeling will not significantly affect ultimate strength verification.

The effects of other time scale factors were also investigated. In the modeling process previously described, the conductive heat transfer process was chosen to establish time scaling; this results in the choice of model time: $\tau_m = n^2\tau_p$. The radiative heat transfer time relationship is $\tau_m = n\tau_p$ for the case where the emissivity of the model is equal to that of the prototype. The radiative heat transfer model time could be matched to the conductive heat transfer model time by increasing the surface emissivity by a factor of $1/n$; however, this is not always possible. As shown in Figure 38, the effects of scaling on

both radiation and convection are approximately the same, and the time-scale relationship is $\tau_m = n\tau_p$. In a situation where both radiation and conduction are important, as is the case for the Mach 3-4 vehicle cross section, scaling might be more closely achieved by selecting an intermediate time scale factor:

$$n^2\tau_p \leq \tau_m \leq n\tau_p$$

for the 1/2 scale model,

$$1/4\tau_p \leq \tau_m \leq 1/2\tau_p$$

The temperatures and thermal stresses achieved at node 111 of the Mach 3-4 vehicle wing lower surface, calculated using a modified time factor of 1/3, are presented in Figures 39 and 40, respectively. Also shown in these figures are the temperatures and stresses for the full-scale cross section and the half-scale cross section using a time scale factor of 1/4 (the case if conductive heating determines the time scale factor). It can be seen that the stresses using a modified time factor of 1/3 match the full-scale cross section stresses closer than those for a time scale factor of 1/4. However, the selection of a single factor for a complete vehicle or component will be extremely difficult because the relative importance of radiation and conduction will vary from location to location in the structure.

1.3.1.2.2 Effect of Modeling on Ultimate Strength - As indicated in Table VI, the theoretical ultimate strength of a model, measured by its allowable stress, is equal to that of the prototype. This means that the theoretical strength of the model, measured in pounds, is n^2 that of the prototype; the theoretical bending strength of the model measured in inch-pounds is n^3 that of the prototype. This theoretical relationship is maintained for a wide range of construction techniques and loadings. Examples, other than those listed in Table VI, are compression or bending of monocoque or semi-monocoque cylinders, lateral pressure applied to spheres or spherical plates, torsion applied to

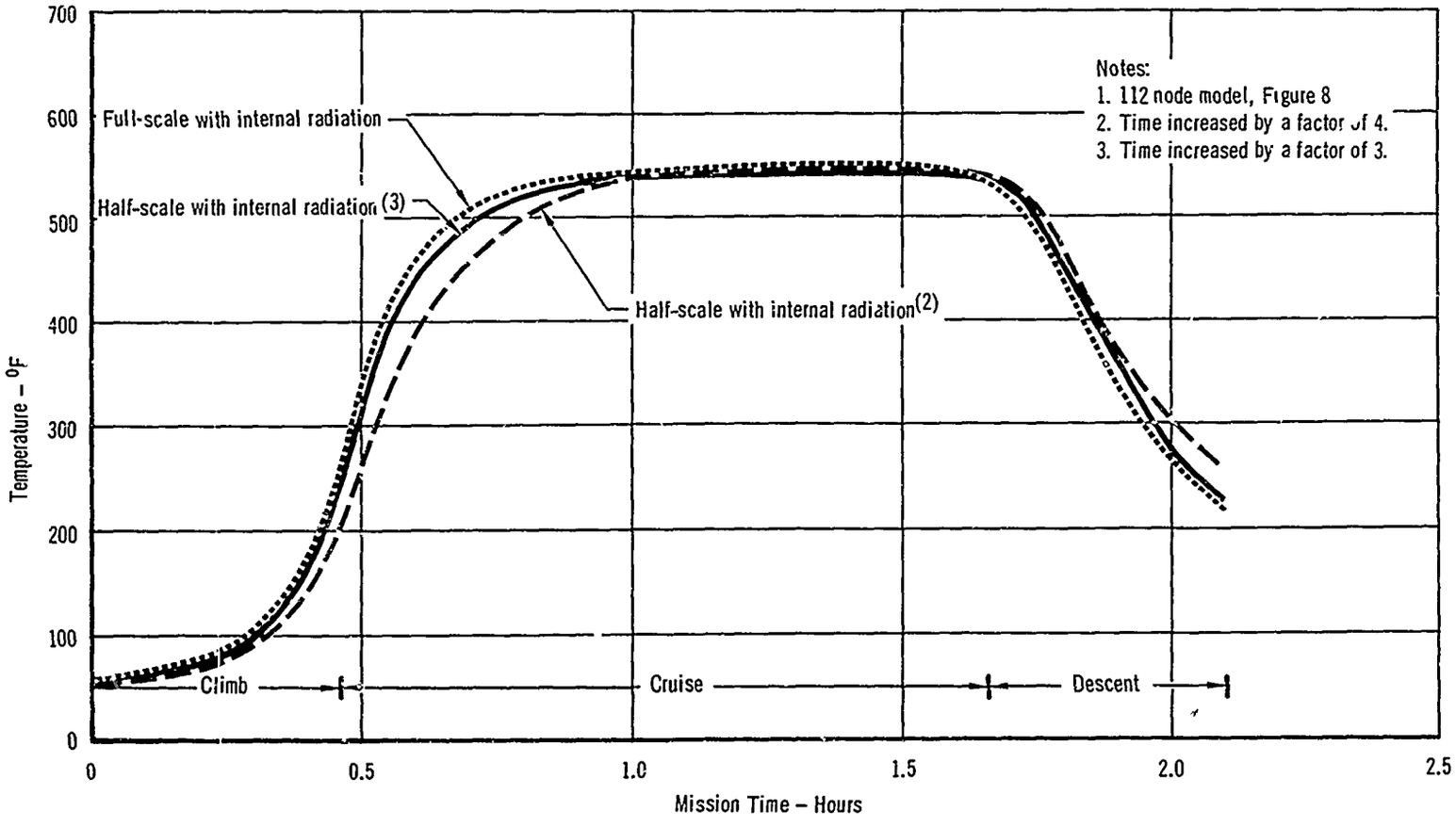

Figure 39 - Effect of Time Scale Factors on Temperature at Node 111 Mach 3-4 Vehicle

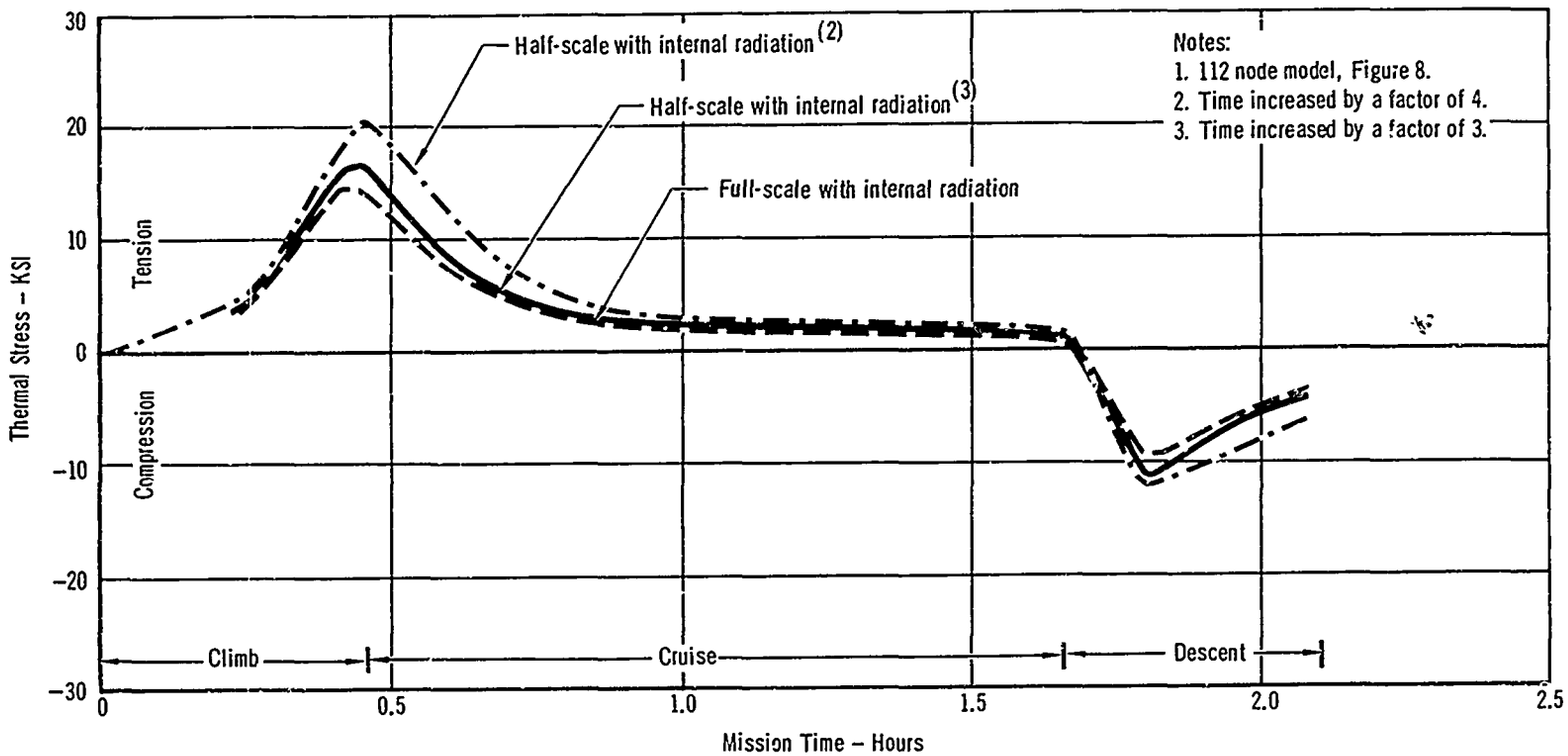

Figure 40 - Effect of Time Scale Factors on Spanwise Thermal Stress at Node 111

Mach 3-4 Vehicle

cylinders, and bending moments applied to multi-web or multi-post beams. In other words, the theoretical relationships have been found to be maintained for almost all arrangements of loading and configurations; a violation of these relationships has not been uncovered in this study. However, available test data indicate that these same relationships will not be completely maintained during testing.

Two areas where present data indicate that perfect modeling would not be attained are in material property size effects and in fastening size effects. The former effects are small; the latter can be significant.

For the expected range of model scale factor ($1/4 \leq n \leq 3/4$), the properties of the common materials are not largely affected by gage or thickness. In general, it can be expected that the model properties will be larger for metallic sheet materials. For example, the specified minimum value of F_{tu} (room temperature) for Ti-8Al-1Mo-1V is 130 ksi for sheet thicknesses greater than 0.188 inches thick and 133 ksi for sheet 0.020 to 0.187 inches thick, a difference of 2.25%. The size effects upon the strength of non-metallics may be much larger; especially when the minimum thickness of the non-metallic is approached. For instance, the manufacture of glass laminates thinner than 0.030 inch having prototype material properties will be difficult, and a model with smaller thickness will usually exhibit less strength than the prototype.

Test data indicate the scaled strength of a bolted, bonded, riveted, or welded joint can be expected to be somewhat greater than the prototype joint; however, this difference for bolted or riveted joints is not expected to be very large. For example, the results of tests on a simple bolted lap shear joint, reported in Section VII, indicated that the failing stress of the full-scale specimen was 0.7% larger than that of the half-scale specimen. In this test, the prototype and model were fabricated from the same sheet stock;

if they were fabricated from sheet gage equal to their thickness, the model would be expected to exhibit greater strength. The model/prototype strength ratio of spot-welds in titanium sheet, however, is an example of a larger variation. Tests have indicated that for most gages, a half-scale model exhibits a greater scaled strength than the prototype by as much as 50%. However, by modification of welding technique, this variation could be reduced. The strength of bonded or continuous welded (e.g. butt-welded) joints would not be expected to exhibit variations of this magnitude.

It has been found that honeycomb construction also would be expected to exhibit non-scaled model strength; in general, the model strength is greater than that of the prototype. For example, while the shear strength for the ribbon direction of 3/8" core - .005 foil - formed of 5052 aluminum alloy is 560 psi, the strength of 3/16" core - .0025 foil of the same material is 600 psi, a difference of about 7%. This trend is reversed as the minimum available foil thickness is approached.

It has been concluded, that although modeling strength will not exactly scale, the scaling error will generally be less than 10%, the error will be predictable, and inaccuracies in thermal stresses caused by modeling do not significantly affect ultimate strength. This leads to the further conclusion that ultimate strength verification of the Mach 3-4 vehicle can be satisfactorily demonstrated by the use of structural models.

1.3.2 Test Facility Analysis - As described in Subsection 1.3.1, while the temperatures and the stress levels in a model of scale factor n must be the same as those in the prototype, the heating and cooling rates are increased by a factor of 1/n. The increase in required heating and cooling rates is expected to result in an increase of the local temperature error, and proper local temperature control on the model surface will be more difficult than on the full-scale complete vehicle. Thus, it is judged that a model will require

more temperature control zones than the prototype vehicle, and not only will there be no savings in quantity of control equipment, but the response time of the control equipment will be less than that for the prototype due to the time scaling factor, n^2.

The similitude laws indicate a reduction of total energy required by a factor of n^3; however, the peak power requirements for the scale model are reduced by only a factor of approximately n times that required for the prototype because of a 1/n scaling increase in heat flux over a test area reduced by a factor of n^2. Because the test systems must be designed to deliver the peak instantaneous demands, the capacity of the power sources for model testing must be approximately n times as large as those required for prototype testing. Since the test systems operate at higher flux levels, their reliability will be diminished.

Heating lamp arrangement has only one degree of freedom, that of spacing, which is inversely proportional to the required heating rate; the effect of specimen to lamp distance is secondary. While the heating rate is scaled by 1/n, the model test lamp spacing must be n times the prototype test lamp spacing over an area n^2 that of the prototype, which results in a total lamp quantity requirement for the model test of n times that for the prototype test.

The results of the detailed analysis of the testing requirements for the Mach 3-4 vehicle are presented in Table V.

1.3.3 Cost Analysis - In contrast to the other testing approaches, engineering design of the model test specimen will require substantial effort. The cost for engineering design includes drawing preparation and, more importantly, the myriad of detail design analysis required by the scaling process; a photograph reduction of the prototype drawings will not be possible or correct. Instead, many engineering tradeoff decisions will be necessary. For example,

the selection of tolerances and surface finish, the choice of a scaled forging or its duplicate in machined form, the determination of welding techniques to obtain scaled strength, and replacement of non-scalable mechanical fasteners with equivalent strength fasteners, will all require resolution. It has been estimated that the cost of the engineering design for the half-scale complete vehicle will be somewhat greater than the sum of the design and fabrication costs for the room temperature test jig. Because of the reduced size, weight, and applied loads, these latter costs are less than for the full-scale complete vehicle test.

The major cost for the half-scale test will be for the tooling required for fabrication of the test specimen. The prototype tooling costs can be prorated over many vehicles; therefore, the prototype design can include manufacturing techniques requiring quite expensive tooling; some of these same techniques are also expected to be required for the model. Although the model tooling need be used only a few times, the cost is still a large fraction of the prototype tooling costs. The fabrication cost will be less for the half-scale model than for the prototype because of reduced size. The large tooling cost for the model causes this technique to be the most expensive of the various approaches. The man-hour cost factors and dollar cost factors for this technique are summarized in Figures 36 and 37.

1.3.4 Conclusions

(a) Fabrication feasibility dictates that scale factors of 1/4, 1/2, or 3/4 be considered for structural verification models, with 1/2 appearing most usable. Other scale factors would require greater use of non-standard hardware or larger deviations from scaled geometry, which would increase the modeling effects on ultimate strength of the specimen or greatly increase procurement costs.

(b) Of all the factors known to be not scalable thermally (radiation, interface conductance, etc.), radiation is of greatest importance for the structures considered.

(c) Using the time scale factor dictated by conductive heat transfer, the thermal stresses in a model tend to be greater than for full-scale structures due to the effects of internal radiation which dictate a different time scale factor.

(d) It is possible to more closely duplicate thermal stresses in a model by the use of a time scale factor somewhere between the values dictated by conductive and radiative heat transfer modes.

(e) Structural models appear satisfactory for the ultimate strength verification of the Mach 3-4 vehicle, the degree of thermal stress simulation having a relatively minor effect in this case.

(f) Although model strength will not scale exactly, the scaling error will be less than 10% and will generally be predictable.

(g) The increased heating and cooling rate requirements in comparison with the prototype test article make the proper temperature control of the model surface more difficult.

(h) Serious drawbacks to the model approaches are the cost of tooling for fabrication of a satisfactory structural model and the engineering effort required to complete model drawings.

1.4 Component Testing

1.4.1 Engineering Analysis - Economics of construction, space, and time, as well as power required for heating and cooling, may be achieved in the laboratory testing of a structure if a small portion or component of the vehicle can be tested separately in a meaningful manner. A theoretical investigation was performed to determine the length of component and heated section required

for a test specimen in which complete vehicle mission temperatures and stresses are duplicated.

A mathematical idealization of a component of the wing cross section was developed to determine the effects of spanwise temperature gradients and stress variations on the ability to achieve mission temperatures and stresses within the structure. This idealization consists of six adjacent chordwise cross sections at one foot spacing which, because of symmetry, actually represents 12 adjacent sections in a component of 12 feet as shown in Figure 41. The cross section nodal numbering system used is indicated in Figure 42. Analytical behavior of each section must be similar to that of the original 112 node idealization, if meaningful data for direct comparison to prior analysis is to be attained. However, computer memory size necessitated a reduction in the number of nodes per cross section down to 22 nodes, accomplished through grouping adjoining nodes of the 112 node model which experience like temperature histories during a typical mission, as shown in Figure 42. Similar to other previously described analyses, a single node in each cross section represents the enclosed air. Two nodes in each adjacent section were used as the upper wing and lower wing surface control nodes for the 22 node model; the temperatures at these nodes were made to follow the temperature-time profiles of Figure 10. An emissivity of .66 was used. Previous analysis on the 112 node model indicated the insignificant role of changes in interface conductance; hence perfect interface conductance was assumed in the 22 node model. The degree to which the 22 node model approximated the 112 node wing box cross section is shown by the temperature-time agreement at the node of maximum thermal stress, nodes 11 and 111, respectively, shown in Figure 43. From these data, it may be concluded that the 22 node model is sufficiently similar to the 112 node model for analysis purposes.

Cross Section	Nodes
1	1–22
2	23–44
3	45–66
4	67–88
5	89–110
6	111–132

Notes: (1) Net heat flux across this plane assumed zero.
(2) No heat transfer across this boundary.
(3) ¼ inch thick titanium alloy end plate. (nodes 133–138)

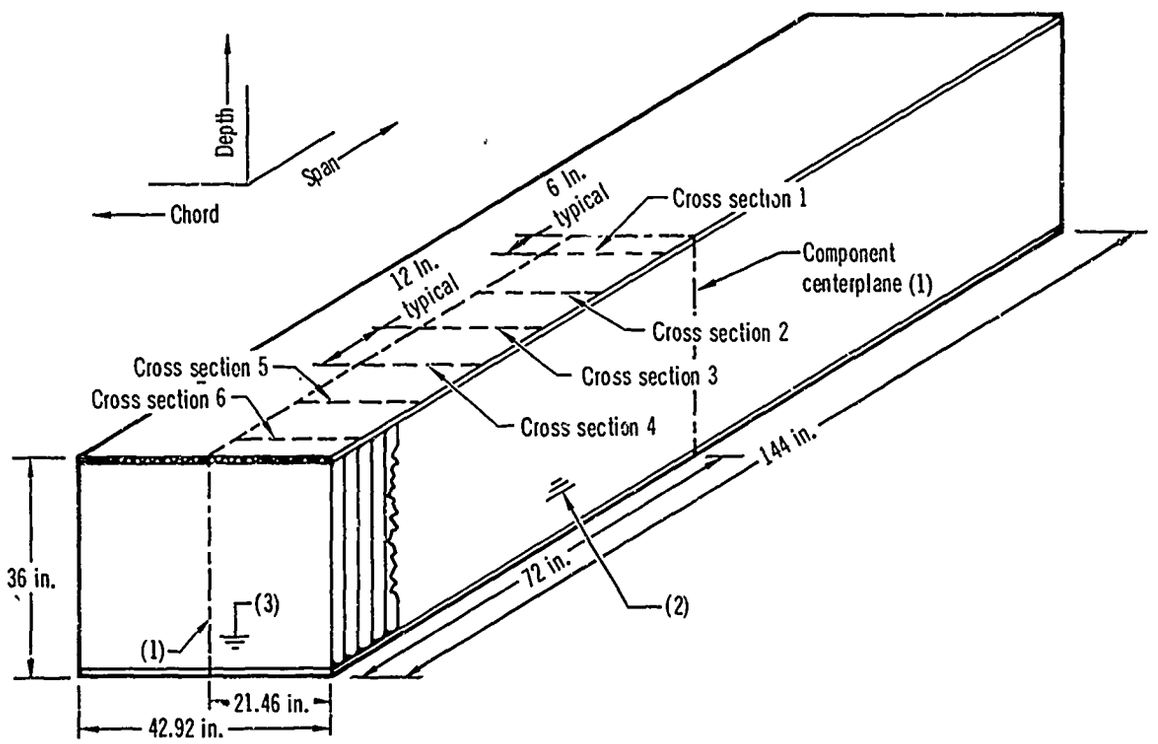

Figure 41 - Wing-Box Component Idealization
Mach 3-4 Vehicle

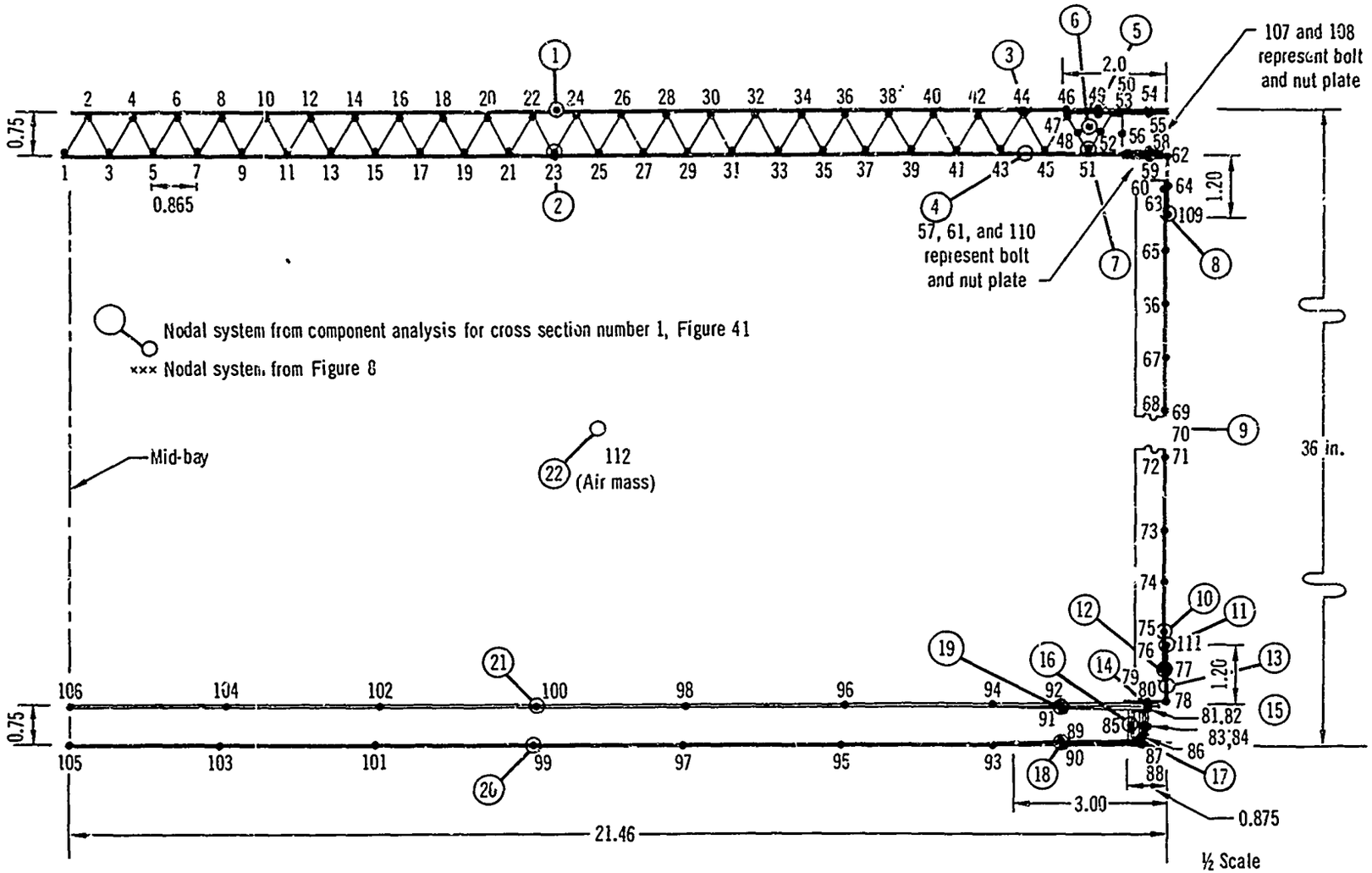

Figure 42 - Component Cross Section Nodal Numbering System Mach 3-4 Vehicle

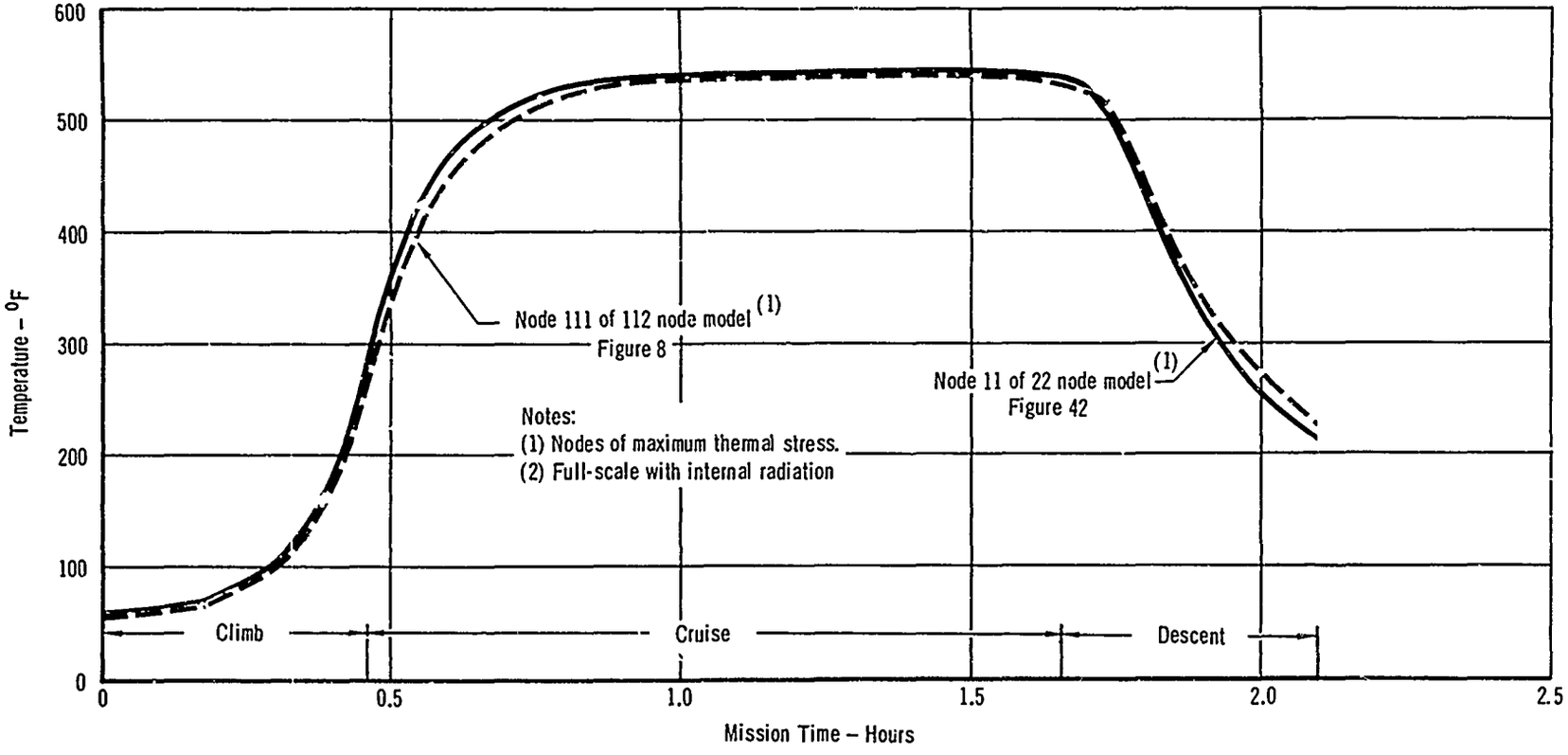

Figure 43 - Comparison of Corresponding Temperatures for 112 Node Wing Cross Section and 22 Node Component
Mach 3-4 Vehicle

The component idealization was completed by including the effect of a titanium alloy end plate idealized into six nodes; hence, the total component includes 138 nodes. Because of symmetry, this idealization represented one quadrant of the entire component. The nodal numbering sequence for adjacent component cross sections is obtainable by adding 22, 44, 66, . . . to the corresponding node number in the first section. Analyses of this idealization included investigations of the effect of internal radiation within the cross section and the effects of heating various lengths of the component. The external surfaces of the unheated portions were assumed to be insulated.

The temperature distribution along the inner end of the spar web attachment tee at the time of peak heating (mission time = .46 hours) is presented in Figure 44 for various heated lengths of the component. This location is the point of maximum thermal stress within the cross section. The uppermost curve represents the temperature developed in an infinitely long component and is the same as shown in Figure 39 for the full-scale complete vehicle analysis with internal radiation and at mission time = .46 hours. All other curves represent spanwise temperature distributions for the same location within each cross section in the 12 foot component. Heating 12, 10, 8, 6, 4, and 2 sections of the 12 section component resulted in a companion decrease in the temperature at this node.

Figure 45 presents the temperature distributions for a component in which three sections are heated with and without the effects of internal radiation; the relative ease in obtaining a suitable "test section" when there is no internal radiation is apparent in the same figure. Because heat is transferred between adjacent layers only by conduction in this case, relatively little heat is dissipated to the externally unheated section, resulting in a uniform temperature over almost all of the heated length. In contrast, a greater percentage

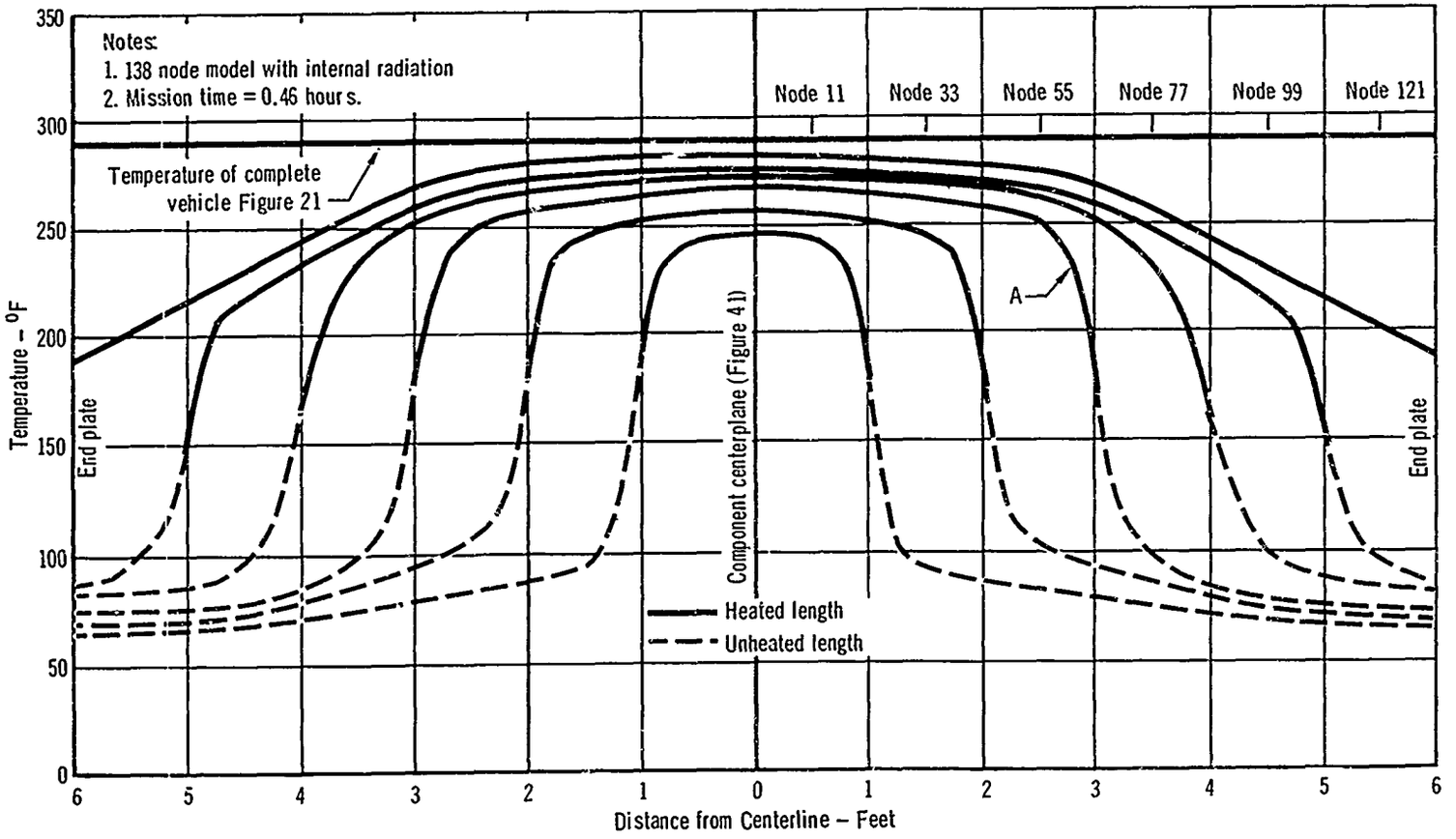

Figure 44 - Component Temperature at Node 111 for Various Heated Lengths Mach 3-4 Vehicle

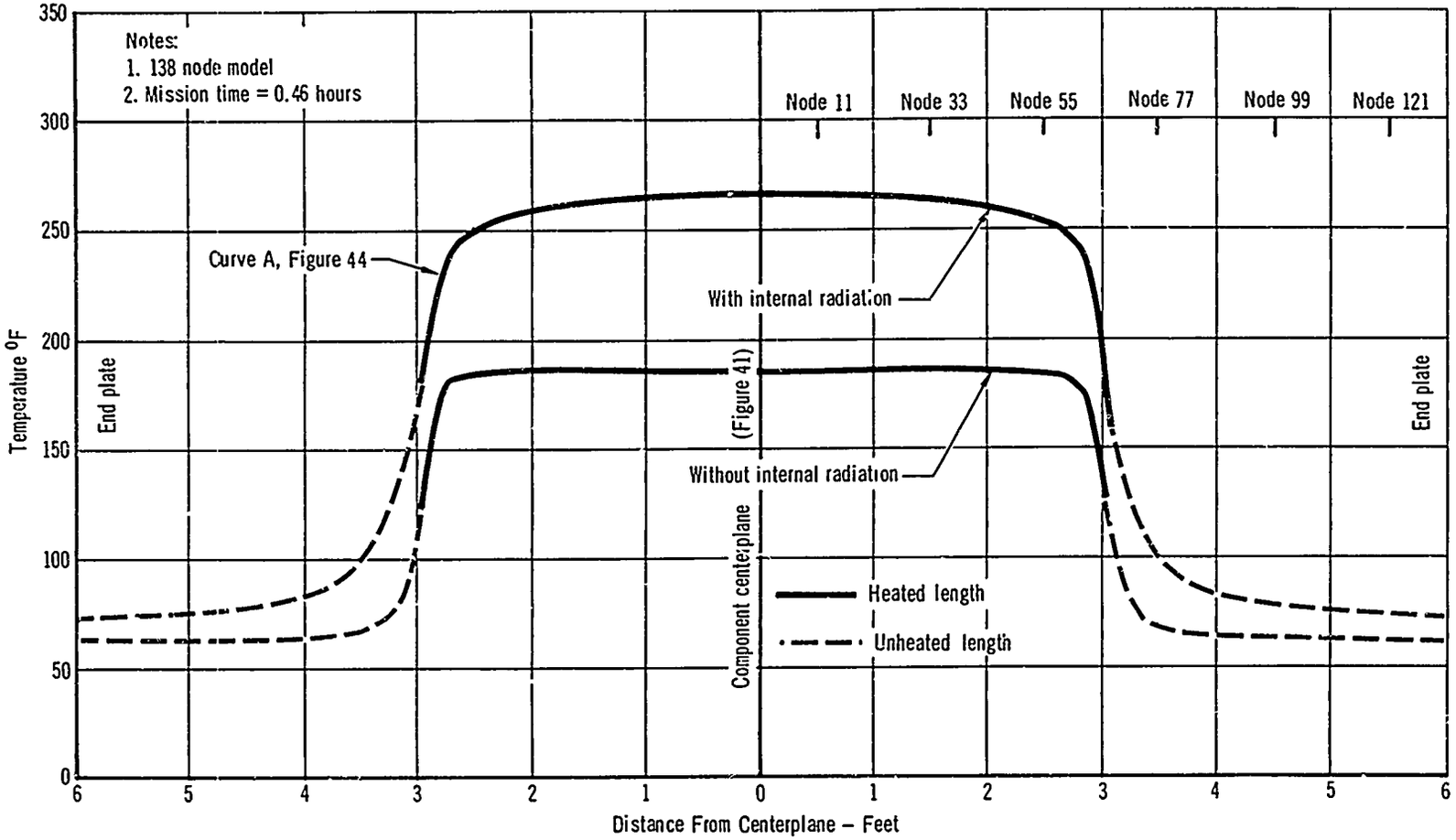

Figure 45 - Effect of Internal Radiation on Component Spanwise Temperature Distribution at Node 111 Mach 3-4 Vehicle

of heat is transferred to the remote unheated areas when internal radiation is included which results in a less uniform temperature distribution. Also, in a finite length component, structural temperatures were found to be lower near the end of the component because of the relative massiveness (heat sink effect) of the assumed end plates. As to be expected, this investigation indicated that the greater the surface heated, the closer the agreement between the temperatures developed in the infinitely long component and the temperatures developed in the test section.

Figure 46 shows the effect of internal radiation on thermal stresses at the nodes of maximum thermal stress when three cross sections of the component are heated. It is apparent from this figure that within the heated areas of the component, the component thermal stresses nearly duplicate those which would be developed in a totally-heated infinite length component. Figure 47 presents the thermal stress variation with time when three cross sections are heated and internal radiation is considered. This corresponds to the same case that was presented in Figure 46 and indicates that the thermal stresses developed in the unheated areas of the component are insignificant.

Temperature distributions in components of the type studied have been found to cause component thermal stresses that are larger than those in the prototype due to the increased thermal gradients. Figure 48 presents component thermal stresses for various heated lengths, computed by not considering structural boundary condition effects and by using the temperature distributions discussed previously. It can be seen that the stresses in a large portion of the component structure are larger than in the prototype.

The development of prototype temperature distributions within a component does not assure the development of prototype thermal stresses; for example, a finite length of the wing cross section is required to exactly reproduce prototype

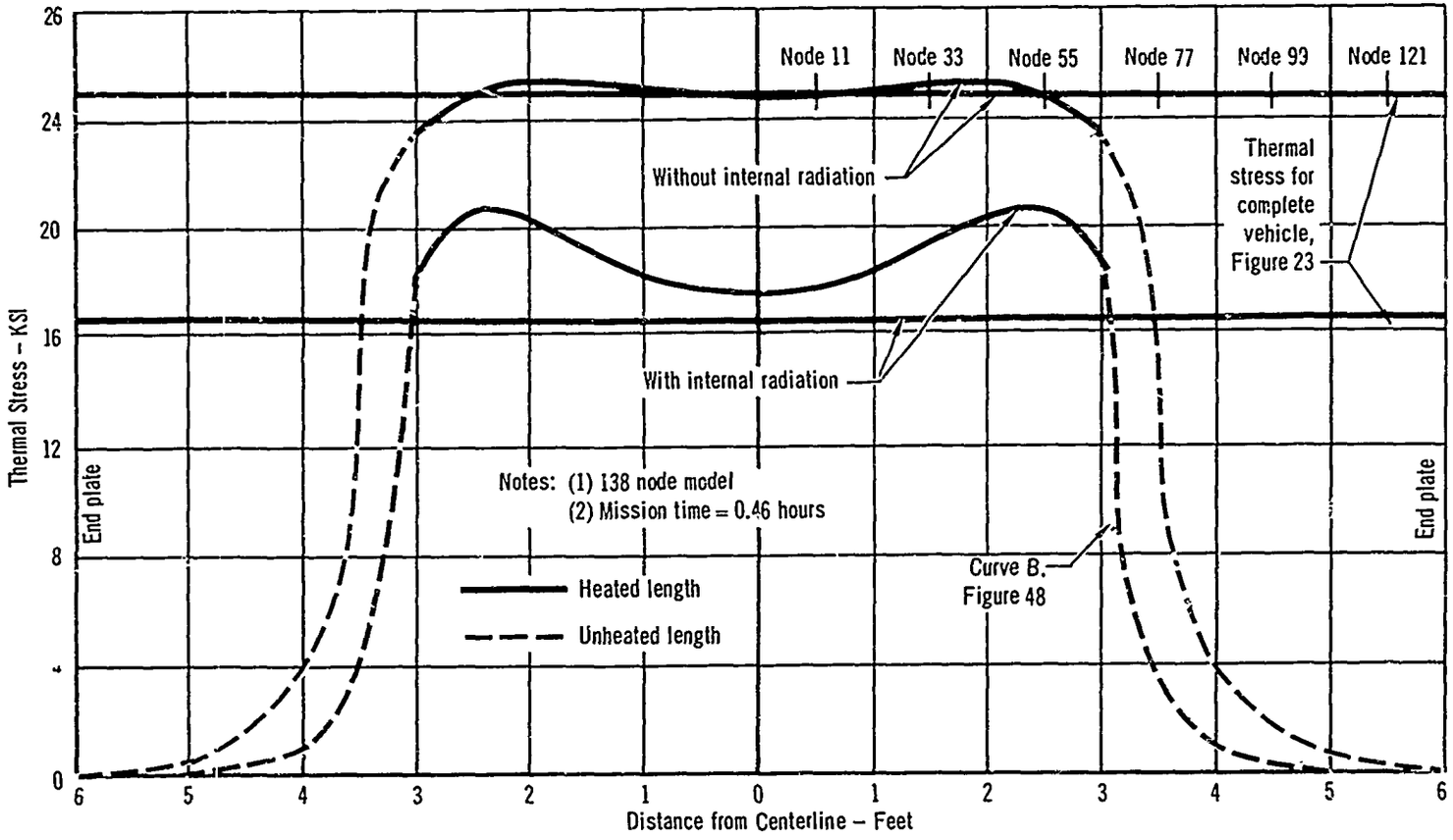

Figure 46 - Effect of Internal Radiation on Component Spanwise Thermal Stress Distribution at Node 111 Mach 3-4 Vehicle

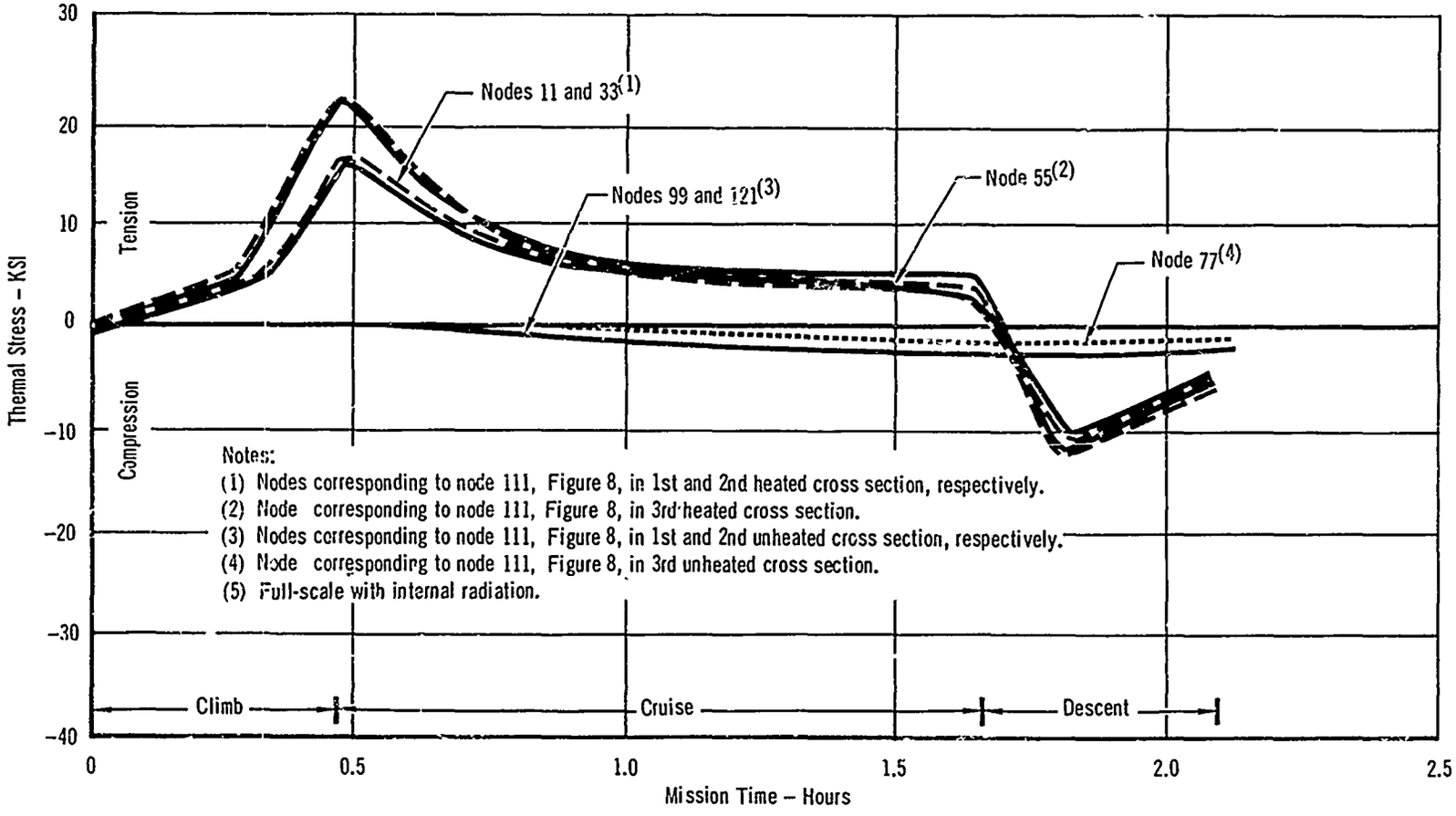

Figure 47 - Component Spanwise Thermal Stress Variation With Time Mach 3-4 Vehicle

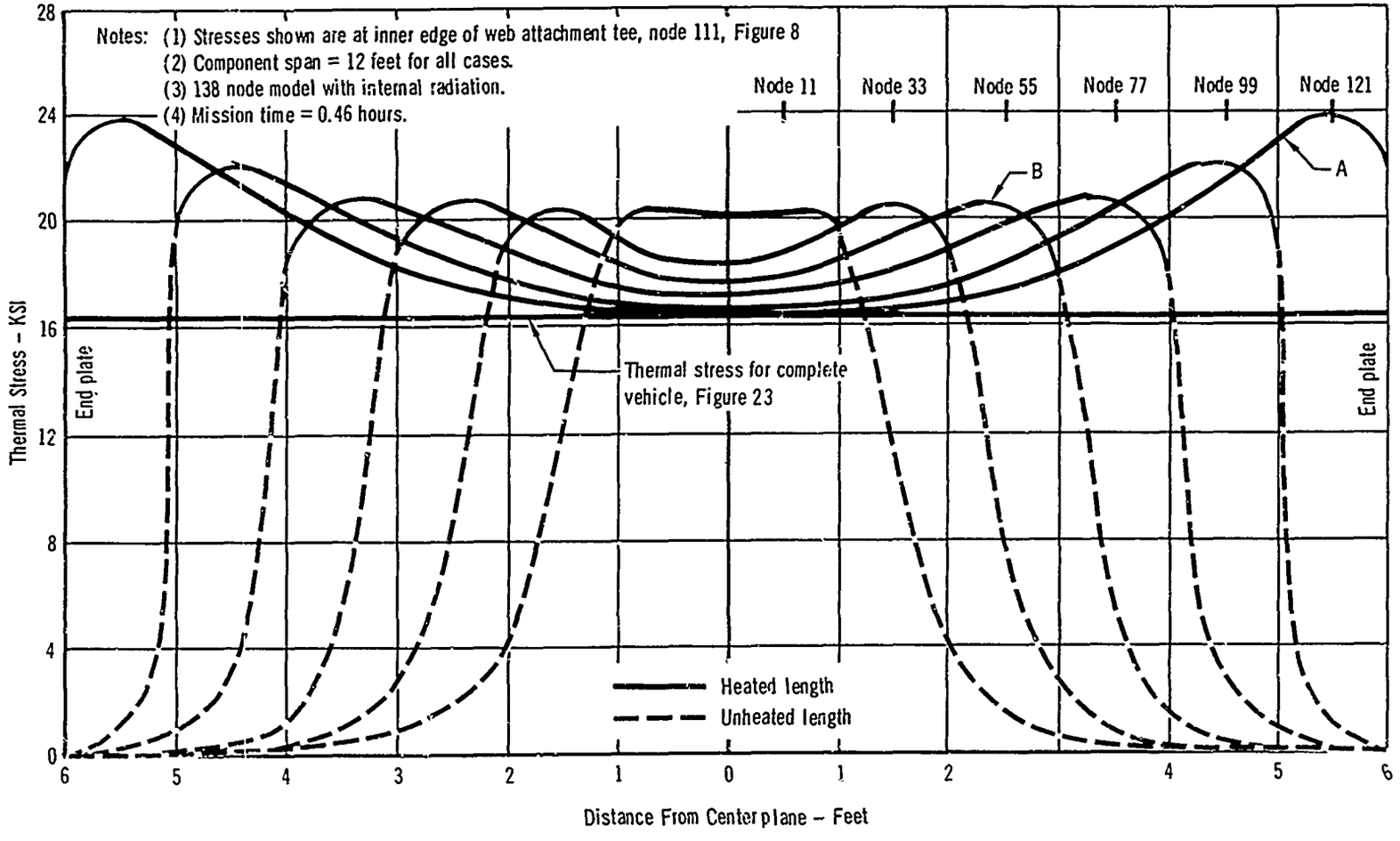

Figure 48 - Component Maximum Thermal Stress for Various Heated Lengths Mach 3-4 Vehicle

thermal stresses because of the structural boundary conditions, i.e., the "shear lag" effect. The results of an analysis of this effect for the inner end of the spar web attachment tee are presented in Figure 49 where the ratio of the stress that would be developed in a component of finite length to the stress that would be developed in the complete vehicle is indicated. It was assumed in this analysis that complete vehicle temperature distributions are maintained throughout the component. This shear lag effect reduces the increase in thermal stresses due to the higher thermal gradients developed in the component.

An estimate of the combined effects of thermal and structural boundary conditions when all cross sections of the component are heated is shown in Figure 50. This figure indicates that the combined effects are expected to cause a thermal stress at the inner end of the web attachment tee and the component centerplane slightly greater than that developed in the prototype. A tradeoff between excessive stresses and higher costs would be used in the practical case to determine the optimum size of the component to be heated. For the particular component considered, direct heating of 6 feet of the 12 foot length appears satisfactory for producing suitably accurate thermal stresses in a component of reasonable size; this results in a test section of approximately 4 feet. Heating a smaller section produces higher than desired thermal stresses, while the heating of larger sections may prove unduly costly without a commensurate increase in test accuracy.

As in the modeling approach, it is concluded that the reproduction of prototype thermal stresses in a component is sufficiently accurate to allow the satisfactory demonstration of ultimate strength by the use of the component approach.

In the component verification testing approach, two different types of components are considered; those of small size to determine the structural

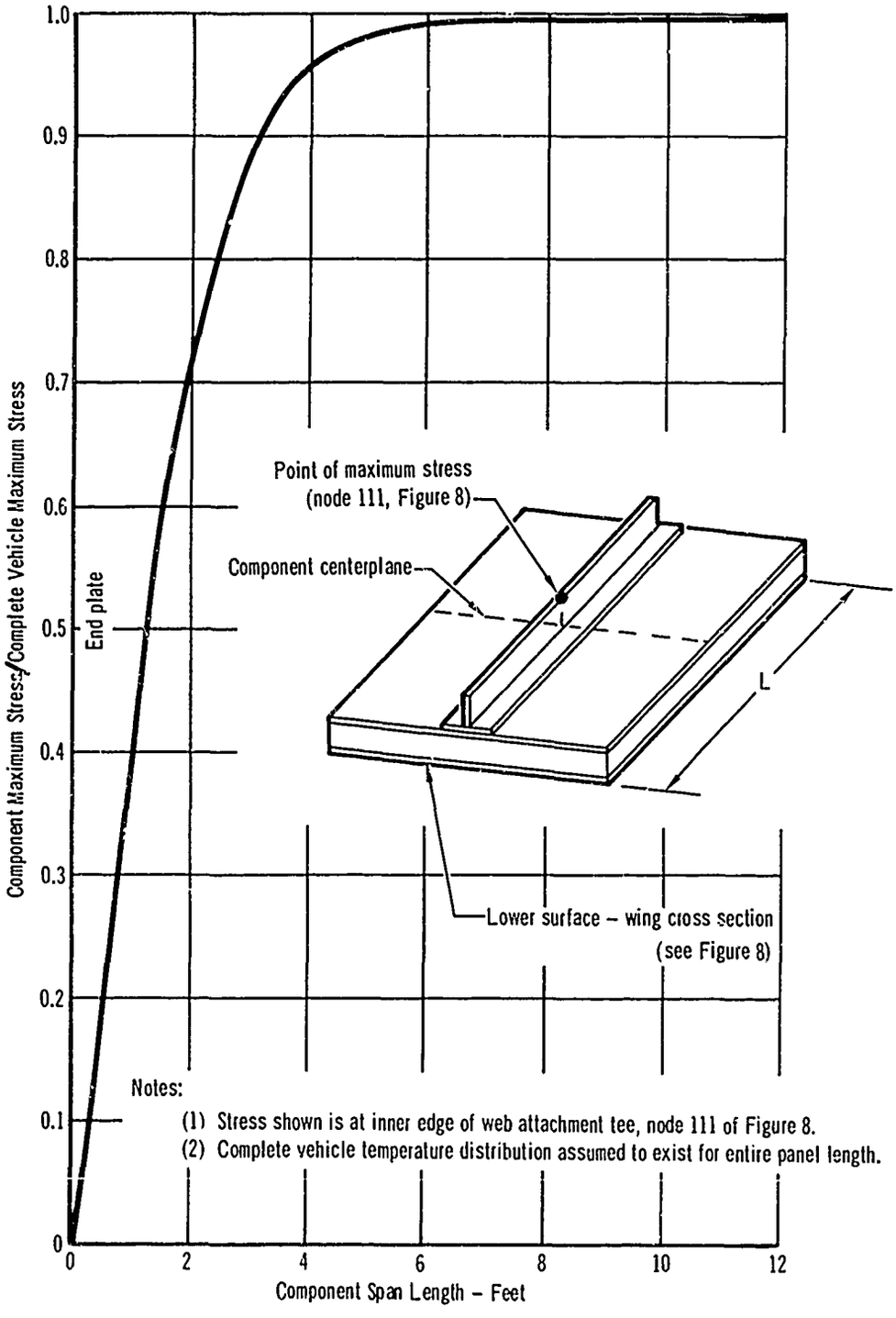

Figure 49 - Effect of Component Span Length on Maximum Spanwise Thermal Stress Mach 3-4 Vehicle

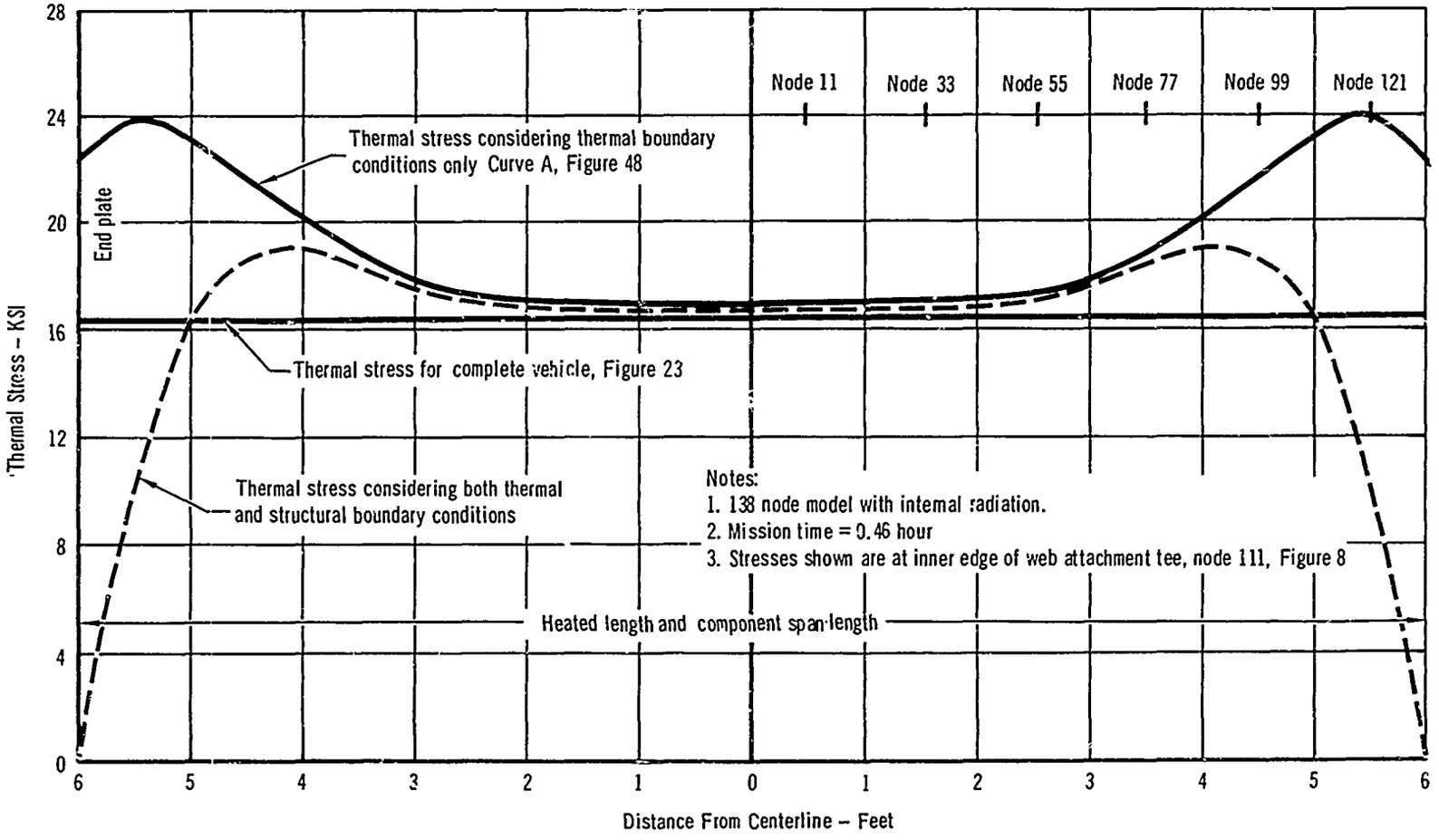

Figure 50 - Effect of Thermal and Structural Boundary Conditions on Component Spanwise Thermal Stress Distribution

Mach 3-4 Vehicle

characteristics of a local area, once a critical section is located, and larger components whose purpose it is to evaluate the structural performance of a major portion of the structure or to reliably locate critical areas. Presented in Figure 51 are the small size components; their total planform area is 65% of the total planform area. The large size components are, on the average, 50% larger in gross size and 4 to 5 times larger in test area size than the components presented in Figure 51, so as to permit the demonstration of the strength characteristics of the complete vehicle.

1.4.2 Test Facility Analysis - The use of components for verification testing will reduce the peak power required and the number of loads applied. By using components, there is a great reduction in the number of test control systems required for any specific test. Another benefit of component testing is the reduction of test complexity, which in turn reduces the probability of a system failure that would cause a premature failure of the test specimen. The component technique requires the jig structure to provide reactions for the applied loads and simulation of prototype stiffness at the component boundary. Also, the use of several components rather than a single complete vehicle test will require more jig design engineering and fabrication man-hours per square foot of area.

The component approach, as applied in the test facility analysis, utilizes the small size components described in the previous subsection. The reduction of area allows a proportionate decrease in total power, cooling, control channel, and instrumentation requirements, as shown in Table V.

1.4.3 Cost Analysis - Engineering design costs have been found to be relatively unimportant in the component approach. Prototype design costs are not applicable, and although the selection of component boundaries and analysis of boundary conditions will require engineering effort, these costs have been

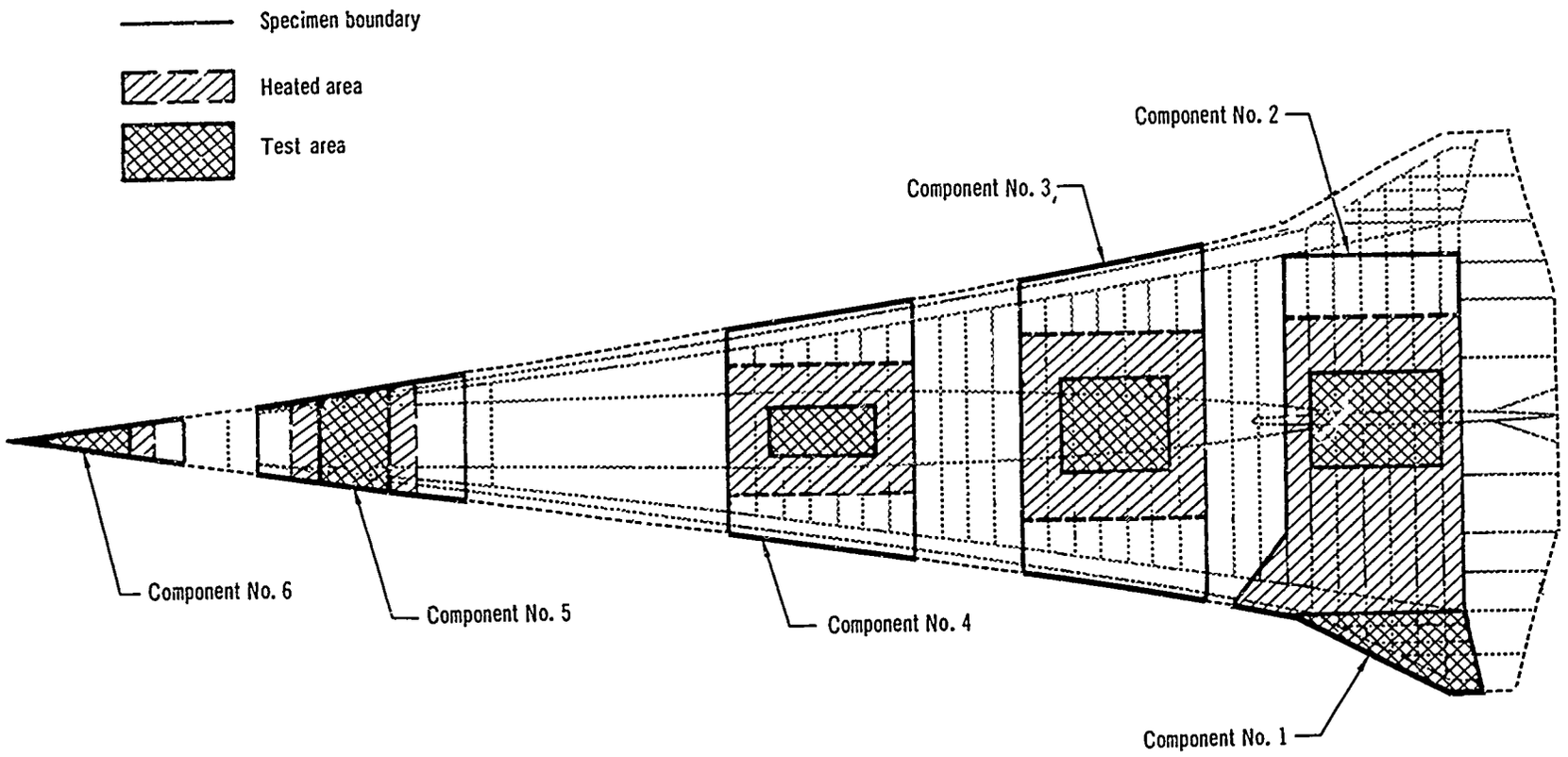

Figure 51 - Small-size Components
Mach 3-4 Vehicle

found to be relatively small. Similarly, the costs of tooling were not significant. Specimen fabrication costs were found to be approximately proportional to the total weight of structure to be fabricated.

Laboratory costs have been determined to be approximately the same for the six components shown in Figure 51 as for the full-scale complete vehicle test, even though the total component area is smaller. This results from the necessity of designing and fabricating several test set-ups, rather than one large one. The results of the cost analysis for the ultimate strength testing of the components shown in Figure 51 for the Mach 3-4 vehicle are presented in Figures 36 and 37. The results of the cost analysis for the ultimate strength testing of large size components are incorporated in the combination testing approach presented in Section VIII.3.

1.4.4 Conclusions

(a) Components for elevated temperature tests become larger than would be anticipated for load application only, because of the requirement for providing suitable thermal boundary conditions. The benefits are the savings of heating rate required at any instant, the reduction in physical size of the test facility, and the capability to use more than one facility at a time.

(b) The presence of internal radiation within a component will generally cause thermal gradients larger than those present in the prototype.

(c) The maximum thermal stresses developed within a component may be larger than in the prototype because of the larger gradients usually present.

(d) The testing costs per square foot of total specimen area will be greater for the component testing approach in comparison to the complete vehicle testing approach due to the additional costs

associated with the design and fabrication of several test set-ups in the component approach.

(e) Components appear satisfactory for ultimate strength verification, since the degree of success associated with the simulation of temperatures and thermal stresses has a relatively minor effect on the ultimate strength of the test article.

1.5 Mechanical Simulation

1.5.1 Engineering Analysis - The primary effects of elevated temperature on structural behavior include:

(a) Material property degradation; this degradation will vary through the cross section because of the temperature variation

(b) The development of thermal stresses and the reduction of stiffness; including the associated reduction of allowable buckling and crippling loads

(c) A change in the shape of the stress-strain curve, causing a modification of the inelastic stress-strain relationships; that is, a change in the F_{cy}/F_{ty} and F_{cy}/E ratios

In the mechanical simulation approach for ultimate strength verification, the testing is performed at room temperature or at some reduced elevated temperature without attempting to duplicate transient temperatures and thermal gradients, but to create the three effects described above by mechanical means. The test loads are increased to account for the above temperature effects but the amount of load increase required is always an area of question in the mechanical simulation approach. The modification of loads can be accomplished in several ways; for example, one method would consist of a simple factoring of material properties at room and elevated temperature. The choice of a simple technique that could readily be understood may be either conservative or

unconservative. An unconservative simple technique using a material property reduction factor coupled with axial stiffness factor where $\Sigma E_n A_n$ is compared at room and elevated temperature is presented in Reference 5. Other simple techniques will usually be conservative or overly conservative. If the load increase required for room temperature testing is based on a detailed analysis, the analysis must be performed twice, once for room temperature and once for elevated temperature. The ratio of the computed failing loads may then be used to determine the applied loads in the room temperature test. In order for this general approach to be accurate, the location and mode of failure must be defined for both room and elevated temperature testing. For example, the computed room/elevated temperature strength ratios for crippling and panel buckling for the upper wing surface are 1.37 and 1.15, respectively, and can be determined from the data presented in Figure 31. Therefore, in the mechanical simulation approach, the applied loads would be increased by 37% if crippling is the basic mode of failure; or by 15% if overall panel buckling is the basic mode of failure. Although the panel buckling allowable, by definition, cannot exceed the crippling allowable, modification of the panel geometry could make it approach the crippling allowable. If such a modification in panel geometry were made, the loads to be applied in a room temperature test would be computed as being 37% greater than those at elevated temperature. Therefore, the mode of failure influences the load ratio to be applied and only a post failure analysis would establish the accuracy of the preselected applied load ratio.

An investigation of this type is described in Reference 5. In that study, only moderate temperature effects on structural elements in a steady-state-temperature condition were considered. The results indicated that this method might be confidently used for ultimate strength verification in the temperature ranges considered.

It is also theoretically possible to simulate a portion of the induced thermal stresses by mechanical loadings without the application of complete temperature distributions. This simulation might be used with some upward adjustment of the magnitude of the applied loads as previously indicated.

One of the inherent limitations of this latter approach is the relatively small number of locations where the stress levels prevailing in the prototype can be reproduced in the specimen. For instance, before the exact thermal stress distribution existing in the prototype can be mechanically applied to a portion of the prototype, all of the structural redundancies inherent in that portion of the structure must be removed. When the removal of these redundancies is not accomplished, the thermal stress distribution is only approximated by the application of mechanical loads. For example, the maximum thermal stress in the wing cross section studied (Figure 8) is at node 111, and for the full-scale wing cross section, this stress was determined to be 16,800 psi tension. The largest compressive stress occurs on the outside surface, node 90, and is 6700 psi. The room temperature application of a bending moment to the cross section that would produce 16,800 psi tension at node 111 would produce 18,300 psi tension at the outside surface. The error in the thermal stress at the outside surface is, therefore, 25,000 psi; the mechanical simulation of thermal stresses is obviously inadequate and virtually impossible in this case.

A considerable measure of engineering judgment is required to select the size and define the completeness of the portion of the vehicle to be tested. Also, considerable judgment is required to select the locations where complete simulation is necessary and to evaluate the effect of simulation errors at other locations. Generally, the technique of applied load augmentation, as discussed previously, is more practicable than direct mechanical simulation of thermal stresses.

Mechanical simulation may be used with any of the specimen types considered (complete vehicle, models, or components) at either room or constant elevated temperature. The combination of mission profile temperature and mechanical simulation defeats the purpose of mechanical simulation and even the combination of constant elevated temperature and mechanical simulation is somewhat incompatible, because the addition of control devices to allow the duplication of transient temperatures is relatively inexpensive in comparison to the original installation of the heating system. Therefore, the most profitable use of mechanical simulation appears to be at room temperature.

1.5.2 Test Facility Analysis - The test facility requirements for the mechanical simulation approach are basically the same as for either the room or constant elevated temperature test of the complete vehicle, model, or components, as appropriate. The use of the mechanical simulation approach simplifies the test procedure, since the heating system is either not required or need not be integrated with the loading system. If the mechanical simulation of thermal stresses is attempted, the loading system will be somewhat more complex. However, in general, this will not affect the total facility requirements. The requirements for testing using mechanical simulation can be determined from Table V for the choice of vehicle type and temperature, room or constant elevated.

1.5.3 Cost Analysis - Engineering design costs are unimportant in this approach, except for the previously discussed cost of designing a half-scale model, if that choice of vehicle type is utilized. The selection of augmented loads, the choice of areas of mechanical simulation of thermal stress, and the additional analysis required to determine ultimate strengths in both design and test conditions will require significant additional engineering effort; however, relative to the total test costs for the Mach 3-4 vehicle, the cost of this

engineering effort is relatively unimportant. The costs for testing using mechanical simulation are approximately the same for a given vehicle whether tested at room temperature or a constant elevated temperature.

1.5.4 Conclusions

(a) One inherent limitation of the approach to simulate induced thermal stresses by mechanical loadings is the relatively small number of locations where the prototype stress levels can be duplicated; this limitation lowers the level of confidence associated with the mechanical simulation approach.

(b) Increases in applied loads to account for thermal effects appears the most practicable version of the mechanical simulation approach.

(c) By definition, tests in which the thermal effects are simulated by mechanical means cannot be expected to produce any thermal effect that cannot be predicted analytically.

(d) Mechanical simulation is not a satisfactory approach to strength verification of the Mach 3-4 vehicle.

2. Mach 12-15 Vehicle

In the following subsections, the four basic approaches to ultimate strength testing of Mach 12-15 vehicle are considered. These basic approaches are: full-scale complete vehicle testing, model testing, component testing, and mechanical simulation of thermal effects. The methodology of evaluation of these approaches is the same as used in Subsection 1 and will not be repeated here.

2.1 Parameters - Many of the parameters discussed in Section IV are unimportant in ultimate strength testing, as discussed for the Mach 3-4 vehicle in Subsection 1.1; the comments for that vehicle are generally applicable to the Mach 12-15 vehicle.

2.2 Complete Vehicle Testing

2.2.1 Engineering Analysis - The analysis of this vehicle parallels the analysis of the Mach 3-4 vehicle. The portion of this vehicle selected for analysis is the centerbody cross section, shown in Figure 13; a 94 node mathematical idealization of this cross section was developed and is shown in Figure 14. Node 55, at the windward location for the ascent portion of the mission, was chosen as the control node, and its assumed temperature history is presented in Figure 15. The assumed heating rate distributions around the body, normalized to the value at node 55, are illustrated in Figure 52 for two mission time ranges; these heat flux distributions are typical of hypersonic conical bodies at small angles of attack.

The various modes of heat transfer included in the analysis are: internal convection, internal radiation, conduction through continuous material and interfaces involving fastening, and radiation to external surroundings.

Surfaces of the double-face corrugated shell are assumed to have an emissivity of 0.8, while the payload is protected from radiation by a reflective covering having an emissivity of 0.15. Assumptions paralleling those for the Mach 3-4 vehicle thermal model have been used for the Mach 12-15 vehicle centerbody. Specifically, they are:

(a) A linearized temperature-time profile for the control node

(b) Infinite depth perpendicular to the plane of the cross section with neither temperature nor heating rate gradients in this direction

(c) Laboratory (1 atmosphere) pressure internal air for convective heat transfer

In the idealization, it was assumed that no conduction paths exist between the skin and the payload; therefore, the internal section is heated only through convection and radiation.

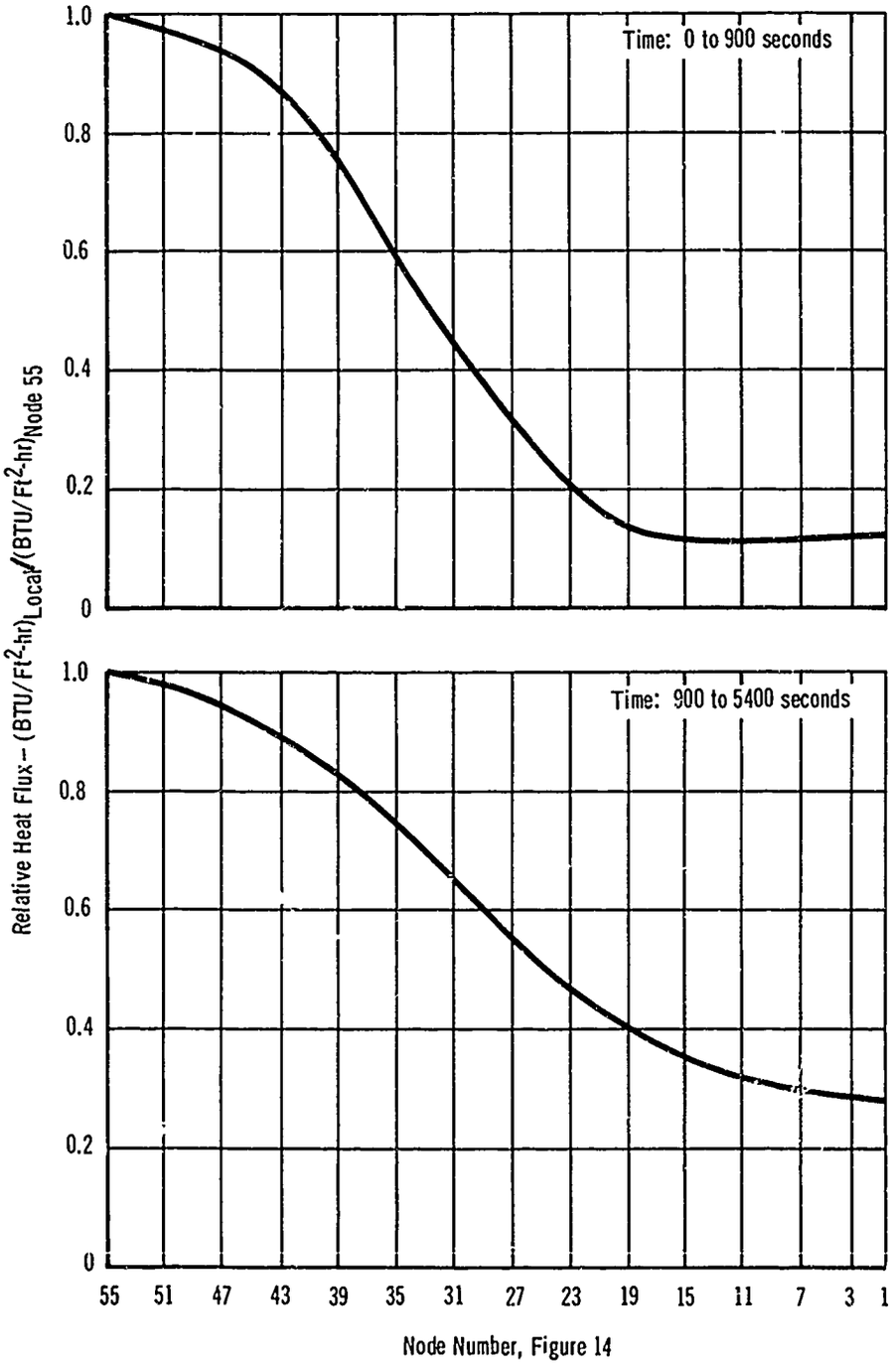

Figure 52 - Circumferential Heating Rate Distribution Mach 12-15 Vehicle

The effects of the radiation from the inner surface of the shell to the payload and between the various nodes of the inner surface have been found to be not as significant as for the Mach 3-4 vehicle. The effects of scaling and radiation on the centerbody heating rates at control node 55 (Figure 14) are indicated in Figure 53 and on the centerbody temperatures at node 1 in Figure 54. While radiation would normally be expected to be a significant factor in testing structures operating at the elevated temperatures attained by the Mach 12-15 vehicle, the results of analysis summarized in Figures 53 and 54 indicated little effect of internal radiation. This resulted from the arrangement of the cross section: a highly reflective coating protects the payload from radiation and the distance between the payload and inner skin is small, largely blocking radiation from the high temperature portion of the cross section to the cooler regions. Essentially, for the Mach 12-15 vehicle centerbody cross section selected, conduction was the dominant mode of heat transfer.

The temperatures described in the previous paragraphs have been used to compute thermal stresses for the Mach 12-15 vehicle centerbody; the elastic thermal stress analysis was similar to that of the Mach 3-4 vehicle. The longitudinal thermal stresses shown in Figure 55 indicate that the maximum thermal stresses in the outer surface (nodes 2 and 56) are tension, which is the usual behavior for such structures. Figure 56 presents the circumferential distribution of the longitudinal thermal stress at the time of maximum compressive stress in node 1.

The thermal stresses for the centerbody, based on temperature distributions computed with and without internal radiation effects, are shown in Figure 57. The close agreement of these stresses confirms that the internal radiation heat transfer process is not significant for the Mach 12-15 vehicle centerbody selected for analysis; however, removal of the payload would cause

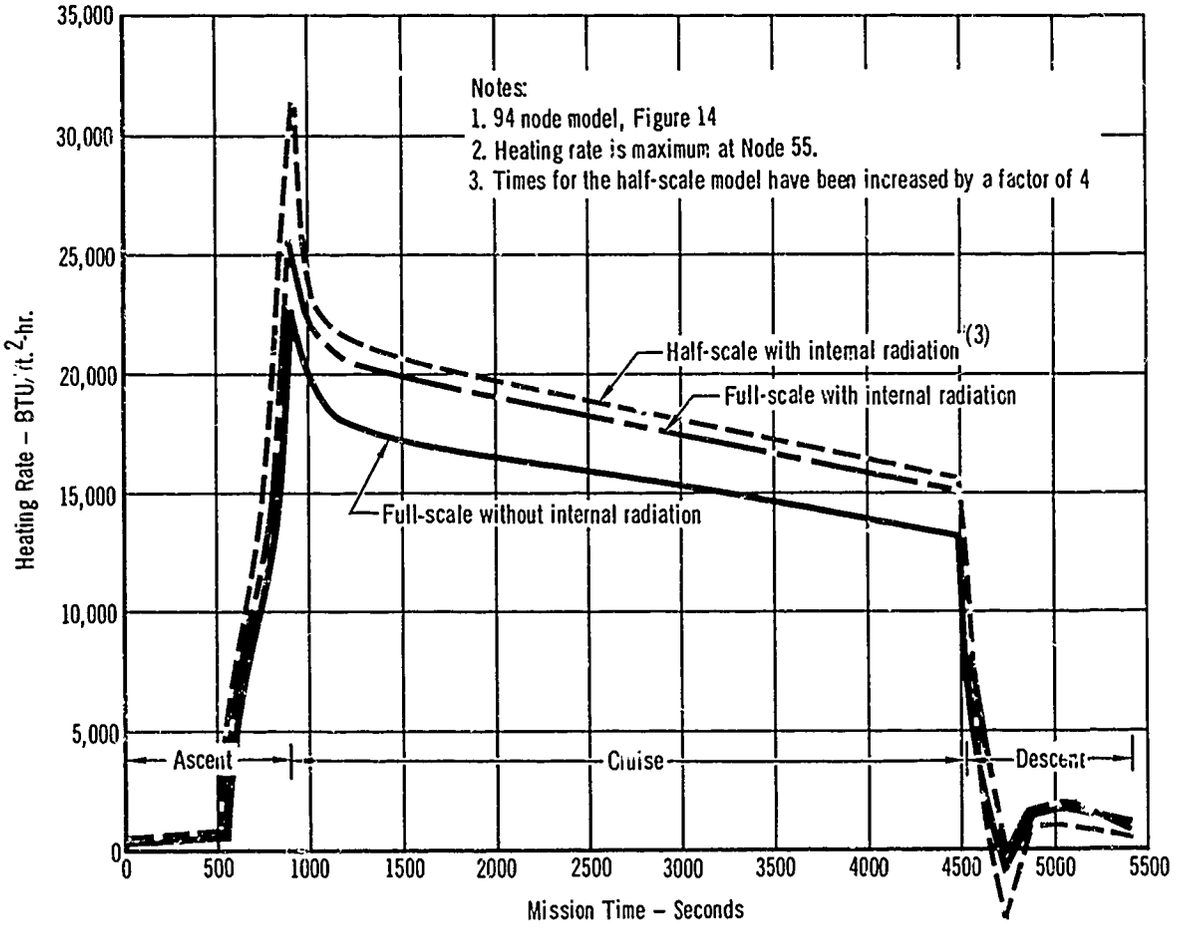

Figure 53 - Scaling and Radiation Effects on Heating Rate at Node 55 Mach 12-15 Vehicle

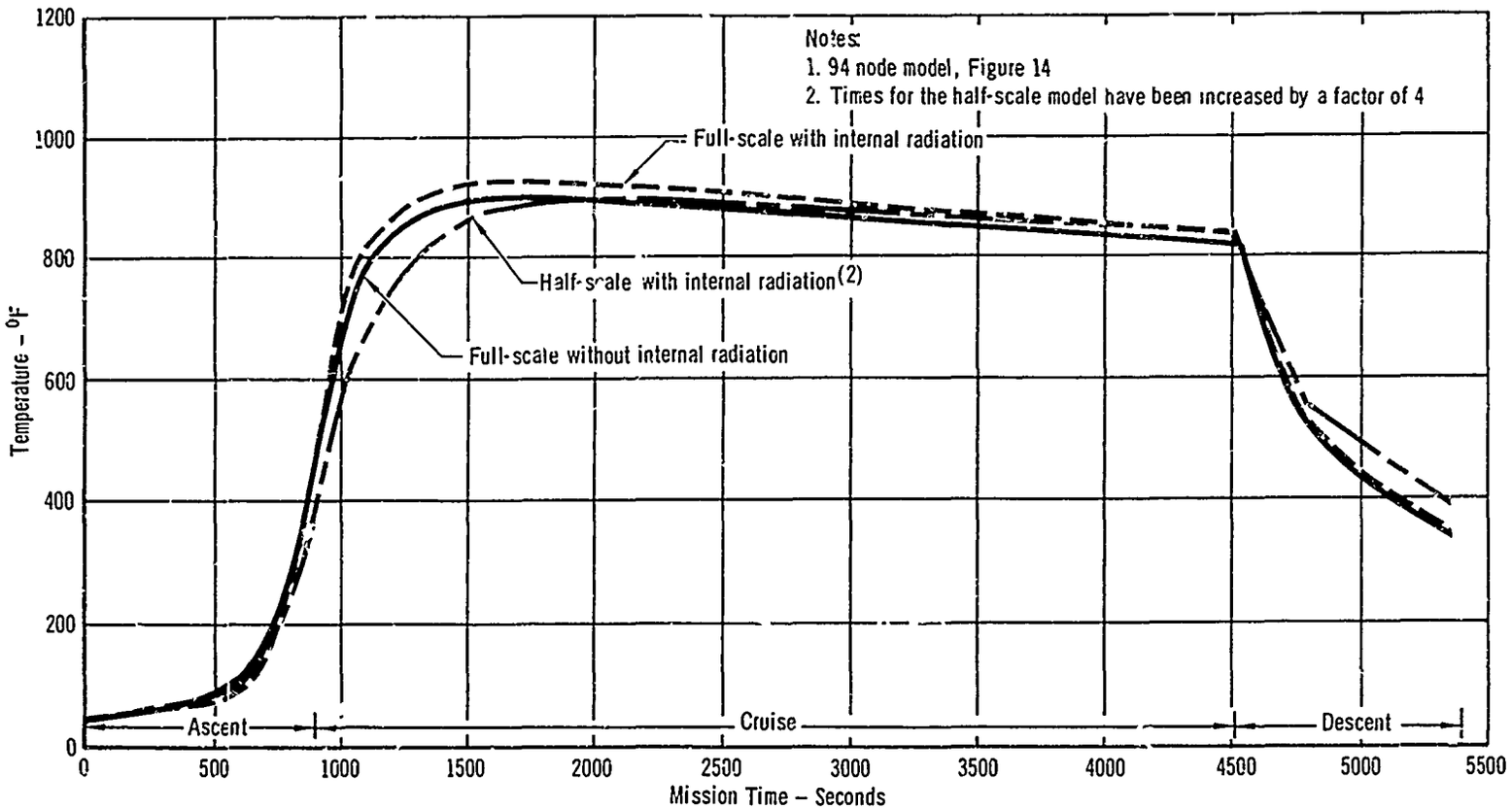

Figure 54 - Scaling and Radiation Effects on Temperature at Node 1 Mach 12-15 Vehicle

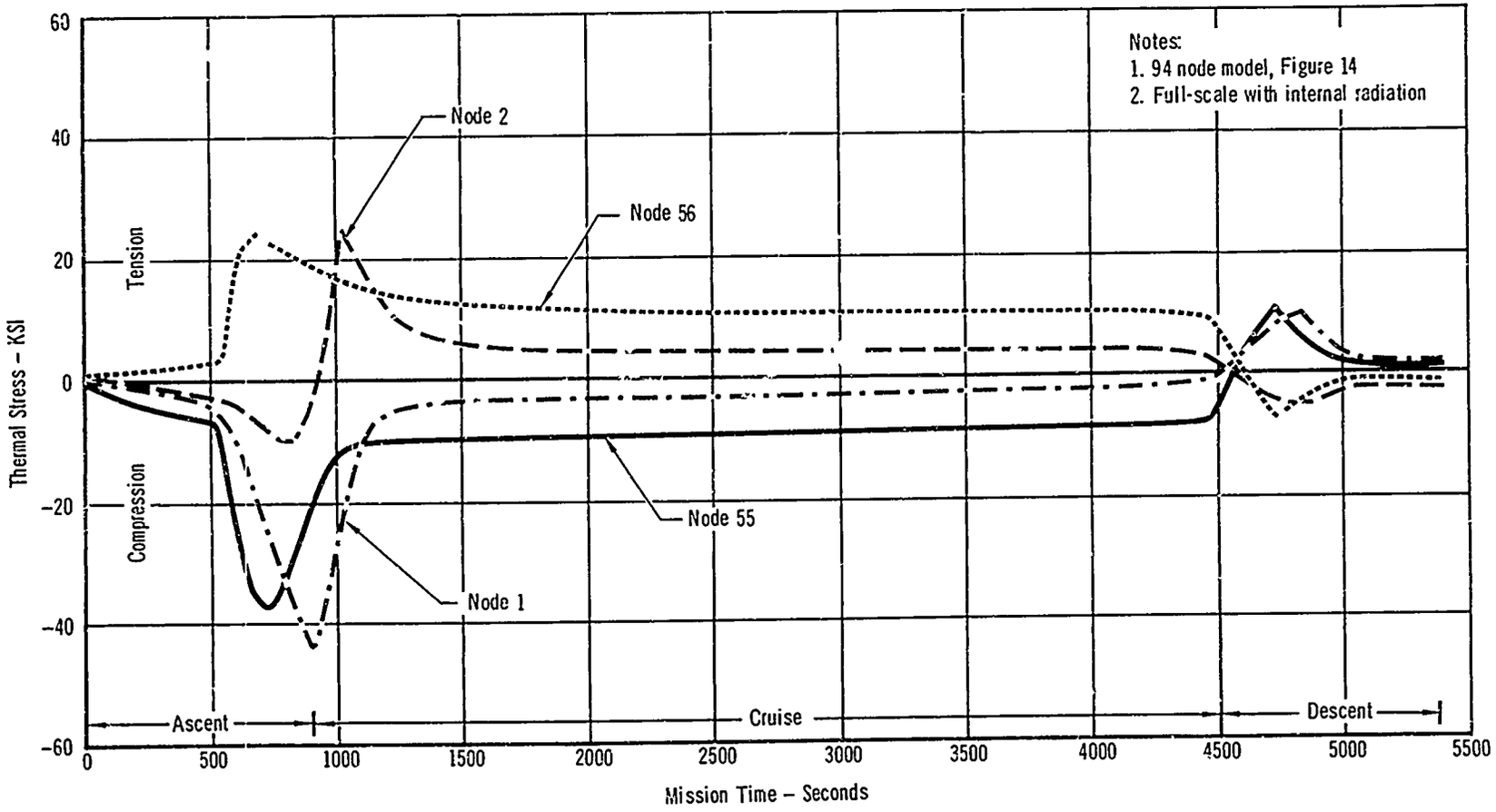

Figure 55 - Longitudinal Thermal Stress Variation With Time Mach 12-15 Vehicle

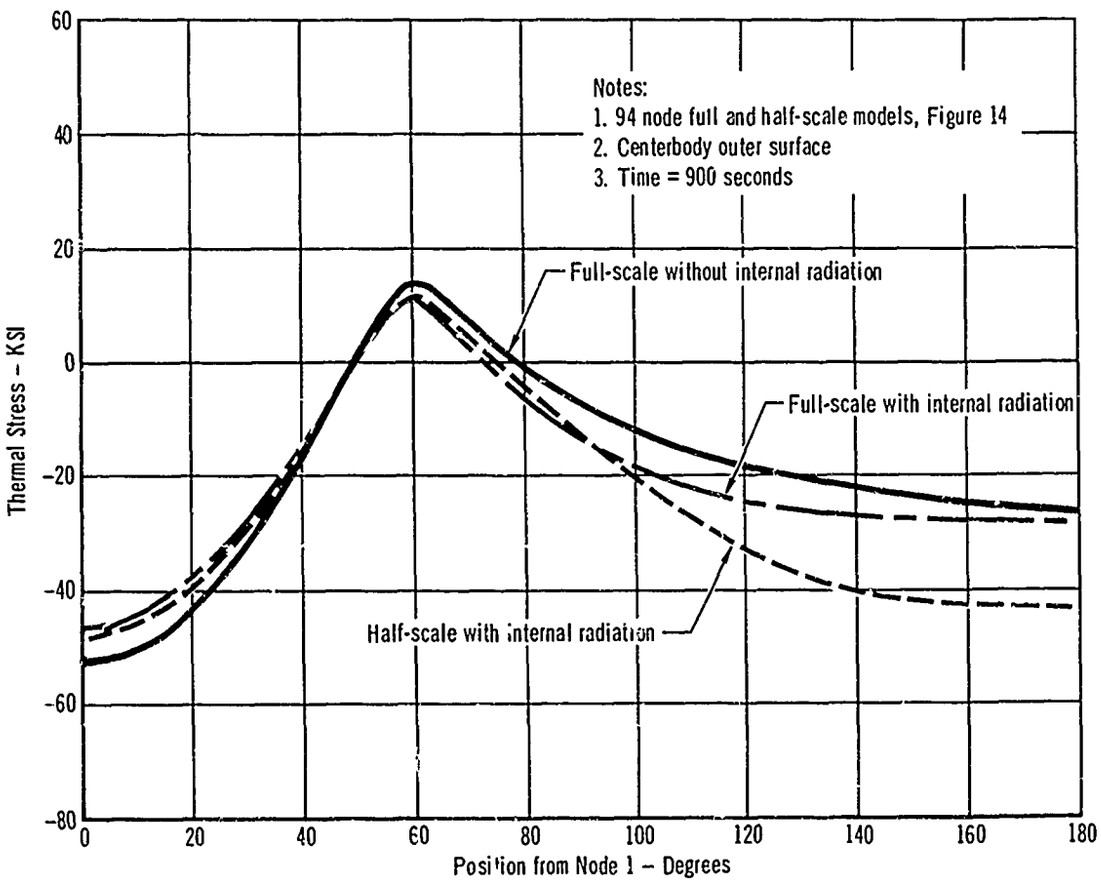

Figure 56 - Scaling and Radiation Effects on Circumferential Distribution of Longitudinal Thermal Stresses Mach 12-15 Vehicle

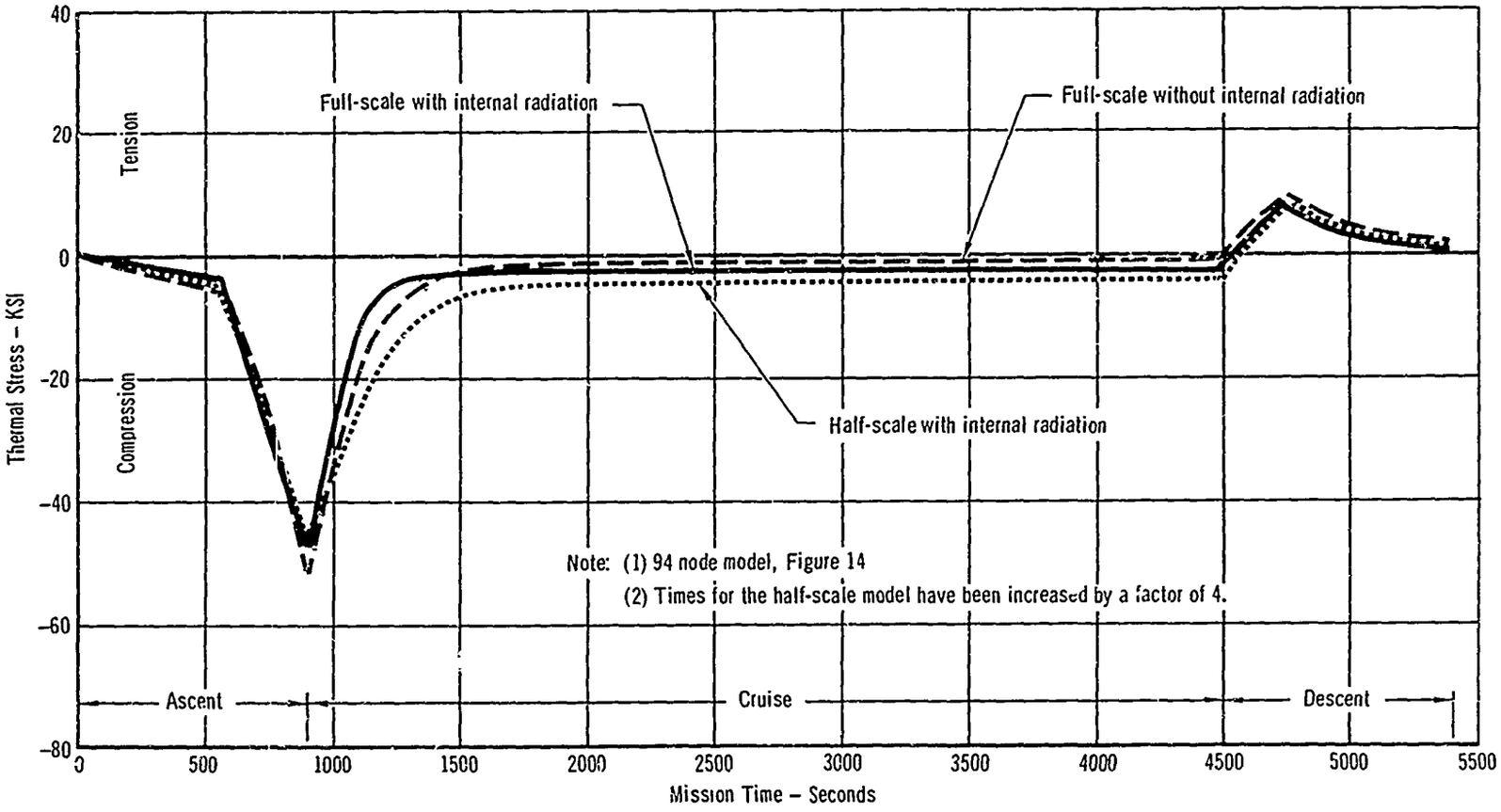

Figure 57 - Scaling and Radiation Effects on Longitudinal Thermal Stress at Node 1 Mach 12-15 Vehicle

radiation effects to become very significant for the range of temperatures considered. Internal convection has also been determined to be a relatively unimportant process for the selected centerbody; thus, conduction is the most significant process affecting thermal stresses.

The computed effect of thermal stress upon ultimate strength of the Mach 12-15 vehicle centerbody is presented in Figure 58. The upper curve represents the ultimate strength limit as affected by material property degradation due to temperature, where local crippling and shell instability are not critical. The middle curve indicates the bending moment that could be developed if local crippling of the corrugated shell were critical. The lowest curve presents the value of the moment that could be developed when shell instability is considered and includes the effects of local crippling and material property degradation. It can be seen that the effects of thermal stress are greatest for instability failure, less for crippling, and negligible for the material failure limit. If the geometry were changed to allow the instability limit to approach the crippling limit, or if the crippling limit were allowed to approach the material limit, the effects of thermal stress would be reduced.

The effect of the thermal environment on the overall stiffness (EI) of the total cross section will be similar to its effect on ultimate strength. However, the effect of thermal stress is not significant at low load levels, where only temperature degradation effects are apparent. At higher load levels, the mode of failure affects the stiffness; the effect being greatest for overall failure, less for local element failure, and negligible for bulk material failure.

The results of the plastic analysis, performed to determine the Mach 12-15 vehicle centerbody stable section ultimate strength, with and without the inclusion of thermal stress effects, are presented in Figure 59. It can be seen that as the bending moment is increased, the plasticity of the material reduces

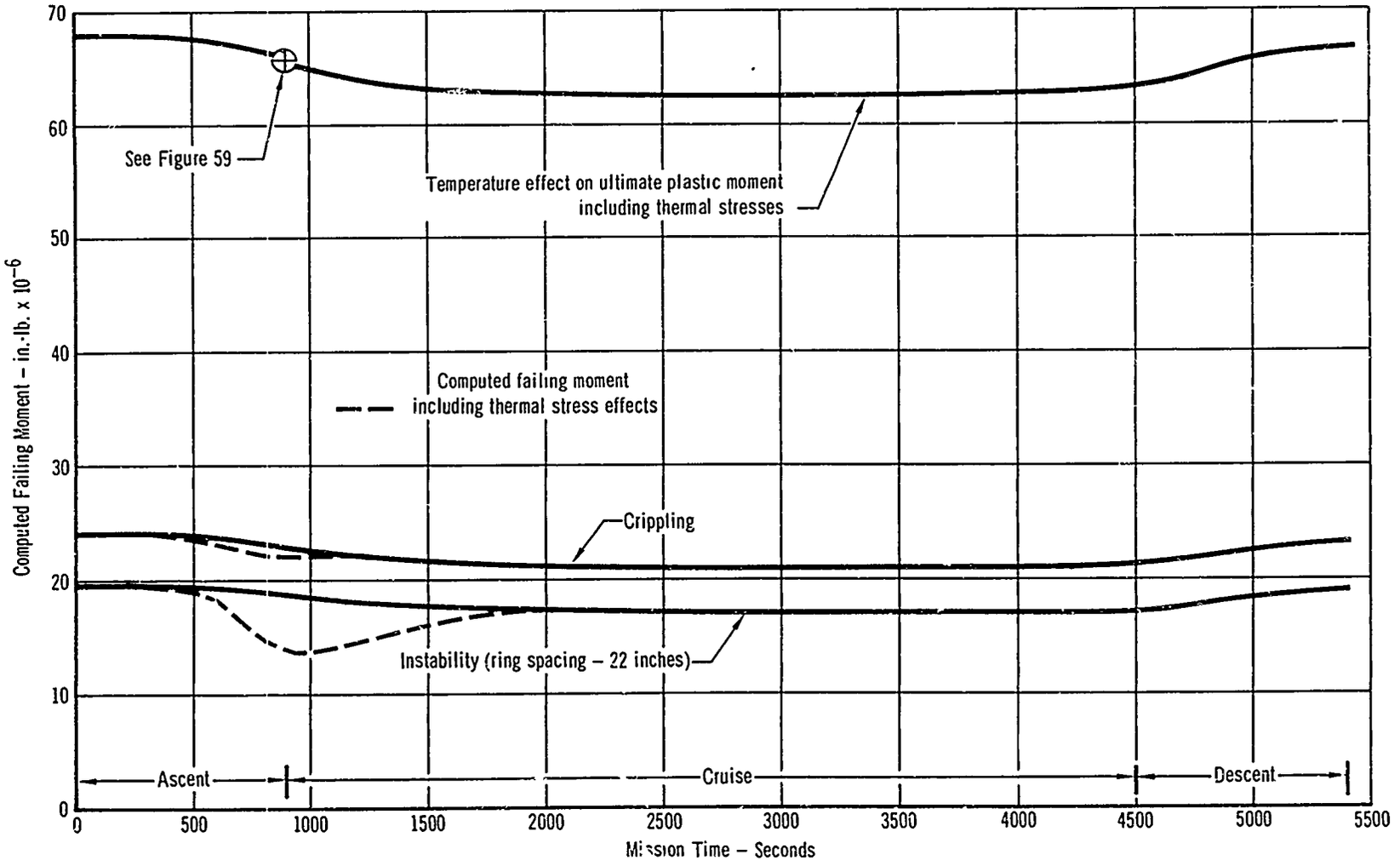

Figure 58 - Computed Centerbody Failing Moment

Mach 12-15 Vehicle

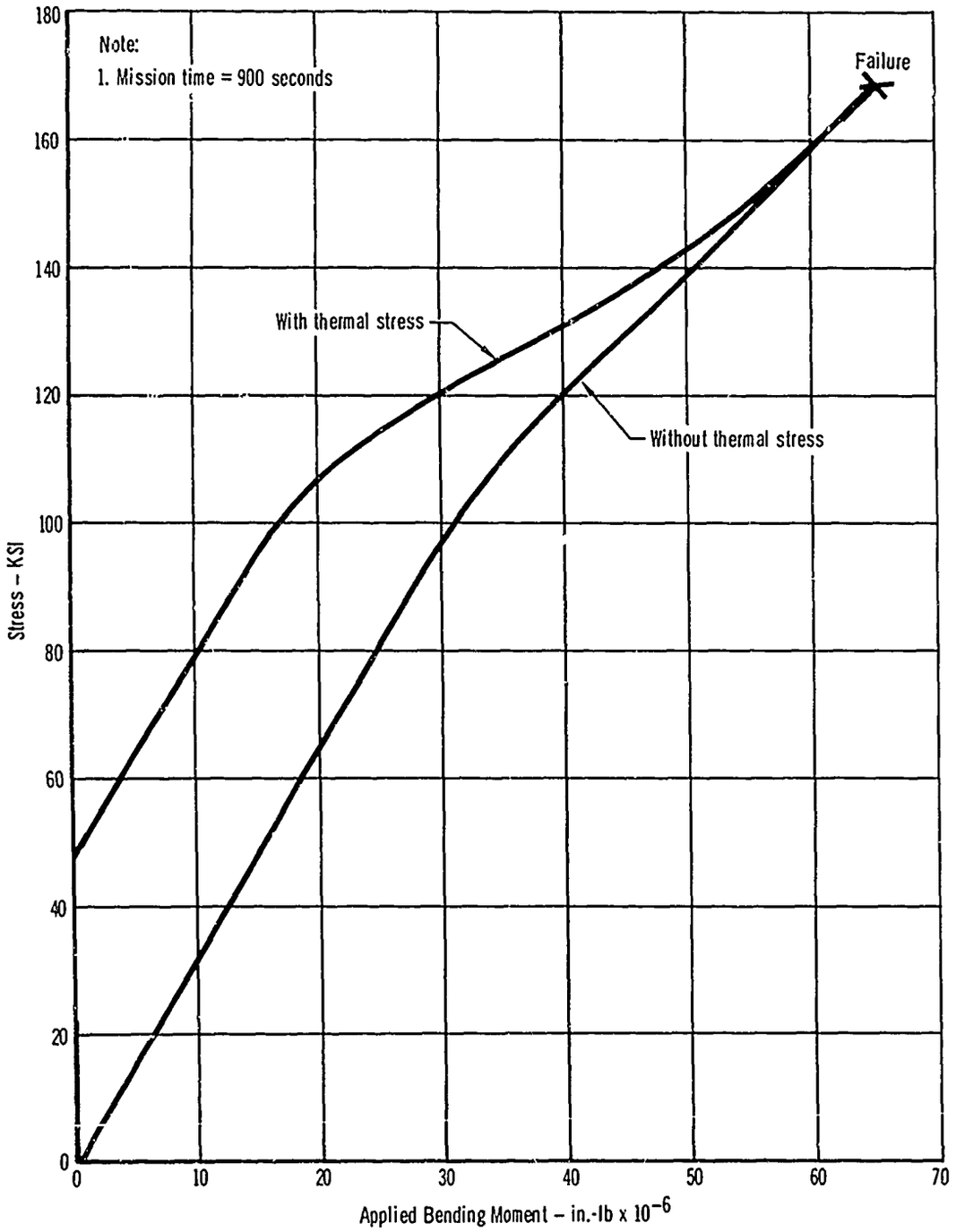

Figure 59 - Centerbody Maximum Stress as a Function of Applied Moment Mach 12-15 Vehicle

both the magnitude and effect of the thermal stress until finally, at computed failure, the thermal stress is negligible. These data are in contrast to that presented in Figure 58 where thermal stresses significantly affect the compressive strength.

2.2.2 Test Facility Analysis - The techniques for evaluating the test complexities for the Mach 12-15 vehicle parallel to those of the Mach 3-4 vehicle are discussed in Subsection 1.2.2. The maximum airframe temperature of the vehicle (1600°F) is well within the capabilities of the same type of lamp system as described for the Mach 3-4 vehicle. The required heating and cooling rates for laboratory simulation are approximately three times as large as for the Mach 3-4 vehicle. The Mach 3-4 vehicle lamp distribution was determined by the need to maintain a uniform flux over the surface, which resulted in a lamp spacing of approximately 4 inches. This lamp spacing could also be adequate for the Mach 12-15 vehicle, since the same lamps could be used at a higher power input. However, assuming no larger change in power input to the lamps, the lamp spacing that would be necessary to produce such large heat fluxes would, in general, be decreased. Consequently, there would be additional complexities associated with the simultaneous application of load and heat under these more severe thermal requirements. The detail requirements for the Mach 12-15 vehicle are presented in Table VIII.

2.2.3 Cost Analysis - The cost analysis of the Mach 12-15 vehicle was performed in the same manner as for the Mach 3-4 vehicle; all costs are presented on a relative basis. For comparison purposes, the ultimate strength verification of the full-scale complete vehicle at room temperature was selected as the base cost values. The total man-hour cost of this test is 0.5 to 0.9 million man-hours and the corresponding dollar cost is 8 to 16 million dollars.

These costs are based on estimates derived from what are believed to be

TABLE VIII
SUMMARY OF ESTIMATED TEST FACILITIES REQUIREMENTS
MACH 12-15 VEHICLE ULTIMATE STRENGTH TESTING

Test Article (1)		Maximum Mission Heat Flux BTU Ft^2-Hr	Maximum Test Heat Flux Required (2) BTU Ft^2-Hr	Effective Maximum Temperature ^oF	Area Heated by Lamps Ft^2	Heating Lamps Required	Maximum Power Required KW	Heat Requirements KW-Hr Flight	Control Channels		Instrumentation		
									Heating (3)	Structural	Strain Gages, Rosettes	Deflection Gages	Thermo-couples
Room Temperature	Full-scale vehicle	14500	0	70	0	0	0	0	0	20	500	50	0
	Half-scale vehicle	19000	↓	70	↓	↓	↓	↓	↓	20	500	50	↓
	Centerbody component	14500	↓	70	↓	↓	↓	↓	↓	3	70	7	↓
	Wing component	16000	0	70	0	0	0	0	0	7	160	15	0
Constant Elevated Temperature	Full-scale vehicle	14500	1250	1100	1050	1500	590	580	250	20	0	50	2000
	Half-scale vehicle	19000	2500	1100	260	750	295	75	250	20	↑	50	2000
	Centerbody component	14500	1250	1100	150	215	85	80	35	3	Note (4)	7	285
	Wing component	16000	1350	1150	330	475	200	195	80	7	0	15	630
Mission Temperature	Full-scale vehicle	14500	7500	1100	1050	1500	3550	1200	250	20	0	50	2000
	Half-scale vehicle	19000	15000	1100	260	750	1780	150	250	20	↑	50	2000
	Centerbody component	14500	7500	1100	150	215	500	170	35	3	Note (4)	7	285
	Wing component	16000	8000	1150	330	475	1200	400	80	7	0	15	630

Notes: 1. See Figure 63 for component locations
2. Maximum test heat flux required is that flux which must be applied to the test article to achieve the desired mission conditions.
3. Control channels with a capacity of 25 KVA.
4. Strain gages cannot be used at testing temperatures.

reasonably representative, typical data; however, they should be considered as gross, first level approximations to actual costs. For instance, it was assumed that laminar flow at a maximum temperature of 1600°F was characteristic of the in-flight conditions. However, if turbulent flow were assumed, the maximum in flight temperature would approach 2800°F, causing a disproportionate increase in these base costs; in fact, this would occur if the maximum temperature were assumed to be 2000°F. For this reason, the relative cost estimates have greater accuracy than any single absolute cost.

Presented in Figures 60 and 61 are the relative man-hour and dollar costs, respectively, for each of the basic approaches. It should be noted that the most significant difference between the Mach 12-15 vehicle and the Mach 3-4 vehicle is the proportionately higher cost of fabricating the Mach 12-15 vehicle. This difference is caused by the more difficult type of construction, combined with the expense of using less conventional material.

2.2.4 Conclusions

(a) The effects of internal radiation on the thermal stresses developed within the Mach 12-15 centerbody selected for analysis are not significant.

(b) The effects of air pressure on the thermal stresses developed within the centerbody enclosure are not significant.

(c) Thermal stresses significantly affect the expected ultimate compression strength of the centerbody but have an insignificant effect on the stable section ultimate strength.

(d) For the mission temperature test of a complete Mach 12-15 vehicle, the heating requirements, either BTU/ft^2-hr. or BTU/hr., are not a serious problem; the real heating problems are associated with equipment reliability and the possibility of producing some serious unwanted and unforeseen thermal effect.

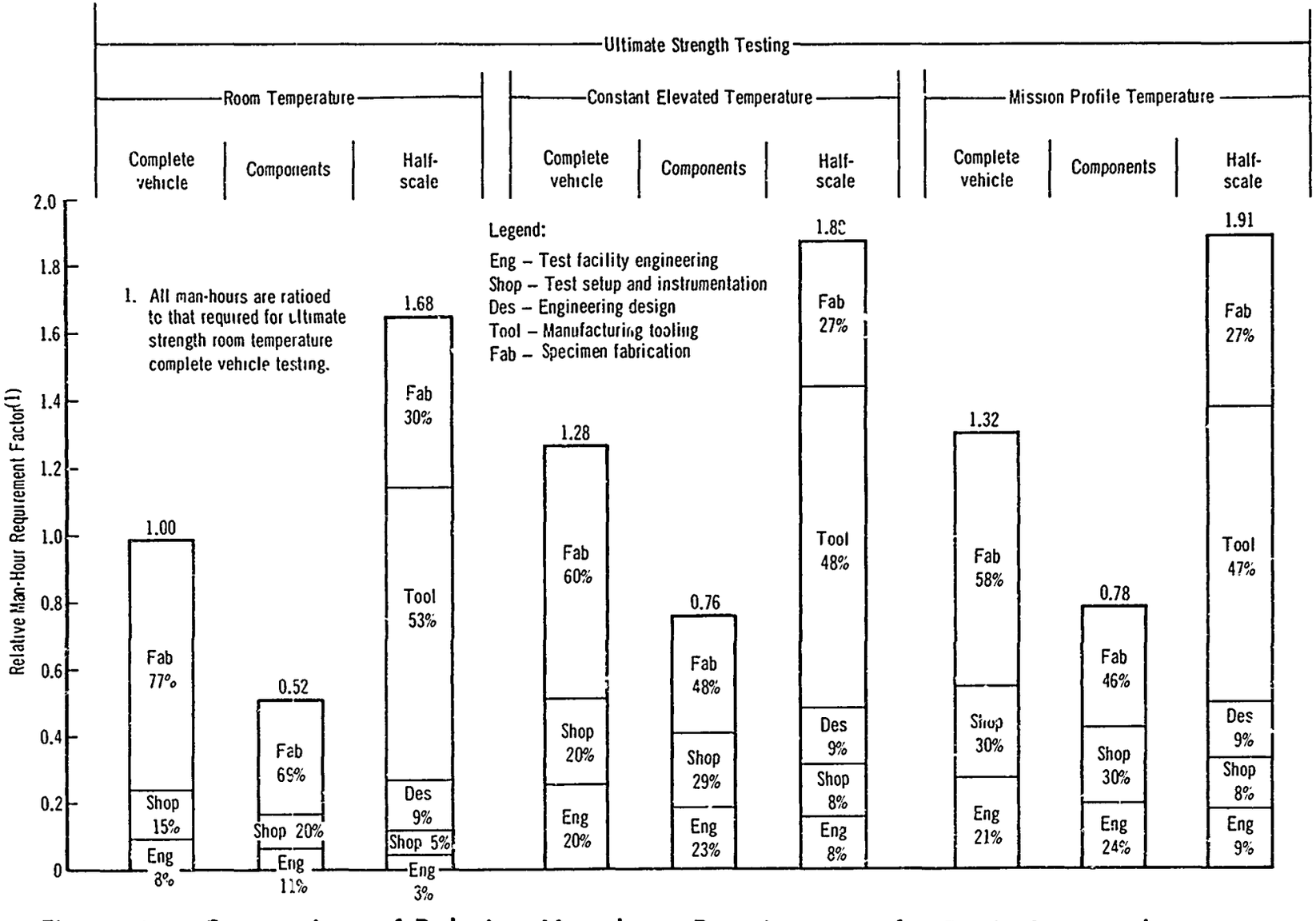

Figure 60 - Comparison of Relative Man-hour Requirements for Basic Approaches Mach 12-15 Vehicle

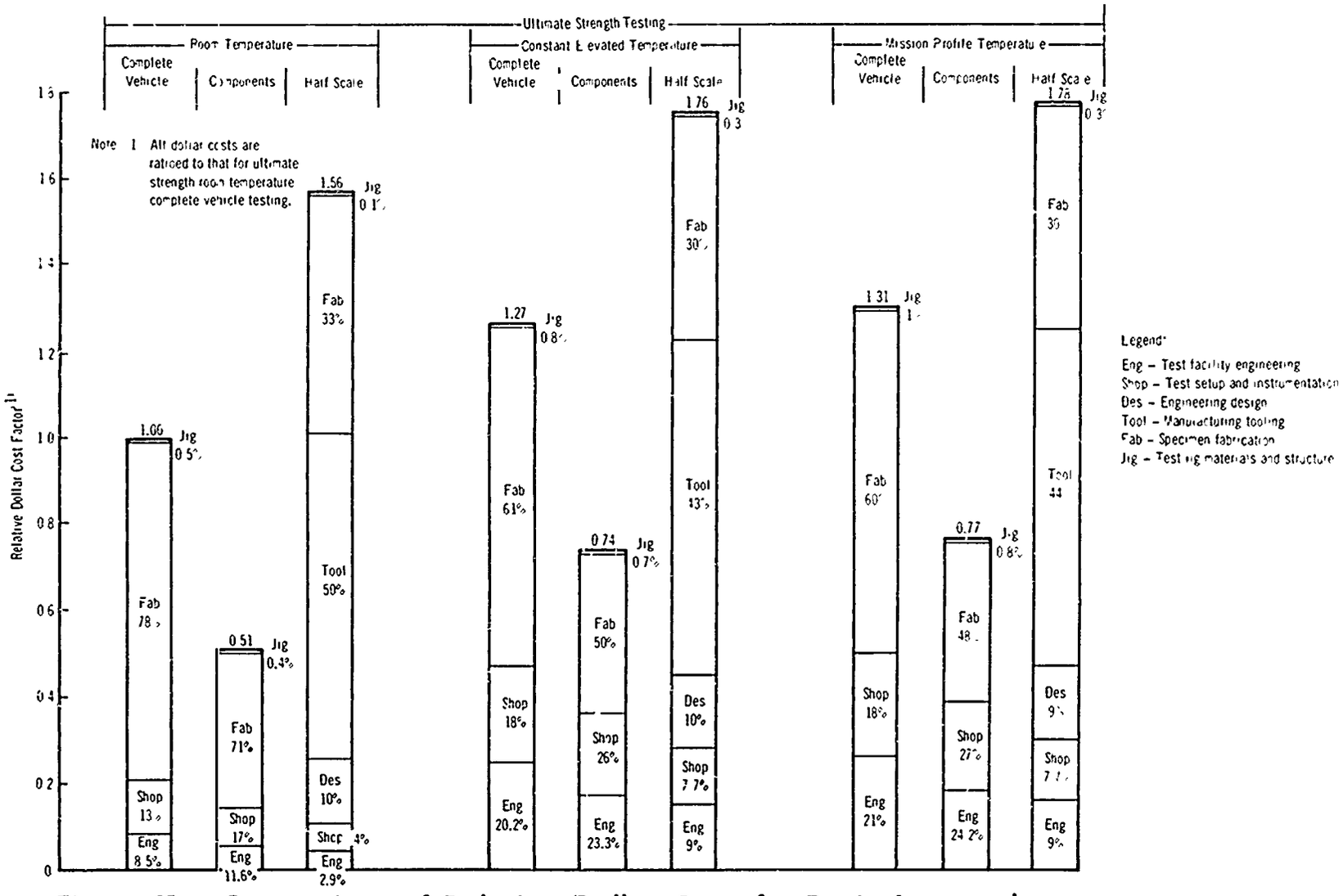

Figure 61 - Comparison of Relative Dollar Costs for Basic Approaches Mach 12-15 Vehicle

(e) Although the test complexities associated with the Mach 12-15 vehicles are greater than those for the Mach 3-4 vehicle due to the more severe thermal environment, the loading and heating systems proposed for use in the Mach 3-4 vehicle testing are generally applicable for the Mach 12-15 vehicle testing.

(f) The cost of the specimen fabrication and the test jig design and fabrication are the most significant costs for complete vehicle ultimate strength tests.

2.3 Model Testing - The ultimate strength verification of the Mach 12-15 vehicle using the basic approach of model testing is discussed in the following subsections. Presented in separate subsections are the engineering analysis, test facility analysis, cost analysis, and conclusions. The effects of the modeling approach are determined by comparisons to results obtained in Subsection 2.2, Complete Vehicle Testing, and in Subsection 1.3 for the Mach 3-4 vehicle.

2.3.1 Engineering Analysis - The description of modeling effects presented in Subsection 1.3.1 for the Mach 3-4 vehicle is applicable to the Mach 12-15 vehicle. The modeling effects were studied in detail by analysis of a half-scale mathematical idealization of the centerbody cross section described in Subsection 2.2.1 and shown in Figure 14.

Analogous to the case for the Mach 3-4 cross section, time for the half-scale model was scaled according to:

$$\tau_m = n^2 \tau_p$$

This scaling is based on the assumption that conduction is the only heat transfer mode. Again, the radiative heat transfer will not be properly scaled unless surface emissivity can be increased to satisfy the following condition:

$$\epsilon_m = \frac{\epsilon_p}{n}$$

With the high emissivity values of the structure ($\epsilon = .8$), proper scaling could not be achieved for the half-scale model. This prototype value of emissivity was also used in the analysis of the half-scale cross section. Internal pressure for the half-scale idealization was one atmosphere, corresponding to laboratory conditions. Analogous to the case of the full-scale cross section, the heating rate producing the prescribed temperature-time history at node 55 was determined by using the assumed circumferential heating rate distributions of Figure 52, with the time reduced by a factor of 1/4. The temperature-time history for node 1 is shown in Figure 54, and the circumferential temperature distribution at the transition between ascent and cruise (225 seconds half-scale time) is presented in Figure 62. Figure 53 presents the heating rate history for the control node (node 55).

Closer agreement in temperature distributions between full and half-scale structures resulted for the Mach 12-15 vehicle than for the Mach 3-4 vehicle. This appears paradoxical because radiation would be expected to be appreciably higher for the Mach 12-15 vehicle since temperatures are greater and radiation necessitates time scaling as:

$$\tau_m = n\tau_p$$

However, further examination of the differences between the two structures clarifies this. First, for the Mach 12-15 vehicle, the entire structure is near the external shell surface; the conduction path inward is rather direct and much more suitable for this mode of heat transfer than in the Mach 3-4 vehicle wing cross section. Second, the presence of the payload prevents the radiation from the hotter windward region of the Mach 12-15 vehicle from reaching and heating the cooler portions of the structure. Therefore, the heat transfer in the circumferential direction of the shell is not significantly affected by internal radiation.

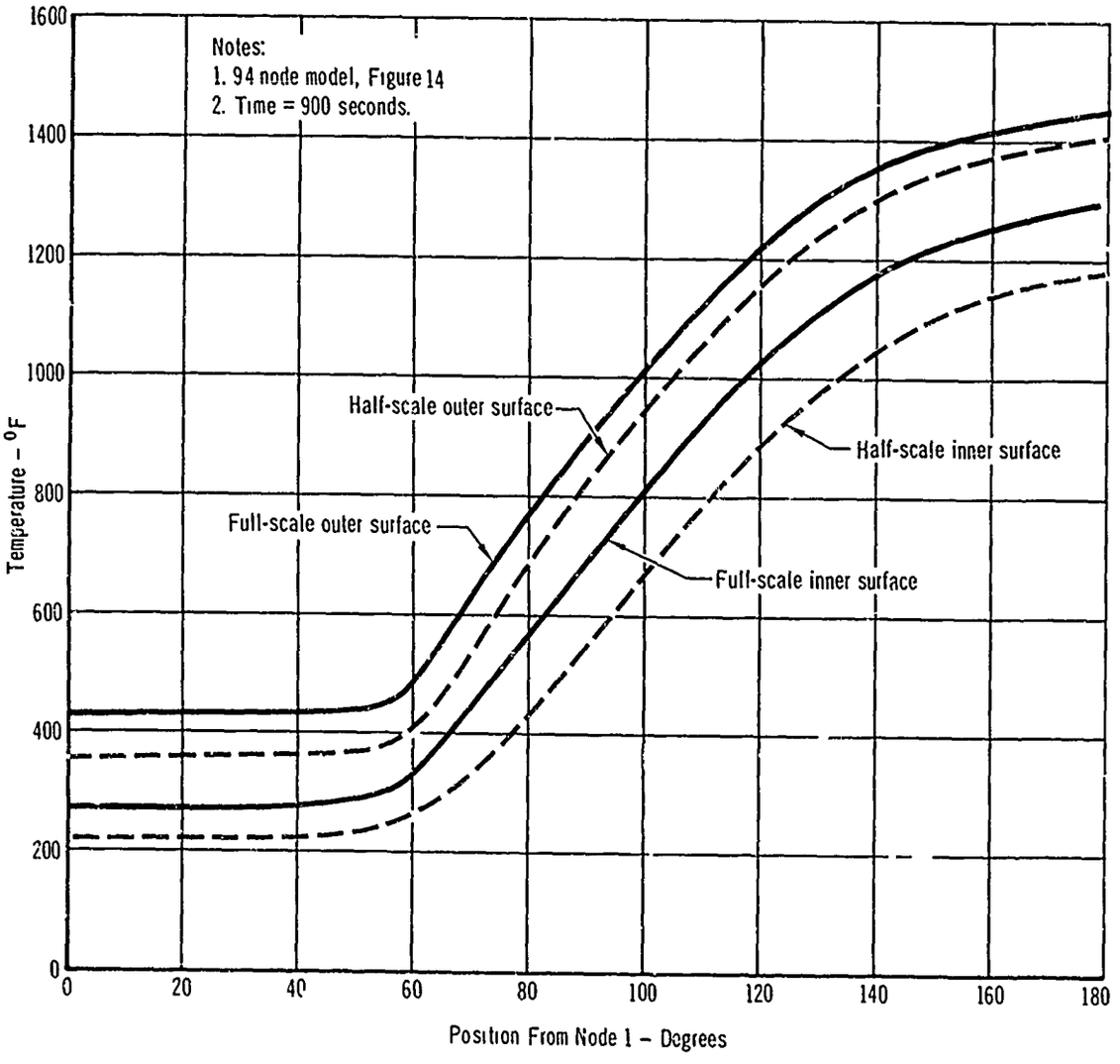

Figure 62- Scaling Effect on Circumferential Temperature Distribution Mach 12-15 Vehicle

The thermal stresses computed for this cross section indicate, as before, that the effects of radiation are not significant. Figure 57 presents the thermal stress history for node 1 (Figure 14) of the half-scale cross section of the Mach 12-15 vehicle centerbody. The magnitude of the thermal stresses computed for the half-scale cross section agrees with those computed for the full-scale cross section; this is in sharp contract to the greater differences determined for the Mach 3-4 vehicle. The closer agreement for the Mach 12-15 vehicle thermal stresses can be explained by considering the importance of the three heat transfer modes: conduction, radiation, and convection. In both the Mach 3-4 vehicle and Mach 12-15 vehicle analyses it was chosen that conductive mode of heat transfer would dictate the selection of model time ($\tau_m = n^2\tau_p$) and, consequently, the radiative and convective heat transfer modes are not scaled properly. However, the close agreement for the full and half-scale analyses and the close agreement for the analyses of the full-scale cross section with and without the effects of internal radiation indicate that radiation is not a significant mode of heat transfer for the Mach 12-15 vehicle. Similar analyses have determined that convection is also not significant. Thus, conduction is the most important heat transfer process for the Mach 12-15 vehicle centerbody configuration selected for study and explains the close agreement of thermal stresses developed in the full and half-scale centerbody models.

It is concluded that although thermal stresses do significantly affect the computed failing moment (the shell instability moment described in Subsection 2.2.1), the close agreement between the full-scale and half-scale model stresses allows the use of a model to verify the ultimate strength of this type of construction.

2.3.2 Test Facility Analysis - The effects of modeling upon the test requirements for the Mach 12-15 vehicle are similar to those for the Mach 3-4

vehicle, as discussed in Subsection 1.3.2. The laboratory heating and cooling rates are increased by a factor of 1/n; for a half-scale model this is a factor of two. In order to maintain heating and cooling flux uniformity proportional to that which would be attained in prototype testing, the lamp and coolant orifice spacing would be reduced to n times that of the prototype. The flux requirements for the half-scale model of this vehicle are the largest of this study; however, they are well within the limitations of the heating and cooling systems described in Subsection 1.2.2. The detailed requirements for the Mach 12-15 vehicle half-scale model are summarized in Table VIII.

2.3.3 Cost Analysis - The costs of the model testing approach for the Mach 12-15 vehicle show a trend similar to that for the Mach 3-4 vehicle. The engineering design costs of the test specimen are greater than the combined costs of designing and fabricating the room temperature test jig. As before, the costs of the tooling for the model are the largest costs for this approach; the actual fabrication costs are proportionally larger for this vehicle than for the Mach 3-4 vehicle because of more expensive manufacturing techniques. The modeling approach is the most expensive ultimate strength verification technique for the Mach 12-15 vehicle. The costs are summarized in Figures 60 and 61.

2.3.4 Conclusions

(a) Fabrication feasibility dictates that the scale factors of 1/4, 1/2, or 3/4 be considered, with 1/2 appearing most usable. Other scale factors would require greater use of non-standard hardware or require larger deviations from scaled geometry, with possible effects on the ultimate strength of the specimen.

(b) For a structure subjected to the thermal environment of the Mach 12-15 vehicle, radiation can be an important factor in the heat transfer process; however, because of its type of construction and

reflective coatings, radiation is less significant for the Mach 12-15 vehicle centerbody cross section than for the Mach 3-4 vehicle wing cross section.

(c) Thermal stresses for models scaled for conductive heat transfer are only slightly greater than full-scale structures.

(d) The effect of thermal stress upon ultimate strength is significant; however, the thermal stress variations caused by modeling are not large enough to significantly affect ultimate strength verification.

(e) Structural models appear satisfactory for ultimate strength verification, the degree of thermal stress simulation having a relatively minor effect in this case.

(f) Serious drawbacks to the model approaches are the cost of (1) tooling for fabrication of a satisfactory structural model, and (2) the engineering effort required to complete model drawings.

2.4 Component Testing - The ultimate strength verification of the Mach 12-15 vehicle using the basic approach of component testing is discussed in the following subsections. The engineering analysis, test facility analysis, cost analysis, and conclusions are presented in separate subsections. Effects of the component approach are determined by comparisons to results obtained in Subsection 2.2, Complete Vehicle Testing, and in Subsection 1.4, Component Testing, Mach 3-4 Vehicle.

2.4.1 Engineering Analysis - The results and conclusions for the wing cross section component of the Mach 3-4 vehicle, discussed in Subsection 1.4, are generally applicable to the wing component of the Mach 12-15 vehicle, with some exceptions. The effects of radiation upon the temperatures and thermal stresses in the mission temperature testing of the complete Mach 3-4 vehicle wing were found to be important; furthermore, the effects of radiation were

found to be significant .n the attempt to duplicate full-scale complete vehicle stresses in a wing component. These latter effects are shown in Figures 46, 47, and 48; Figure 46 presents a comparison of temp ratures in the component with and without the effects of internal radiation. This figure indicates that the temperature of the full-scale complete vehicle can readily be attained in a component if radiation effects are not present in either structure; however, with radiation included, the full-scale complete vehicle temperature is not developed in the component due to the effect of length on the radiation shape factors. If a similar structural configuration were used in a Mach 12-15 vehicle wing, with appropriate changes in material, the effects of radiation would be more important and the attainment of full-scale complete vehicle temperature distributions would be more difficult than in the Mach 3-4 vehicle wing. However, no quantitative analysis has been performed on such a component for the Mach 12-15 vehicle since adequate qualitative conclusions can be drawn from the Mach 3-4 vehicle component analysis.

A different result would be expected in the centerbody component illustrated in Figure 63. While radiation would normally be expected to be a significant factor in all portions of the Mach 12-15 vehicle, Figures 53 and 54 indicate that the effects of internal radiation in the centerbody cross section are small compared to those of conduction. This results from the design of the cross section, as discussed in Subsection 2.2.1; a reflective coating protects the payload from radiation, and the payload blocks the radiation from the hotter to cooler portions of the shell. Essentially, conduction is the only heat transfer process of significance for this component. The previous analysis for the Mach 3-4 vehicle indicated that the attainment of proper temperatures in a component is easier if internal radiation is negligible, as indicated in Figure 46.

Therefore, considering temperature distributions only, it is concluded that

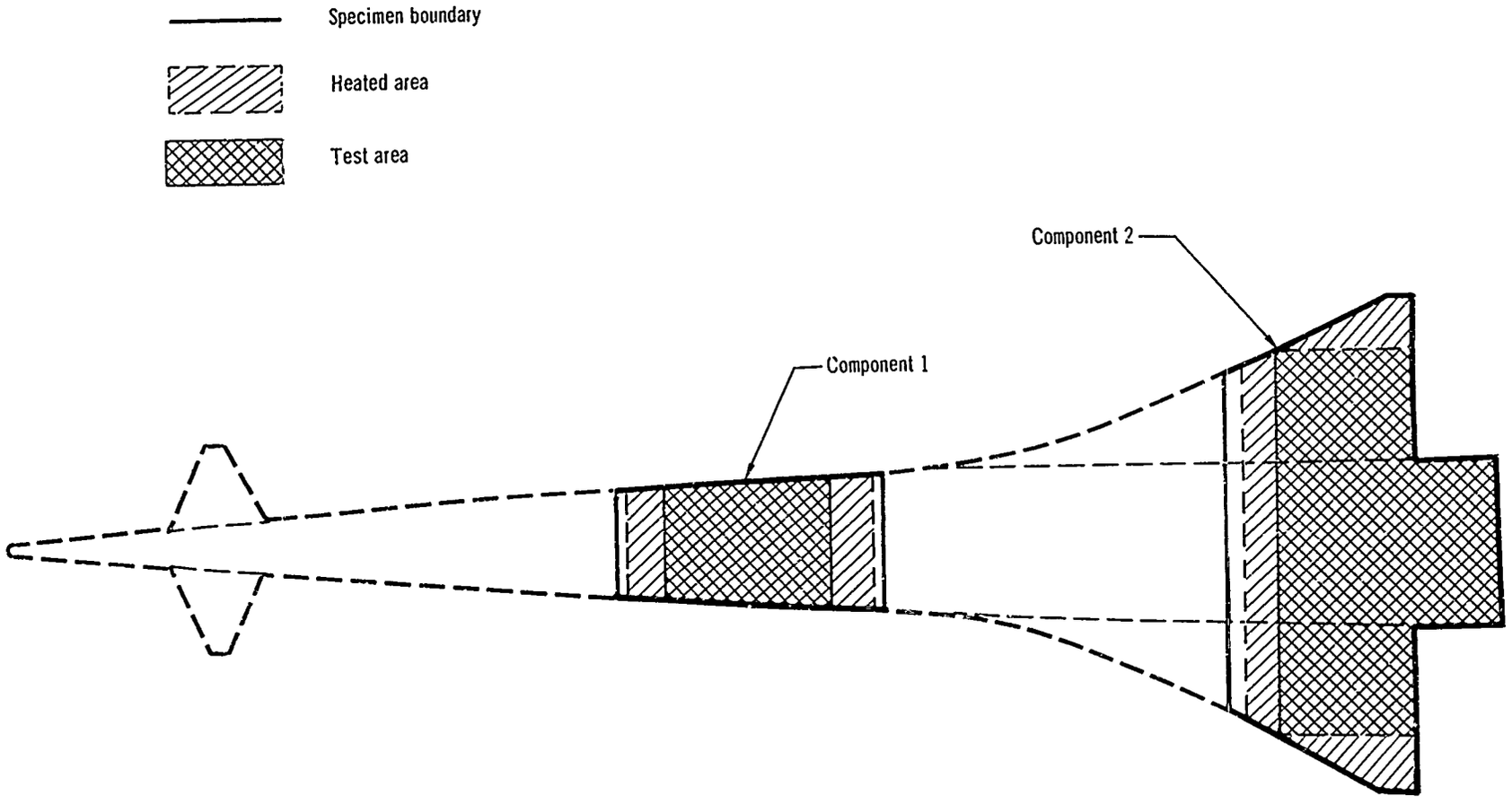

Figure 63 - Small-size Components

Mach 12-15 Vehicle

a component of relatively small length may be employed for a section of the complete vehicle in which the internal radiation is small, compared with one in which an appreciable portion of the heat transfer occurs through internal radiation. In the Mach 3-4 vehicle the component length was 3 to 4 times the wing cross section depth and width, and a suitable test section resulted when approximately 50 percent of this structure was heated. Hence, for a similar ratio of component length to width (diameter) for the Mach 12-15 vehicle, the heated portion could justifiably be less than 50 percent. The seemingly more difficult process for the Mach 12-15 vehicle is seen to actually be simpler due to the structural design. It should again be noted that any change in payload characteristics could result in radiation becoming a significant parameter.

The effects of structural boundary conditions are more important for the Mach 12-15 vehicle centerbody component than for the Mach 3-4 vehicle wing component. The results of the analysis of the Mach 12-15 vehicle component are presented in Figure 64. Both of these analyses assume that the complete vehicle temperature distributions exist throughout the entire component length. A length of 4 to 6 feet is sufficient for the Mach 3-4 vehicle wing component; however, a length of 15 feet is required for the Mach 12-15 vehicle centerbody component.

This difference in behavior is explained by the differences in the type of thermal gradients and stresses. The thermal stress at node 111 of the Mach 3-4 vehicle is caused by the difference in temperatures between this location and the average temperature of the skin; the thermal stresses are caused by temperature gradients of adjoining structure. In contrast, the major portion of the thermal stress in the Mach 12-15 vehicle centerbody is caused by the circumferential temperature difference in locations on the structure, separated by a large portion of the shell circumference. Therefore, a larger component length

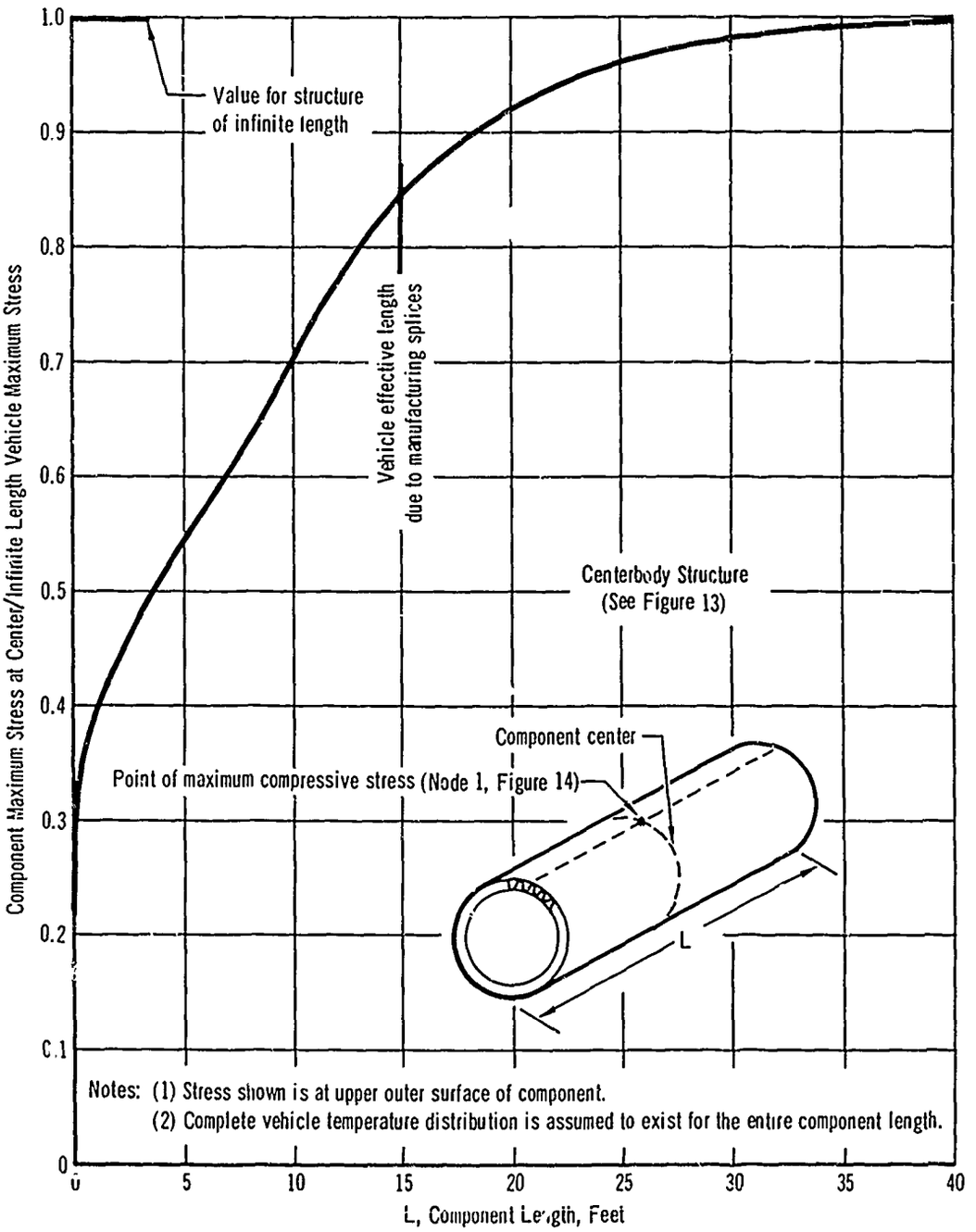

Figure 64 - Effect of Component Length on Maximum Longitudinal Thermal Stress Mach 12-15 Vehicle

is required to develop the same percentage of full-scale complete vehicle thermal stresses. The component length indicated in Figure 63 is 10 feet. Figure 64 indicates that the maximum thermal stress developed in a component 10 feet in length is approximately 70% of that developed in an infinite length full-scale complete vehicle. In the analysis, it was assumed that complete vehicle temperature distributions are maintained throughout the component. The effects of the temperature distributions actually present in the component would tend to increase thermal gradients and, thus, the maximum thermal stresses. However, in contrast to the results of the component analysis for the Mach 3-4 vehicle, it is expected that the combined effects of thermal and structural boundary conditions would cause the maximum thermal stress developed in the component to be less than in the complete vehicle. The computed effects of thermal stress upon ultimate strength, as indicated in Figure 58, are important and, therefore, the errors in thermal stresses caused by the component approach will affect the ultimate strength demonstrated in tests. However, the resulting error in ultimate strength will be less on a percentage basis than the error in thermal stress; hence, it is concluded that components may be used to adequately verify the ultimate strength of this type configuration.

2.4.2 Test Facility Analysis - The component approach for the Mach 12-15 vehicle allows the same testing economies as for the Mach 3-4 vehicle and the same testing flexibilities with regard to instantaneous power requirements, possibility of using multiple test sites, etc. The total planform area of the components shown in Figure 63 is approximately 55% of the vehicle planform area; this allows a proportionate decrease in the total testing requirements as shown in Table VIII.

2.4.3 Cost Analysis - In the component testing cost analysis for this vehicle, the equipment reliability and useful life have been included in the

determination of relative costs. The jig costs for the components include estimates of jig weight and the number of strain gages, thermocouples, actuators, and lamps required. Since it was assumed that all control equipment necessary to perform the tests would be available, their cost is not included in the analysis. The engineering design of the components including the selection of boundaries and analysis of boundary conditions will not cause significant costs. Similarly, the costs of tooling are not important because of the prototype tooling availability; the cost of fabricating the specimens is approximately proportional to the weight of structure to be fabricated.

Laboratory costs for the Mach 12-15 vehicle component approach are less than the costs for complete vehicle test. This is in contrast to the laboratory costs for the Mach 3-4 vehicle where the component approach is somewhat more expensive. This difference is caused by the selection of six components for the Mach 3-4 vehicle and only two components for the Mach 12-15 vehicle; it is more economical to provide fewer test set-ups with larger portions of the total structure included. The results of the cost analysis for the ultimate strength testing of the components are presented in Figures 60 and 61.

2.4.4 Conclusions

(a) Components for the elevated temperature tests become larger than would be anticipated for load application only, because of the requirement for providing suitable thermal boundary conditions. The benefits are the savings of heating rate required at any instant, the reduction in physical size of the test facility, and the capability to use more than one facility at a time.

(b) The effects of radiation on temperature and thermal stresses are larger for the Mach 12-15 vehicle wing cross section than for the Mach 3-4 vehicle wing cross section because of the higher temperatures.

(c) The presence of internal radiation within a component will generally cause thermal gradients larger than in the prototype due to the effect of length on the radiation shape factors.

(d) The maximum thermal stresses developed within a component similar to the Mach 3-4 vehicle wing component will generally be larger than in the full-scale complete vehicle, because of the larger temperature gradients usually present.

(e) The maximum thermal stresses developed within the centerbody component will generally be smaller than in the full-scale complete vehicle, because of the structural boundary conditions.

(f) The effects of radiation in the Mach 12-15 vehicle are potentially greater than in the Mach 3-4 vehicle, requiring that greater care be used in the selection of component size and boundary conditions in the Mach 12-15 vehicle.

(g) The testing costs per square foot of specimen will be more when several components rather than a single complete vehicle is used.

(h) The test complexities associated with the simultaneous application of load and temperature will be larger than for the Mach 3-4 vehicle component testing.

(i) Components appear satisfactory for ultimate strength verification in which the degree of temperature and thermal stress simulation has a relatively minor effect.

2.5 Mechanical Simulation - The ultimate strength verification of the Mach 12-15 vehicle using the basic approach of mechanical simulation is discussed in the following subsections The engineering analysis, test facility analysis, cost analysis, and conclusions are presented in separate subsections. The effects of the mechanical simulation are determined by comparisons to results obtained in

Subsection 2.2, Complete Vehicle Testing, and in Subsection 1.5 for the Mach 3-4 vehicle.

2.5.1 Engineering Analysis - The discussion of the mechanical simulation approach as applied to the Mach 3-4 vehicle (Subsection 1.5.1) is also applicable to the Mach 12-15 vehicle. The three temperature effects (material property degradation, thermal stresses, and the modification of inelastic stress-strain relationships such as the F_{cy}/F_{ty} and F_{cy}/E ratios) may be simulated at room temperature by modification of the test loading. Figure 58 indicates the effects of temperature and thermal stress on computed centerbody failing moment. The computed room/elevated temperature strength ratios for crippling and instability of the shell are 1.09 and 1.44, respectively. The test loads must be increased by 9% if crippling is the basic mode of failure; by 44%, if shell instability is the basic mode of failure. As with the Mach 3-4 vehicle, prior knowledge of the mode of failure is important in that the mode of failure influences the choice of load increase to be used at room temperature.

2.5.2 Test Facility Analysis - The discussion of test facility analysis, cost analysis, and conclusions presented for the Mach 3-4 vehicle are also applicable to the Mach 12-15 vehicle.

The facility requirements for the mechanical simulation approach are basically the same as for either the room or constant elevated temperature test of the complete vehicle, component or model, as appropriate. This technique simplifies the test procedure; the heating system is either not required or need not be integrated with the loading system. If the mechanical simulation of thermal stress is attempted, the loading system will be somewhat more complex. However, in general, this will not affect the total facility requirements. The requirements for testing using mechanical simulation can be determined from Table VIII for the choice of vehicle type and temperature, room or constant elevated.

2.5.3 Cost Analysis - Engineering design costs are unimportant in this approach, except for the previously discussed cost of designing a half-scale model, if that choice of vehicle type is utilized. The selection of augmented loads, the choice of areas of mechanical simulation of thermal stress, and the additional analysis required to determine ultimate strengths in both design and test conditions will require additional engineering effort. Relative to the total costs, however, the cost of this engineering effort is not important. The costs of testing using mechanical simulation are approximately the same as indicated in Figures 60 and 61 for the choice of vehicle type and test temperature, room or constant elevated.

2.5.4 Conclusions

(a) One inherent limitation of the attempt to simulate induced thermal stresses by mechanical loadings is the relatively small number of locations where the prototype stress levels can be duplicated.

(b) Increases in applied loads to account for thermal effects appears to be the most practicable use of the mechanical simulation approach, but this method is dependent upon the availability of adequate techniques of analysis to predict failure in the actual thermal environment.

(c) By definition, tests in which the thermal effects are simulated by mechanical means cannot be expected to produce any thermal effect that cannot be pre-analyzed or predicted.

(d) Mechanical simulation as a general testing approach for the Mach 12-15 vehicle does not have the technical merit of a complete vehicle mission temperature test and, therefore, cannot be used without auxiliary tests.

SECTION VII

FATIGUE STRENGTH VERIFICATION TESTING OF THE MACH 3-4 VEHICLE

BASIC APPROACHES

The discussion of ultimate strength testing of the Mach 3-4 vehicle presented in Section VI.1 is generally applicable to fatigue testing as well, including the results obtained in the thermal analyses. However, in general, fatigue strength is more sensitive to errors attendant upon the use of the various testing approaches than is ultimate strength testing. For example, analysis indicates the effect of thermal stresses on ultimate strength of the wing cross section to be small; however, the effect upon fatigue strength may be large, as indicated in Subsection 2.1. Accordingly, this section considers problems expected to arise in the fatigue strength testing of this vehicle, and focuses attention on areas that affect fatigue strength significantly more than ultimate strength.

1. Parameters Considered

In contrast to ultimate strength testing, all of the parameters discussed in Section IV have an effect on fatigue life and must be considered in the establishment of a fatigue life verification test program; they are, however, not of equal importance. The effect of some of these parameters may be assessed by theoretical considerations; the effect of other parameters may be assessed by a combination of theoretical techniques and analysis of test data; finally some parameters can be investigated only by testing. The parameters that may be investigated by theoretical techniques are those causing variations in temperatures and, subsequently, in thermal stress. These parameters include:

Model size

Surface emissivities

Interface conductances

Parameters to be investigated by combinations of analysis and available test data include:

Creep

Load spectrum

Ground-air-ground cycle

Material degradation caused by temperature

Parameters that may be investigated only by testing, or to a very limited extent by analysis, include:

Metallurgical changes

Corrosion

Manufacturing residual stresses

Specimen-to-specimen variability

In this study, the investigation has been limited to the parameters amenable either to analysis or to analysis and test. The results are discussed in the following sections.

2. Complete Vehicle Testing

2.1 Engineering Analysis

2.1.1 Thermal Analysis - In mission temperature fatigue testing, the structure is subject to numerous heating and cooling cycles, while in the ultimate strength testing cooling is not required. If it were necessary to cool the specimen to exact pre-flight conditions before initiation of each reheat cycle, the heating and cooling requirements would increase, and the aggregate test time would be large. Accordingly, an alternate test schedule was studied in which the reheating is begun while the structural temperatures are still elevated. This was found to significantly reduce, (1) the cooling requirements during that portion of the mission, (2) the subsequent heat input to the structure, and (3) the total test time.

Two reheat profiles, along with the original control temperature profile, are presented in Figure 65 for the wing lower outer surface. Reheat profile 1 commences immediately following termination of the first mission when control node 93 is at 150°F. Reheat profile 2 is initiated after node 93 has been cooled to 60°F and represents usual laboratory procedure. Figure 66 presents thermal stress variation resulting from the recycling temperature profiles. For reheat profile 1, the maximum thermal stress exhibits an 18 percent decrease from the original profile, while for reheat profile 2, as expected, the maximum thermal stress is only 2 percent less than the corresponding thermal stress for the original profile. This difference in results can be explained by examination of the temperature profile of node 111 in Figure 67. It can be seen that for reheat profile 1 node 111 was unable to cool before the reheating began, while for reheat profile 2 considerable cooling had occurred at this node before reheating. Thus, for reheat profile 2, the temperature gradients, as indicated by the differences in temperature between node 93 and node 111, closely duplicate those of the original profile. However, a significant time disadvantage is realized by using reheat profile 2 due to additional cool-down time required. This time disadvantage would cause the theoretical laboratory testing time to be approximately 25% longer than true mission time. Consequently, a profile similar to reheat profile 1 would be preferred. Towards this end, an analysis was performed to determine the shape of another immediate reheat profile which still achieves the desired thermal stress while not appreciably altering mission maximum temperatures. This study indicated that by doubling the temperature-time slope of reheat profile 1, the maximum thermal stress achieved during mission flight is duplicated and test time is reduced to approximately 85% of the mission time and 65% of reheat profile 2. In doing this, however, the peak surface heating rate is increased to 1.3 times the corresponding mission value.

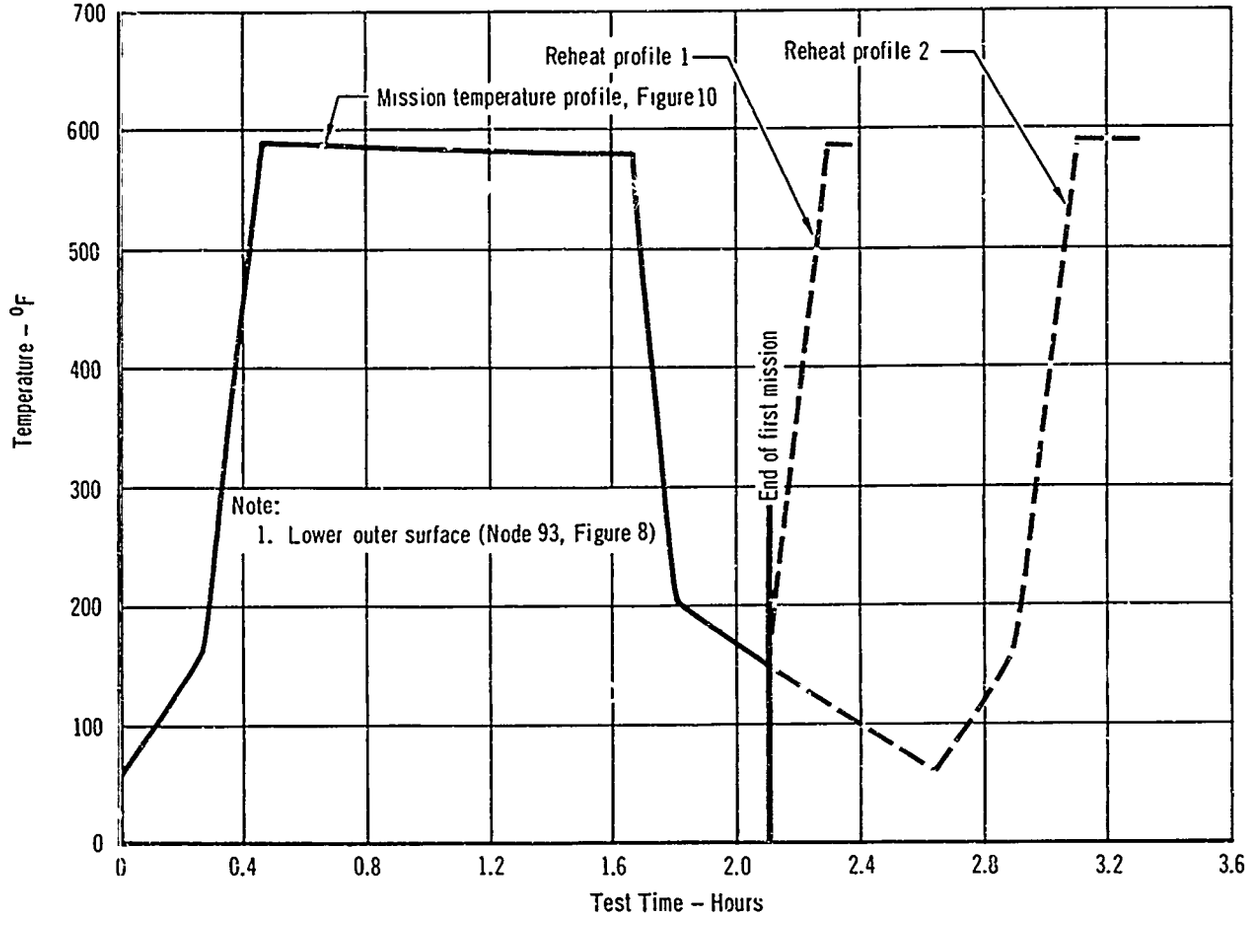

Figure 65 - Reheat Temperature Profiles
Mach 3-4 Vehicle

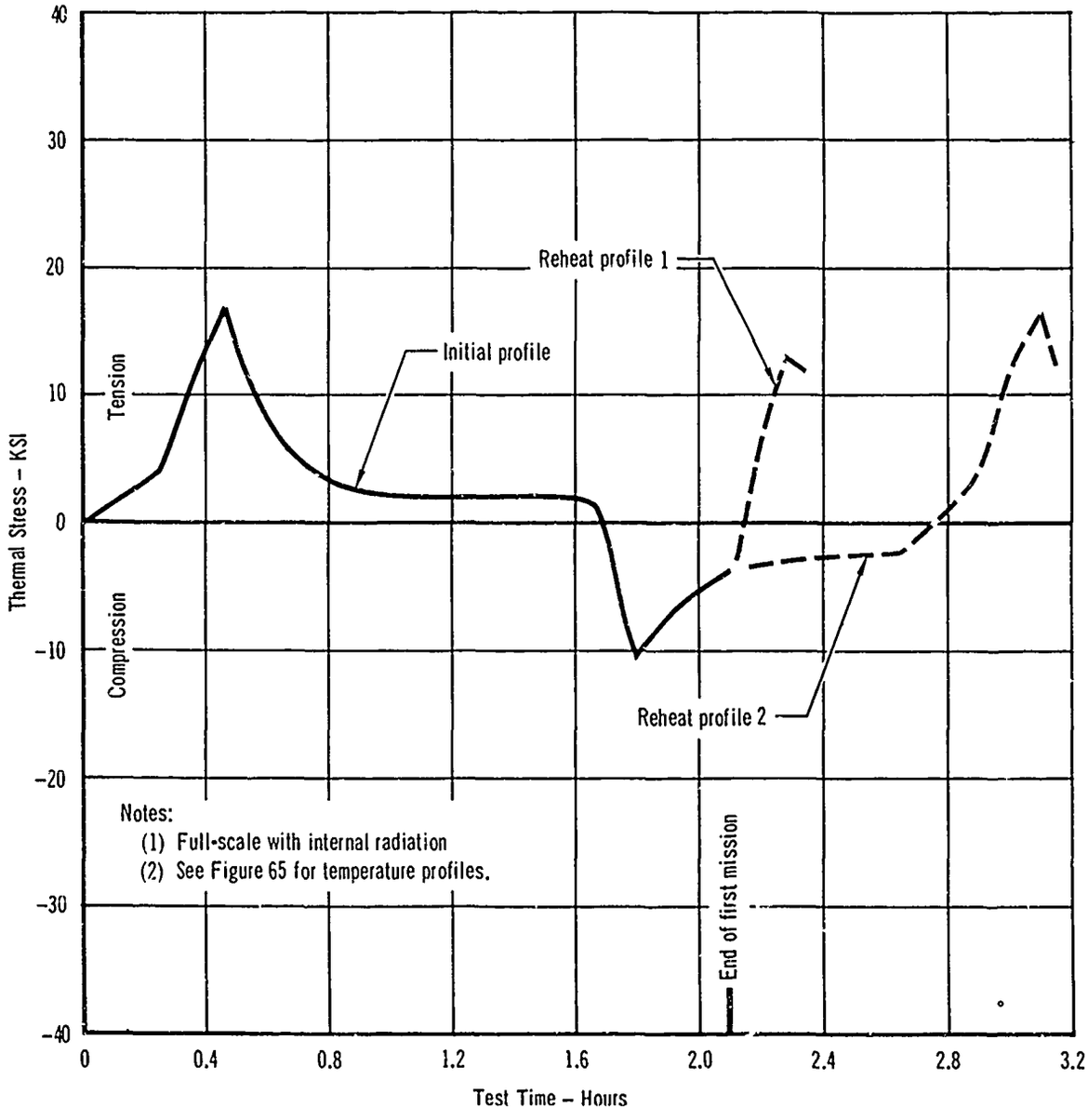

Figure 66 Effect of Alternate Reheat Profiles on Spanwise Thermal Stress at Node 111
Mach 3-4 Vehicle

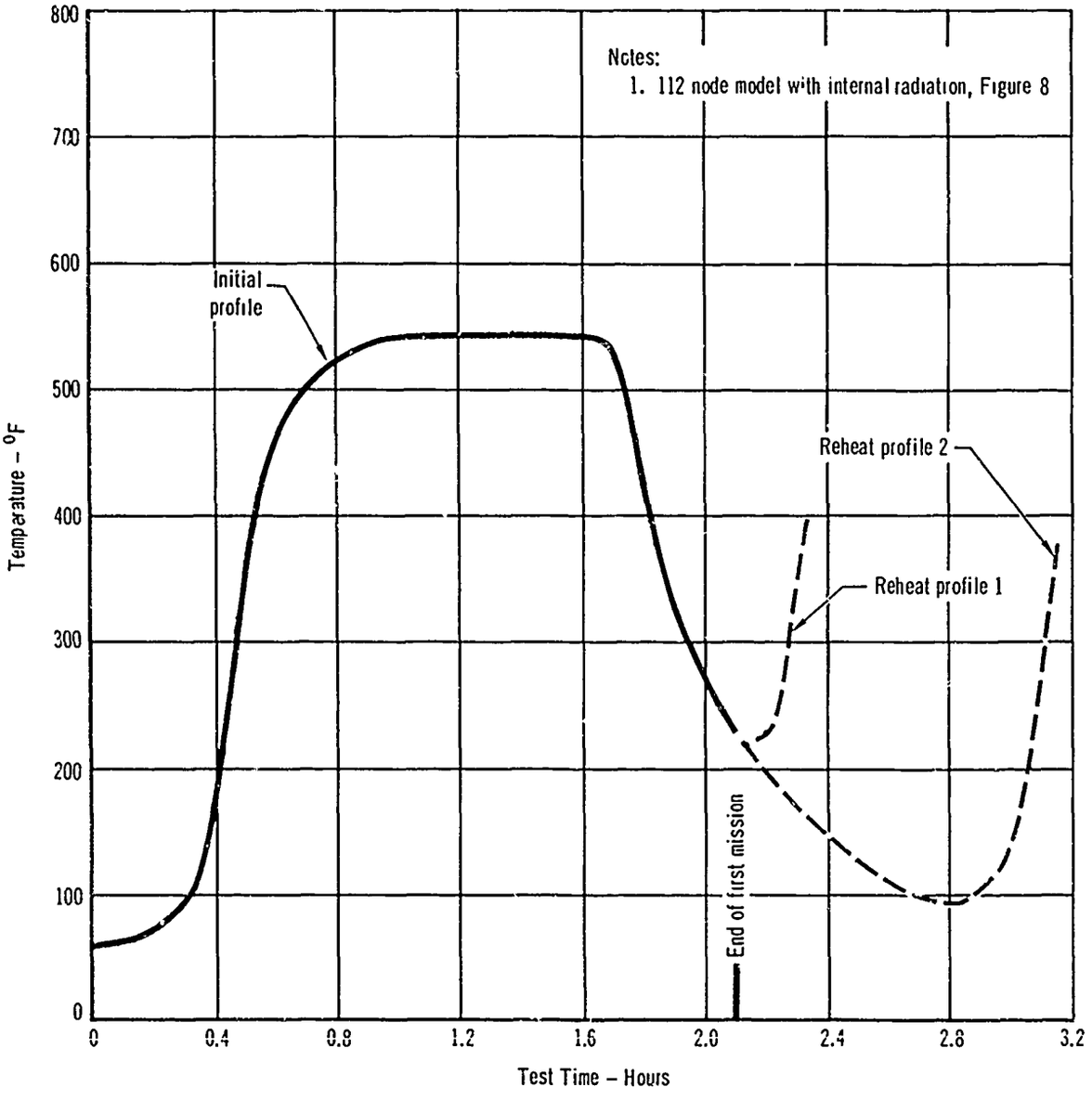

Figure 67 - Effect of Alternate Reheat Profiles on Temperature at Node 111 Mach 3-4 Vehicle

2.1.2 Fatigue Life Analysis - In order to investigate the effects of various parameters on the fatigue life of a 8Al-1Mo-1V duplex-annealed titanium structure, a representative constant-life fatigue diagram (Figure 68) has been determined for the Mach 3-4 vehicle wing cross section for the expected temperature range (R.T. to 600°F) and stress concentration factor (K_T = 4-5). The gust, maneuver, and combined load spectra for this vehicle are presented in Tables II, III, and IV (Section V), respectively. The fatigue life of the Mach 3-4 vehicle was determined by means of the Palmgren-Miner hypothesis with the use of the representative fatigue life diagram (Figure 68) and the combined gust-maneuver load spectrum (Table IV). The results of this analysis for nodes 90 and 111 are presented as curves A in Figures 69 and 70, respectively.

2.1.2.1 Effect of Thermal Stresses on Fatigue Life Without the G-A-G Cycles - A fatigue analysis has been performed to determine the effects of thermal stresses on the fatigue life of the Mach 3.4 vehicle. Thermal stresses are additive to the maneuver mean and gust mean flexural stresses. Their estimated effects upon the fatigue life are presented as curves B in Figure 69 for a maximum thermal stress at node 90 of approximately -5 KSI and in Figure 70 for a maximum thermal stress at node 111 of approximately +25 KSI (see also Figures 22 and 23). Note that the calculated effect on fatigue life of the thermal stress history produced at the lower outer surface of the wing (node 90) is negligible, while the corresponding effect at the lower inner surface of the wing (node 111) is more pronounced. However, the flexural mean stress at node 111 is less than at the outer surface of the wing, since the node is closer to the neutral axis of the cross section. Therefore, this analysis, which does not include the effects of the ground-air-ground cycle, indicates that fatigue at node 111 is less critical than at node 90, in the desired range of life (40,000 flights).

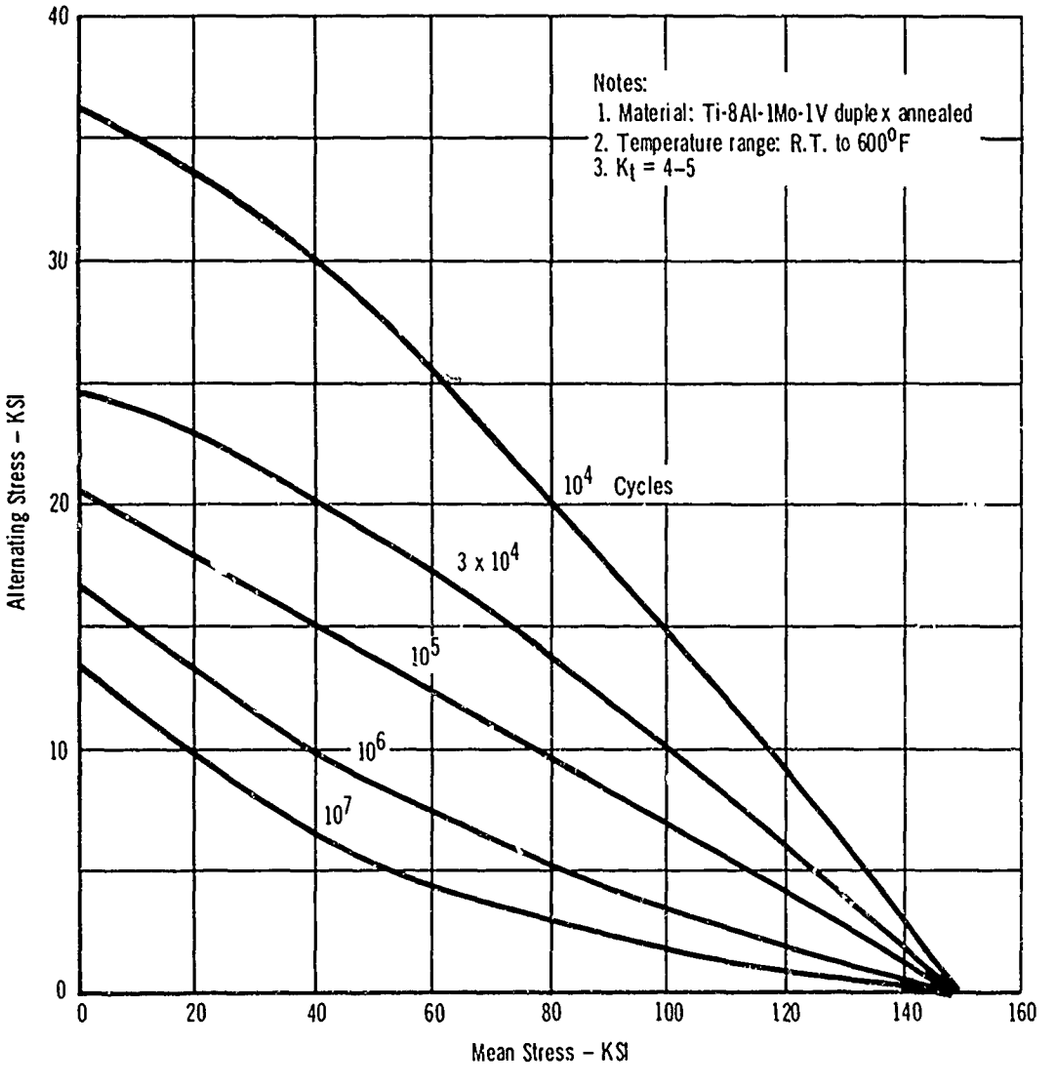

Figure 68 - Representative Modified-Goodman Diagram

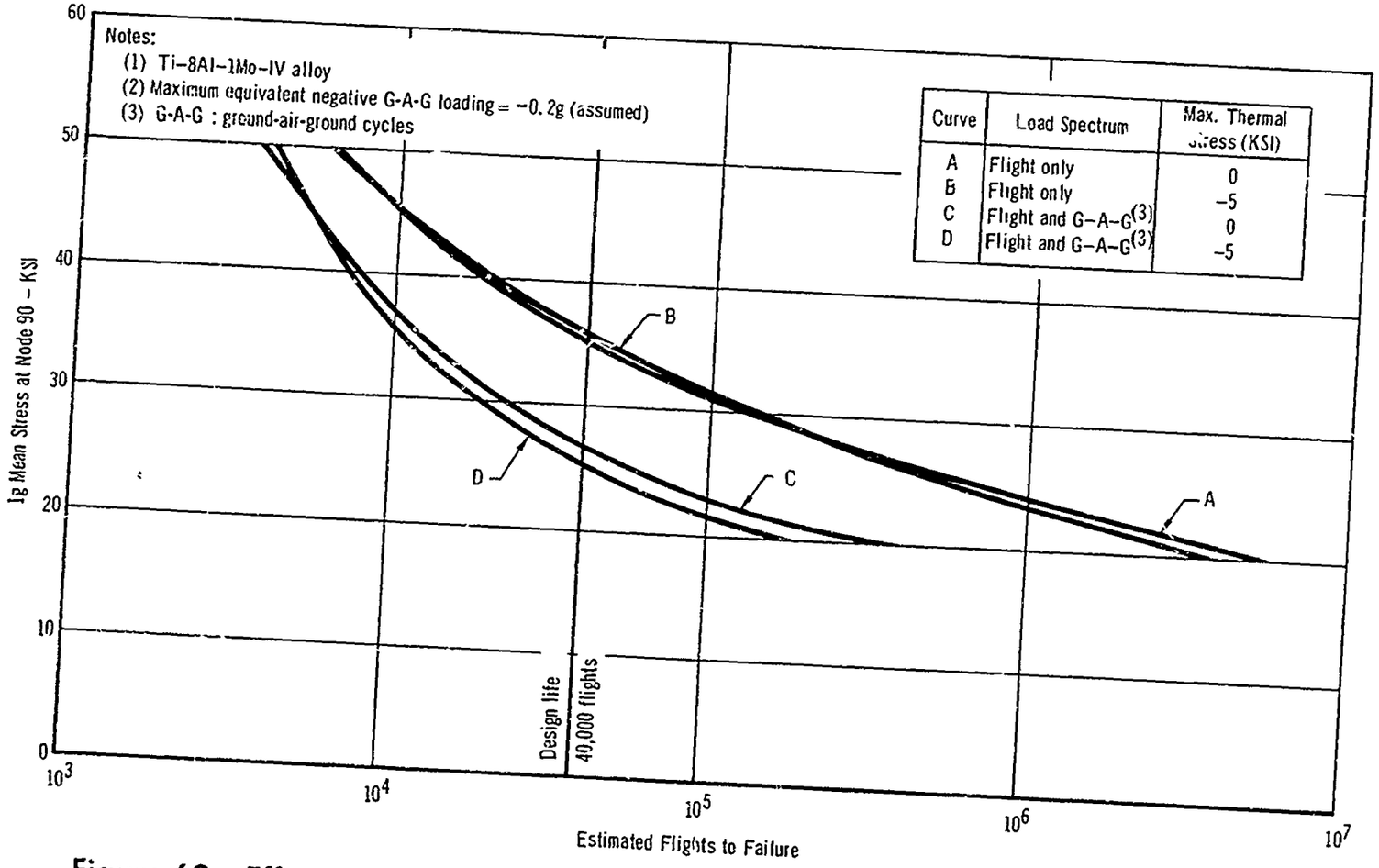

Figure 69 - Effect of Thermal Stress on Estimated Flights to Failure at Node 90 Mach 3-4 Vehicle

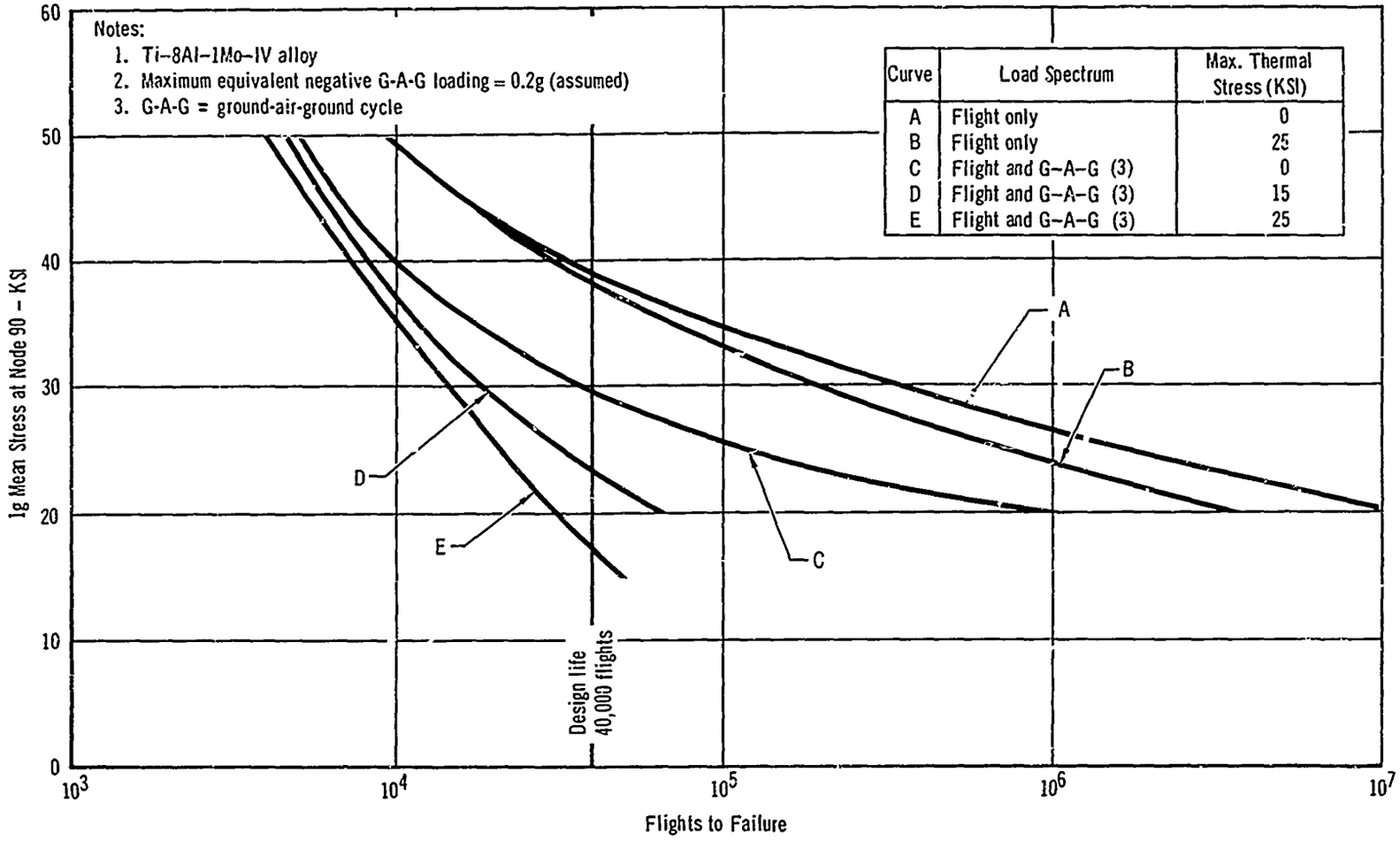

Figure 70 - Effect of Thermal Stress on Estimated Flights to Failure at Node 111 Mach 3-4 Vehicle

2.1.2.2 Effect of G-A-G Cycles on Fatigue Life - To determine the effects of the G-A-G cycles on fatigue life, the gust, maneuver, and thermal stress data discussed previously were used in combination with the G-A-G cycles assumed to occur during the mission. For the Mach 3-4 vehicle, it is assumed that for the ground portion of the cycle the maximum compressive stress in the tension skin during landing impact is equivalent to -0.2g; therefore, the complete G-A-G cycle includes this -0.2g load level and the maximum gust or maneuver loading which occurs during the subsequent flight. A modification of the conventional application of the Palmgren-Miner technique was used to compute the effects on fatigue life caused by the application of G-A-G cycles; the results are presented as curves C in Figures 69 and 70. In this analysis it was considered that the peak of the G-A-G cycle is developed when the maximum positive gust or maneuver load factor occurs during each flight; the alternating stress is one-half the difference between this stress and the negative stress developed during the ground portion of the cycle. Figure 71 indicates the relative effect of G-A-G cycles on the fatigue life at node 90 when such cycles are applied in conjunction with flight loads. It is seen that the G-A-G cycles account for approximately 91% of the fatigue damage.

To determine the accuracy of the modified Palmgren-Miner technique used to determine the fatigue life with the inclusion of G-A-G cycles, a similar analysis was performed for literature-reported fatigue test results on 7075-T6 aluminum-alloy edge notched specimens having a stress concentration factor of 4. By using the variable-amplitude loading spectrum presented in Reference 6 and the constant amplitude S-N curves presented in Reference 7, the predicted flights to failure for the aluminum specimens were calculated and then compared to the test results presented in Reference 6. Figure 72 presents the results of this analysis and indicates close agreement between the predicted and achieved flights

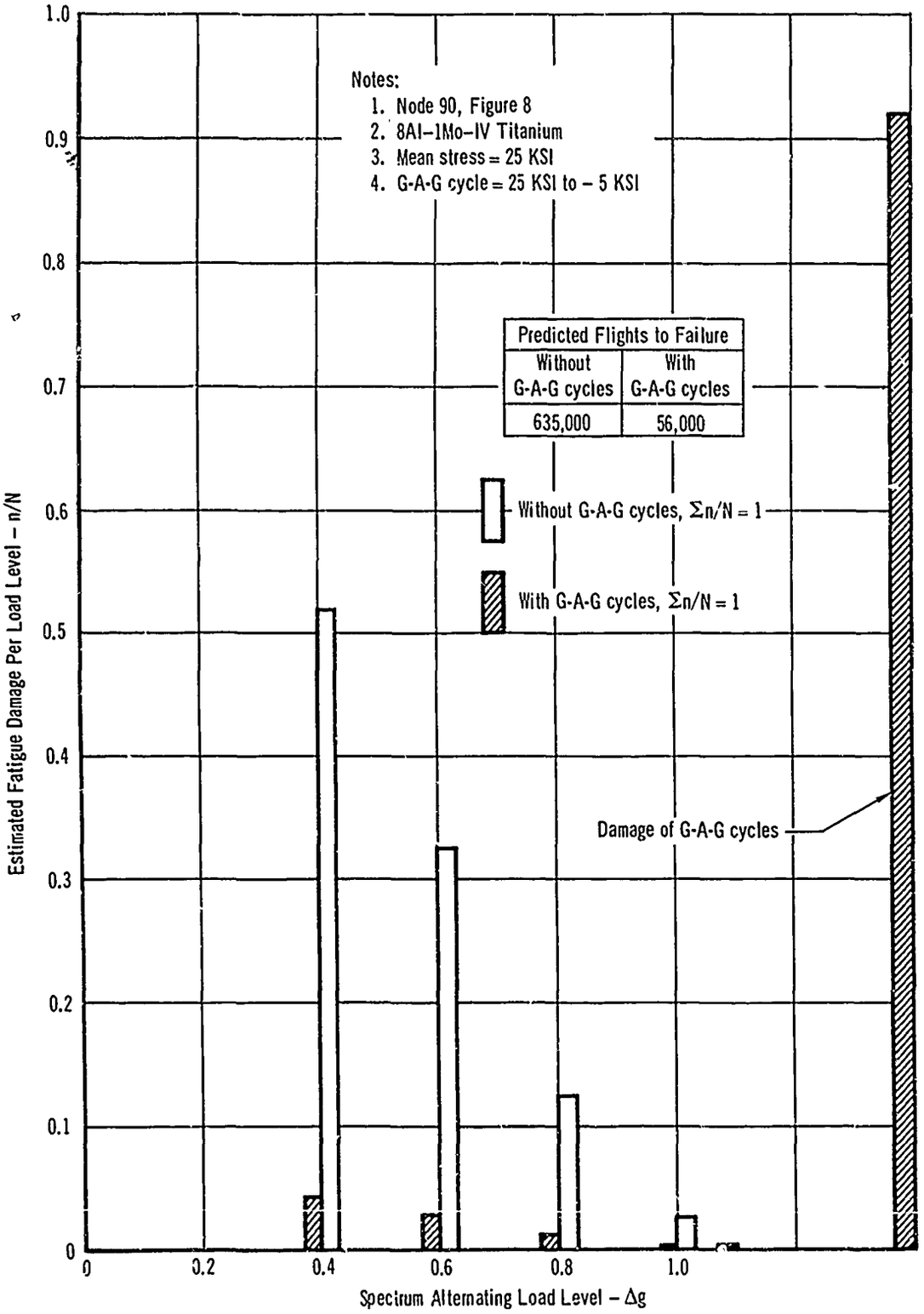

Figure 71 - Effect of Ground-Air-Ground Cycles on Fatigue Damage Mach 3-4 Vehicle

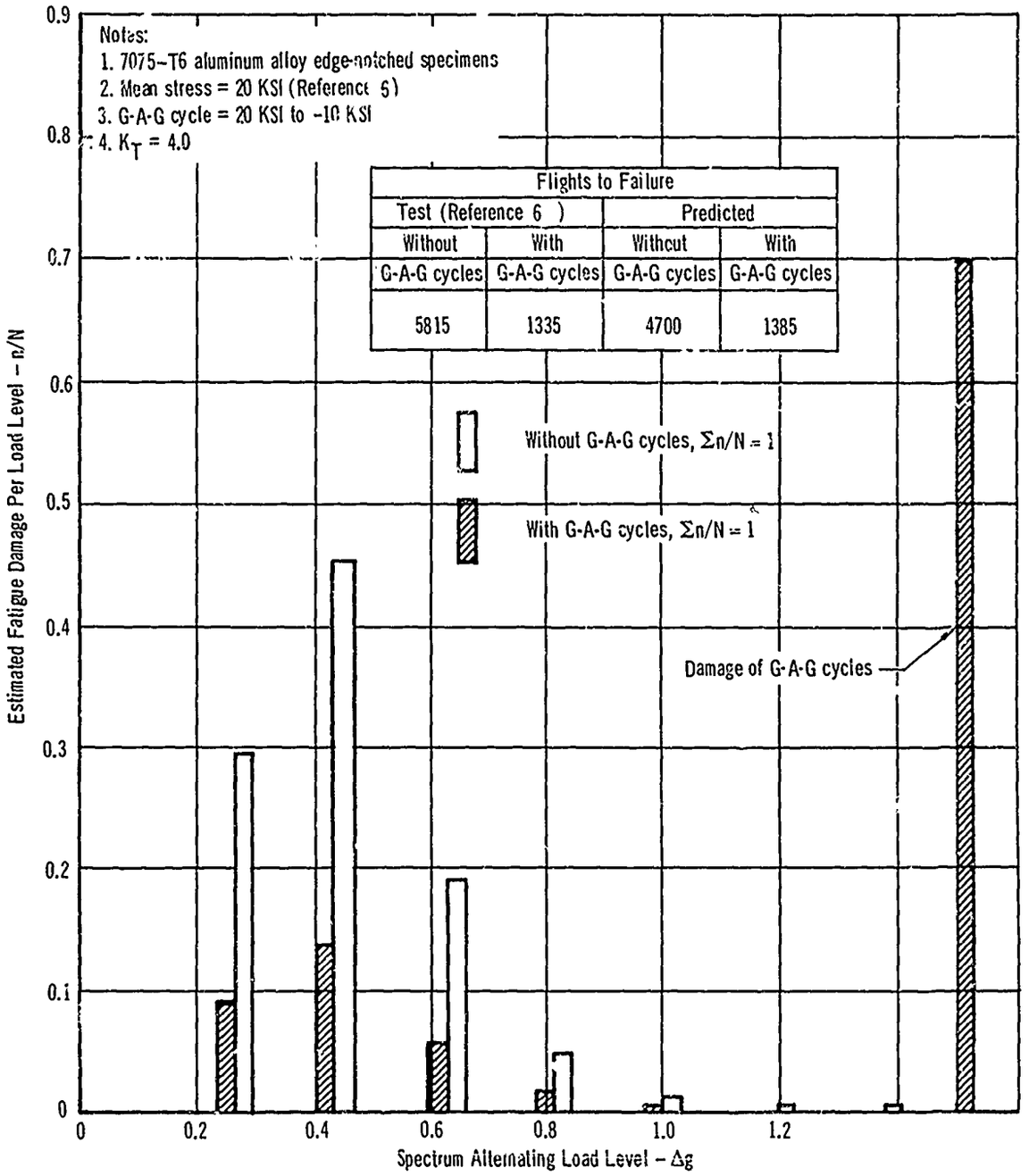

Figure 72 - Effect of Ground-Air-Ground Cycles on Fatigue Damage - Correlation With Tests

to failure when the G-A-G cycles are included, thus providing a partial confirmation of the method used for the Mach 3-4 fatigue life calculations.

The discrepancy between the predicted and achieved flights to failure when flight loads only are considered is due to the conservatism of the Palmgren-Miner technique for randomized spectrum loading, where beneficial residual stresses can increase the fatigue life of the test article. The significant reduction in life with the insertion of G-A-G cycles is attributed to the change in residual stresses at the base of the discontinuity which are either reduced or reversed, depending on the magnitude of the G-A-G cycle. In either case, the succeeding cycles will contribute damage at a much greater rate than if the G-A-G cycles were not applied.

2.1.2.3 Effect of Thermal Stresses on Fatigue Life With G-A-G Cycles - Curve D in Figure 69 presents the effect of thermal stresses on the fatigue life at node 90, with the G-A-G cycles considered; curves D and E in Figure 70 present similar data for node 111. At node 111, there is little computed fatigue damage induced by thermal stresses when only flight loads are considered, since the superimposed thermal stresses developed during the mission increase only the mean stress in the fatigue life computation using the Palmgren-Miner hypothesis. To determine the fatigue life when the G-A-G cycles are included, a modified Palmgren-Miner fatigue analysis was performed. In this analysis it was assumed that the peak magnitude of thermal stress occurring each flight superimposed on the peak stress of the G-A-G cycle. Consequently, the superimposed thermal stresses increased both the mean and alternating stresses by an amount equal to one-half of the peak thermal stress. Therefore, when thermal stresses and G-A-G cycles are both included, a greater decrease in life is evidenced. At node 90, where relatively small thermal stresses are induced, the effect of thermal stresses upon fatigue life when the G-A-G cycles are included is not as pronounced as at node 111.

Figure 73 indicates the relative effect of the combined thermal stresses and G-A-G cycles as compared to maneuver and gust cycles on fatigue damage at node 90; Figure 74 presents similar data for node 111. At both locations, the synergistic effects of thermal stresses and G-A-G cycles on the total fatigue damage is pronounced; especially at node 111 when relatively large tensile thermal stresses are realized. This is apparent in Figure 75 where a summary of the estimated flights to failure for various loading conditions is presented.

2.1.2.4 Effects of Creep Strains on Fatigue Life - For the 8Al-1Mo-1V duplex-annealed titanium alloy, the macroscopic effect of creep deformations on the fatigue life of the Mach 3-4 vehicle has been found to be negligible. This is illustrated in Figure 76 where creep plastic deformations are shown to be small compared to short time plastic deformations due to mechanical loads. If the inelastic strain effect on fatigue life is due to the magnitude of plastic flow, creep deformations contribute only a small amount to the total damage compared to deformations caused by short time maneuver loads. Consequently, the macroscopic effects of creep deformations on the fatigue life of the Mach 3-4 vehicle are expected to be negligible for notched specimens formed of the titanium alloy considered. Furthermore, based on tests reported in the literature, it is tentatively concluded that the microscopic creep effects due to changes in metallurgical structure in notched specimens of this material are also small.

2.2 Test Facility Analysis - The test facility for fatigue testing of the Mach 3-4 vehicle will be very similar to the ultimate strength test facility described in Section VI, with two possible exceptions: equipment required for cooling and desired accuracy of load or temperature simulation.

It is probable that the critical condition or conditions for the ultimate strength verification testing occur during the climb portion of the mission, or

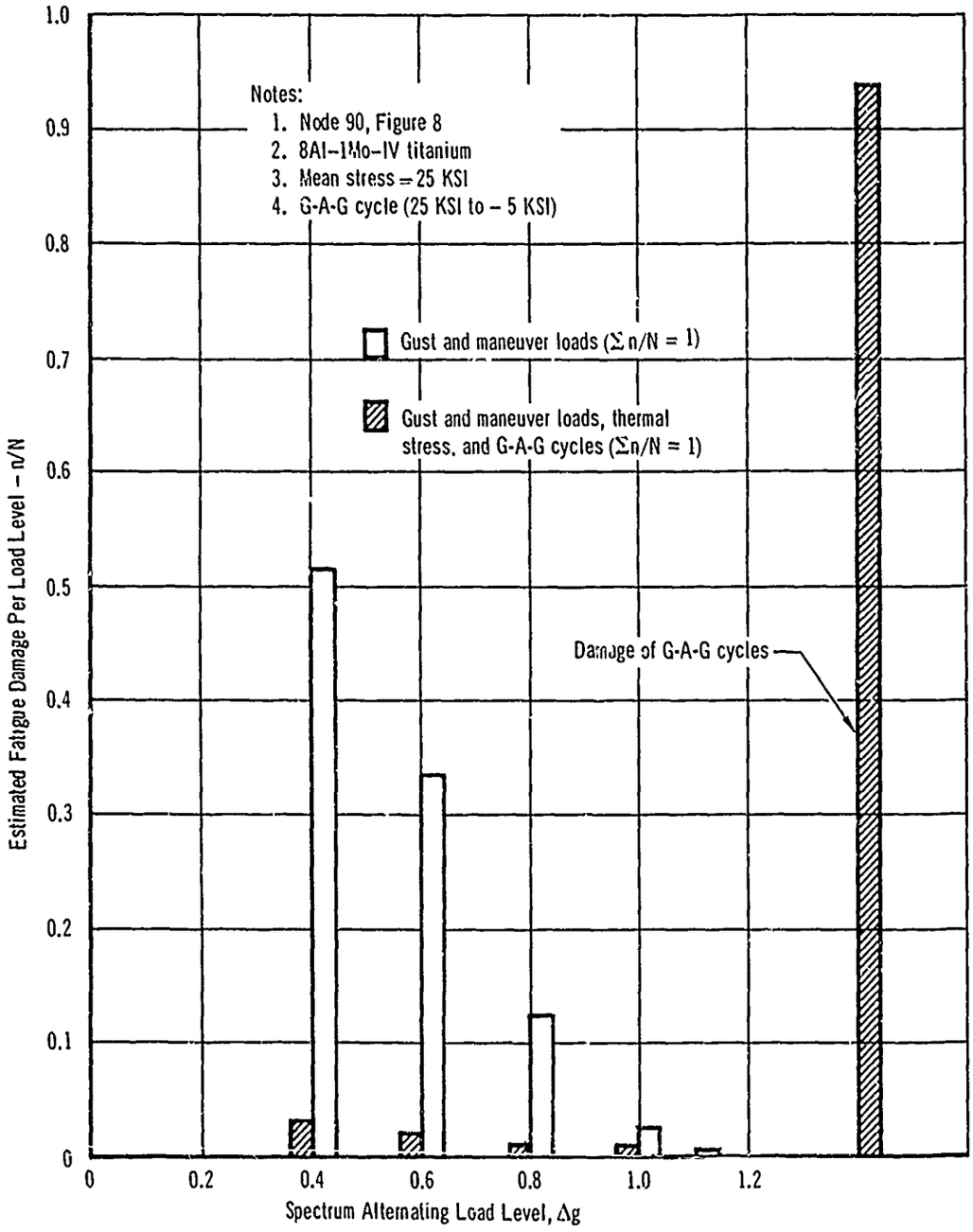

Figure 73 - Effect of Thermal Stress and Ground-Air-Ground Cycles on Fatigue Damage at Node 90 Mach 3-4 Vehicle

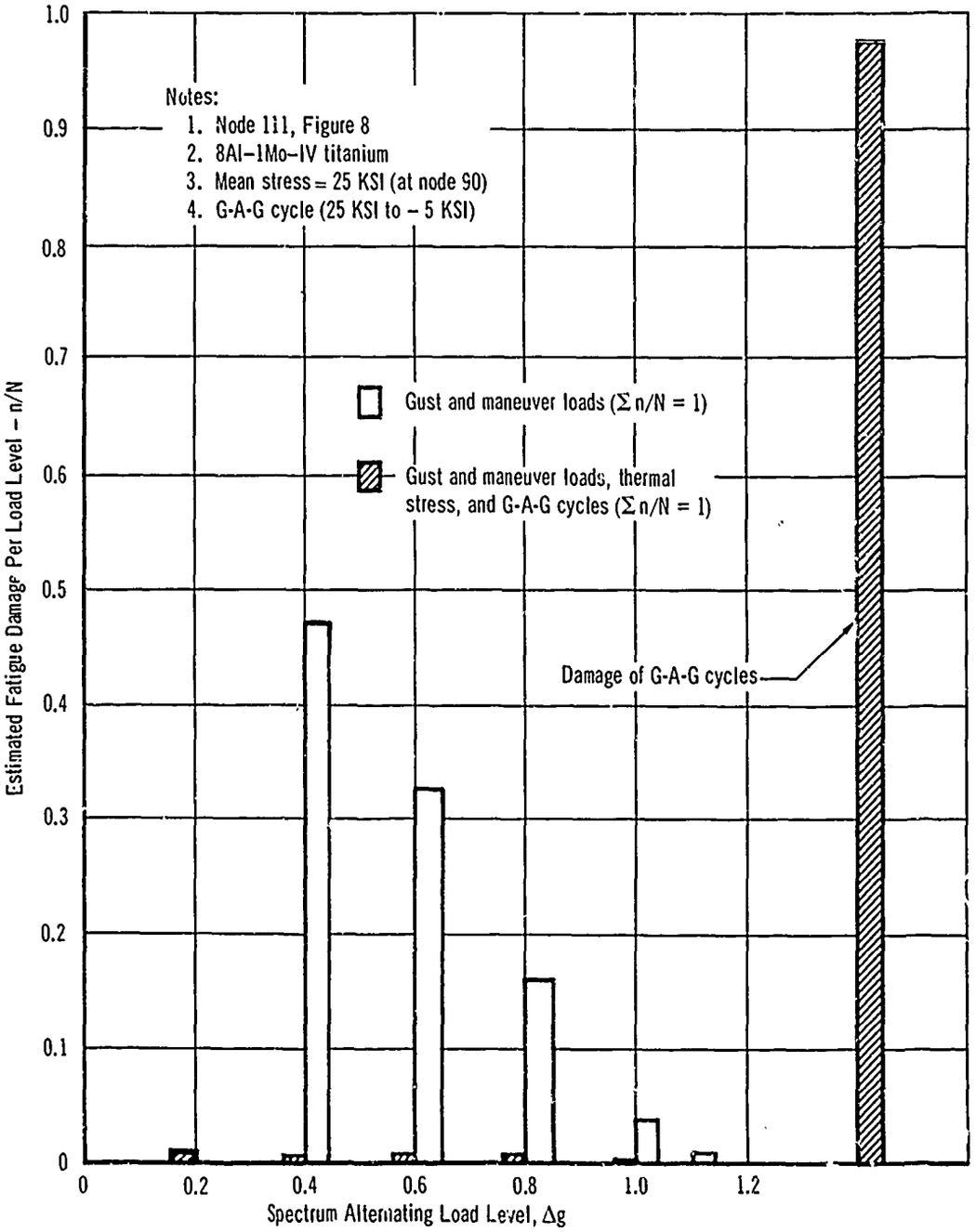

Figure 74 - Effect of Thermal Stress and Ground-Air-Ground Cycles on Fatigue Damage at Node 111
Mach 3-4 Vehicle

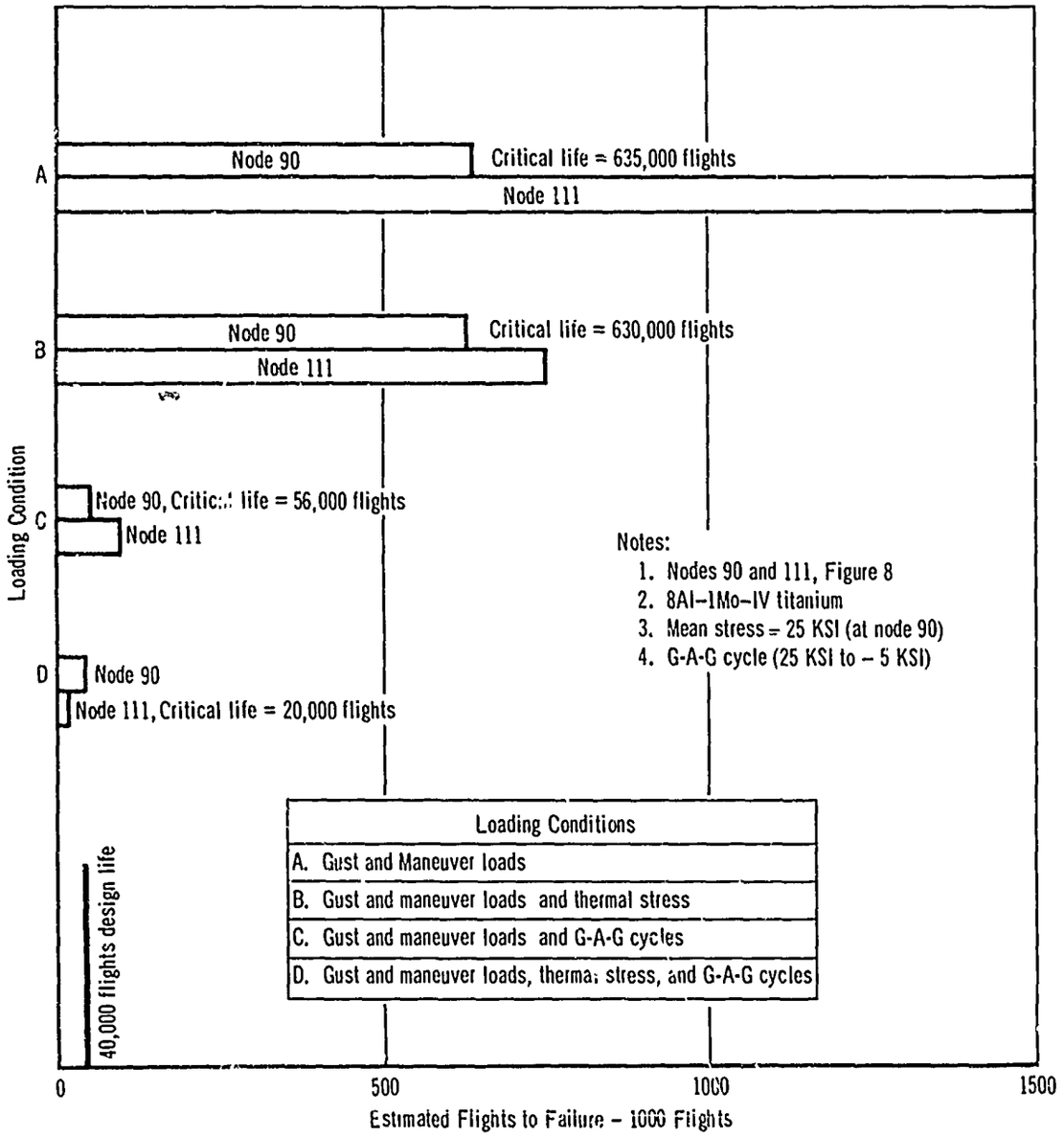

Figure 75 - Effect of Thermal Stress and Ground-Air-Ground Cycles on Estimated Flights to Failure Mach 3-4 Vehicle

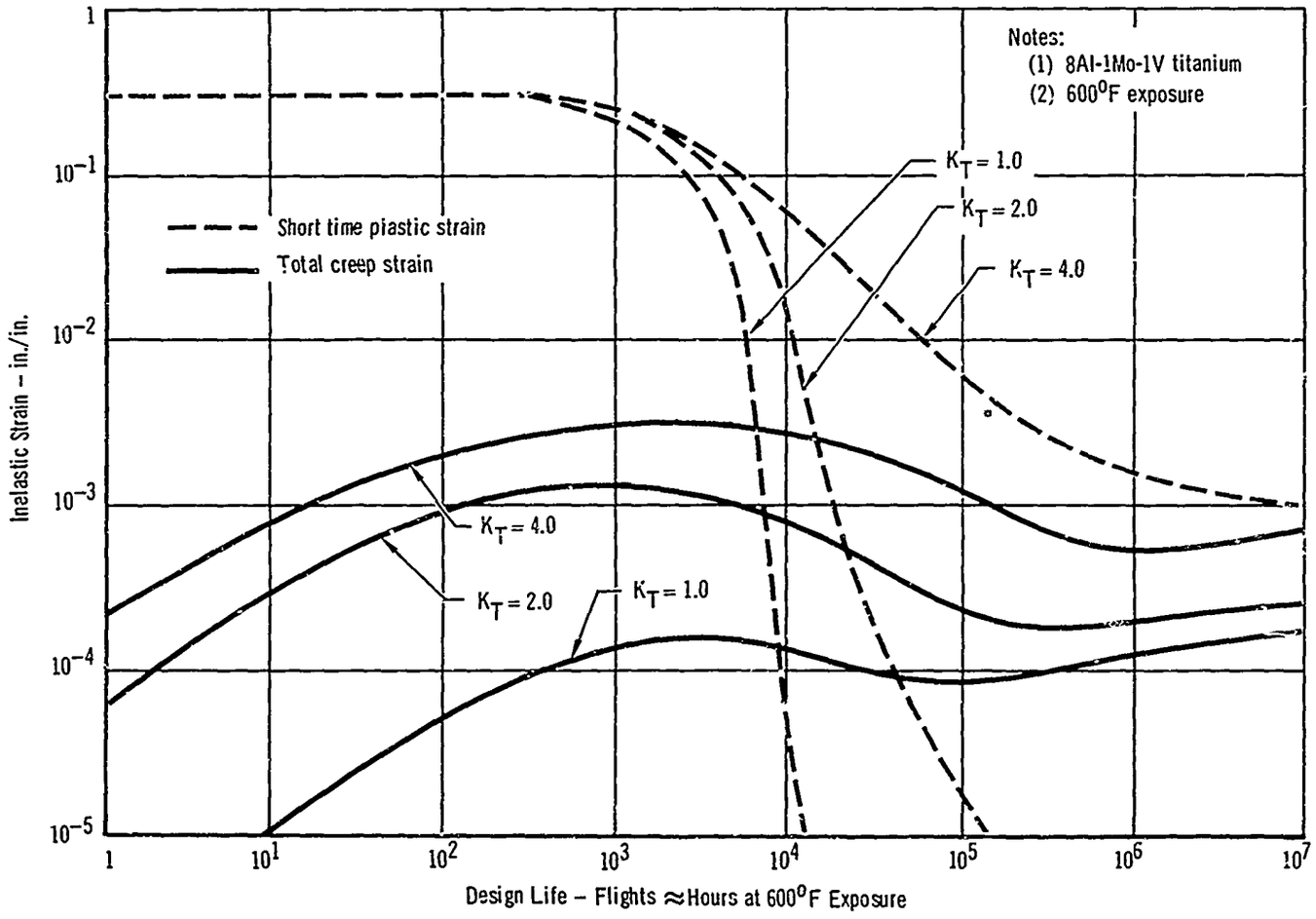

Figure 76 - Effect of Design Life on Short Time Plastic Strain and Creep Strain Mach 3-4 Vehicle

at the end of climb, which coincides with the time of maximum thermal stress for much of the structure. Cooling is not required for duplication of either of these conditions; however, mission simulation of temperatures for fatigue testing does require cooling. If accurate duplication of temperatures during cooling were not required a gross technique would be sufficient, although "natural" cooling obtained by merely deactivating the heating system would require too large of an elapsed test time. The coolant system design is discussed in Section VI.1.2.2 and the required mass flow of cooling air is indicated in Table V.

The second difference between ultimate and fatigue testing lies in the desired accuracy of load and temperature simulation. As was indicated in Subsection 2.1.2.3, thermal stresses can have a major influence on the fatigue life of a structure; consequently, the automatic load and temperature control equipment must be more reliable in fatigue testing than in ultimate strength testing. However, the simultaneous cyclic application of load and temperature presents a problem in that the possibility of system failures occurring is increased, causing an increase in down time. It has been assumed in the present study that the facility requirements presented in Table V are applicable.

2.3 Cost Analysis - The engineering and manufacturing costs for the fatigue test specimen will be almost identical to those of the ultimate strength test specimen; these costs are discussed in Section VI.1 2.3.

The basic difference in the costs between fatigue testing and ultimate strength testing is that of test performance. The increased costs of fatigue testing are due to the power required to heat and cool the specimen, lamp and other equipment replacement, man-hours required for test operation and maintenance, and man-hours required for facility and specimen maintenance or repair. These man-hour costs are proportional to the total time required for

the completion of the test; they are indicated in Figure 36. The test performance costs are shown in Figure 37; the power and man-hour costs are combined into a single category titled test performance, which includes downtime; the equipment is included in the jig cost category.

The constant elevated temperature technique for fatigue testing does not require a cooling system. This reduction in test complexity allows companion reductions in test staff and in total time required to perform the test. Further, the room temperature testing approach offers greater economies than do the mission or constant elevated temperature approaches.

2.4 Conclusions - The following conclusions, identical to those determined for the complete vehicle testing approach applied to ultimate strength verification testing, are applicable to a complete vehicle fatigue testing.

(a) The effects of internal radiation within the wing cross section on thermal stress are significant.

(b) The effects of interface conductance between the surfaces of the wing cross section and air pressure within the wing cross section on thermal stress are not significant.

(c) The effects of relatively small test control temperature error may be expected to cause significant deviations in thermal stress, and therefore in fatigue life, if the G-A-G cycle is included.

(d) Heat flux, either BTU/hr. or BTU/ft^2-hr., is not a serious problem; the real heating problems are associated with equipment reliability, the possibility of producing some serious unwanted and unforeseen thermal effect, and the difficulty of controlling temperatures over large areas.

The following conclusions are different from those determined for the complete vehicle testing approach applied to ultimate strength verification

testing and are basically applicable to mission temperature fatigue testing:

(a) For vehicles designed for long fatigue life, such as the Mach 3-4 vehicle, analysis indicates that creep is not of major significance, and hence its simulation is of secondary importance.

(b) For the fatigue strength verification testing of certain portions of the Mach 3-4 vehicle (wing carry-through, inner wing, etc.), G-A-G cycles are extremely important.

(c) Thermal stresses are not of significant importance for fatigue life simulation, if only flight loads are considered. However, if the ground-air-ground cycle is included in the testing program, the thermal stress simulation becomes important.

(d) The additional requirement for cooling causes the mission temperature fatigue test to be more complex, and therefore more difficult than the mission temperature ultimate strength test.

(e) The test cooling requirements for this vehicle are more restrictive than the heating requirements due to the large cooling requirements at moderate temperatures where re-radiation is not significant.

(f) The largest additional cost for fatigue rather than ultimate strength testing is caused by the man-hours required for test performance.

3. Model Testing

3.1 Engineering Analysis - The engineering analysis pertaining to ultimate strength considerations in model testing described in Section VI.1.3.1 are also applicable to the fatigue verification testing using models. The effects in temperature errors caused by modeling are more important in fatigue strength verification than in ultimate strength verification, because of the greater importance of thermal stresses on fatigue life. Temperature profiles for the point of maximum thermal stress (node 111, Figure 8) are shown in

Figure 39. The use of a structural model generally causes temperatures at such internal locations to be lower than for the prototype, and this greater temperature difference between the outer and inner surfaces of the wing structure induces thermal stresses that are larger in the model than in the prototype. This effect of modeling upon thermal stresses is shown in Figures 22 and 23. In Figure 23, the maximum thermal stress at node 111 in the full-scale complete vehicle is 16,800 psi, while in the half-scale cross section, it is 20,500 psi. The effect of this difference in thermal stress on estimated flights to failure may be determined from Figures 69 and 70; for a 1g mean stress at node 90 of 25,000 psi with the G-A-G cycle, Figure 69 indicates the full-scale cross section at a thermal stress of 16,800 psi would fail at 29,000 flights and the half-scale cross section at a thermal stress of 20,500 psi would fail at 23,500 flights. Consequently, the analysis to determine the effect of modeling on fatigue life as affected by thermal stress indicates that a half-scale model, fatigue tested at mission temperatures, would fail in 81% of the life of a similarly tested full-scale complete vehicle.

Other parameters that will be non-scalable in a fatigue model, indicated in Table VII, include creep, cyclic rate, surface finish, tolerances, and stress gradients. For the same stresses in a model and a full-scale complete vehicle, creep is not a scalable factor, if the test is performed at mission temperatures; this results from model test time scaling as the square of the model scale factor. Thus, four minutes of test time in the full-scale vehicle would be replaced by one minute in the model and, therefore, the correct amount of creep would not be produced in the model fatigue test at the same stress levels. It is also true that the interaction between creep deformation and thermal and mechanical load deformations would not be accurately reproduced in the model fatigue test at the same stress levels. However, as indicated in

Subsection 2.1.2.4, creep macroscopic deformations are small in comparison to the plastic strains developed by short term gust or maneuver cycles; therefore, the macroscopic strain effects of creep are judged to be not significant. Similarly, the microscopic metallurgical effects are not expected to be significant for alloys whose transformation temperatures are much higher than the exposure temperature; therefore, the fatigue life of the half-scale model should not be significantly affected by the non-scalable creep effects.

The desired scale factor for cyclic rate (load frequency) from prototype to model is the square of the linear scale factor (see Table VII). Therefore, the fatigue loads must be applied four times as rapidly to the model as to the full-scale complete vehicle, if mission temperatures are used. This relatively small change in laboratory load frequency is not expected to have a significant effect on fatigue life.

Generally, surface finishes and tolerances will not be scaled in a model. It is expected that surface finish will be approximately the same in the full-scale structure and model; the maintenance of scaled tolerances in a model will be difficult.

The desired stress gradient in a model is 1/n that of the full-scale complete vehicle; for a half-scale model, the stress gradient would be twice that of the full-scale vehicle. So, for a given size of surface imperfection in both the prototype and model, the volume of the highly stressed metal region is considerably less in the model than in the full-scale vehicle. Due to the impossibility of scaling of material parameters such as grain size or hardened particle spacing, this smaller volume of highly stressed material is expected

to increase the life of the model in comparison to that of the prototype. Closely related to this are the effects of specimen size; if the model were fabricated with scaled geometry, scaled stress gradients, equal stress concentrations, scaled surfac finish, scaled tolerances, and scaled metallurgical structure (grain size, etc.), the deviation between the fatigue life of a model and the fatigue life of the prototype would, theoretically, be insignificant.

A McDonnell sponsored test program has been conducted to evaluate the effect of modeling on fatigue life. The fatigue lives of full and half-scale single-shear bolted lap joint specimens were determined by test and compared to the results of tests conducted on specimens of the same nominal geometric configuration as presented in Reference 8. The full-scale test specimens were made from a single sheet of bare 2024-T3 stock of 0.125" thickness; the half-scale specimens were obtained by chem-milling the basic sheet to the required 0.063" thickness. A description of the specimens is presented in Figure 77; a summary of the results is contained in Table IX. Figure 78 presents the fatigue lives of the full and half-scale specimens, as well as the results of alclad sheet specimen tests reported in Reference 8. On the basis of these tests, it appears that the ultimate strength characteristics of the McDonnell-tested half-scale specimens are scalable. However, the fatigue tests indicate that the fatigue lives are not scalable, since at stresses less than 25 KSI, the half-scale specimens exhibited a greater fatigue life than the full-scale specimens.

An apparent contradiction to the results for the bolted lap joint tests was found in Reference 9 in which the results obtained from the flexural fatigue testing of bare 2024-T3 aluminum alloy of triangular coupon specimens mounted as cantilever beams were reported. These specimens were rigidly attached along one edge of the triangular shape coupon and were designed to

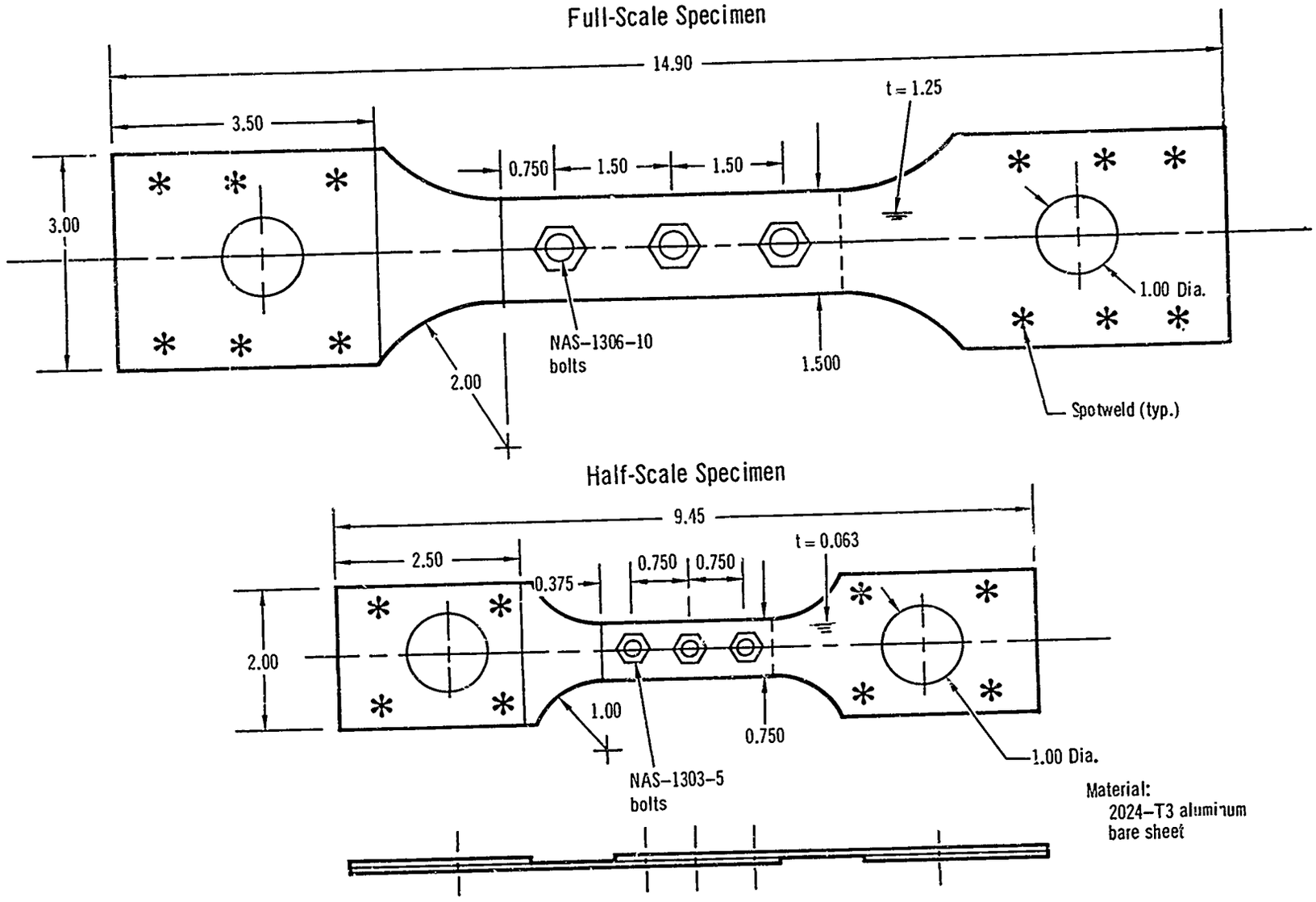

Figure 77 - Bolted Lap Joint Fatigue Specimens

TABLE IX
SUMMARY OF BOLTED LAP JOINT TESTS

Bolted Lap Joint Ultimate Strength Tests

Specimen	Width (In.)	Ave. Thickness (In.)	Geometry (1)	Ultimate Failing Load (Lb.)
1	1.5075	0.1278	Full-scale	9950
2	0.7500	0.0637	Half-scale	2390

Bolted Lap Joint Fatigue Tests

Specimen	Width (In.)	Ave. Thickness (In.)	Maximum Load (Lb.)	Minimum Load (Lb.)	Fatigue Life (1000 Cycles)
Full-scale specimens(1)					
3	1.5045	0.1276	5600	1400	69
4	1.5085	0.1276	5600	1400	39
5	1.5025	0.1275	5600	1400	43
6	1.5000	0.1277	3730	930	168
7	1.5020	0.1275	3730	930	131
8	1.5055	0.1280	3730	930	63
Half-scale specimens(1)					
9	0.7509	0.0640	1400	350	59
10	0.7497	0.0647	1400	350	64
11	0.7511	0.0640	1400	350	41
12	0.7476	0.0647	930	230	389
13	0.7512	0.0641	930	230	104

Notes: 1. See Figure 77 for specimen geometry.
2. 2024-T3 material.

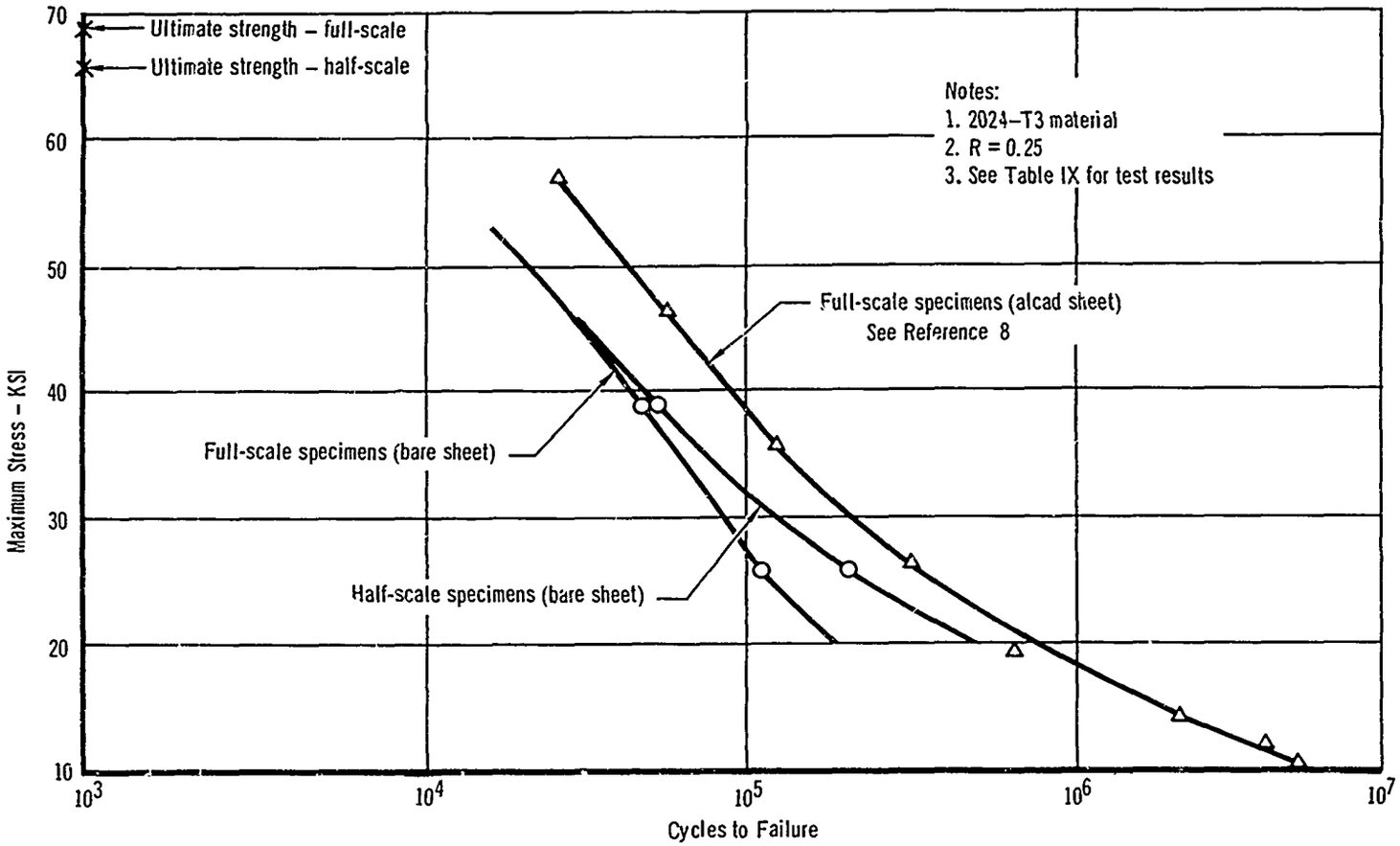

Figure 78 - Fatigue Life of Full-Scale and Half-Scale Bolted Lap Joints

cause crack initiation at the center of the long edge when the specimen vibrated in the first bending mode. The results of these tests indicate that the one-third scale specimens exhibit shorter fatigue lives than the full-scale specimens. No clear explanation is available for this behavior at this time.

Three phenomena may be considered in the investigation of the effects of modeling on fatigue life: crack initiation, crack propagation, and finally, failure. Crack initiation is considered first. For the case in which fatigue cracks initiate from holes or fillets, where the crack must be initiated before propagation may occur, the fatigue life of a one-half scale model may exceed the fatigue life of the full-scale specimen by a factor of five. For the case in which the cracks are modeled, that is, they are proportioned to the thickness and/or the width of the weld bead and occur in the same number as in the prototype, the model is expected to exhibit greater fatigue life than the prototype. However, for the case in which the cracks in the model and prototype are the same size, that is, they are caused by the basic welding process and are not properly scaled, the model fatigue life would be expected to be less than that of the full-scale specimen.

For the second phenomenon, a study was made of the results reported in Reference 10 to evaluate the crack propagation rates and residual strength characteristics of flat sheet specimens made of L73 material containing cracks. It was determined that the critical crack length and the rate of crack propagation are a function of the size of the specimen, which agrees with other test data. From Figure 79 it can be seen that the scaled critical length in the 1/3 scale model is longer than that of the prototype, which would indicate that the model would have fatigue life greater than that of the full-scale specimen. However, other data presented in that reference indicate that (1) as the actual width of the plate is decreased, the rate of crack propagation

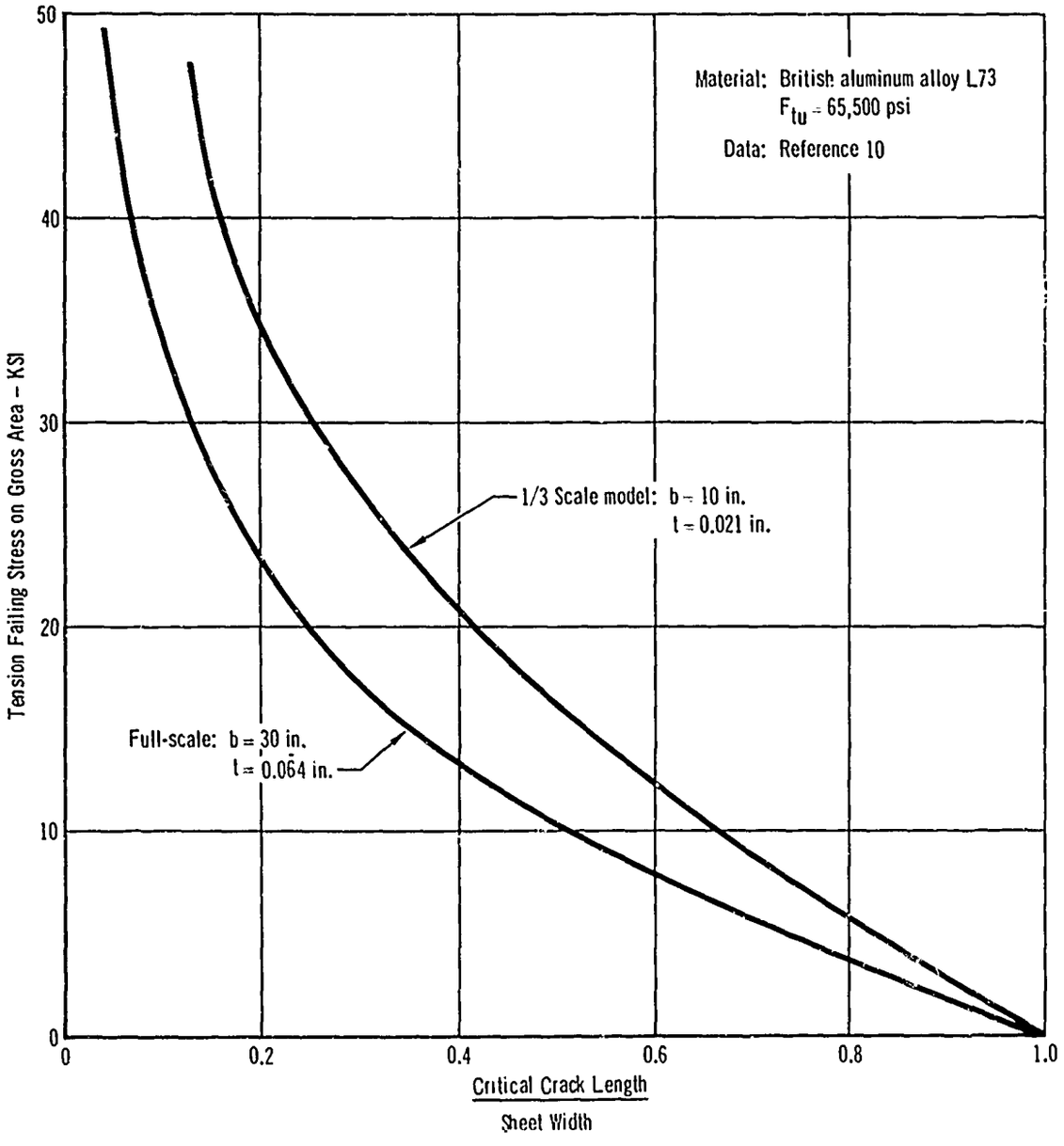

Figure 79 — Effect of Scaling on Residual Tension Strength of Aluminum Sheet Containing Cracks

increases, which would tend to decrease the fatigue life of the model in relation to that of the prototype, and (2) as the actual thickness of the plate is decreased, the rate of crack propagation is reduced in relation to the prototype. The data presented are somewhat inconclusive as to the extent of compensation between these effects, making the prediction of the relative fatigue life between models and prototypes on the basis of rate of crack propagation questionable.

Consequently, if a reasonably accurate fatigue life prediction of a full-scale structure is to be made from model testing, a further investigation into important parameters such as crack size, crack initiation period, stress history, and rate of crack propagation is required. Such investigation would be beyond the scope of this study, but might be given consideration in future efforts in this field. Since the precise definition of the value of some of these parameters is difficult, the level of confidence in the prediction of fatigue life in a full-scale complete vehicle after testing of a scaled model is currently low.

3.2 Test Facility Analysis - The analysis of the test facility requirements is quite similar to that of the full-scale complete vehicle; it is assumed that the fatigue and ultimate strength test facilities would be identical with the exception that cooling is required for fatigue testing and not for ultimate strength testing. The description of the basic differences in the modeling approach in contrast to the complete vehicle approach is presented in Section VI.1.3.2. The test requirements are presented in Table V and indicate that the increase in required heating and cooling rates will result in no savings in the quantity of control equipment since proper local temperature control on the model surface becomes more difficult than on the full-scale complete vehicle.

3.3 Cost Analysis - The engineering and manufacturing costs for the fatigue test specimen will be almost identical to those of the ultimate strength

test specimen; these costs are discussed in Section VI.1.3.3. The cost of designing and fabricating the test fixture will be the same as for the ultimate test. The basic difference in costs between the ultimate and fatigue tests is caused by test performance. The cost of test performance for scale models is less than for the complete vehicle because of its reduced size and power requirements. The difference in cost of test performance for this approach, however, is minor in comparison to the total cost because of the large tooling cost for specimen fabrication. The costs for the fatigue tests are indicated in Figures 36 and 37.

3.4 Conclusions - The following conclusions, identical to those determined for the modeling approach applied to ultimate strength verification testing, are applicable to model fatigue testing:

(a) Fabrication feasibility dictates that scale factors of 1/4, 1/2, or 3/4 be considered for structural verification models with 1/2 appearing most usable. Other scale factors would require a greater use of non-standard hardware or require greater deviations from scaled geometry, which could have effects on the fatigue life of the specimen or greatly increase procurement costs.

(b) Of all the thermal factors known to be not scalable (radiation, interface conductance, etc.), radiation is of greatest importance for the structures considered.

(c) Thermal stresses in tests of models where the time scale factor is correct for conductive heat transfer tend to be greater than for full-scale structures due to the effects of internal radiation, which dictate a different time scale factor.

(d) It is possible to more closely duplicate thermal stresses in a model by the use of a time scale factor somewhere between the values dictated by conductive and radiative heat transfer modes.

(e) Serious drawbacks to the model approaches are the cost of tooling for fabrication of a satisfactory structural model, and secondly, the engineering effort required to complete model drawings.

The following conclusions are different than those determined for the modeling approach for ultimate strength verification testing and are basically applicable to mission temperature testing:

(f) The effect of the increased thermal stresses in the model may decrease the fatigue life below that of the full-scale complete vehicle.

(g) The non-scaling of creep in a model is not expected to significantly affect the model fatigue life.

(h) The change in cyclic rate (load frequency) required for mission temperature testing is not expected to significantly affect the fatigue life.

(i) Three phenomena of fatigue: crack initiation, crack propagation, and failure are affected differently by the modeling process. Therefore, the model fatigue life may be either greater or less than that of the full-scale specimen, depending on detailed design features.

(j) The present level of confidence for the prediction of fatigue life for a complete vehicle after testing of a scale model is small.

4. Component Testing

4.1 Engineering Analysis - The analysis presented in Section VI.1.4.1 is also applicable to the fatigue test verification. There is not the same

large difference in confidence for fatigue and ultimate strength testing of components as for models.

A component of the Mach 3-4 vehicle has been analyzed to evaluate the effect of the use of components on fatigue life. It has been determined that the maximum calculated thermal stress in the component test area selected is greater than the maximum thermal stress in the same area of the full-scale complete vehicle; the results of this study are presented in Figure 48. For the case in which all six cross sections are heated, the maximum thermal stress is approximately 50% greater than than that of the complete vehicle. In general, as the heated area of the component is decreased, the magnitude of thermal stress at the location of the web attachment tee is increased in the area of testing. However, due to the effect of the structural boundary, a finite length of structure is required to develop complete vehicle thermal stresses. This effect causes the thermal stresses at the component ends to be decreased as indicated in Figure 49, tending to offset the increase in thermal stress mentioned previously. The net of these two effects is still expected to cause the maximum thermal stresses developed within a component to be larger than those in the complete vehicle.

The selection of the critical area of the complete vehicle is not a simple task. For example, during the fatigue tests on seventy-two P51D "Mustang" wings presented in Reference 11, fatigue failures were obtained in several quite different areas of the wings. It is important that all critical areas of the complete vehicle be encompassed by the selected components, if fatigue strength verification of the complete vehicle is to be achieved. Once the component area is selected, however, the fatigue strength determination will be only as good as the simulation of the thermal and mechanical boundary conditions. Usual engineering judgment and analysis during the specimen design will allow these boundary conditions to be established without great difficulty.

4.2 Test Facility Analysis - The analysis of the test facility requirements for component fatigue testing is similar to that of the complete vehicle fatigue test; it is assumed that the fatigue and ultimate test facilities would be identical with the exception that cooling would be required for fatigue testing. The advantages obtained from the use of the component approach are more significant for fatigue verification testing than for ultimate strength verification testing. These advantages include the reduction in the number of test control systems required for any specific test site and the companion reduction in control systems that must be operable at a specific time. This reduction in system requirements will enhance the reliability of the test performance; a greater ratio of test time/down time will be achieved. The test facility requirements for component fatigue testing are presented in Table V.

4.3 Cost Analysis - The engineering and manufacturing costs for the fatigue test specimens will be almost identical to those of the ultimate strength components. These costs are discussed in Section VI.1.4.3. The cost of designing and fabricating the test fixture will be nearly equal to that of the ultimate strength test, except for the addition of cooling for mission temperature tests. The basic difference in costs between the ultimate and fatigue tests is caused by test performance. The cost of test performance for room temperature component tests is greater than for room temperature complete vehicle tests, because of the need for staffing of multiple test set-ups. However, the addition of either constant elevated or mission temperatures in any test will increase the test complexity with a corresponding reduction in the ratio of test time/down time. This reduction is greater for a complete vehicle test than for a single component test, which causes the test performance cost to be greater for the complete vehicle tests than for the corresponding component

tests when temperature is added to the test environment. The costs for fatigue testing are indicated in Figures 36 and 37.

4.4 Conclusions - The following conclusions, almost identical to those determined for ultimate strength testing of components, are considered applicable to component fatigue testing:

(a) Components for elevated temperature tests become larger than would be anticipated for load application, only because of the added length requirement to provide suitable thermal boundary conditions. The benefits are the savings of heating rate required at any instant, the reduction in physical size of the test facility, and the capability to use more than one facility at a time.

(b) The effect of internal radiation will generally cause component thermal gradients to be larger than in the prototype; hence, the maximum thermal stresses developed within a component may be larger than in the prototype because of these larger gradients.

(c) The testing costs per square foot of specimen will be more when several components rather than a single complete vehicle are tested at room temperature; the opposite is true when elevated temperature tests are considered.

(d) Components appear satisfactory for fatigue strength verification testing; however, greater accuracy in temperature and thermal stress simulation is required in ultimate strength verification testing.

5. Mechanical Simulation

5.1 Engineering Analysis - The discussion of the mechanical simulation approach as applied to the ultimate strength verification of the Mach 3-4 vehicle (Section VI.1.5.1) is generally applicable to the fatigue strength verification of the Mach 3-4 vehicle. The temperature effects (material property degradation, thermal stresses, and the modification of inelastic stress-strain relationships such as the F_{cy}/F_{ty} and F_{cy}/E ratios) may be partially simulated at room temperature or constant elevated temperature by modification of the test loading, but it is not expected that mechanical simulation of thermal stress is practicable. Instead, an increase in applied loads, the increase computed to account for the thermal effects, is a more attractive technique. The test may be performed at room or constant elevated temperature; if a room temperature test is used, the load increase must account for both material property degradation and thermal stresses. If a constant elevated temperature test is used, only thermal stresses need be simulated. In contrast to ultimate strength verification testing, the use of constant elevated temperature rather than mission temperature in fatigue strength verification testing provides considerable savings in test costs and elapsed time.

The computed effect on fatigue life of not reproducing the thermal stresses can be determined from Figures 69 and 70. The range of computed load augmentation that would be required to create the same fatigue damage as do the thermal stresses is presented in Figure 80. This range was computed for only two locations in the structure; the range for the entire structure would be larger. This range, rather than a single value of load augmentation, constitutes the inherent weakness of the mechanical simulation approach. In this analysis it is assumed all loads, mean, gust and maneuver, and G-A-G are increased proportionately. Other techniques are conceivable; for example,

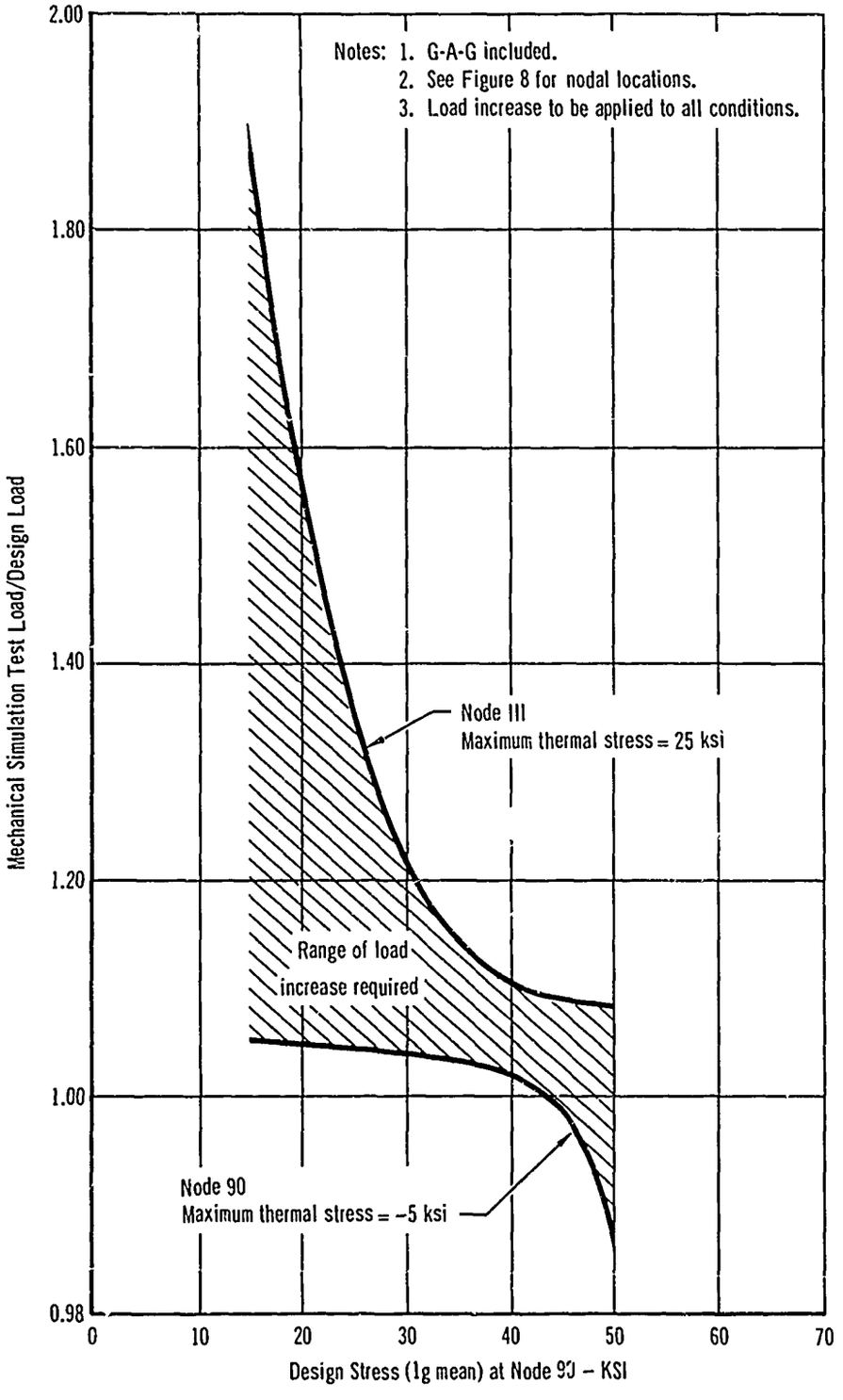

Figure 80 - Comparison of Load Increase Required for Mechanical Simulation of Thermal Stress Fatigue Damage Mach 3-4 Vehicle

increasing only the mean stress level may be a more logical technique for some cases. However, the same problem presented in Figure 80 will arise using any technique; that is, no single factor may be used with confidence for all values of predicted fatigue life and for all locations within the structure. Therefore, both the critical area and expected life must be preselected in order to allow the required load augmentation to be computed. Because of these requirements, a low level of confidence is associated with this approach.

5.2 Test Facility Analysis - The facility requirements for the mechanical simulation approach are basically the same as for either the room or constant elevated temperature test of the complete vehicle, component, or model, as appropriate. The mechanical simulation technique simplifies the test procedure; the heating system is either not required or need not be integrated with the loading system. If the mechanical simulation of thermal stresses is attempted, the loading system and its design may be somewhat more complex; however, in general, this will not affect the total facility requirements. The requirements for testing using mechanical simulation can be determined from Table V for the choice of vehicle type and temperature, room or constant elevated.

5.3 Cost Analysis - Engineering design costs are relatively unimportant in the mechanical simulation approach, except for the previously discussed cost of designing a half-scale model, if that choice of vehicle type is utilized. The selection of augmented loads, the choice of areas of mechanical simulation of thermal stress, and the additional analysis required to determine the amount of load increase required will cause additional engineering effort. Relative to the total costs, however, the cost of this engineering effort is not important. The costs for testing using mechanical simulation

are approximately the same as indicated in Figures 36 and 37 for the choice of vehicle type and test temperature, room or constant elevated.

5.4 Conclusions

(a) One inherent limitation of the attempt to simulate induced thermal stresses by mechanical loadings is the relatively small number of locations where the prototype thermal stress levels can be duplicated simultaneously.

(b) Increasing applied loads to account for thermal stress effects rather than for the thermal stress itself appears to be the most practicable use of the mechanical simulation approach.

(c) By definition, tests in which the thermal effects are simulated by mechanical means cannot produce any thermal effect that cannot be pre-analyzed or predicted.

(d) The use of increased loads to compensate for thermal effects requires the pre-selection of the critical area and fatigue life, which inherently results in a low level of confidence in this approach.

SECTION VIII

EVALUATION AND SELECTION OF PROPOSED APPROACHES

1. Introduction

Several basic approaches to structural verification testing have been considered in this study. In Sections III through VII, the technical evaluation of the main aspects of these approaches has been presented; in this section, their cost and time evaluation is discussed. Following this, combination approaches are discussed and rated. Finally, the selected approaches are presented.

All approaches considered consist of one or more of the following test types: (1) full-scale complete vehicle test, (2) structural model test, (3) full-scale component tests, and (4) mechanical simulation test. Each test type can be conducted in one or more of the following temperature environments: (1) room temperature, (2) constant elevated temperature, or (3) mission temperatures.

A basic approach, as used in this study, is defined as a single test type performed in any one of the temperature environments listed above. The following nine basic approaches have been evaluated for the Mach 3-4 vehicle ultimate and fatigue strength testing and for the Mach 12-15 vehicle ultimate strength testing:

(a) full-scale complete vehicle at

room temperature

constant elevated temperature

mission profile temperatures

(b) structural model at

room temperature

constant elevated temperature

mission profile temperatures

(c) full-scale components at

room temperature

constant elevated temperature

mission profile temperatures

The cost and test time evaluation for the appropriate basic approach at room or constant elevated temperature can be considered applicable to mechanical simulation testing.

An evaluation of each basic approach led to the conclusion that not all of these approaches would satisfy the requirements of a meaningful vehicle strength verification test program, and that some were not acceptable. Combination approaches were then developed, formed of more than one basic approach. A combination approach is an approach in which one or more of the several test types (full-scale complete vehicle test, structural model tests, component tests, or mechanical simulation tests) are performed in one or more of the thermal environments (room temperature, constant elevated temperature, or mission temperatures). The purpose of a combination approach is to provide a means of performing structural verification testing of the vehicle in a manner essentially equal in technical merit to the full-scale complete vehicle test at mission temperatures. This latter test was chosen as the basis of comparison for all combination approaches: if it were not for test costs, time, and complications, this approach would be the prime candidate for testing, being generally acceptable as a verification testing approach. Alternate combination testing approaches should have comparable technical merit, obtainable at less cost, or in less time, or with

fewer test complications. Technical merit is defined as the applicability of test results, assuming the test is performed satisfactorily, to the prediction of the prototype strength in the mission environment.

The combination approaches developed for the Mach 3-4 and 12-15 vehicles are presented in Tables X and XI, respectively. A qualitative technique was used in developing these combination approaches. Each of the nine basic approaches previously described in this subsection was augmented by additional tests, sufficient to cause the total technical merit of the combination to be reasonably comparable to that of the full-scale complete vehicle test at mission temperatures. After elimination of the less desirable approaches thus obtained, there remained six combinations for ultimate strength testing of each vehicle and eight combinations for fatigue testing of the Mach 3-4 vehicle as shown in Tables X and XI, respectively. The exact definition of the details of these tests and their sequence of application requires much more investigation of critical conditions for the vehicle in question, a more complete structural description, a detailed evaluation of the specification requirements for the vehicle to be tested, etc. For example, it may be necessary to use more than one small component at mission profile temperature in Combination A, Table X, for the ultimate strength testing for the Mach 3-4 vehicle. If this were necessary, then more components would probably also be required in the use of approaches B, C, E, and F, while the absolute costs of the test programs would increase, the relative costs would not be significantly changed.

As described in Section IV, the testing performed in a basic or combination approach does not refer to a single test, nor is it assumed that such a single test, at one time, can substantiate the vehicle strength in any meaningful manner. It is recognized, for instance, that in the case of ultimate strength

TABLE X
DESCRIPTION OF COMBINATION APPROACHES
MACH 3-4 VEHICLE

Ultimate Strength Testing Combinations

Symbol	Description[1]
A	1 Complete vehicle at room temperature 1 Small component at mission profile temperature
B	6 Large components at room temperature 1 Large component at mission profile temperature
C	6 Large components at mission profile temperature
D	1 Complete vehicle at mission profile temperature
E	1 Half-scale vehicle at mission profile temperature 2 Small components at mission profile temperature
F	1 Half-scale vehicle at room temperature 1 Small component at room temperature 2 Small components at mission profile temperature

Fatigue Strength Testing Combinations

Symbol	Description[1]
A	6 Large components at room temperature 2 Large components at mission profile temperature
B	6 Large components at constant elevated temperature 1 Large component at mission profile temperature
C	1 Complete vehicle at room temperature 2 Large components at mission profile temperature
D	1 Complete vehicle at constant elevated temperature 1 Large component at mission profile temperature
E	6 Large components at mission profile temperature
F	1 Half-scale vehicle at constant elevated temperature 2 Large components at mission profile temperature
G	1 Half-scale vehicle at mission profile temperature 2 Small components at mission profile temperature
H	1 Complete vehicle at mission profile temperature

[1] A small component is a representative portion of the airframe, selected to verify a single critical section. See Figure 51. A large component is a major portion of the airframe, the total of six, when combined, have a total area equal to that of the complete vehicle.

TABLE XI

DESCRIPTION OF COMBINATION APPROACHES

MACH 12-15 VEHICLE

Ultimate Strength Testing Combinations

Symbol	Description(1)
A	1 complete vehicle at room temperature. 1 small component at mission profile temperature.
B	2 large components at room temperature. 1 small component at mission profile temperature.
C	2 large components at mission profile temperature.
D	1 complete vehicle at mission profile temperature.
E	1 half-scale vehicle at mission profile temperature. 1 small component at mission profile temperature.
F	1 half-scale vehicle at room temperature. 1 large component at mission profile temperature.

(1) A small component is a representative portion of the airframe, selected to verify a single critical section. See Figure 63. A large component is a major portion of the airframe, the two have a total area equal to that of the complete vehicle.

testing. a sizable number of critical conditions must be applied to the vehicle structure to substantiate the strength in various areas of the structure, and although several conditions can sometimes be applied simultaneously, some of the remainder must be applied separately. It is this whole group of tests - all those which would normally be applied to the complete structure - which are the tests that would be applied in a single combination approach.

The methodology used in estimating technical merit, test costs, and test time of the approaches is presented in Subsection 2, followed by the related data for the basic approaches in Subsection 3. The evaluation and rating of the combination approaches are discussed in Subsection 4. The selected approaches are presented in Subsection 5.

2. Methodology of Approach Evaluation

In order to best compare the several possible approaches for ultimate and fatigue strength verification, the advantages and disadvantages of each were converted, insofar as possible, into a quantitative form. Three bases of comparison - technical merit, cost, and time have been established for the approaches under consideration. These three factors have been used to permit the selection of the best approach on a cost effectiveness basis for ultimate strength testing and a cost-time effectiveness basis for fatigue strength testing. As indicated in Subsection 1, all combination approaches have been established so that their technical merits were essentially equal to each other and comparable to that of the complete vehicle mission temperature testing program. As indicated in Subsection 2.2, time is not a critical parameter in ultimate strength testing; hence approaches to ultimate strength testing of both vehicles have been ranked by their respective costs only. However, approaches to fatigue testing, where time is important, have been ranked by their respective products of cost and elapsed time. These costs and

cost-time products have been normalized to the values for the mission temperature test of the complete vehicle; the reciprocals of these normalized values are termed the cost effectiveness and cost-time effectiveness factors for ultimate and fatigue strength verification, respectively. The combination approaches found to have the highest factors have then been selected, such selections being one of the objectives of the study.

Only the combination approaches have been judged to have a technical merit equal to that of the full-scale complete vehicle mission testing; therefore, only the combination approaches and not the basic approaches were rated as to cost effectiveness and cost-time effectiveness and were used in the final selections. However, pertinent data for all basic approaches are presented in Subsection 3 for completeness.

2.1 Method of Estimating Test Costs - In order to determine the cost associated with the fabrication of the test specimens, the number of man-hours required to design the specimens, to fabricate the required tooling, and to complete the manufacturing of the test specimens were determined for all approaches. These man-hours were then translated into dollar costs including all factors, contingencies, overhead, etc., normally included, except profit. It should be carefully noted that while the costs, both unit and total, are based on data believed to be reasonably applicable, they are not intended to represent actual cost estimates and cannot in any event be construed as contractual cost proposals.

The principal factors considered are discussed in the following subsections.

2.1.1 Test Specimen Fabrication Costs - For certain approaches, some of the individual costs which would be expected to enter into the total test specimen fabrication cost may actually be negligible. For example, for the

approach in which the full-scale complete vehicle is utilized, little additional engineering effort is required to design either the specimen or the tooling for specimen fabrication, because the production drawings and tooling may be used directly. However, for any scale model approach, the test program cost for these same items is significant. In both of the above examples, and in all other cases, the specimen fabrication costs include raw material, equipment, fabrication, and assembly effort required to produce the test specimen.

2.1.2 Test Performance Costs - In the determination of costs associated with test performance, all materials and man-hour costs have been included within the assumptions described in Section IV. The facility has been assumed to exist in all cases, as described in Section IV, and no costs have been included for its construction, lease, or depreciation. Control and monitoring equipment and centers have also been assumed to exist. Costs have been included for fabrication of the specimen and the loading network and structure, installation of thermocouples, strain gauges, etc., fabrication and installation of cooling systems as required, all materials of an expendable nature, system hook-up and check-out, and performance of the testing. Although small, the cost of jig work has also been included and comprises the cost of the static structure unique to the specimen to be tested, the lamp costs, load actuators, strain and deflection gages, and thermocouples.

2.2 Method of Estimating Test Time Required - Time spans necessary to perform the fatigue tests of all approaches for the Mach 3-4 vehicle are presented in Subsection 3.3. These time spans are indexed relative to the time when the first prototype vehicle proceeds to system installation and checkout, and when the manufacturing tooling is first available for test specimen fabrication. This reference date has no special significance other than

it is easily identified, and usually corresponds to the beginning of fabrication of the ultimate strength test article.

Time considerations would not be important for any of the approaches considered if testing could be expected to be completed well before the test data are required. For ultimate strength verification, it is estimated that these data would be required shortly after the prototype's first flight for the Mach 3-4 vehicle and some time before first flight for the Mach 12-15 vehicle. For fatigue strength verification of the Mach 3-4 vehicle, the fatigue test data should be available before any of the prototype vehicles accumulates one-half of its design life. This is consistent with the assumed requirement of exhibiting, in the fatigue test, a life twice the service life of the flight vehicle. From the analysis of the time spans required to perform the tests, it has been concluded that all tests associated with the ultimate strength verification approaches under consideration for both vehicles could be accomplished within 24 months of the above reference date; therefore, test time is not given consideration in evaluating the overall merit of the combination approaches considered. For fatigue testing, however, time is of prime importance and has been considered and weighed in the final evaluation.

3. Man-hour, Dollar Cost, and Test Time Estimates for the Basic Approaches

The basic approaches evaluated in this study are the complete vehicle approach, the modeling approach, the component approach, and the mechanical simulation approach; all considered at room temperature, constant elevated temperature, or at mission temperatures. Man-hour and dollar costs of these basic approaches are described in the following subsections. As indicated in Subsection 2, no ratings of the basic approaches have been performed.

3.1 Man-hour Estimates - The estimated man-hours for the basic approaches for the ultimate and fatigue strength verification tests of the Mach 3-4 vehicle

are presented in Figure 36. Man-hours for the basic approaches for the ultimate strength verification of the Mach 12-15 vehicle are presented in Figure 60. For all of these data, the man-hours were determined for the extent and quantity of work described in Subsection 2.

In these man-hour data, a large quantity is shown for tooling required for the half-scale model. These costs are considerably less than those for tooling of the complete vehicle, as only the tooling required for structural fabrication and assembly is necessary (no systems included). Other factors considered were the reduced size of the structure and the more temporary and, therefore less costly, nature of the tooling for the half-scale model, since only a few are expected to be fabricated.

3.2 Dollar Cost Estimates - Using the man-hours from Subsection 3.1, total test costs have been estimated for each of the basic approaches. These dollar costs, presented in Figure 37 for the Mach 3-4 vehicle and in Figure 61 for the Mach 12-15 vehicle, are the total costs associated with that basic approach specified for the particular vehicle.

3.3 Test Time Estimates - As discussed above, no test time data are presented for ultimate strength verification of either vehicle because they are less than 24 months and therefore are considered non-critical. Estimated test times for each of the basic approaches for fatigue strength verification of the Mach 3-4 vehicle are summarized in Figure 81. These include the total time required to perform the specified fatigue tests, indexed to the time when the specimen is delivered to the test facility. All times are ratioed to that required for complete vehicle mission temperature testing. The design service life for this vehicle is 20,000 flights in 40,000 hours; with an assumed requirement of exhibiting in test a life twice that of the design service life, the test would require the simulation of 40,000 flights and [illegible]00 hours. It is expected

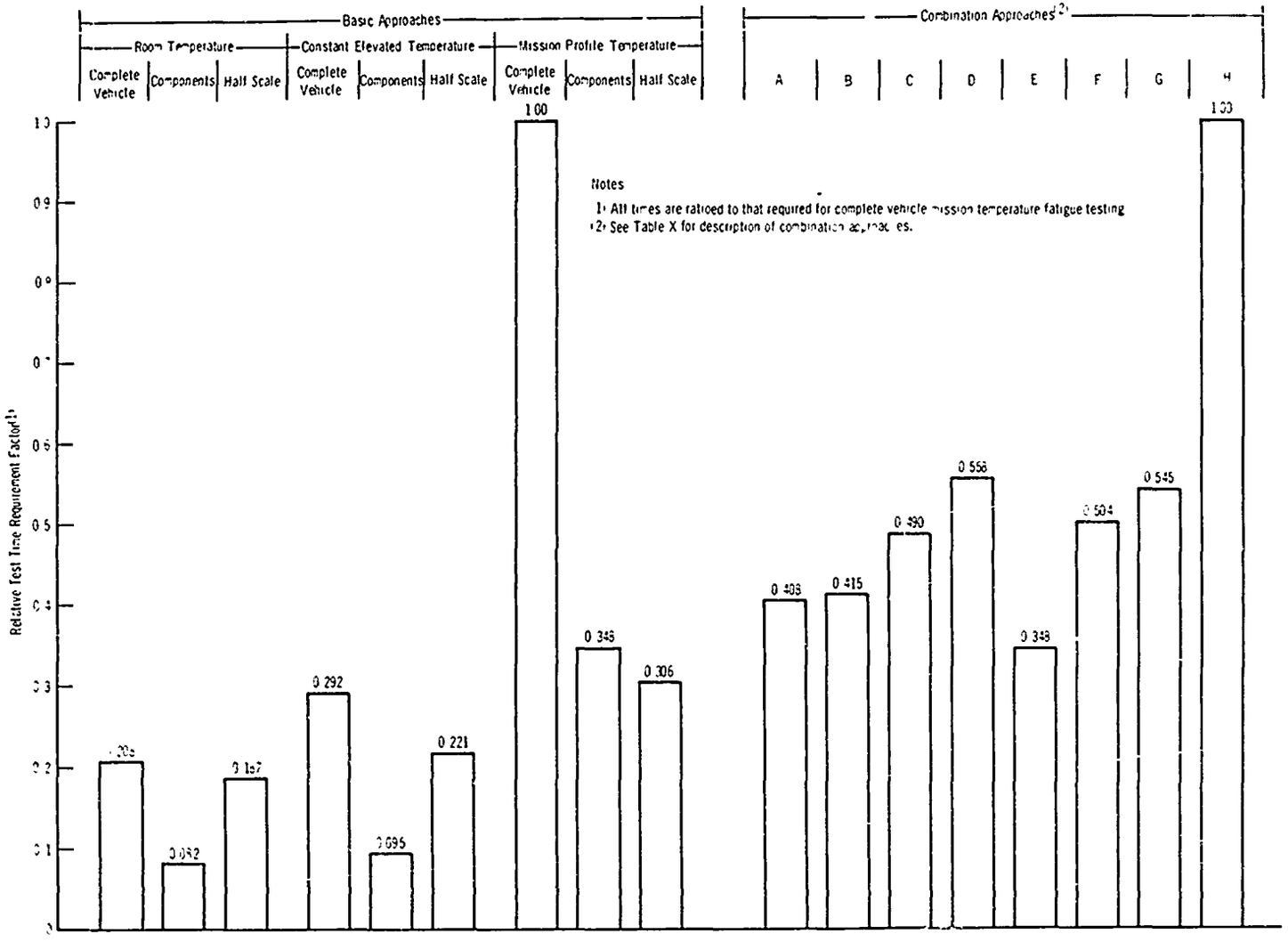

Figure 81 - Comparison of Relative Fatigue Test Time Requirement Factors Mach 3-4 Vehicle

that the test time could be shortened, perhaps using the techniques of Reference 3. However, the lower limit of the time required to satisfactorily simulate mission thermal stresses is approximately one hour per flight; therefore, 40,000 hours are required to simulate 40,000 flights. Using full time operation - 24 hours a day, 7 days a week - this test would require 4.6 years to complete. Considering the testing efficiencies expected for this type test, the time required to perform this test is estimated to be between 15 and 25 years.

4. Combination Approaches

4.1 Purpose of Combination Approaches - As described in the introduction to this section, the selection of proposed approaches is accomplished on a cost effectiveness or a cost-time effectiveness basis. Such a rating system must be fashioned so as to be most applicable to a typical strength verification test program. The primary purpose of such a test program is to verify the structural integrity of a given vehicle, i.e., to provide test data of sufficient technical merit to define vehicle strength. Thus, to be considered acceptable, an approach must have a minimum technical merit, equal to some preestablished norm.

As indicated in the introduction to this section, the established norm of technical merit has been assumed in this study to be that of the mission temperature environment tests of the full-scale complete vehicle. It is judged that none of the other basic approaches have this level of technical merit; these other basic approaches must, therefore, be augmented with some additional testing in order to form a combination approach of a technical merit comparable to the established norm. Accordingly, all combination approaches which are shown in Table X for the Mach 3-4 vehicle and in Table XI for the Mach 12-15 vehicle, have been tailored to have an estimated technical merit comparable to the mission temperature testing of the full-scale complete vehicle.

This concept has a strong analogy to cost effectiveness study methods where the scope of the task to be performed is held constant and the costs are determined in order to produce that fixed value of effectiveness (which, in this study, is the technical merit).

An alternate cost effectiveness concept, which is sometimes also used, considers costs constant and evaluates the approach or method which would yield the highest effectiveness - the converse of that previously described. This alternate concept is believed to be more applicable in cases where the total task is not expected to be performed by a single activity and the evaluation is performed to see how much of the total task can be performed for a fixed cost. No work has been performed in this study utilizing this alternate concept, because it is not considered applicable to strength verification testing.

4.2 Description of Combination Approaches - Combination approaches, estimated to have technical merit approximately equal to that of mission environment testing of the full-scale complete vehicle, are listed in Table X and Table XI for the Mach 3-4 and 12-15 vehicles, respectively. It should be noted that two different types of components are specified in these tables: small components and large components.

Large components are defined as test specimens of a size sufficient to permit, in test, the strength evaluation of a significant portion of the vehicle. For the Mach 3-4 vehicle, for example, it has been assumed that six such large components may be used for strength evaluation of the total vehicle. The total size and weight of the components are comparable to that of the complete vehicle. On the other hand, the size of small components such as shown in Figures 51 and 63 for the Mach 3-4 and 12-15 vehicles, permit the strength evaluation of only local areas; the location of such a critical area is

determined in either large component tests or complete vehicle tests, performed at room or constant elevated temperatures. The large components are, on the average, 50 percent larger in gross size than small components but 4 to 5 times larger in test area size, allowing the strength substantiation of a more significant portion of the overall vehicle.

Man-hour costs for the combination approaches applicable to the Mach 3-4 vehicle and the Mach 12-15 vehicle are presented in Figures 82 and 83, respectively. Costs based on these man-hours are presented in Figures 84 and 85. Both costs and man-hours for approaches utilizing large components have been determined using the same basic method of cost analysis as for the small components, that is, based on component size and weight data. Test times to complete the fatigue tests on the Mach 3-4 vehicle are shown in Figure 81.

4.3 Ratings of Combination Approaches - The relative ratings of the combination approaches described in the previous section are presented in Figures 86 and 87, for the Mach 3-4 and Mach 12-15 vehicles, respectively. As stated before, the combination approaches for ultimate strength testing of both vehicles have been ranked by their respective costs; the combination approaches for fatigue testing of the Mach 3-4 vehicle have been ranked by their respective product of cost and elapsed time. These cost and cost-time products have been normalized to the values for the complete vehicle, mission temperature test; the reciprocal of these normalized values are termed the cost effectiveness factors and cost-time effectiveness factors for ultimate and fatigue strengths, respectively. In these data a higher rating indicates the better approach. For ultimate strength approaches, the relative rating represents estimated cost differences between approaches, while for fatigue strength approaches, the relative ratings include both cost and time differences between approaches.

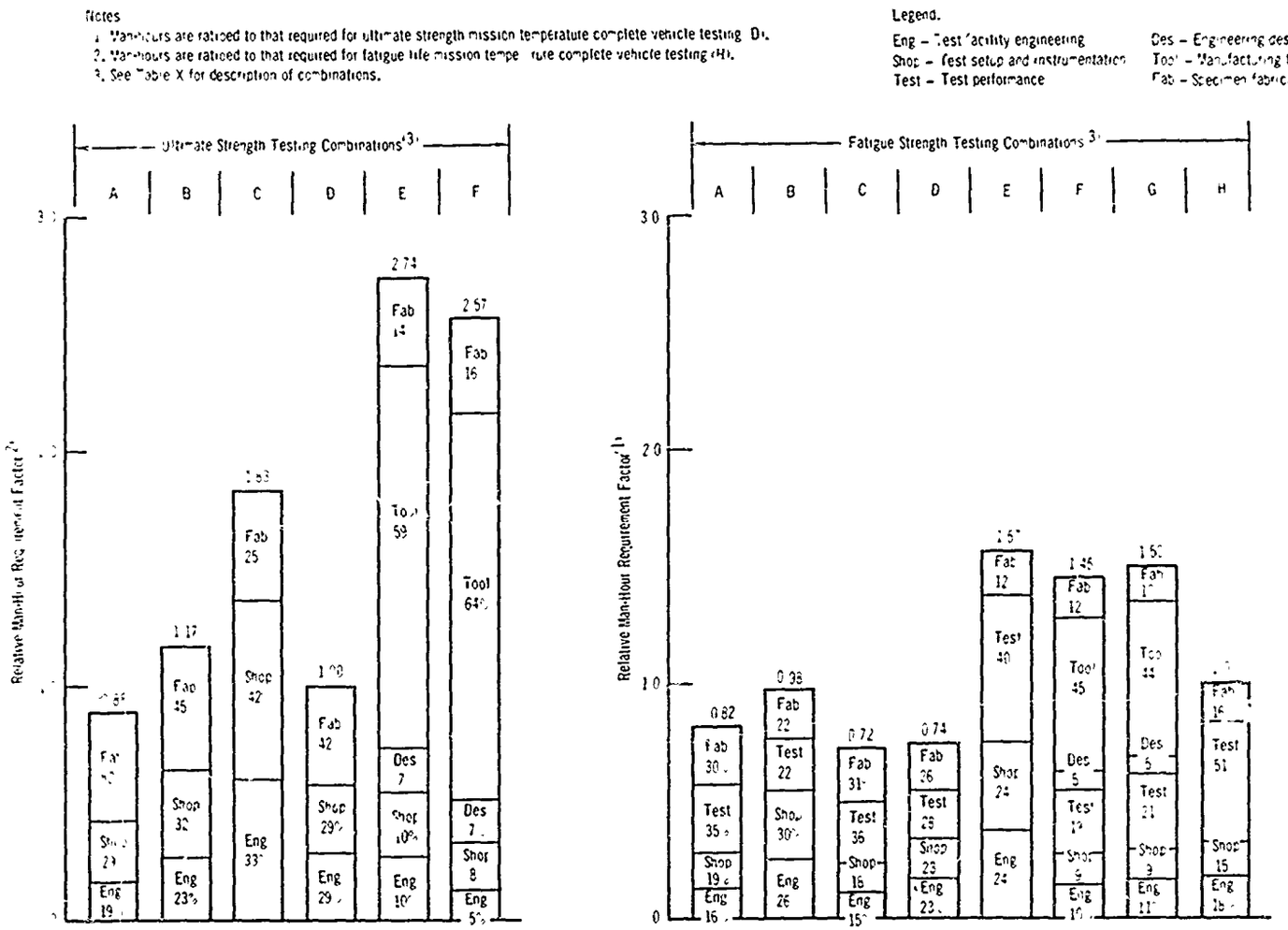

Figure 82 - Comparison of Relative Man-hour Requirements for Combination Approaches Mach 3-4 Vehicle

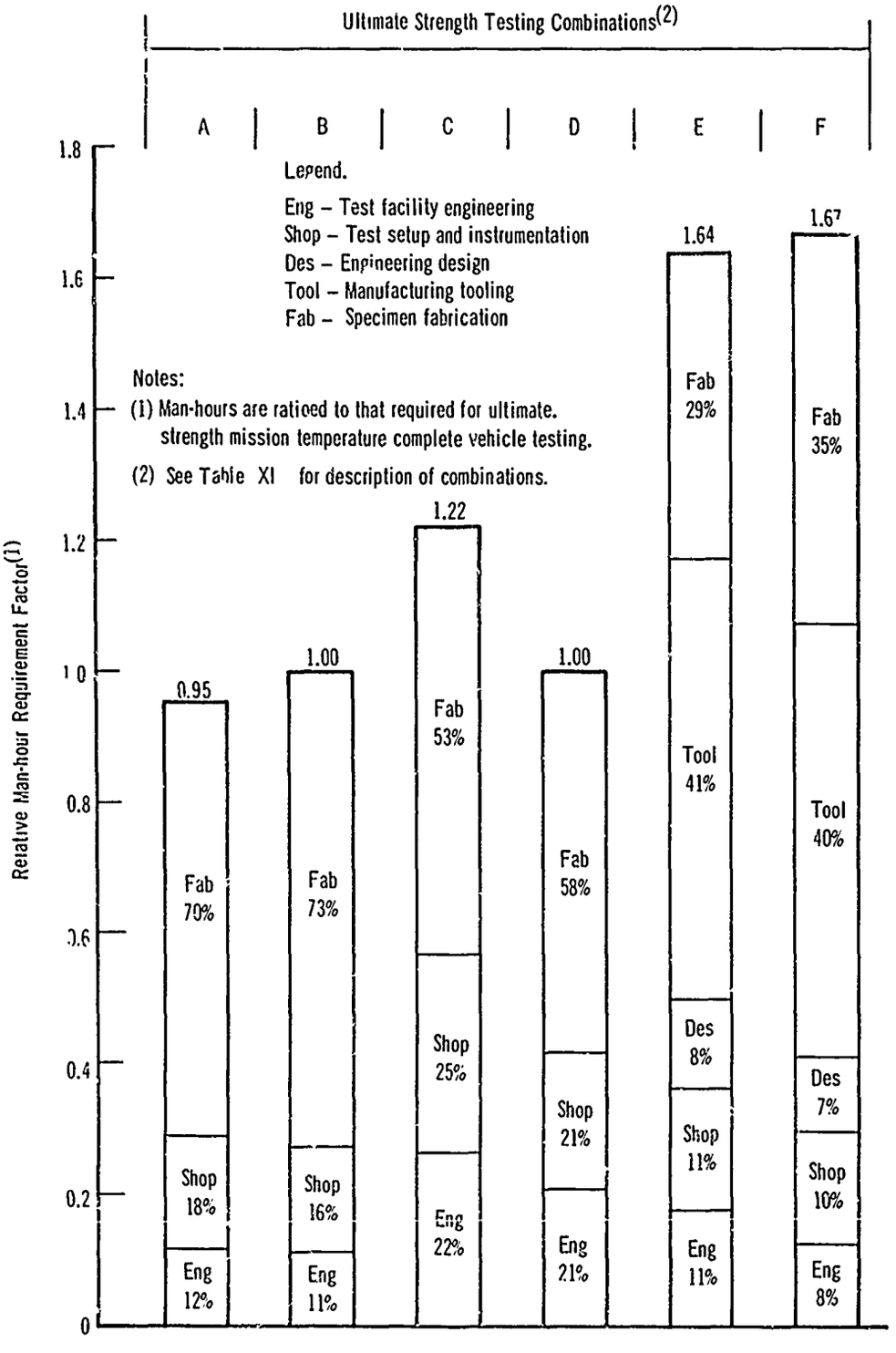

Figure 83 - Comparison of Relative Man-hour Requirements for Combination Approaches Mach 12-15 Vehicle

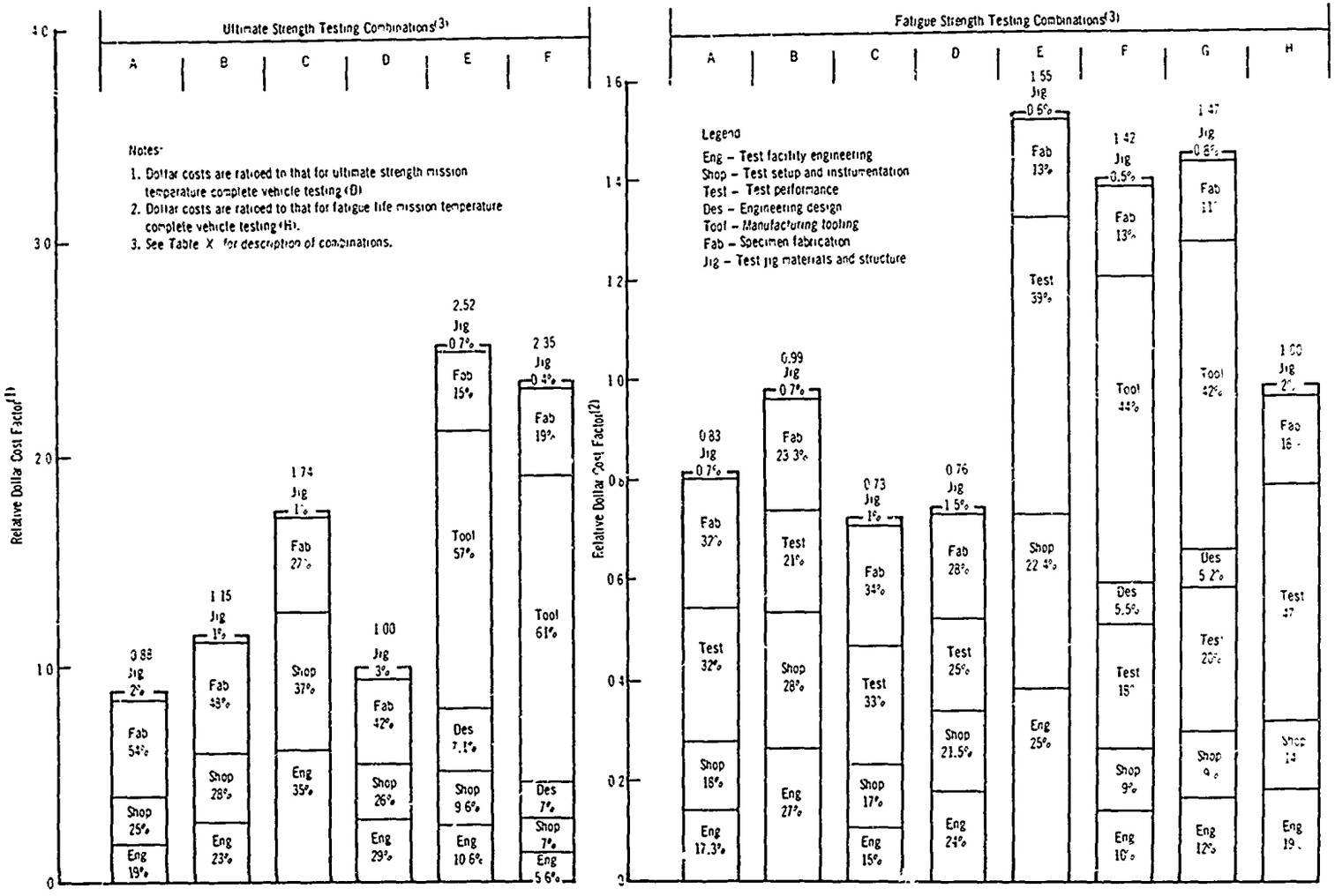

Figure 84 - Comparison of Relative Dollar Costs for Combination Approaches Mach 3-4 Vehicle

Notes:
(1) Dollar costs are ratioed to that for ultimate strength mission temperature complete vehicle testing.
(2) See Table XI for description of combinations.

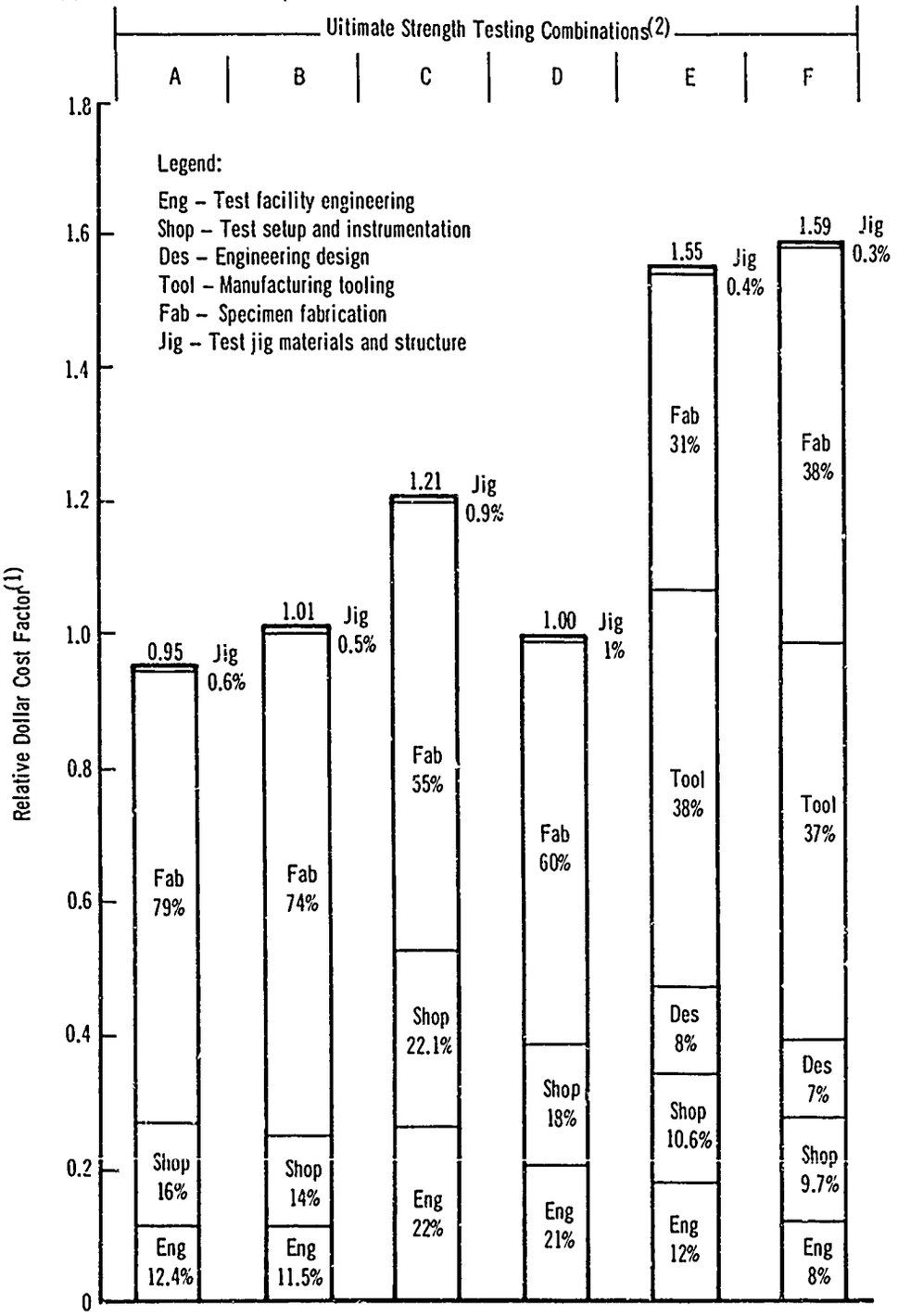

Figure 85 - Comparison of Relative Dollar Costs for Combination Approaches Mach 12-15 Vehicle

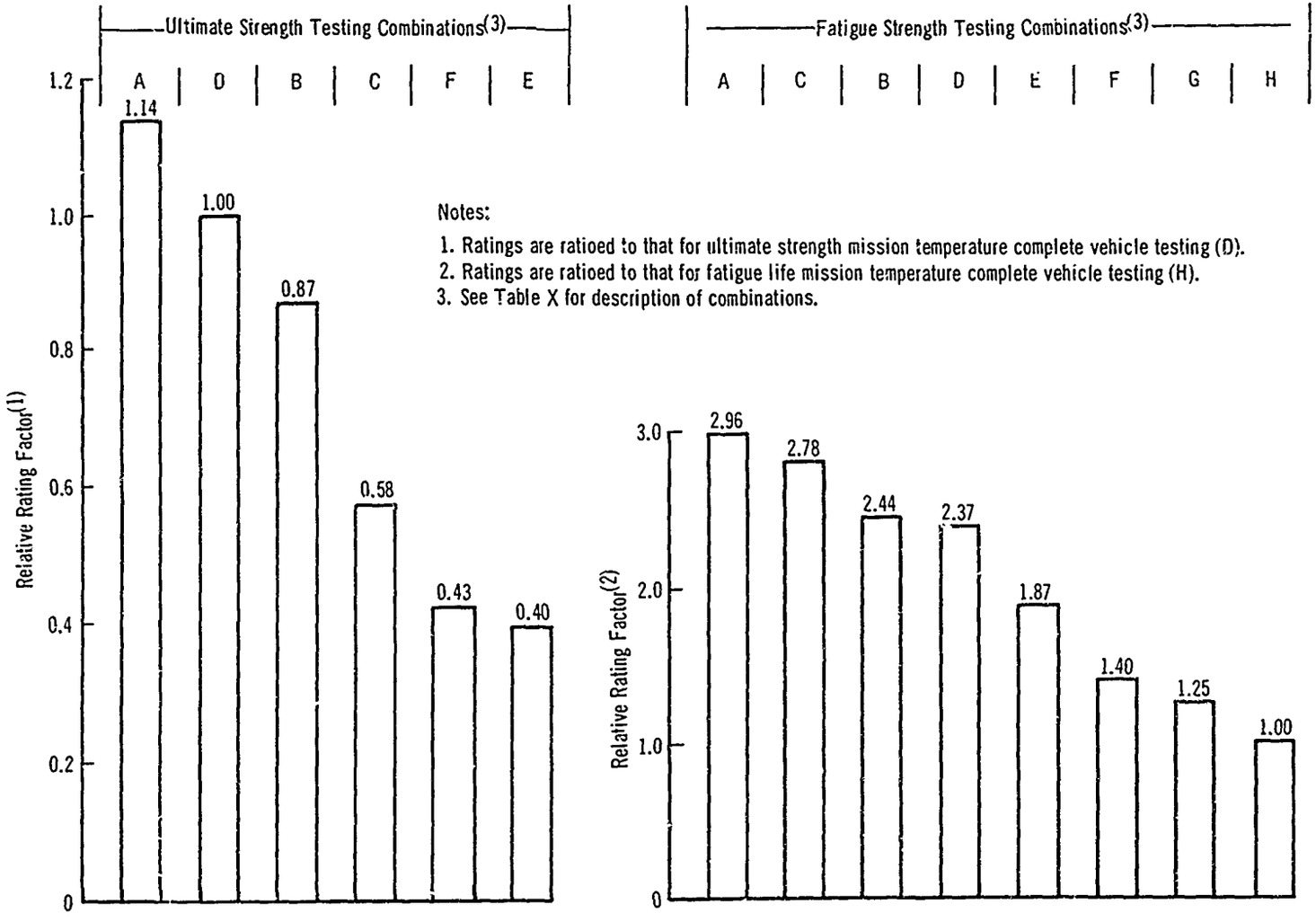

Figure 86 - Comparison of Relative Rating Factors for Combination Approaches Mach 3-4 Vehicle

Notes:

(1) Ratings are ratioed to that for ultimate strength mission temperature complete vehicle testing.

(2) See Table XI for description of combinations

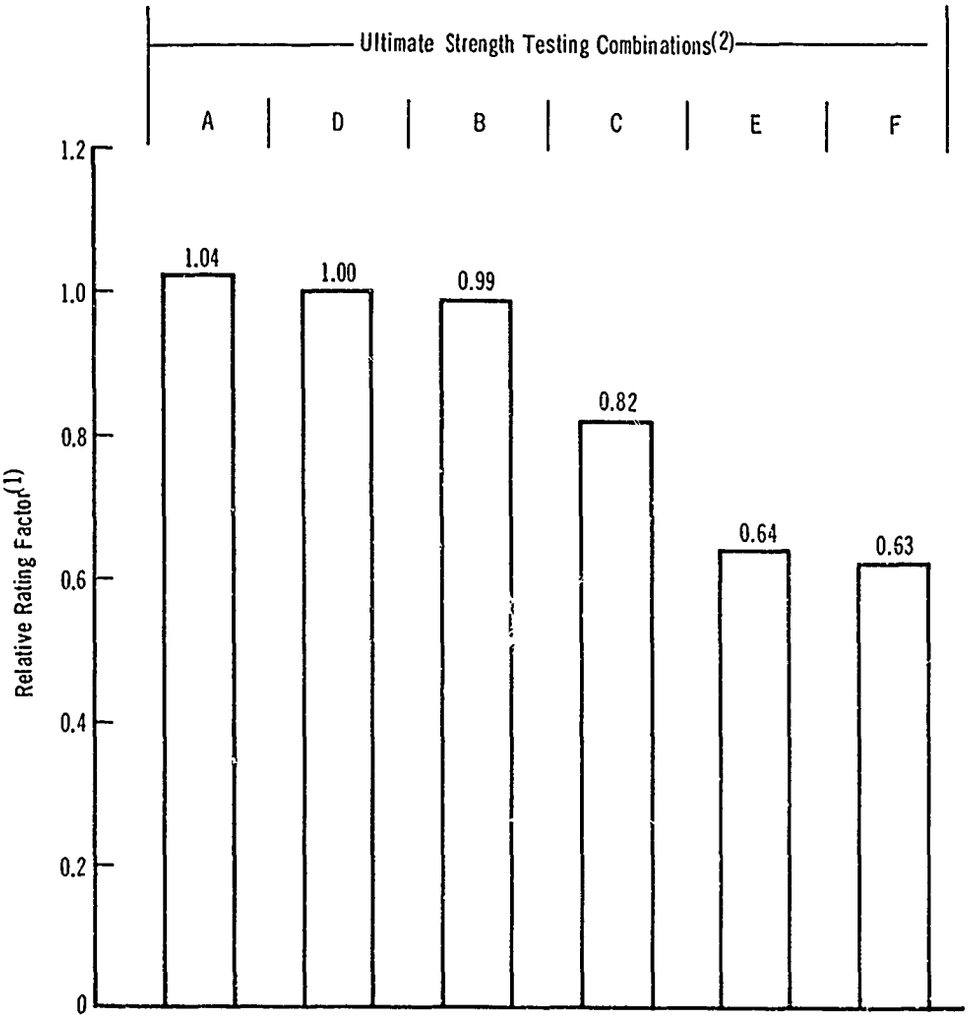

Figure 87 Comparison of Relative Rating Factors for Combination Approaches Mach 12-15 Vehicle

These relative rating values for all approaches can be obtained from the relative cost data and relative time data presented in Figures 81, 84, and 85. For all ultimate strength approaches for both vehicles, the relative ratings shown in Figure 86 or Figure 87 are simply the reciprocals for the relative dollar cost factors shown in Figures 84 and 85. This is to say, the higher the relative cost, the lower the relative rating and vice versa. For all the fatigue strength approaches for the Mach 3-4 vehicle shown in Table X, the relative rating value shown in Figure 86 is the reciprocal of the product of relative dollar cost shown in Figure 84 and relative test time requirement factor shown in Figure 81. Again, the higher either the relative cost or relative test time, the lower the relative rating, and vice versa.

Several general conclusions may be drawn from these data:

(a) For ultimate strength verification of the vehicles studied, only a small reduction in relative rating is associated with mission profile temperature testing of the complete vehicle, the approach which rates a close second for both vehicles.

(b) For fatigue strength verification of the Mach 3-4 vehicle, where cost-time effectiveness has been used as a rating criterion, the approaches with the highest resulting rating are those in which only small portions of the structure are fatigue tested at mission profile temperatures due to both time and cost considerations.

(c) Despite the many scaling advantages, the modeling approach has a low rating resulting from the large specimen fabrication tooling costs.

The best approaches for each vehicle and strength testing are those with the highest relative rating. These selected approaches are presented in the following subsection.

5. Selected Approaches

5.1 Mach 3-4 Vehicle

5.1.1 Verification of Vehicle Ultimate Strength -

Selected Approach:

This approach consists of one complete vehicle tested at room temperature to locate the critical area(s), followed by a test at mission profile temperatures of a small component containing the section which failed in the complete vehicle room temperature test to establish the ultimate strength level under mission temperatures (Combination Approach A, Table X). Relative Rating = 1.14 (Figure 86).

Approach Rated Second:

This approach consists of one complete vehicle tested at mission profile temperatures (Approach D, Table X). Relative Rating = 1.00 (Figure 86).

Approach Rated Third:

This approach consists of six large components tested at room temperature to locate the critical section, followed by one large component containing the section which failed in the component room temperature tests to establish the ultimate strength level under mission temperatures (Combination Approach B, Table X). Relative Rating = 0.87 (Figure 86).

5.1.2 Verification of Vehicle Fatigue Strength -

Selected Approach:

This approach consists of six large components tested at room temperature to locate critical areas, followed by two large components tested at mission profile temperatures to determine Mach 3-4 vehicle fatigue life. (Combination Approach A, Table X). Relative Rating = 2.96 (Figure 86).

Approach Rated Second:

This approach consists of one complete vehicle tested at room temperature to locate the critical area(s), followed by a test at mission profile temperatures of two large components to establish the vehicle fatigue strength under mission temperatures. One large component would include the area of the vehicle which failed first in room temperature tests and the second component would include either the area which failed second or the next most critical section determined by analysis (Combination Approach C, Table X). Relative Rating = 2.78 (Figure 86).

5.2 Verification of Mach 12-15 Vehicle Ultimate Strength

Selected Approach:

This approach consists of one complete vehicle tested at room temperature to locate the critical area(s), followed by a test at mission profile temperatures of a small component containing the section which failed in the complete vehicle room temperature test to establish the ultimate strength level under mission temperatures (Combination Approach A, Table XI). Relative Rating = 1.04 (Figure 87).

Approach Rated Second:

This approach consists of one complete vehicle tested at mission profile temperatures (Combination Approach D, Table XI). Relative Rating = 1.00 (Figure 87).

Approach Rated Third:

This approach consists of two large components tested at room temperature to locate the critical section, followed by one large component containing the section which failed in the large component room temperature tests to establish the ultimate strength level under mission temperatures (Combination Approach B, Table XI). Relative Rating = 0.99 (Figure 87).

SECTION IX

PROPOSED TEST PROGRAM TO CONFIRM THE VALIDITY OF SELECTED APPROACHES

1. General Scope and Purpose

As described in Section I, one of the goals of this study program is the definition of a test program to confirm the validity of the selected approaches for: (1) the ultimate and fatigue strength verification of the Mach 3-4 vehicle, and (2) the ultimate strength verification of the Mach 12-15 vehicle. The selected approaches are discussed in Section VIII; they are repeated below.

Mach 3-4 Vehicle

Selected Approach for Verification of Vehicle Ultimate Strength - This approach consists of one complete vehicle tested at room temperature to locate the critical area(s), followed by a test at mission profile temperatures of a small component containing the section which failed in the complete vehicle room temperature test to establish the ultimate strength level under mission temperatures. (Combination Approach A, Table X.) Relative Rating = 1.14 (Figure 86).

Selected Approach for Verification of Vehicle Fatigue Strength - This approach consists of six large components tested at room temperature to locate critical area(s), followed by two large components tested at mission profile temperatures to determine Mach 3-4 vehicle fatigue life. (Combination Approach A, Table X.) Relative Rating = 2.96 (Figure 86).

Mach 12-15 Vehicle

Selected Approach for Verification of Vehicle Ultimate Strength - This approach consists of one complete vehicle tested at room temperature to locate the critical area(s), followed by a test at mission profile temperatures

of a small component containing the section which failed in the complete vehicle room temperature test to establish the ultimate strength level under mission temperatures. (Combination Approach A, Table XI.) Relative Rating = 1.04 (Figure 87).

The approaches have been selected or the basis of (1) a cost-effectiveness study for ultimate strength verification, and (2) a cost-time effectiveness study for fatigue strength verification; the methodology used in the evaluation is described in Section VIII. It is important to note that each of these selected approaches utilizes either the full-scale complete vehicle, or an appropriate number of components, tested at room temperature to locate critical areas, followed by one or more components tested at mission temperature to determine the vehicle actual mission strength. The use of components does not require substantiation or confirmation; a simple awareness of the potential problems associated with components will usually lead to a satisfactory design and test. However, the correctness of the hypothesis that vehicles in constant temperature tests will fail in the same areas, if not necessarily at the same load or life, as in mission profile temperature tests, does require confirmation. The proposed test program is designed to evaluate the above hypothesis.

It should also be noted that a test program to confirm the correctness of the concept of using room or constant elevated temperature tests to locate critical areas is not a substantiation of the mechanical simulation approach. To confirm its applicability and correctness, the following premises of the mechanical simulation approach would require test evaluation: (1) that the precise location of either a fatigue or an ultimate strength failure in a complex elevated temperature structure can be predetermined analytically,

(2) that a single mechanical loading can be applied which simulates both the mission mechanical and thermal loadings, and (3) that vehicle mission ultimate or fatigue strength may be deduced from test results where premises (1) and (2) were used. In the selected approaches previously described, however, the only assumption made is that room temperature or constant elevated temperature ultimate or fatigue strength tests will fail in the same general area as in mission temperature tests, hereinafter referred to as the similar critical section concept; mission profile temperature tests are then conducted on components containing the critical area to determine actual vehicle strength. The purpose of the proposed test program is to confirm the correctness of this similar critical section concept.

2. Recommended Tests - General

In the selected approaches, room temperature tests are utilized to locate critical areas for both ultimate strength and fatigue strength verification. However, it should be noted that the ratings of the selected ultimate strength approaches are 1.14 for the Mach 3-4 vehicle and 1.04 for the Mach 12-15 vehicle, indicating, as described in Section VIII, only a 14% and 4% improvement, respectively, over the basic approach of full-scale complete vehicle testing at mission temperatures.

This lack of significant gain by use of the similar critical section concept is not true, however, for the selected fatigue strength testing approach. In the fatigue verification of the Mach 3-4 vehicle, the similar critical section concept appears in the four highest rated approaches as shown in Figure 86, and the selected approach has a rating over 50% higher than the highest approach not using this concept. Hence, it is seen that significant cost and time savings, over one third, are possible by the use of the selected approach for fatigue strength tests, but only smaller savings, about 10%, are

possible for ultimate strength tests. For these reasons, it is recommended that the proposed test program be focused on the evaluation of the validity of the similar critical section concept for vehicle fatigue strength test approaches. Further, in order to be most applicable to testing needs in the near future, it is recommended that the test program be directed toward application to the Mach 3-4 vehicle and therefore incorporate spectrum loading, based on the maneuver load factor and gust load factor data described in this report.

Generally, a test program to confirm the validity of any concept includes tests which determine both the individual and the synergistic effects of all pertinent parameters. In the proposed test program, focused on confirming the validity of the similar critical section concept in fatigue testing, it shall be necessary to perform identical fatigue loading tests in three temperature environments: (1) at room temperature, (2) at a constant elevated temperature, and (3) at mission profile temperatures. The constant elevated temperature fatigue tests are recommended because (1) the specimens will probably fail in the same area as in mission temperature tests, (2) approaches utilizing constant elevated temperature fatigue tests to locate critical areas also offer significant cost, time and complexity savings over mission profile temperature testing, and (3) the results of this program may indicate that room temperature fatigue tests are not satisfactory in locating similar critical areas. The location of failures in the mission profile temperature tests will be used to judge the validity of the similar critical section concept previously described, by comparison to the location of failures in either the room temperature or constant elevated temperature tests. Both coupon and component tests are proposed. It is recommended that the effect of the ground-air-ground cycle loads be included in the evaluation.

3. Detailed Description of Recommended Tests

The essence of the test program proposed herein is as follows:

(1) Coupon fatigue tests under both constant amplitude and spectrum loading to provide basic material property fatigue data and to evaluate whether the relative fatigue performance, that is, order of failure of specimens containing two different stress concentrations, remains constant with changes in temperature history. The latter would serve as an indication of preliminary confirmation of the similar critical section concept in actual structures.

(2) Small structures or component fatigue tests under a spectrum fatigue loading to provide a confirmation of the critical section concept in actual structures.

It is important in this proposed test program, as it is in all fatigue evaluation programs, that the specimens be especially well made, that all stock used be from the same basic heat, and that the test set-up and performance be especially well monitored and controlled.

The proposed test program is outlined in Table XII; the loading spectrum is defined in Table XIII. It is recommended that a titanium alloy, either Ti-6Al-4V or Ti-8Al-1Mo-1V, be used as the base material for all specimens, both coupons and components. It would be most useful to select specimen design, material, test definition, etc., which have been utilized in a previous or current program, where some of the required testing may have already been accomplished. Thus, to save costs, the final selection of material and specimen design may be made on that basis. It should be noted that the recommended program does not evaluate the behavior of a specific alloy but rather is designed to evaluate general material behavior to a fatigue environment; therefore, the actual material choice is less important.

TABLE XII
PROPOSED TEST PROGRAM
COUPON TESTS

Group I – Constant Amplitude Fatigue Coupon Tests

Specimen Configuration	Test Stress Levels and Desired Life	Number of Specimens per Stress Level	Loading Ratio, R Min. Load / Max. Load	Test Temperature	Total Number of Specimens to be Tested	Estimated Test Time in Hours (1)
Nos. 1 and 2: Multiple central hole specimen K_T = 2.5 and 2.8 Figure 88 Nos. 3 and 4: Multiple edge notch specimen K_T = 2.5 and 2.8 Figure 88	Low stress Life $\approx 10^6$ cycles Medium stress Life $\approx 5 \times 10^4$ cycles Intermediate stress Life $\approx 10^3$ cycles High stress Life $\approx 10^2$ cycles	12 (3 per configuration)	R = 0.25	Room temperature	48	2,000
				500°F	48	2,000
				Total:	96	4,000

Group II – Spectrum Fatigue Coupon Tests

Specimen Configuration	Test Stress Levels and Equivalent Mission Life	Number of Specimens per Stress Level	Test Series	Test Temperature	Total Number of Specimens to be Tested	Estimated Test Time in Hours
Nos. 1 and 2: Multiple central hole specimen K_T = 2.5 and 2.8 Figure 88 Nos. 3 and 4: Multiple edge notch specimen K_T = 2.5 and 2.8 Figure 88	Low stress Life $\approx$ 8000 hours (2) Medium stress Life $\approx$ 800 hours (2) High stress Life $\approx$ 80 hours (2)	12 (3 per configuration)	(A) Spectrum loading only Table XIII	Room temperature	36	3,552 (1,3)
				500°F	36	3,552 (1,3)
				Mission temperatures Table XIII	36	35,520 (2)
				Subtotal:	108	42,624
No. 1: Multiple central hole specimen K_T = 2.8 Figure 88 No. 2: Multiple edge notch specimen K_T = 2.8 Figure 88	Low stress Life $\approx$ 8000 hours (2) Medium stress Life $\approx$ 800 hours (2) High stress Life $\approx$ 80 hours (2)	6 (3 per configuration)	(B) Spectrum loading plus thermal stresses Table XIII	Room temperature	18	1,776 (1,3)
				Mission temperatures Table XIII	18	17,760 (2)
				Subtotal:	36	19,536

Notes:
(1) Based on simultaneous testing of 3 specimens in series and 5 cps loading rate.
(2) Design mission time.
(3) Based on a time reduction factor of 10 for room temperature and 500°F tests compared to design mission time.

TABLE XII (Continued)
PROPOSED TEST PROGRAM
COUPON TESTS

Specimen Configuration	Test Stress Levels and Equivalent Mission Life	Number of Specimens per Stress Level	Test Series	Test Temperature	Total Number of Specimens to be Tested	Estimated Test Time in Hours
No. 1: Multiple central hole specimen K_T = 2.8 Figure 88 No. 2: Multiple edge Notch specimen K_T = 2.8 Figure 88	Low stress Life≈8000 hours(2) Medium stress Life≈800 hours(2) High stress Life≈80 hours(2)	6 (3 per configuration)	(C) Spectrum loading plus G-A-G loads Table XIII	Room temperature	18	1,776(1,3)
				Mission temperatures Table XIII	18	17,760(2)
				Subtotal:	36	19,536
Nos. 1 and 2: Multiple central hole specimen K_T = 2.5 and 2.8 Figure 88 Nos. 3 and 4: Multiple edge notch specimen K_T = 2.5 and 2.8 Figure 88	Low stress Life≈8000 hours(2) Medium stress Life≈800 hours(2) High stress Life≈80 hours(2)	12 (3 per configuration)	(D) Spectrum loading plus G-A-G loads plus thermal stresses Table XIII	Room temperature	36	3,552(1,3)
				500°F	36	3,552(1,3)
				Mission temperatures Table XIII	36	35,520(2)
				Subtotal:	108	42,624
				Total:	288	124,320
				Grand total for constant amplitude and spectrum fatigue coupon tests:	384	128,320

Notes:
(1) Based on simultaneous testing of 3 specimens in series and 5 cps loading rate.
(2) Design mission time.
(3) Based on a time reduction factor of 10 for room temperature and 500°F tests compared to design mission time.

TABLE XII (Continued)
PROPOSED TEST PROGRAM
COMPONENT TESTS

Group III – Spectrum Fatigue Component Tests

Specimen Configuration	Test Stress Levels and Equivalent Mission Life	Number of Specimens per Stress Level	Test Series	Test Temperature	Total Number of Specimens to be Tested	Estimated Test Time in Hours (1)
Test component See Figure 89	Low stress Life ≈ 8000 hours(2)	3	Spectrum loading plus thermal stresses Table XIII	Room temperature	6	2,640(3)
				500°F	6	2,640(3)
	Medium stress Life ≈ 800 hours(2)			Mission temperatures Table XIII	6	26,400(2)
				Subtotal:	18	31,680
Test component See Figure 89	Low stress Life ≈ 8000 hours(2)	3	Spectrum loading plus G-A-G loads plus thermal stresses Table XIII	Room temperature	6	2,640(3)
				500°F	6	2,640(3)
	Medium stress Life ≈ 800 hours(2)			Mission temperatures Table XIII	6	26,400(2)
				Subtotal:	18	31,680
				Total:	36	63,360

Notes:
(1) Based on testing one specimen at a time.
(2) Design mission times.
(3) Based on a time reduction factor of 10 for room temperature and 500°F tests compared to design mission time.

TABLE XIII
TEST SPECTRUM DEFINITION

Mission Time (HR)	0–0.23	0.23–0.26	0.26–0.34	0.34–0.46	0.46–1.66	1.66–1.73	1.73–1.84	1.84–1.91	1.91–2.10
Temperature (°F)(4)	R.T. – 150	150–160	160–330	330–590	590–580	580–385	385–193	193–180	180–150
Thermal Stress (KSI)(4)	0–4	4–5	5–10	10–20	20–2	2–(–3)	(–3)–(–10)	(–10)–(–7)	(–7)–0
Δg = 0.2	782,381	308,626	576,089	893,746	2,087,434	1,082,018	590,026	265,744	681,045
Δg = 0.4	6,535	2,231	4,046	6,170	12,440	17,320	9,620	4,140	11,686
Δg = 0.6	466	82	156	111	534	642	359	151	392
Δg = 0.8	53	3	6	9	25	36	20	9	21
Δg = 1.0	11	–	–	–	1	2	1	–	1
Δg = 1.1	2	–	–	–	–	–	–	–	–

Notes:
(1) Spectrum is for 20,000 flights.
(2) Load during cycle is $1g \pm \Delta g$.
(3) Add one ground-air-ground cycle per flight (equivalent in stress to –0.2g).
(4) Temperatures and thermal stresses shown are end points corresponding to the times shown.

In the following subsections, the individual portions of the test program are discussed in more detail.

3.1 Coupon Tests - As shown in Table XII, two categories of coupon tests are proposed: (1) constant amplitude coupon fatigue tests to provide basic material property fatigue data and preliminary evaluation of the similar critical section concept, and (2) spectrum coupon fatigue tests to provide a further check of the similar critical section concept under spectrum loading. In the tests, four specimen configurations are utilized, two central hole specimens with stress concentration factors of 2.5 and 2.8, respectively, and two edge notch specimens also with stress concentration factors of 2.5 and 2.8, respectively. The specimen configurations are shown in Figure 88. These two values of stress concentration factors have been selected to represent two values far enough apart to result in discernibly different fatigue test results, but close enough so as to permit a preliminary check on the similar critical section concept. The recommended values of stress concentration, 2.5 and 2.8, are reasonable compromises between values that are easily reproduced and the somewhat higher values exhibited by typical structures.

The specimen configurations shown in Figure 88 utilize a multiple stress concentration design. The purpose of the multiple pattern incorporated within each specimen is to reduce scatter by evaluating the "weakest of five" nominally identical stress raisers. This concept has been used successfully in the fatigue testing conducted under Reference 3 contract where, under a similar testing environment, test scatter was extremely small and the location of failure was random among six identical stress concentrations.

The use of these coupon fatigue tests to provide a preliminary check on the similar critical section concept is based on the following idealization. All complete structures contain a variety of stress concentrations, ranging

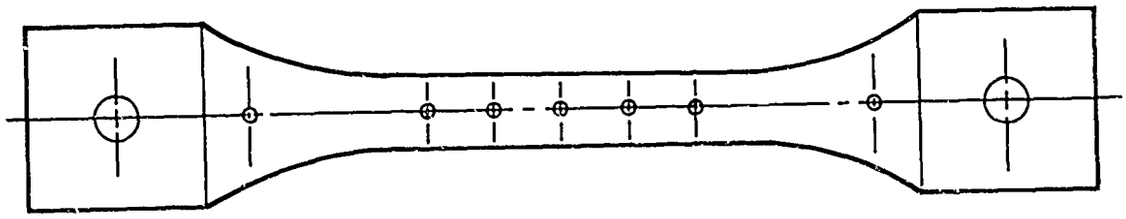

Multiple Central Hole Specimen – K_t = 2.5 or 2.8

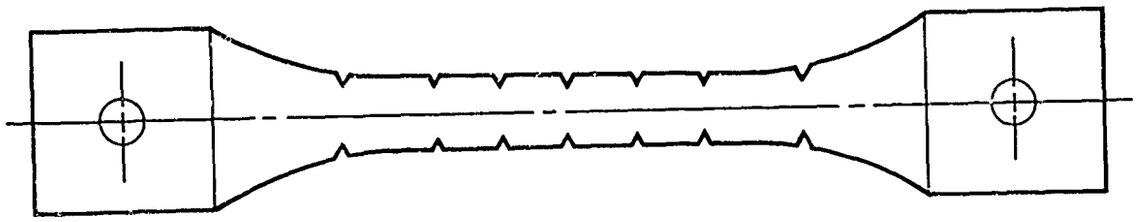

Multiple Edge Notch Specimen – K_t = 2.5 or 2.8

Figure 88- Coupon Test Specimens

in numerical value from 1.0 to the critical value approaching 4.0, and in type such as edge notch, central hole, local imperfections, etc. During fatigue testing, the failure will usually initiate from a single point of the critical stress concentration. If the point from which fatigue failure will initiate does not change whether tested at room temperature, constant elevated temperature, or mission temperature, the similar critical section concept would tend to be validated. Therefore, if in the coupon tests, where different types and values of stress concentrations are used, the relative fatigue performance remains essentially constant, regardless of the temperature environment, it may indicate a preliminary confirmation of the desired similar performance in the complete structure test.

Each of the two categories of fatigue tests are described subsequently.

3.1.1 Constant Amplitude Fatigue Coupon Tests - As previously described, the purpose of the constant amplitude fatigue coupon tests is to provide basic material property fatigue data to aid in the definition of loading for the remaining coupon tests and component tests and to provide a limited check on the similar critical section concept.

As shown in Table XII, constant amplitude, R = 0.25, fatigue tests are recommended to be performed at room temperature and 500°F. It is also recommended, as shown in Table XII, that four stress levels be used for each configuration, and that three specimens be tested at each stress level. The test quantities are defined in Table XII.

3.1.2 Spectrum Fatigue Coupon Tests - The spectrum fatigue coupon tests are designed for the following three purposes: (1) to provide a further check on the similar critical section concept over that provided by the constant amplitude tests, (2) to provide an evaluation, on a coupon basis, of the individual and synergistic effects of the G-A-G cycle and thermal stresses on

fatigue life, and (3) to aid in the test definition and need for the component tests described in Subsection 3.2. The further check on the similar critical section concept will be obtained with the same philosophy as used in the constant amplitude tests, a comparison of the location of failures, but now in three environments of room temperature, 500°F, and mission profile temperatures. The evaluation of the individual and synergistic effects of the G-A-G cycle and thermal stresses on fatigue life will be made on the basis of results of fatigue tests in which the G-A-G cycle and thermal stresses are or are not included. The test definition of the component tests will be made on the basis of a review of the general test results. Detailed aspects of the spectrum fatigue coupon tests are discussed below.

The definition of the spectrum fatigue coupon tests to be performed is presented in Table XII. These tests utilize the same coupon configurations as used in the constant amplitude fatigue tests and are shown in Figure 88. As shown in Table XII, the spectrum fatigue coupon tests are divided into four series which are all possibilities of the basic mission spectrum loading, with and without thermal stress simulation and the G-A-G cycle. As shown in Table XIII, the inclusion of thermal stresses in a coupon specimen is simulated by means of adjusting the mean mechanical stress level by an amount equal to the desired thermal stress. The landing loads portion of the G-A-G cycle is introduced to the specimen by application of a compressive load on a one-per-flight basis; the combination of the maneuver and thermal loadings provide the remaining portion of the G-A-G cycle.

In some cases, as shown in Table XII, a complete range of tests is not proposed for all four groups; this has been done for cost reasons and it is judged that reasonable conclusions may be drawn for the reduced scope of Groups B and C by review of the related results in Groups A and D. Also, for

cost reasons, only three stress levels are proposed for evaluation; but again, this reduction, supported by the more complete range of constant amplitude tests, is not expected to significantly reduce the value of the program. As with the constant amplitude tests, only three specimens are required for a single test definition, due to the multiple stress concentration specimen design which is expected to reduce test scatter.

The successful completion of these spectrum fatigue coupon tests will provide a check on the similar critical section concept of sufficient merit to indicate whether the more expensive and time consuming component fatigue tests are warranted. Additionally, they will provide needed fatigue data on the relative importance of the G-A-G cycle and thermal stresses on fatigue life.

3.2 Component Tests - The purpose of the component tests is to provide a confirmation of the similar critical section concept as applied to tests of complete structures. The design of the component specimens should be compatible with structural requirements of the Mach 3-4 vehicle. A proposed specimen configuration is shown in Figure 89.

A test set-up should be designed to simultaneously heat and load the tension panel of the specimen to the load specimen defined in Table XIII. In the mission temperature component tests, the thermal stresses will be applied by means of thermal gradients. The proposed test sequence is outlined in Table XII. These tests no longer utilize two different stress concentration factors as in the coupon tests, but instead allow the structure to choose its point of failure initiation in a fashion similar to a full-scale complete vehicle structure.

As shown in Table XII, only component fatigue tests with and without G-A-G cycle are proposed since the thermal stresses will be present whenever the mission profile temperatures are applied. However, it is proposed that the

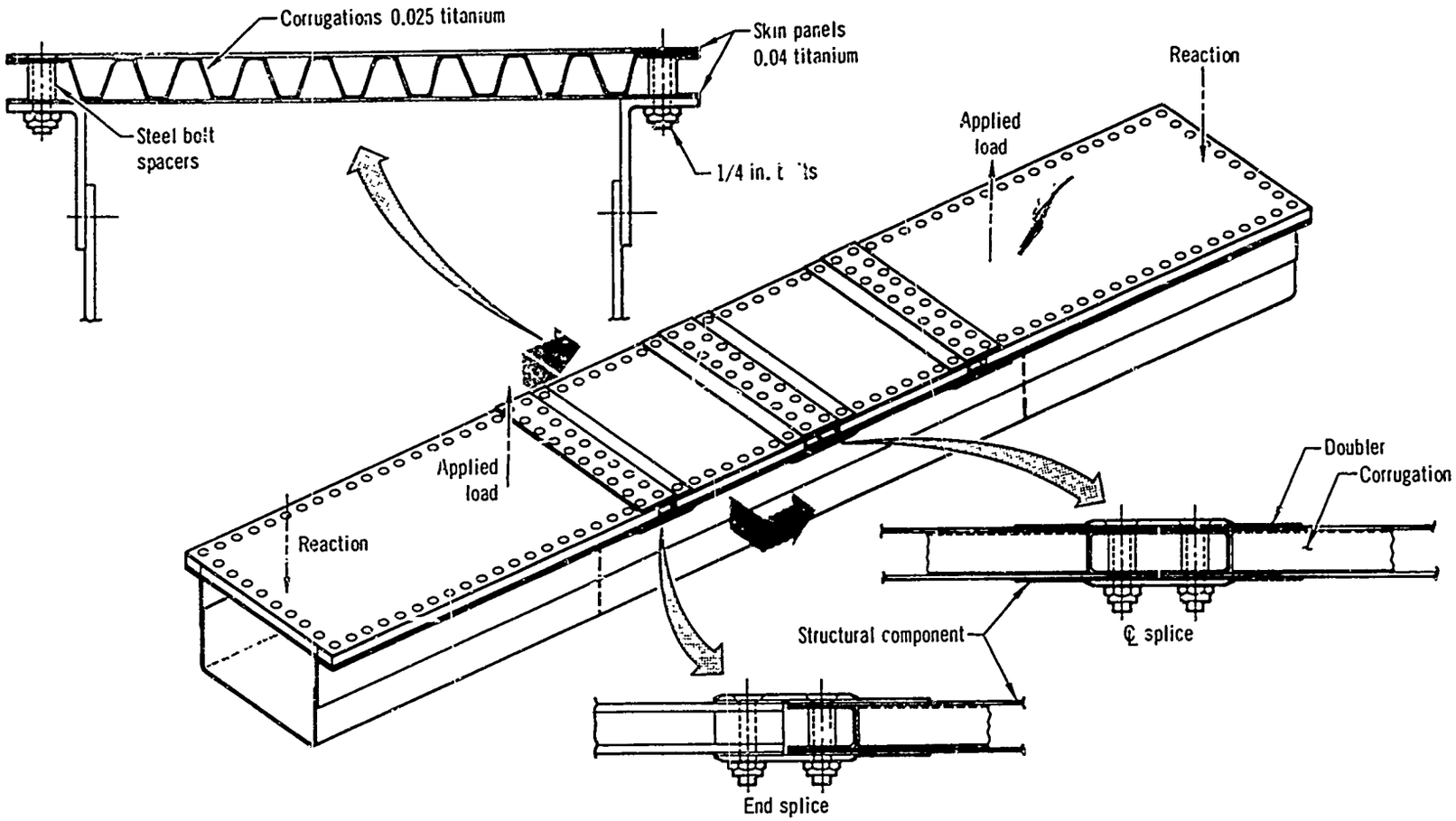

Figure 89 · Component Test Specimen

decision of whether to simulate the missing thermal stresses in the constant temperature. room temperature, and 500°F tests await the completion of the Groups A and B coupon tests. A tentative conclusion, based on the results of this study, would be to omit the thermal stress effect in the constant temperature fatigue tests.

Confirmation of the similar critical section concept will be obtained from the component tests if the location of failure in the constant temperature environments is the same as the location of failure which occurs in the mission profile tests. It should also be realized that if the structure has a number of locations with identical stress concentrations, the location of failure may be random; also, in some cases, the point of failure initiation may not be discernible. In these cases, as supplemented by the coupon data, equivalent life failures in any of many identical stress concentration areas may also be considered as confirmation of the concept of similar critical sections. Such a test substantiation of the similar critical section concept provides confirmation of the selected approaches as described in the first part of this section.

SECTION X

REFERENCES AND BIBLIOGRAPHY

In this section a list of references cited in the text and a bibliography of data pertaining to the subject covered in the study are presented. A cross index of bibliography subjects is presented in Table XIV, in which the numbers shown refer to the bibliography list number. In Table XIV, a particular entry indicates that the corresponding document in the bibliography has data pertaining to both the topic and approach of that matrix position.

REFERENCES

1. Lowndes, H. B., and Cavanagh, R. L., "Airframe Structural Testing - Where Do We Go from Full Scale?," RTD-TDR-63-4197, Part I, March 1964.

2. Boggs, B. C., "The Science of Thermal Simulation - Strength Testing," ASD-TR-61-394, September 1961.

3. FDL-TDR-64-52, "Study to Determine the Suitability of Compressing the Time of Mission Profile During Elevated Temperature Fatigue Testing on Large or Full Scale Vehicles," September 1964.

4. RTD-TDR-63-4235, "Development and Test of a Laboratory System for Simulation of Aerodynamic and Radiative Cooling of Structures," April 1964.

5. Gehring, R. W., and Maines, C. H., "Application of Applied Load Ratio Static Test Simulation Techniques to Full-Scale Structure, Volume IV, Summary of Results, Conclusions and Recommendations," North American Aviation Report NAEC-ASL-1094, Volume IV, August 1966.

6. Naumann, E. C., "Evaluation of the Influence of Load Randomization and of Ground-Air-Ground Cycles on Fatigue Life," NASA TN D-1584, October 1964.

7. Naumann, E. C., Hadrath, H. F., and Guthrie, D. E., "Axial-Load Fatigue Tests of 2024-T3 and 7075-T6 Aluminum-Alloy Sheet Specimens Under Constant-and-Variable-Amplitude Loads," NASA TN D-212, December 1959.

8. Jackson, L. R., et al., "The Fatigue Characteristics of Bolted Lap Joints of 24S-T Alclad Sheet Materials," NACA TN 1030, October 1946.

9. Gray, C. L., "Study in the Use of Structural Models for Sonic Fatigue," ASD-TR-61-547, April 1962.

10. Harpur, N. F., "Crack Propagation and Residual Strength Characteristics of Some Aircraft Structural Materials," Fatigue of Aircraft Structures, p.219-248, MacMillan Company, 1963.

11. Kepert, J. L., and Payne, A. O., "Interim Report on Fatigue Characteristics of a Typical Metal Wing," NACA TM 1397, March 1956.

TABLE XIV
BIBLIOGRAPHY COMPILATION
STRUCTURAL VERIFICATION TESTING

Topic	Model	Component	Full-Scale	Mechanical Simulation of Thermal Effects	General
General	1, 2, 4, 17, 44, 45	2, 21, 22	20	43	
Loading techniques			19, 22, 35		2, 18. 23, 26, 43
Heating techniques			19, 33		18, 24, 26
Cooling techniques			18		24, 26
Ultimate strength			22, 27	29, 30, 31, 32	18, 19, 26
Fatigue strength	2, 5	21, 22, 37, 38, 40, 47	13, 19, 22, 25, 27, 28		6, 15, 18, 20, 23, 26, 34, 42
Material properties					15, 23
Thermal stress	1, 3, 7, 8		25, 27, 28	29, 30, 31, 32	13, 14, 15, 16, 41
Creep	8		20, 25, 27, 28		
Joints					22, 27
Stress concentration			25, 28		
Design criteria			22, 26, 27, 36		2
Crack propagation	5	40	22, 27		46
Thermodynamic analysis	1. 3, 7, 8, 9, 10, 11, 12		33		

BIBLIOGRAPHY

1. Hayes, J., "Structural Modeling," Literature Search No. 523, Jet Propulsion Laboratory, California Institute of Technology, March 1963.

2. RTD-TDR-63-4197, Part 1, "Proceedings of Symposium on Aeroelastic and Dynamic Modeling Technology," Research and Technology Division, Aerospace Industries Association, September 1963.

3. O'Sullivan, W. J., "Theory of Aircraft Structural Models Subject to Aerodynamic Heating and External Loads," NACA TN 4115, September 1957.

4. Goodier, J. N., and Thomson, W. T., "Applicability of Similarity Principles to Structural Models," NACA TN 993, July 1944.

5. Gray, C. L., "Study in the Use of Structural Models for Sonic Fatigue," ASD-TR-61-547, April 1962.

6. Jackson, L. R., et al, "The Fatigue Characteristics of Bolted Lap Joints of 24S-T Alclad Sheet Materials," NACA TN 1030, October 1946.

7. Molyneux, W. G., "Scale Models for Thermo-Aeroelastic Research," Technical Note: Structures 294, Royal Aircraft Establishment, March 1961.

8. Calligeros, J. M., and Dugundju, J., "Similarity Laws Required for Experimental Aerothermoelastic Studies," Technical Report 75-2, Part 2 - Hypersonic Speeds, Aeroelastic and Structures Research Laboratory, Massachusetts Institute of Technology, February 1961.

9. Adkins, D. L., "Scaling of Transient Temperature Distributions of Simple Bodies in a Space Chamber," AIAA Paper 65-660.

10. Vickers, J. M. F., "Thermal Scale Modeling," Astronautics and Aeronautics, May 1965.

11. Bevans, J. T., et al, "Prediction of Space Vehicle Thermal Characteristics," AFFDL-TR-65-139, October 1965.

12. Barzelay, M. E., Tong, K. E., and Holloway, G. F., "Effect of Pressure on Thermal Conductance of Contact Joints," NACA TN 3295, May 1955.

13. Barrois, W., and Ripley, E. L., "Fatigue of Aircraft Structures," MacMillan, 1963.

14. Gatewood, B. E., "Thermal Stresses," McGraw Hill, 1957.

15. Boley, B. A., Freudenthal, A. M., and Liebowitz, H., "High Temperature Structures and Materials," MacMillan, 1964.

16. Boley, B. A., and Weiner, J. H., "Theory of Thermal Stresses," John Wiley and Sons, 1960.

BIBLIOGRAPHY (Continued)

17. Langhaar, H. L., "Dimensional Analysis and Theory of Models," John Wiley and Sons, 1951.

18. Boggs, B. C., "The Science of Thermal Simulation - Strength Testing," ASD-TR-61-394, September 1961.

19. Ripley, E. L., and Maxwell, R. D. L., "A Review of the Work in the United Kingdom on the Fatigue of Aircraft Structures During the Period May 1963 - April 1965," Technical Report 65-193, Royal Aircraft Establishment, August 1965.

20. Atkinson, R. J., "The Testing of Supersonic Transport Structures in Fatigue," Technical Note: Structures 359, Royal Aircraft Establishment, June 1964.

21. Schijve, J., "Estimation of Fatigue Performance of Aircraft Structures," S.T.P. No. 338, American Society for Testing and Materials, 1962.

22. Plantema, F. J., and Schijve, J., "Full Scale Fatigue Testing of Aircraft Structures," Pergamon Press, 1961.

23. Naumann, E. C., "Evaluation of the Influence of Load Randomization and of Ground-Air-Ground Cycles on Fatigue Life," NASA TN D-1584, October 1964.

24. RTD-TDR-63-4235, "Development and Test of a Laboratory System for Simulation of Aerodynamic and Radiative Cooling of Structures," April 1964.

25. FDL-TDR-64-52, "Study to Determine the Suitability of Compressing the Time of Mission Profile During Elevated Temperature Fatigue Testing on Large or Full Scale Vehicles," September 1964.

26. AFFDL-TR-65-42, "A Study to Determine Environments Required to Simulate Design Conditions on Structures for Future Aerospace Vehicles," May 1965.

27. WADD-TR-60-140, Part 1, "Investigation of Thermal Effects on Structural Fatigue," August 1960.

28. Padlog, F., and Schmitt, A., "A Study of Creep, Creep Fatigue, and Thermal-Stress-Fatigue in Airframes Subject to Aerodynamic Heating," WADC-TR-58-294, July 1958.

29. Engle, R. L., and Gehring, R. W., "A Feasibility Study of Applied Load Ratios to Simulate Elevated Temperature Static Tests at Room Temperatures," North American Aviation Report NA62H-973, May 1963.

30. Gehring, R. W., and Maines, C. H., "Application of Applied Load Ratio Static Test Simulation Techniques to Full-Scale Structures; Volume I, Methods of Analysis and Digital Computer Programs," North American Aviation Report NAEC-ASL-1094, Volume I, December 1965.

BIBLIOGRAPHY (Continued)

31. Gehring, R. W., and Lumm, J. A., "Application of Applied Load Ratio Static Test Simulation Techniques to Full-Scale Structures; Volume II, Material Properties Studies and Evaluation," North American Aviation Report NAEC-ASL-1094, Volume II, January 1966.

32. Gehring, R. W., and Maines, C. H., "Application of Applied Load Ratio Static Test Simulation Techniques to Full-Scale Structures; Volume IV, Summary of Results, Conclusions and Recommendations," North American Aviation Report NAEC-ASL-1094, Volume IV, August 1966.

33. Malcolm, J. R., and Slack, R. L., "Comparison of Relative Costs of Thermal Analysis Methods for Hypersonic Vehicle Compartments," WADD TR 60-768, July 1961.

34. Naumann, E. C., Hardrath, H. F., and Guthrie, D. E., "Axial-Load Fatigue Tests of 2024-T3 and 7075-T6 Aluminum-Alloy Sheet Specimens Under Constant-and-Variable-Amplitude Loads," NASA TN D-212, December 1959.

35. Nederveen, A., et al, "Experimental Details of Testing a Full-Scale Structure With Random and Programmed Fatigue Load Sequences," NLR Report S. 608, January 1964.

36. Shuler, W. T., "Large Cargo Airplane Structural Considerations," Society of Automotive Engineers Paper 660669, October 1966.

37. Schijve, J., et al, "Fatigue Lives Obtained in Random and Program Tests of Full-Scale Wing Center Sections," NLR Report S.611, December 1963.

38. Schijve, J., "Fatigue Loads Applied on a Full-Scale Structure in Random and Programmed Sequences," NLR Report S.609, April 1964.

39. Schijve, J., and Broek, D., "Fatigue Test Results of Two Full-Scale Wing Center Sections Under Ground-to-Air Cycle Loading," NLR-TM S.635, April 1965.

40. Schijve, J., et al, "Fatigue Tests with Random and Programmed Load Sequences, With and Without Ground-to-Air Cycles. A Comparative Study on Full-Scale Wing Center Sections," AFFDL-TR-66-143, October 1966.

41. Timoshenko, S., and Goodier, J. N., "Theory of Elasticity," McGraw-Hill Book Company, 1951.

42. Ketola, R. N., "A Full Scale Structural Fatigue Test Program," AIAA Paper 64-444, July 1964.

43. Lowndes, H. B., and Cavanagh, R. L., "Airframe Structural Testing - Where Do We Go from Full Scale?", RTD-TDR-63-4197, Part I, March 1964.

44. Hetenyi, M., "Handbook of Experimental Stress Analysis," John Wiley and Sons, 1950.

45. Ezra, A., "Scaling Laws and Similitude Requirements for Valid Scale Model Work," Martin Company Report 63K19, June 1964.

UNCLASSIFIED
Security Classification

DOCUMENT CONTROL DATA - R&D

(Security classification of title, body of abstract and indexing annotation must be entered when the overall report is classified)

1. ORIGINATING ACTIVITY (Corporate author) THE MCDONNELL COMPANY ST. LOUIS, MISSOURI	2a. REPORT SECURITY CLASSIFICATION UNCLASSIFIED 2b GROUP N/A

3. REPORT TITLE

Approaches to Structural Verification Testing of Mach 3-15 Vehicles

4. DESCRIPTIVE NOTES (Type of report and inclusive dates)
Final Report

5. AUTHOR(S) (Last name, first name, initial)
Finn, Joseph C.
Garrett, Ramon A.
Dill, Harold D.

6. REPORT DATE	7a. TOTAL NO. OF PAGES	7b. NO. OF REFS
December 1967	253	45

8a. CONTRACT OR GRANT NO. AF33(615)-3418 b. PROJECT NO. 1347 c. Task No. 134703 d.	9a. ORIGINATOR'S REPORT NUMBER(S) AFFDL-TR-67-82 9b. OTHER REPORT NO(S) (Any other numbers that may be assigned this report) N/A

10. AVAILABILITY/LIMITATION NOTICES This document is subject to special export controls and each transmittal to foreign governments or foreign nationals may be made only with prior approval of AFFDL (FDTE); WPAFB, Ohio 45433.

11. SUPPLEMENTARY NOTES None	12. SPONSORING MILITARY ACTIVITY Air Force Flight Dynamics Laboratory, Structures Branch, Wright-Patterson AFB, Ohio 45433

13. ABSTRACT

Several alternate techniques are investigated for the structural verification testing of future aerospace vehicles. The investigation has a twofold objective: (1) to develop criteria for fatigue and ultimate strength verification testing of aerospace structures experiencing large thermal inputs over large areas, and (2) to establish a test program for the substantiation of the criteria thus obtained.

The primary approach evaluated is reducing the size of the test article and hence the thermal input required by means of scaled structural models or components. A secondary approach is simulation of thermal effects by mechanical means. Two vehicle configurations are used for relative evaluation: a large Mach 3-4 vehicle similar to the SST and a smaller Mach 12-15 hypersonic manned vehicle. Detailed thermodynamic, strength, and test facilities and cost data relating to testing approaches, and combinations of approaches, of these two configurations are presented. From these data several conclusions are drawn. A comparison of cost is developed for the testing approaches; the most attractive combinations of approaches are selected and testing verification programs for these combinations are defined.

This abstract has been approved for public release. Its distribution is unlimited.

DD FORM 1 JAN 64 1473

UNCLASSIFIED
Security Classification